

**Mammalian Cell Culture:  
High Throughput  
Applications of Oxygen  
Sensor Plates and Cellular  
Physiological Studies Using  
<sup>13</sup>C-Labeling**

**Dissertation  
zur Erlangung des Grades  
des Doktors der Naturwissenschaften  
der Naturwissenschaftlich-Technischen Fakultät III  
Chemie, Pharmazie, Bio- und Werkstoffwissenschaften  
der Universität des Saarlandes**

**von  
Rahul Ravi Deshpande M.Tech  
Saarbrücken, Germany  
2007**

**Tag des Kolloquiums:**

**Dekan:**

**Berichterstatter:**

कर्मण्ये वाधिकारस्ते  
मा फलेषु कदाचन ।  
मां कर्मफलहेतुर्भूः  
मा ते सङ्गोस्त्वकर्मणि ॥  
- From *Bhagwad Gita*



# Acknowledgements

No man is an island. Any successful completion of work or achievement cannot be said to be a truly individual effort. Such is the case with the completion of my thesis. This small part of my thesis gives me not only an opportunity, but also great pleasure to thank those who have helped and supported me along the way.

First and foremost my heartfelt thanks to my doctoral guide, Prof. Elmar Heinzle, for giving me an opportunity to work in his group and, for the continued support and guidance during the work. The discussions we had together are the main driving factor behind the work described in this thesis. His passion for work and a friendly disposition make him truly an endearing person, whom you automatically come to respect.

Thanks to my second official referee Prof. Dr. Friedrich Gifforn for reviewing this dissertation.

Special thanks to Dr. Tae Hoon Yang for the helpful discussions and guidance, especially during the second part of my doctoral work involving metabolic flux analysis. I will always remember the long evenings in the lab, the kebabs, Thai/Chinese food and the trips to Moloco and KFC along with Masoud.

The analytical lifeline of Technische Biochemie, Michel Fritz, requires a special mention. It would not have been possible to do the analytics carried out in the thesis without his help. Thank you for being a patient and wonderful human being.

Thanks to Prof. Christoph Wittmann for helpful discussions and support.

Thanks to my project collaborators, Dr. Ruth Mass, Yvonne Kirsch, Dr. Gernot John, Dr. Christian Krause and Dr. Harald Waltenberger for the work comprising of microtiterplates; my special gratitude for Dr. Ruth Mass and Yvonne Kirsch of Pharmacelsus GmbH (Saarbruecken, Germany) for the data concerning the adherent and primary cell lines.

I would like to thank the Deutsche Bundesstiftung Umwelt (DBU) and the University of Saarland for the financial support.

My thanks and appreciation goes out to all my colleagues, both former and present, at the Technische Biochemie. Here the following former members of Technische Biochemie, Svenja, Ditte, Sathish, Vidya and Arno, deserve special mention. Not only were they great colleagues but are also dear friends.

Thanks to Svenja and Andrea for introducing me to microtiterplates and cell culture respectively.

Thanks to Robert and Frau Witte for the smooth running of lab.

Special people deserve special mention. Hence, my gratitude to three such people whom I have the very good fortune of calling as my friends, Lucia, Masoud and Uenal. Thanks for being such great friends.

Thanks to Simone B and Christoph B for helping me with the German part of thesis and also other helps.

For Ilka M, Maria L, Maria S, Simone B, Alex S, Christoph B and Mathias S, my good friends (notice the alphabetical order) in the lab as well as outside, a very special thank you for spending the weekends and evenings with this “so lonely” creature.

A special credit to a lovely friend from France, Karen M, without whom, I don’t think I would have been able to speak even the “butler” German that I do now.

To my Parents, I would like to say, that no amount of thank you would show the appreciation I have for you and for everything you have done for me. To my brother, Anand, a big hug for being there for me. To Usha Kaki, Baba, Sadhana and Shreeram, my gratitude for the love showered on me. To all my friends; thanks for liking me.

To all those who are not mentioned here, maybe due to lack of my memory power, my deepest apologies and a very big thank you.





# CONTENTS

<b>Acknowledgements</b> .....	<b>v</b>
<b>1 ABSTRACT</b> .....	<b>1</b>
<b>2 ZUSAMMENFASSUNG</b> .....	<b>2</b>
<b>3 INTRODUCTION</b> .....	<b>3</b>
3.1 Objective.....	3
3.2 Thesis organization.....	4
<b>4 MICROTITER PLATES IMMOBILIZED WITH OXYGEN SENSOR</b> .....	<b>5</b>
4.1 Introduction .....	5
4.2 Materials and methods.....	6
4.2.1 Cell lines and stock maintenance.....	6
4.2.2 Oxygen-sensor microtiter plate .....	8
4.2.3 Culture enumeration and viability assay .....	9
4.2.4 Microtiter plate (MTP) growth of cells .....	10
4.3 Respiration rate measurements.....	11
4.3.1 Motivation and theory .....	11
4.3.2 Uptake rates and $K_{La}$ measurements.....	12
4.3.3 Growth of CHO cells.....	13
4.3.4 On-line measurement of oxygen uptake rates .....	16
4.3.5 Culture viability based on OUR .....	17
4.4 Medium optimization .....	22
4.4.1 Motivation and theory .....	22
4.4.2 Statistical experimental design.....	23
4.4.3 Cell growth and oxygen uptake rate (OUR) determination.....	27
4.4.4 Results and discussion .....	28
4.4.5 Conclusions .....	37
4.5 Cytotoxicity Testing .....	38
4.5.1 Motivation and theory .....	38
4.5.2 Cytotoxic compounds.....	39
4.5.3 Microtiter plate (MTP) growth of cells and cytotoxicity assay.....	39
4.5.4 Comparison of oxygen uptake rates with MTT assay .....	40
4.5.5 Growth of primary and adherent cells on MTP.....	41
4.5.6 Cytotoxicity assays and $LC_{50}$ determination .....	44
4.5.7 Z'-Factor of assay.....	48

4.5.8	Cell death kinetics .....	48
4.5.9	Conclusions .....	52
<b>5</b>	<b>PHYSIOLOGICAL INVESTIGATIONS ON CHO CELLS.....</b>	<b>53</b>
5.1	Introduction .....	53
5.2	Review of cellular biochemistry.....	54
5.3	Metabolic flux analysis.....	67
5.3.1	Methodology.....	67
5.3.2	Metabolic flux analysis in mammalian cells .....	72
5.4	Materials and methods.....	74
5.4.1	Cell line and culture conditions.....	74
5.4.2	Cell viability assays .....	74
5.4.3	Chemicals .....	74
5.4.4	Dry weight determination.....	74
5.4.5	Sampling for analysis .....	75
5.4.6	Quantification of extracellular metabolites .....	75
5.4.7	Gas chromatography-mass spectrometry analysis.....	76
5.4.8	Online monitoring of oxygen in spinner flasks .....	79
5.5	Investigative physiological studies on CHO cell.....	85
5.5.1	Theory.....	85
5.5.2	[U- <sup>13</sup> C]Glucose studies of metabolism.....	86
5.5.3	Parallel labeling studies for metabolic studies .....	123
<b>6</b>	<b>CONCLUSIONS.....</b>	<b>174</b>
<b>7</b>	<b>OUTLOOK.....</b>	<b>176</b>
<b>8</b>	<b>REFERENCES .....</b>	<b>179</b>
<b>9</b>	<b>APPENDIX.....</b>	<b>194</b>
9.1	Symbols and abbreviations.....	194
9.2	Berkeley Madonna program for kla determination .....	197
9.3	Equations for the biochemical metabolic model in Figure 5.2.1 .....	198
9.4	Equations for the biochemical metabolic model in Figure 5.6.13 .....	201
9.5	Biomass composition of CHO cells.....	204





## 1 ABSTRACT

Innovative 96-well microplates equipped with optical oxygen sensors were applied for high throughput applications for mammalian cell culture. The oxygen uptake rates of the cells could be calculated from online monitoring of dissolved oxygen. The microplates were applied for process development using statistical experimental design with regard to medium optimization offering significant cost benefits and reducing the time generally required to carry out the process. With viability assay developed using the microplates, the toxicity of compounds could be tested in primary cells as well as adherent and suspension cells. The advantage of this assay over the presently available assays includes its kinetic nature and that the cells could be processed for further studies.

The physiology of Chinese hamster ovary (CHO) cells was investigated by isotopic labeling studies. Cells were grown in parallel in multiple labeled carbon substrates. Based on the carbon isotope distribution in the metabolites, a model for the metabolism of pyruvate is proposed. There was evidence for the cytosolic compartmentation of pyruvate. The model proposes that this might be due to metabolic channeling occurring in glycolysis. Moreover, from the data, metabolism of glycine and serine was investigated. It is seen that the reverse glycine cleavage system and the glyoxylate cycle is active in CHO cells. Relative fluxes in the major metabolic pathways of CHO cells were estimated.

## 2 ZUSAMMENFASSUNG

In der vorliegenden Arbeit wurden 96-well Mikrotiterplatten, ausgestattet mit optischen Sauerstoffsensoren, für die „high throughput“-Anwendung mit Säuger-Zellkulturen eingesetzt. Die Sauerstoff-Aufnahmeraten der Zellen konnten dabei durch online Messung des gelösten Sauerstoffs bestimmt werden. Die verwendeten Mikrotiterplatten wurden zur Mediumoptimierung mittels „statistical experimental design“ mit entsprechender Senkung von Kosten und Zeit eingesetzt. Außerdem konnte mit den Mikrotiterplatten die Toxizität von Substanzen für Primärzellen sowie für adhären und in Suspension wachsenden Zellen durch Einsatz eines „viability assays“ bestimmt werden. Der hier angewendete Ansatz bietet gegenüber den bisher verfügbaren Tests den entscheidenden Vorteil, einer dynamischen Messung und dass die Zellen für weitere Studien verwendet werden können.

Des Weiteren wurde die Physiologie von Chinese hamster ovary (CHO) Zellen durch  $^{13}\text{C}$ -Markierungsstudien untersucht. Zellen wurden zu diesem Zweck auf Kohlenstoff-markierten Substraten kultiviert. Basierend auf der Kohlenstoffverteilung im Stoffwechsel wurde ein Modell für den Pyruvat-Metabolismus vorgeschlagen. Dabei ergaben sich Hinweise auf eine zytosolische Kompartimentierung von Pyruvat bedingt durch „Metabolic Channeling“ in der Glycolyse. Im Glycin/Serin-Stoffwechsel waren das „reverse Glycin Cleavage System“ und der Glyoxylat-Weg in CHO-Zellen aktiv.

### 3 INTRODUCTION

#### 3.1 Objective

The history of cell culture dates back to early twentieth century. However, it was only during the 1940's and 1950's that there was a rapid development in the techniques for cell culture. Mammalian cells are cells which are generally part of an organ of an organism, differentiated to perform specific functions. These cells can be extracted and be grown *in vitro*. Many of them survive but do not multiply *in vitro*. However, cells can acquire the ability to proliferate indefinitely either by random mutation or by genetic transformation. Many immortalized cell lines derived from various organs and organisms are now commercially available. The cell lines can either be adherent, i.e. requiring a support for growth or can grow in suspension. The Chinese hamster ovary (CHO) cell line was developed at the end of the 1950 (Puck et al., 1958) and it is available both as an adherent and as a suspension cell line. These cells are routinely used in biological and medical research. However, the main usage of these cell lines has been in the production of proteins for therapeutic and diagnostic purposes. The main advantage of using these and other mammalian cell lines for production is their ability to produce proteins with the correct conformation and post-translational modifications. CHO cells are also routinely used for cytotoxicity testing (Hsie and Schenley, 1983). In this regard it is important to develop methods which can lead to process improvements such as development of high throughput methods for large scale handling of the cells. Moreover, it is also important to have a better understanding of the cellular metabolism. The development of high throughput methods with a better understanding of the cellular metabolism would result in superior industrial cell culture processes as well as knowledge of the effect various environmental conditions have on the cellular physiology. The objective of this thesis is to develop methods for quantitative physiological studies as well as for high throughput application for the CHO cells. The high throughput applications are achieved using innovative 96-well microplates equipped with optical sensors for oxygen monitoring. Methods are developed for quantitative physiological studies for application in the technique of metabolic flux analysis.

### **3.2 Thesis organization**

The thesis is organized in two major parts. The first part of the thesis deals with the high throughput application of innovative 96-well microplates equipped with optical sensors for oxygen monitoring. These plates are shown to be applicable for high throughput respiration measurements, medium optimization for cellular growth and *in vitro* cytotoxicity testing. The second part of the thesis deals with the quantitative physiological studies of the cellular metabolism. A brief review of cellular biochemistry and the technique of metabolic flux analysis are given. It is followed by the development of methods required for the generation of data required for flux analysis. Physiological interpretations concerning the cellular physiology obtained from the experiments performed with labeled substrates are then presented.

## **4 MICROTITER PLATES IMMOBILIZED WITH OXYGEN SENSOR**

### **4.1 Introduction**

Advances in molecular biology, human genetics and functional genomics continue to produce increasing numbers of molecular targets available for therapeutic intervention. This, coupled with major increases in compound collections produced by combinatorial technologies, has fuelled an important need for improvements in high-throughput capabilities (Hertzberg and Pope, 2000). Moreover, with the advances in the production of biologicals, high throughput methods are needed for acceleration of process development. Mammalian cells have become an integral part in the process of drug screening and also for the production of biologically important proteins. Hence high throughput methods catering to mammalian cell culture are needed.

Generally microplates are used for the routine culturing of cells. Microplates are available for the growth of both adherent and suspension cell cultures in static condition. They are presently available in 6, 8, 12, 24, 96, 384, 1536 and 3456 well formats. Each well of the plate can be used for cell culture. The choice of the format depends upon the end application of the cell culture. Many well plates are used simultaneously for screening drugs and for other biochemical assays. However, monitoring of cell growth in these well plates is problematic. Most of the methods of determining cell viability are end-point assays and hence the cells cannot be processed further. In this part the use of novel 96-well microplates immobilized with optical oxygen sensors as a method for the online monitoring of cell growth is described. Moreover the application of these plates for process development as well as cytotoxicity screening is described.

## 4.2 Materials and methods

### 4.2.1 Cell lines and stock maintenance

Chinese Hamster Ovary (CHO) cell line T-CHO ATIII, obtained from Gesellschaft fuer Biotechnologische Forschung mbH (Braunschweig, Germany), was one of the cell lines used for this work. The cells produce recombinant Antithrombin III, which has clinical applications for its coagulation inhibitory activity. The cells are grown in suspension and are adapted to serum free medium. CHO-S-SFM II (GIBCO, Invitrogen Corporation, USA), a serum free medium for CHO suspension cells was used for the routine growth and maintenance of cells. A 1 mL cryopreserved aliquot of the cells was rapidly thawed to 37 °C and washed twice with pre-warmed medium to remove any traces of cryoprotectant before inoculating the cells at a density of  $1-2 \times 10^5$  cells mL<sup>-1</sup> in 15-25 mL of medium. The cells were grown in 250 mL spinner flasks (Techne, Staffordshire, United Kingdom) placed in an incubator (INCO2, Memmert GmbH + Co.KG, Schwabach, Germany) set at 37 °C and 88 % relative humidity with an overlay of 12 % CO<sub>2</sub>. The spinner flasks were placed on a stirrer (Model 104-S, Techne, Staffordshire, United Kingdom) which has maximum speed of 80 rpm. To demonstrate the application of the plates for medium optimization, the cells were adapted to grow in a protein and peptide free, chemically defined media (SMIF 6, Life Technologies, Karlsruhe, Germany).

Cryopreserved stock aliquots were prepared from cells grown in CHO-S-SFM II. The cryoprotectant solution was serum free medium CHO-S-SFM II with 10 % Dimethyl sulfoxide (DMSO). Typically  $4-10 \times 10^6$  viable cells mL<sup>-1</sup> in the cryoprotectant solution were taken and aliquots of 1 mL volumes in 2 mL plastic cryovials were prepared. Due to the non-availability of a programmable freezer the following steps of slow freezing were followed. Initially the cryovials were held at 4 °C for 2-3 h and then transferred to a well insulated Styrofoam box. This Styrofoam box was then held at -20 °C for 5-6 h and then transferred immediately to -70 °C for overnight cooling. The cryovials were then removed from the box and quickly stored in liquid nitrogen storage canisters till further usage.

The other suspension cell line used in this work was HL-60 (human acute myeloid leukemia). The cell line was obtained from German collection of microorganisms and cell cultures (DSMZ) (Braunschweig, Germany) and Roswell Park Memorial Institute (RPMI) 1640 medium with 10 % fetal bovine serum (FBS) was used for growth. These cells are also adapted for suspension growth and were grown in 250 mL spinner flasks placed in a 12 %

CO<sub>2</sub> humidified gas controlled incubator at 37 °C. The process of thawing and freezing was similar to the one described above with the only change being in the medium used and the cryoprotectant solution in this case being RPMI 1640 medium with 10 % FBS with either 10 % glycerol or 10 % DMSO. Stocks were made both with 10 % Glycerol and 10 % DMSO due to the potential toxicity and differentiation caused by DMSO.

Both the cells cultures were maintained in growth phase by changing the media using the serial dilution method. Cells were grown in spinner flasks till a density of about  $2 \times 10^6$  cells mL<sup>-1</sup> for CHO cells and around  $1 \times 10^6$  cells mL<sup>-1</sup> for HL-60 cells, centrifuged, transferred at a cell density of  $2-3 \times 10^5$  cells mL<sup>-1</sup> in fresh media into spinner flasks and allowed to grow. The HL-60 cells were harvested at a lower cell density since they can potentially differentiate at high cell densities.

The culture of the adherent cell line human colon carcinoma cell line Caco-2 and primary rat hepatocytes for toxicity studies were carried out in cooperation with the firm Pharmacelsus GmbH, Saarland University, Saarbrücken, Germany.

The human colon carcinoma cell line Caco-2 (DSMZ, Braunschweig, Germany) was cultured in Dulbeccos Modified Eagle Medium (DMEM) pH 7.6. The following supplements were added: Minimum Essential Medium with Non-Essential Amino Acids (1X), 100 U ml<sup>-1</sup> Penicillin, 100 µM ml<sup>-1</sup> Streptomycin and 10 % fetal calf serum (FCS). For growth studies 44 mM HEPES were added. All reagents were purchased from C.C. Products GmbH (Cell Culture Products, Neustadt, Germany). The cells were seeded to 25 cm<sup>2</sup> culture flasks (Greiner Bio-One GmbH, Frickenhausen, Germany) and cultivated at 37°C in a humidified incubator with 5 % CO<sub>2</sub>. The medium was changed every 2 days and the cells were passaged at 90 % confluence.

Hepatocytes were isolated from male Wistar rats (250-350 g, Harlan-Winkelmann, Germany) by an *in situ* enzymatic perfusion (Seglen, 1976). After the two-step collagenase perfusion, the liver was transferred in ice cold Hank's medium and the hepatocytes were liberated from the connective-vascular tissue by shaking the liver. The cells suspension was then filtered through sterile gauze (250 µm mesh openings). This cell suspension was then diluted 1:1 with WME-I (Williams medium E with 10 % FCS and 50 µg/ml Gentamycin) to inactivate collagenase. In order to achieve high purity the cell suspension was centrifuged at 50 g and 4 °C for 20 min over a 30 % Percoll gradient (Nussler et al., 2001). The supernatant with non-parenchymal and dead cells was removed, and the final cell pellet was resuspended in 10 ml growth medium (Williams medium E with 1 µM Insulin, 15 mM HEPES, 100 U/ml Penicillin, 100 µg/ml Streptomycin, 50 µg/ml Gentamycine, 1.4 µM Hydrocortisone and 10

% FCS). With this protocol approximately  $5 \times 10^8$  cells per rat liver were obtained and the viability was greater than 80 % as determined by trypan blue exclusion staining. All cell culture reagents were purchased from C.C. Products GmbH (Cell Culture Products, Neustadt, Germany).

#### 4.2.2 Oxygen-sensor microtiter plate

The oxygen-sensor microtiter plates (MTP) were provided by PRESENS, Precision Sensing GmbH (Regensburg, Germany). The ‘U’ bottomed well plates (OP96U) were used for the growth of suspension cells while the flat bottomed (OP96F) plates were used for the primary and adherent cell lines. OXOPLATE OP96U (Figure 4.2.1) is a sterile polystyrene micro plate in the common 96 round well format, supplied with lid. An oxygen sensor is immobilized on the bottom of each well. This sensor can be read out from the bottom side with a commercially available reader. The OXOPLATE OP96F is similar with the round well format replaced by flat well.



**Figure 4.2.1:** Oxoplate (OP96U) 96 well round bottom MTP with integrated oxygen sensor.

The sensor contains two different dyes. One is the oxygen indicator. Its phosphorescence intensity  $I_{ind}$  is dependent on the concentration of oxygen in the sample filled into the well. The other dye is the reference. Its fluorescence intensity  $I_{ref}$  is independent of the oxygen concentration.

Using the luminescence intensities, the ratio  $I_R$  can be calculated. This referenced signal  $I_R$  corresponds to the concentration of oxygen.

$$I_R = \frac{I_{ind}}{I_{ref}} \quad (4.2.1)$$

Calibration is done by the determination of zero point by the chemical removal of dissolved oxygen using sodium dithionite or sodium sulfite and by subsequent saturation with oxygen from air.

The relationship between fluorescence intensity and dissolved oxygen concentration is nonlinear and described by the Stern-Volmer equation for collision quenching:

$$\frac{I_R}{I_{R,0}} = \frac{1}{1 + K_{SV}[O_2]} \quad (4.2.2)$$

Where  $I_{R,0}$  is the fluorescence intensity ratio in the absence of oxygen,  $I_R$  is the fluorescence intensity ratio at the oxygen concentration  $[O_2]$  and  $K_{SV}$  is the Stern-Volmer constant. More information and detailed procedures are described elsewhere (John et al., 2003).

Measurements were carried out in two fluorescence readers, both equipped with integrated shakers and temperature control (Fluostar, BMG Labtechnologies, Offenburg, Germany and Fluoroskan Ascent, Labsystems, Finland) using dual kinetic mode. The former was used generally for static culture and the latter for suspension culture due to the availability of higher shaking rates. The fluorescence intensities were measured with the filter combinations 544 nm/650 nm and 544 nm/590 nm. The first combination measured fluorescence depending on oxygen concentration, whereas the latter showed the oxygen independent constant fluorescence of the reference signal.

### 4.2.3 Culture enumeration and viability assay

Cells were counted using a Neubauer hemocytometer. Cell concentration and viability were determined using the trypan blue exclusion method (Morris et al., 1997). 50  $\mu$ L of the cell suspension was diluted 1:1 in a 0.4 % trypan blue in Phosphate Buffered Saline (pH 7.5). Viable cells exclude the dye while the non-viable cells are stained blue.

Cell vitality and metabolic activity were also compared using the MTT assay (Morris et al., 1997) using standard protocol. Briefly a stock solution of 5 mg mL<sup>-1</sup> of 3-(4,5-Dimethylthiazol-2-yl)-2,5-diphenyltetrazolium bromide (MTT stain) (Sigma-Aldrich Chemie GmbH, Steinheim, Germany) was prepared in Phosphate Buffered Saline (pH 7.5) and filtered through a 0.22  $\mu$ m filter to sterilize and remove any insoluble matter. Wells of a 96-well

microtiter plate were filled with 100  $\mu\text{L}$  of cell suspension; to this was added 10  $\mu\text{L}$  of MTT solution and incubated at 37 °C for 2 h in a humidified incubator. Yellow MTT (a tetrazole) is reduced to insoluble purple formazan by the mitochondria of living cells. The insoluble formazan is solubilised using acidified propanol (0.04 M HCl in propan-2-ol) and the absorbance of the resulting solution is read at a test wave length of 570 nM and a reference wavelength of 630 nM (for cell debris).

#### **4.2.4 Microtiter plate (MTP) growth of cells**

The cells were grown in the absence of CO<sub>2</sub> incubation thus affecting the bicarbonate buffering of the medium. To provide additional buffering capacity, the CHO-S-SFM II medium was modified by the addition of HEPES (Sigma-Aldrich Chemie GmbH, Steinheim, Germany) buffer. The final concentration of the HEPES buffer in the medium was 35 mM. Inoculum cultivations were made using modified medium in spinner flasks with incubation. Cells in the growth phase were harvested and centrifuged for 10 min at 1000 rpm and 4 °C (Function Line, Heraeus Instruments, Osterode, Germany). The resulting pellet was suspended in fresh medium. Volume was adjusted to give an initial viable cell density from  $3 \times 10^5$  cells/ml to  $6 \times 10^5$  cells/ml. From this, aliquots of 200  $\mu\text{L}$  were transferred to the wells of the microplate, covered with lid and cultivated in the fluorescence reader (Fluoroskan Ascent, Labsystems, Finland) at 37 °C and 660 rpm (orbital) with a shaking diameter of 2 mm.

## 4.3 Respiration rate measurements

### 4.3.1 Motivation and theory

O<sub>2</sub> uptake rates of animal cells are well known indicators for metabolic activity and can be used to predict the state of growth (Ramirez and Mutharasan, 1990; Eyer et al., 1995; Ducommun et al., 2000; Schoenherr et al., 2000). This has been applied for laboratory and large scale cell cultures in fermentors using electrodes but rarely for small scale cultures. The critical issue of O<sub>2</sub> availability and mixing in small scale cultivations is generally overlooked (Weiss et al., 2002) and this can affect the final research outcome as O<sub>2</sub> influences growth and product formation (Ozturk and Palsson, 1990b). For small scale cell culture, microplates are generally used both for adherent as well as suspended cells in static condition. But monitoring of culture has remained a problem and is achieved mainly by off-line measurements.

Newly developed microplates with O<sub>2</sub> sensors have been described very recently and used for monitoring respiration of microorganism (Stitt et al., 2002; John et al., 2003). John et al. (2003) reported mass transfer characteristics in 96 well plates, based on fluorescence O<sub>2</sub> sensing. O'Riordan et al. (2000) determined dissolved O<sub>2</sub> in microplates by measuring fluorescence phase shift. They were able to detect the activity of the fission yeast *Schizosaccharomyces pombe* above 10<sup>4</sup> cells ml<sup>-1</sup>. These applications have been directed towards cultivation of bacterial or yeast cells which have high respiratory activities compared to mammalian cells. Hynes et al. (2003) measured dissolved O<sub>2</sub> in microplates using a dissolved O<sub>2</sub> sensor and applied it to mammalian cell monitoring.

In this chapter, the application of microplates with immobilized dissolved O<sub>2</sub> sensor for the determination of O<sub>2</sub> uptake rates and specific uptake rates of suspended mammalian cells is described. The measured data is evaluated using simple models and compared with cultures in spinner flask. The possibility of simplifying and accelerating the measurement for potential high-throughput measurements is investigated.

### 4.3.2 Uptake rates and $K_{La}$ measurements

Oxygen uptake rate can be determined from a stationary liquid phase  $O_2$  balance,

$$\frac{d[O_2]_{aq}}{dt} = k_L a ([O_2]_{aq}^* - [O_2]_{aq}) - OUR \quad (4.3.1)$$

where  $[O_2]_{aq}$  and  $[O_2]_{aq}^*$  are the dissolved oxygen concentrations in the liquid phase and in equilibrium with the gas phase, respectively, and  $k_L a$  is the volumetric liquid phase mass transfer coefficient. The first term in the right hand side of the equation represents the transfer rate of oxygen from the atmosphere into the medium and  $OUR$  is the oxygen uptake rate of cellular, enzymatic or chemical reactions. For cellular processes,

$$OUR = q_{O_2} X \quad (4.3.2)$$

where  $q_{O_2}$  is the specific oxygen uptake rate and  $X$  is the viable cell number.

$[O_2]_{aq}$  was measured using the oxygen sensor coated microplate in conjunction with the fluorescence reader. The  $k_L a$  was determined experimentally, for the cultivation conditions, using sodium dithionite (Fluka Chemie AG, Buchs, Switzerland) by the method earlier (John et al., 2003) using the software BERKELEY MADONNA.

The estimated  $k_L a$  was  $0.9 \text{ h}^{-1}$  thus giving a maximum oxygen transfer rate of  $0.21 \text{ mM h}^{-1}$  (Figure 4.3.1). This value is not as high as reported in previous literature (Hermann et al., 2003) but may be attributed to the presence of a lid during the measuring process.

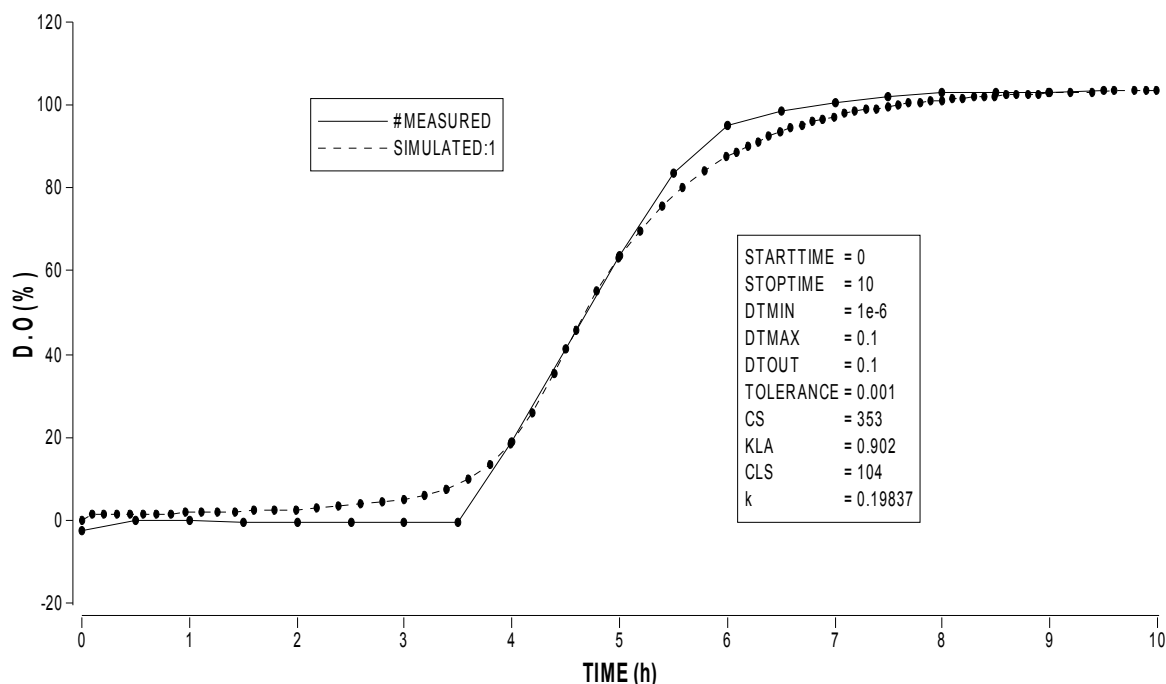


**Figure 4.3.1:** Dynamic estimation of  $k_{La}$  using dithionite. The rise of oxygen is first order and  $k_{La}$  is estimated from liquid phase oxygen balance using a simulation program of BERKELEY MADONNA. The value is found to be  $0.9 \text{ h}^{-1}$ , giving a maximum oxygen transfer rate of  $0.21 \text{ mM h}^{-1}$ . The abbreviations in the inbox are explained in the program supplied in Appendix.

### 4.3.3 Growth of CHO cells

To check the applicability of the oxoplates, an initial simple experiment with cell culture was carried out. T CHO ATIII cells were seeded at different densities in quadruplicates ( $1.6 \times 10^6$ ,  $8 \times 10^5$ ,  $4 \times 10^5$  and  $2 \times 10^5 \text{ Cells mL}^{-1}$ ) in Oxoplate OP96U and grown in Fluorescence reader (Fluostar, BMG Labtechnologies, Offenburg, Germany) at  $37^\circ\text{C}$  under ambient atmospheric conditions. The cycle time was 30 minutes with orbital shaking at 70 rpm (shaking diameter of 3 mm) for 5 minutes before the readings. Cultivation was carried out for 90 hrs with readings being taken every 30 min. Figure 4.3.2 shows the oxygen profile of the cells and as it is evident from the figure, the oxygen profile corresponds to the growth profile and is density dependent. Thus, the cells with higher cell density start initially with lower dissolved oxygen and as the time progresses the oxygen levels increase. This is most probably

due to the loss of viability of the cells, as this phenomenon is observed with a cell density dependent delay in the various cultures.

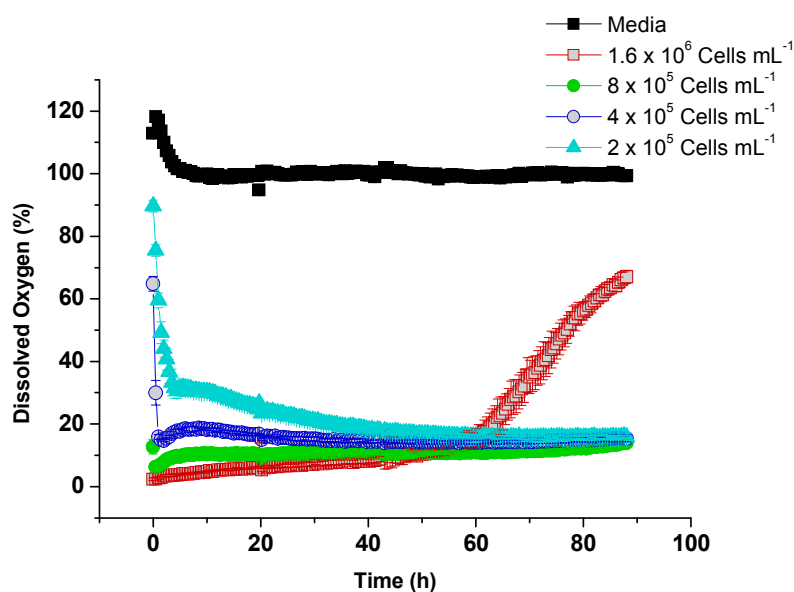


**Figure 4.3.2:** Oxygen profiles of CHO cells with different cell densities. Cells were cultured at different cell densities in triplicates in the oxoplate. The error bars depicting the standard deviation are indicated on each of the curve.

CHO cells were cultivated parallel in microtiter plate and spinner flask. The plate was read every 30 min for the entire cultivation period of 48 h with the shaking parameters given in material and methods section. The breakup of the cycle time for shaking and measurement is given elsewhere (John et al., 2003). The outer wells of the plate were not used for cultivation and were filled with water to reduce evaporation (John et al., 2003). Only 8 innermost wells were read, 4 for calibration and 4 replicates for cell growth. Sampling from the plate was done regularly to compare the growth in MTP with spinner flask. The method of “sacrificial wells” was employed for the sampling of cells, with two wells extracted for every time point. Sampling was done starting from “sacrificing” the wells on the periphery, proceeding towards the center. Sterility was ensured during cultivation and sampling.

Figure 4.3.3 gives the growth characteristics in both systems. The growth of cells was compared by doing viability assay on regularly timed samples. The pH of the samples was measured to check the buffering effect in the absence of  $\text{CO}_2$  incubation. From the data plot it is clear that the growth of cells in both systems is comparable for a 48 h period. There is an

increase in pH at the initial phase of growth in MTP. This can be due to the effect of CO<sub>2</sub> evolution from bicarbonate in the medium.

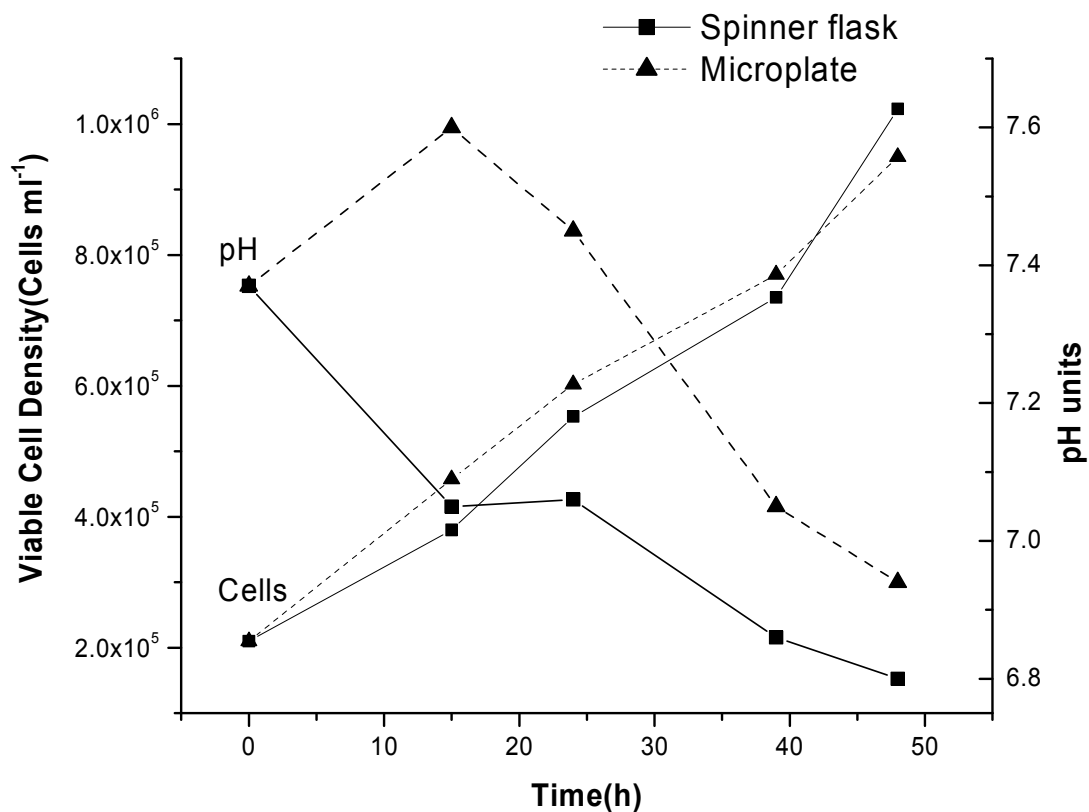


**Figure 4.3.3:** Growth Comparison of CHO cells in oxygen sensor coated MTP (without CO<sub>2</sub> incubation) with spinner flask (in CO<sub>2</sub> incubator). MTP cultivations were carried out in the Fluoroskan Ascent reader at 37°C and at 660 rpm (orbital) with a shaking diameter of 2 mm.

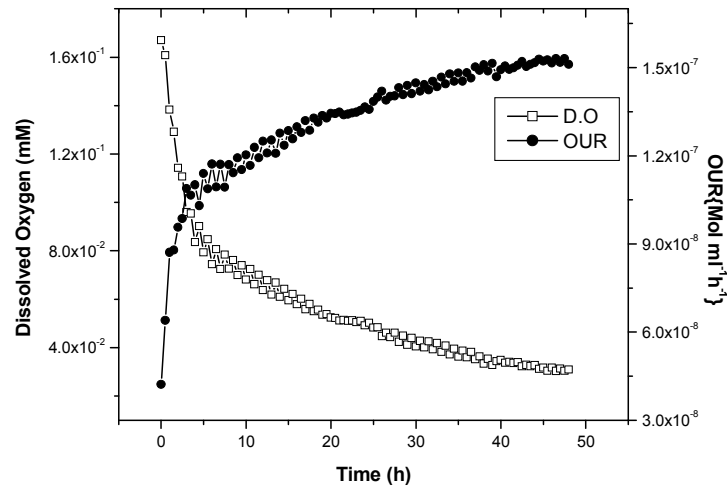
The dissolved oxygen profile of the above cell growth in MTP is given in Figure 4.3.4 (A). As seen, the shaking at the rate employed ensured that there was no oxygen limitation during the entire cultivation period.

#### 4.3.4 On-line measurement of oxygen uptake rates

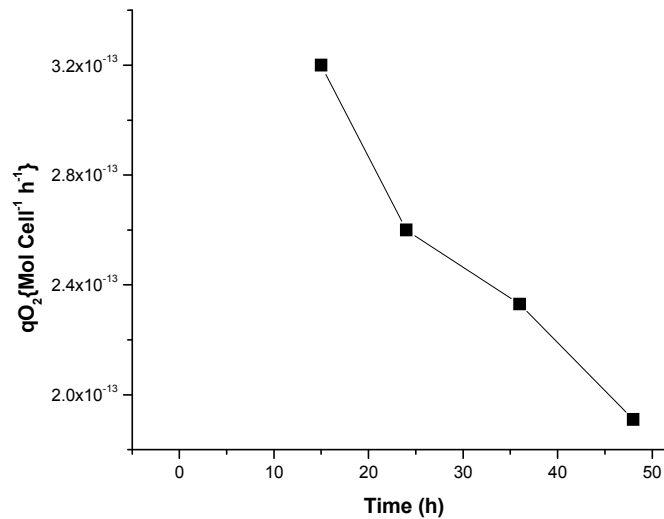
The oxygen uptake rates of cells offer a valuable insight into culture viability and its metabolic activity. For the determination of oxygen uptake rate from the dissolved oxygen profile of cell growth, the oxygen transfer rate into the system should be known.

This transfer rate is dependent on the mass transfer coefficient ( $k_La$ ) of the system which was determined as described earlier. The oxygen uptake rate of the cells was calculated from the oxygen mass balance (Eq. 4.3.1) by using the derivative of the dissolved oxygen profile and the estimated  $k_La$ . The so called “respirogram” [Figure 4.3.4 (A)] of the cells is thus obtained, giving a measure of the respiratory activity of the cells.

Figure 4.3.4 (B) depicts the specific oxygen uptake rate ( $q_{O_2}$ ) of the cells, calculated from OUR and the cell counts in parallel wells, at different time points. The specific oxygen uptake is found to decrease with time with a value of  $3.2 \times 10^{-13} \text{ Mol } (O_2) \text{ Cell}^{-1} \text{ h}^{-1}$  at 15 h cultivation going down to  $1.8 \times 10^{-13} \text{ Mol } (O_2) \text{ Cell}^{-1} \text{ h}^{-1}$  at 48 h. This value is in accordance to the values reported in earlier studies (Ducommun et al., 2000). The decrease of  $q_{O_2}$  is most likely due to the effect known as "crowding phenomenon", which refers to the decrease in specific oxygen uptake rate with increasing cell densities (Trubel and Barnikol, 1998).



(A)



(B)

**Figure 4.3.4:** (A) The online dissolved oxygen (D.O) profile with the respirogram of the CHO cell growth in oxygen sensor coated MTP. The respirogram was constructed by estimation of oxygen uptake rates (OUR) using the D.O profile. (B) The specific oxygen uptake rates at different time points calculated from OUR and the viable cell counts of parallel wells given in Figure 4.3.3

### 4.3.5 Culture viability based on OUR

It was also of interest to measure oxygen uptake rates of sampled cells. A simple method, described earlier for yeast using a different system, was followed (O’Riordan et al., 2000). Cells in exponential growth phase from a spinner flask were harvested and centrifuged for 10

min at 1000 rpm and 4°C. These were re-suspended in fresh medium at various cell densities. 150 µl of the suspended cells were added on to the plates and layered with mineral oil (Sigma-Aldrich Chemie GmbH, Steinheim, Germany) to reduce oxygen transfer. The layer of oil does not totally prevent the transfer of oxygen. Oil may act as a reservoir for oxygen, but as seen from Figure 4.3.5 the transfer of oxygen to the liquid is significantly reduced by applying an oil layer. The oxygen drop was noted every 2 minutes in the reader for 1 h. Initially, dissolved oxygen decreased linearly showing zero order kinetics. Since gas-liquid mass transfer was found to be negligible in comparison to the consumption rate under these conditions, the OUR of the cells was estimated using the liquid phase oxygen balance (Eq. 4.3.1) and setting  $k_{La}$  to be zero.

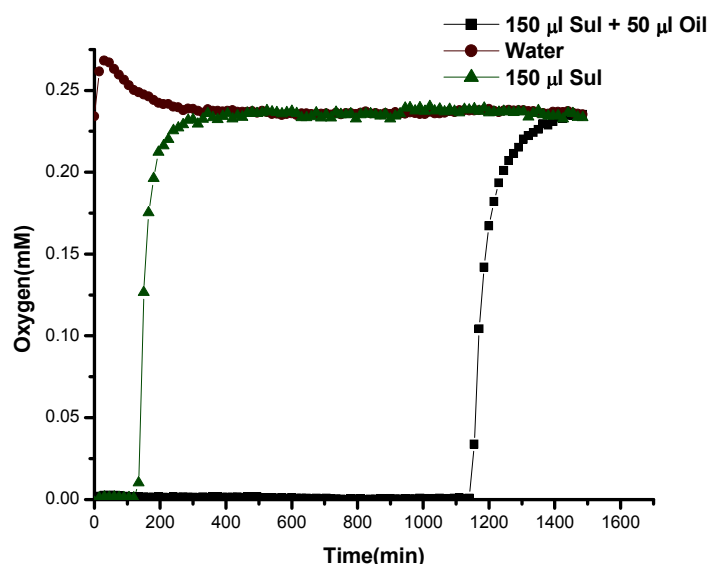


**Figure 4.3.5:** The comparison of oxygen transfer without layer of mineral oil and with the presence of a layer of mineral oil on top. 150 µl of 1 % Sodium sulphite solution was layered with was 50 µl mineral oil (150 µl Sul + 50 µl oil) and the oxygen transfer compared with 1 % Sodium sulphite solution (150 µl Sul). The sulphite removes the oxygen from water. The transfer of oxygen is slower with the presence of mineral oil.

Figure 4.3.6 shows the plot of *OUR* vs. *cell density* which was found to be linear and compared well with the MTT assay. The specific oxygen uptake rate was determined from the slope of the plot. The value of  $3.18 \times 10^{-13} \text{ mol } (O_2) \text{ Cell}^{-1} \text{ h}^{-1}$  obtained is in agreement with the results obtained during the continuous monitoring of cell growth which had a value of  $3.2 \times 10^{-13} \text{ mol } (O_2) \text{ Cell}^{-1} \text{ h}^{-1}$  at 15 h of cultivation [Figure 4.3.4 (B)].

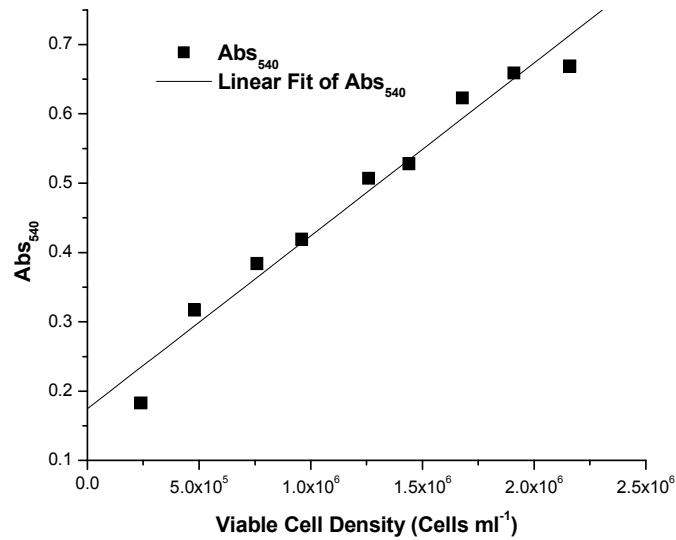
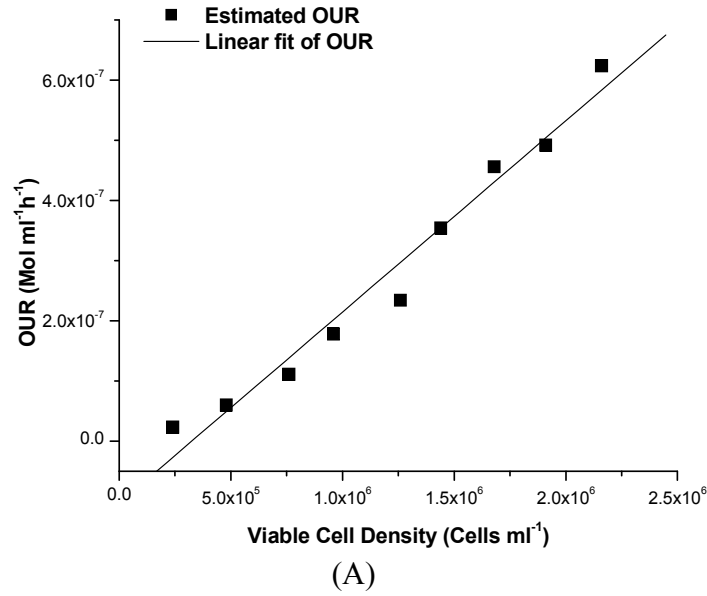


**Figure 4.3.6:** (A) Oxygen uptake rate (OUR) of sampled cells, from a spinner flask, at various dilutions was determined by layering it with mineral oil. The viable cell density was determined using trypan blue. The OUR is estimated from liquid phase oxygen balance with no oxygen transfer. The slope of the fitted curve gives the average specific oxygen uptake rate and is equal to  $3.18 \times 10^{-13} \text{ Mol } (O_2) \text{ Cell}^{-1} \text{ h}^{-1}$ .

(B) The sampled cells were also assayed using MTT ( $Abs_{540}$ ).

A method for a quick assay to measure viability was explored. The dissolved oxygen concentrations at a given time point were plotted against the respective cell densities (Figure 4.3.7). The plots were found to be linear, for a short time over a long range and vice versa.

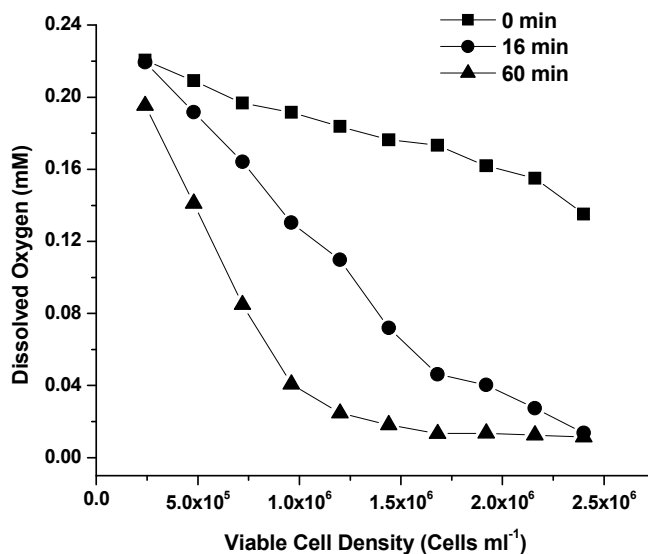


**Figure 4.3.7:** The dissolved oxygen concentration at a few time points for different cell densities prepared from a spinner flask culture when layered with mineral oil.

The method was also tried without the use of oil layer. The hypothesis that cells in same phase of growth i.e. cells having the same specific oxygen uptake rates should show a linear relationship with regard to the dissolved oxygen (D.O) concentration at a particular time was tested using the oxoplate OP96U. Actively growing cells from a spinner flask culture were taken and serially diluted using media. 200  $\mu$ l of each of these were then seeded in the Oxoplate, incubated in the Fluoroskan Ascent reader at 37 °C for 30 min and then shaken at a speed of 250 rpm before the measurement (Figure 4.3.8). The relationship was found to be linear to a maximum cell density of  $1 \times 10^6$  cells mL<sup>-1</sup>. This method can thus be used as a quick reference for viable cell density measurements compared to other time consuming assays (MTT, ATP etc).

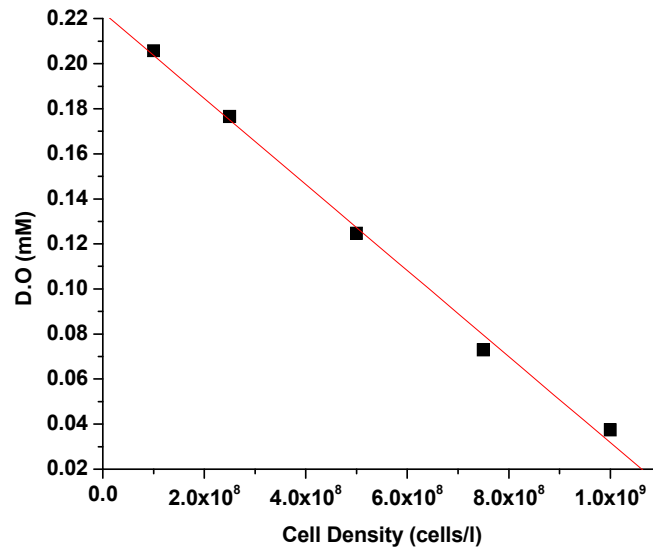


**Figure 4.3.8:** Relationship between Dissolved Oxygen and Cell Density. It was found to be linear till a cell density of maximum  $1 \times 10^6$  cells  $\text{mL}^{-1}$ . This can be used as a quick assay method.

The methods developed here will not only provide an avenue for process control but also pave way for important interpretations with relation to oxygen uptake, culture viability etc. We show their applicability in process optimization by using them for medium optimization and also in drug testing as a tool for cytotoxicity testing in the subsequent chapters.

## 4.4 Medium optimization

### 4.4.1 Motivation and theory

Development of processes involving mammalian cell cultures producing therapeutically important proteins is generally very time consuming. Medium optimization plays a key role in this process (Hesse and Wagner, 2000). Classically this is done by the addition or deletion of components, one at a time, to see their influence on the process. However, this approach has a lot of problems associated with it including false optimums, much experimentation, no information of interactions etc. Therefore, statistical design is used to minimize experimental efforts and provide relevant information (Ertola et al., 1995; Massart et al., 1997). Essential items to start such optimization are the selection of potentially influencing parameters, the measurement of the output and the method of experimental design applied. The selection of input variables depends strongly on the specific problem. The inputs could involve specific individual components of a media or complex media supplements or operating variables such as pH or temperature. The output is generally the growth rate or production rate (Castro et al., 1992; Lee et al., 1999). However, for the primary phases this is generally the cell proliferation. Recently Chun et al. (2003) applied statistical experimental design to identify growth factors in an overall effort to accelerate recombinant CHO medium development with cell proliferation as the output variable. In this context the measurement of oxygen uptake rate (OUR) as the output parameter is of high interest because it is a known indicator for metabolic activity and directly reflects culture viability (Ramirez and Mutharasan, 1990; Eyer et al., 1995; Ducommun et al., 2000; Schoenherr et al., 2000). Despite the use of experimental design strategies the number of experiments required for optimization studies is still large considering the large number of potential influencing parameters in mammalian cell culture (Palmqvist et al., 1999; Adinarayana and Ellaiah, 2002). Therefore, high-throughput methods for cultivation and on-line monitoring such as 96 well microtiter plates with on-line oxygen sensing are needed. The application of these plates for culture viability measurements using oxygen uptake rate has been shown in the previous chapter. The viability-OUR relationship changes if the specific OUR is changing. One can, however, expect that in almost any case less favorable media composition would decrease both culture viability as well as cell specific OUR. This additive effect would even simplify finding an optimum media composition. Here we show the applicability of these microplates

for medium optimization using statistical experimental design with oxygen uptake rate as a parameter.

#### **4.4.2 Statistical experimental design**

In an experiment, one or more process variables (or factors) are deliberately varied in order to observe the effect these changes have on one or more response variables. The (statistical) design of experiments (*DOE*) is an efficient procedure for planning experiments so that the data obtained can be analyzed to yield valid and objective conclusions. DOE begins with determining the objectives of an experiment and selecting the process factors for the study. An *Experimental Design* is the laying out of a detailed experimental plan in advance of doing the experiment. Well chosen experimental designs maximize the amount of "information" that can be obtained for a given amount of experimental effort.

It is common to begin with a process model of the 'black box' type, with several discrete or continuous input factors that can be controlled, i.e. varied at will, and one or more measured output responses. Experimental data are then used to derive an empirical (approximation) model linking the outputs and inputs.

A common experimental design is one with all input factors set at two levels each. These levels are called 'high' and 'low' with a range width of '+1' and '-1', respectively. A design with all possible high/low combinations of all the input factors is called a full factorial design in two levels. If there are  $k$  factors, each at 2 levels, a full factorial design has  $2^k$  runs. For example the two-level, full factorial design for three factors, namely the  $2^3$  design has eight runs (not counting replicates or centre point runs). Graphically, we can represent the  $2^3$  design by the cube shown in Figure 4.4.1.

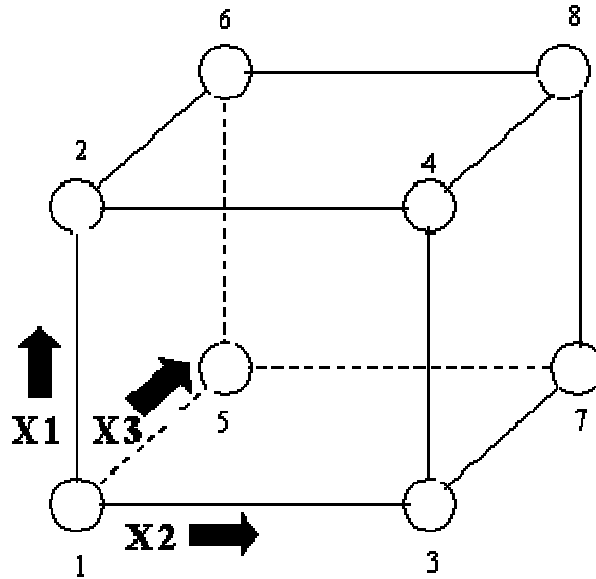


**Figure 4.4.1:** A  $2^3$  two-level, full factorial design; factors X1, X2, X3. The arrows show the direction of increase of the factors. The numbers '1' through '8' at the corners of the design box reference the 'Standard Order' of runs [Figure derived from NIST statistical handbook (<http://www.itl.nist.gov/div898/handbook>)]

The present experiments are aimed to show the applicability of microplates with immobilized oxygen sensors as a system to study media optimization in primary stages. The protein and peptide free, chemically defined media SMIF 6 was used for the study. The medium components varied were inorganic salt mixture (A), glutamine (B) and glucose (C). The  $2^3$  full factorial central composite design used in response surface methodologies was applied. This consists of the evaluation of the relationship between controlled experimental factors and the measured response, in this case being the oxygen uptake rate of the cells at the end of cultivation time.

For statistical calculations, the variables were coded as according to the following equation.

$$x_i = (X_i - X_0) / \Delta X \quad (4.4.1)$$

Where  $x_i$  is the  $i^{th}$  coded value of the variable  $X$ ,  $X$  is the variable A, B or C,  $X_i$  is the  $i^{th}$  natural value of  $X$ ,  $X_0$  is the centre value of  $X$  and  $\Delta X$  is the step change value of  $X$ . The range and levels of the factors varied are given in the Table 4.4.1.

**Table 4.4.1:** Range and levels of the factors varied in optimization experiments.

CODED VALUES	INORGANIC SALTS (A) (% Conc.)	GLUTAMINE (B) (% Conc.)	GLUCOSE (C) (% Conc.)
-2	33.33	33.33	33.33
-1	66.66	66.66	66.66
0	100	100	100
1	133.33	133.33	133.33
2	166.66	166.66	166.66
<b><math>\Delta X</math></b>	<b>33.33</b>	<b>33.33</b>	<b>33.33</b>

% Concentration refers to the concentration as a percentage used in the original medium.

Six star points and six centre point replicates were employed in the design for the fitting. The star points and the factorial points were done in triplicate, thus requiring a total of 48 experiments. All the experiments were carried out in one run using a single microtiter plate with immobilized oxygen sensors, thus reducing the blocking effects (inter-experiment variations). The central points were taken as those in which the cells were known to be viable, and in which the stock cells were prepared, i.e. the concentrations in the chemically defined medium used for the cell growth. These concentrations were designated as 100 % and step changes were applied. The tabulation of the experimental variations and the observed response are given in Table 4.4.2.

MICROTITER PLATES IMMOBILIZED WITH OXYGEN SENSOR

**Table 4.4.2:** Medium formulations according to the statistical design with observed and predicted response. The predicted response is obtained from the regression model developed.

Run No.	A	B	C	Observed Response OUR ( $\times 10^{-6} \text{ M h}^{-1}$ )	Predicted Response OUR ( $\times 10^{-6} \text{ M h}^{-1}$ )
1	-1	-1	-1	0.093	0.11
2	-1	-1	-1	0.119	0.11
3	-1	-1	-1	0.109	0.11
4	1	-1	-1	0.093	0.085
5	1	-1	-1	0.062	0.085
6	1	-1	-1	0.096	0.085
7	-1	1	-1	0.119	0.13
8	-1	1	-1	0.137	0.13
9	-1	1	-1	0.132	0.13
10	1	1	-1	0.149	0.15
11	1	1	-1	0.145	0.15
12	1	1	-1	0.142	0.15
13	-1	-1	1	0.144	0.14
14	-1	-1	1	0.140	0.14
15	-1	-1	1	0.134	0.14
16	1	-1	1	0.138	0.12
17	1	-1	1	0.095	0.12
18	1	-1	1	0.135	0.12
19	-1	1	1	0.143	0.16
20	-1	1	1	0.153	0.16
21	-1	1	1	0.16	0.16
22	1	1	1	0.135	0.12
23	1	1	1	0.125	0.12
24	1	1	1	0.1	0.12
25	-2	0	0	0.023	0.051
26	-2	0	0	0.09	0.051
27	-2	0	0	0.048	0.051
28	2	0	0	0.014	0.021
29	2	0	0	0.005	0.021
30	2	0	0	0.043	0.021
31	0	-2	0	0.16	0.15
32	0	-2	0	0.159	0.15
33	0	-2	0	0.16	0.15
34	0	2	0	0.17	0.16
35	0	2	0	0.166	0.16
36	0	2	0	0.17	0.16
37	0	0	-2	0.15	0.15
38	0	0	-2	0.155	0.15
39	0	0	-2	0.153	0.15
40	0	0	2	0.161	0.16
41	0	0	2	0.158	0.16
42	0	0	2	0.156	0.16
43	0	0	0	0.168	0.16
44	0	0	0	0.160	0.16
45	0	0	0	0.162	0.16
46	0	0	0	0.155	0.16
47	0	0	0	0.160	0.16
48	0	0	0	0.143	0.16

Run 1-24 represent the Factorial Design, Run 25-42 are the Star points and Run 43-48 are the Central points.

#### 4.4.3 Cell growth and oxygen uptake rate (OUR) determination

The cell inoculum was grown in the chemically defined media in spinner flasks with CO<sub>2</sub> incubation and provided with additional buffering by the addition of 35 mM HEPES. All the different media compositions used for the study were prepared with 35 mM HEPES buffering to carry out the cultivation without CO<sub>2</sub> incubation and a lower concentration of sodium bicarbonate. Cells in growth phase were harvested and equal volume (containing equal no. of viable cells) was transferred to 1.5 ml tubes, centrifuged and re-suspended in the various media compositions to give a final viable cell concentration of  $1 \times 10^5$ -  $2 \times 10^5$  cells/ml. This ensured that the final viable cell concentration inoculated into each media formulation was the same. 200µl of these were transferred to the wells of the microplate, covered with lid and cultivated in the fluorescence reader at 37°C and 660 rpm (orbital) with a shaking diameter of 2 mm. The plate was read every 30 min for the cultivation period of 72 hours. The outer wells of the plate were not used for cultivation and were filled with water to reduce evaporation. All the other wells were used for the experimentation which included the calibration points of the plate. At the end of 72 h, it was seen that the evaporation from the wells varied from 25µl at the well designated as B11 (outermost used for the growth experiment) to 15µl at the innermost well (D6). The evaporation was the highest in the outermost wells (A1, A2, A12 etc), which were not used for the study. This uneven evaporation across the plate, which was always below 15 %, is one of the limitations of the system leading to variable osmolalities in different wells. However, it has been shown that an increase of up to 20 % in osmolality has no effect on growth rate in case of CHO cells (Kimura and Miller, 1996).

Oxygen uptake rate was estimated for each of the wells using a stationary liquid phase O<sub>2</sub> balance using equation (4.3.1) supplied in the materials and methods section and given below (John et al., 2003),

$$\frac{d[O_2]_{aq}}{dt} = k_L a ([O_2]_{aq}^* - [O_2]_{aq}) - OUR \quad (4.4.2)$$

where  $[O_2]_{aq}$  and  $[O_2]_{aq}^*$  are the dissolved oxygen concentrations in the liquid phase and in equilibrium with the gas phase, respectively, and  $k_L a$  is the volumetric liquid phase mass transfer coefficient.  $[O_2]_{aq}$  was measured using the oxygen sensor coated microplate in conjunction with the fluorescence reader. The saturation oxygen concentration  $[O_2]_{aq}^*$  is 0.21

mM, which is the solubility of oxygen in water at 37°C. The  $k_{La}$  was determined experimentally as  $0.9 \text{ h}^{-1}$ , as has been shown before, for the cultivation conditions, using sodium dithionite (Fluka Chemie AG, Buchs, Switzerland).

#### **4.4.4 Results and discussion**

##### **On-line oxygen profile and oxygen uptake rate**

In the previous chapter, the oxygen uptake rates of cells, measured using oxygen sensor coated microplate, were shown to be directly related to culture viability. The online dissolved oxygen profiles obtained are converted to the oxygen uptake rates by using equation (4.4.2). Figure 4.4.2 shows both the dissolved oxygen profile as well as the uptake rate of two different media formulations. Figure 4.4.2(A) shows the profile and uptake for medium formulation with the coded values  $A=0$ ,  $B=0$  and  $C=0$ . Figure 4.4.2(B) shows the same with the medium formulation of coded values  $A=2$ ,  $B=0$  and  $C=0$ . From the figure it can be seen that there is a marked difference in the profiles of both, with the former showing a higher final oxygen uptake than the latter. This effect is most probably due to the presence of certain component or components in toxic concentrations. Thus by comparing the two profiles a preliminary idea on the effect of different compositions can be obtained. From the figure it is clear that a high concentration of inorganic salt mixture causes a decrease in cell vitality. Also potential components limitations could be identified with 72 h oxygen profiles.

The final oxygen uptake obtained for each formulation after 72 h is listed in Table 4.4.2.

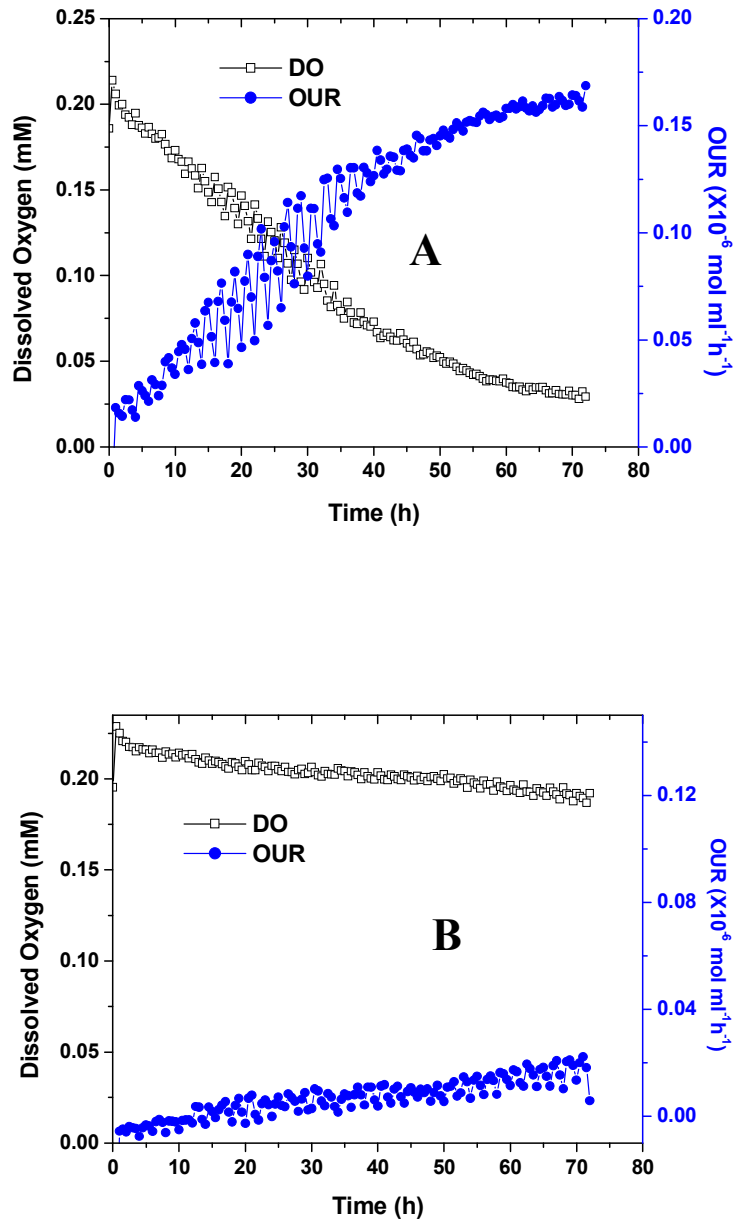


**Figure 4.4.2:** The dissolved oxygen and oxygen uptake profile of two media formulations. (a). Media formulation with compositions known to support viability (A=0, B=0 & C=0), (b). Media formulation with higher amount of inorganic salt mixture (A=2, B=0 & C=0). Concentration levels A, B and C are specified in Table 4.4.1.

### Development of regression equation

The experimentations were carried out using the  $2^3$  full factorial central composite design. Design Expert 6.0 (Stat Ease Inc, Minneapolis, US) was used for the regression analysis. A second order polynomial model (which includes the linear, quadratic and the interaction terms) is generally adequate to describe the system. But this was found to have a lack of fit with an F-value of 3.14 (Massart et al., 1997). So a reduced third order model was applied. The model is described by the equation

$$\begin{aligned} OUR = & b_0 + b_1 * A + b_2 * B + b_3 * C + b_4 * A^2 + b_5 * AB + b_6 * AC + b_7 * BC \\ & + b_8 * A^2B + b_9 * A^2C + b_{10} * ABC \end{aligned} \quad (4.4.3)$$

where A is the concentration of inorganic salt mixture, B is the concentration of glutamine and C is the concentration of glucose. Also  $b_0$  is the intercept coefficient and  $b_{i=1...6}$  are the coefficients referring to the measures of effect of the various variables involving A, B, and C. This model was not aliased (confounded) and therefore could be applied. The analysis of variance (ANOVA) of the model demonstrates that the model is significant (Table 4.4.3), as is evident from Fisher F test ( $F_{\text{model}} = 42.20$ ) and a low probability of failure ("Prob>F"= $<0.0001$ ) (Massart et al., 1997). The "Lack of Fit F-value" of 0.52 implied that the Lack of Fit was not significant relative to the pure error. The goodness of fit was checked by the determination coefficient ( $R^2$ ). For this analysis, the value of the determination coefficient ( $R^2=0.92$ ) showed that there was a good agreement in the model and the responses. The adjusted determination coefficient ( $\text{adj.}R^2=0.856$ ) too indicated significance of the model. The application of the methodology yielded the following equation with the estimated coefficients,

$$\begin{aligned} OUR = & 0.16 - 7.517 * 10^{-3} A + 2.079 * 10^{-3} B + 1.575 * 10^{-3} C - 0.030 A^2 + 3.206 * 10^{-3} AB \\ & - 4.851 * 10^{-3} AC - 9.011 * 10^{-3} BC + 9.926 * 10^{-3} A^2B + 7.335 * 10^{-3} A^2C - 6.729 * 10^{-3} ABC \end{aligned} \quad (4.4.4)$$

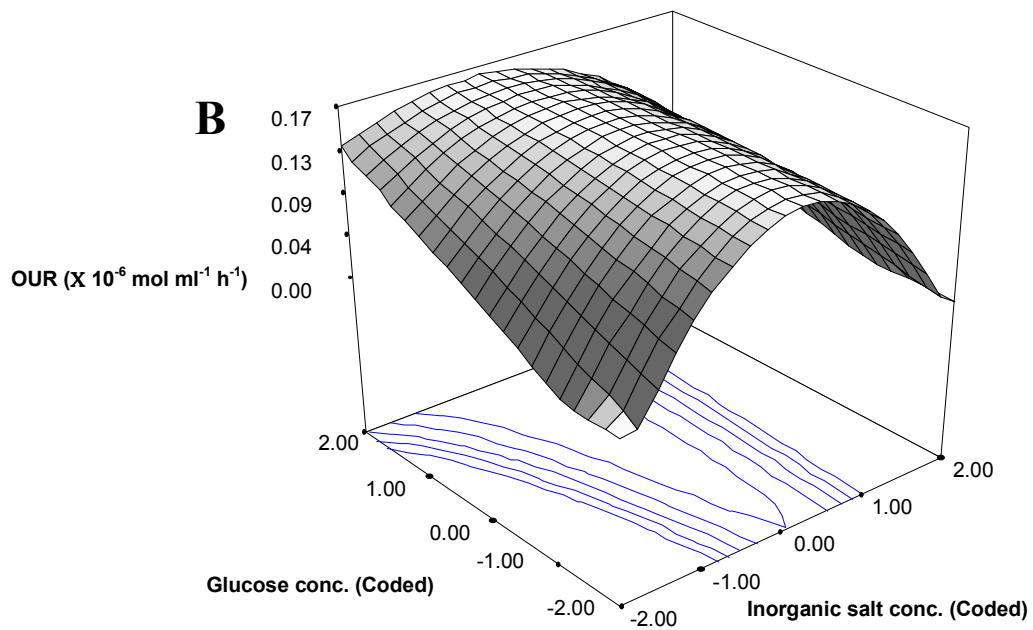
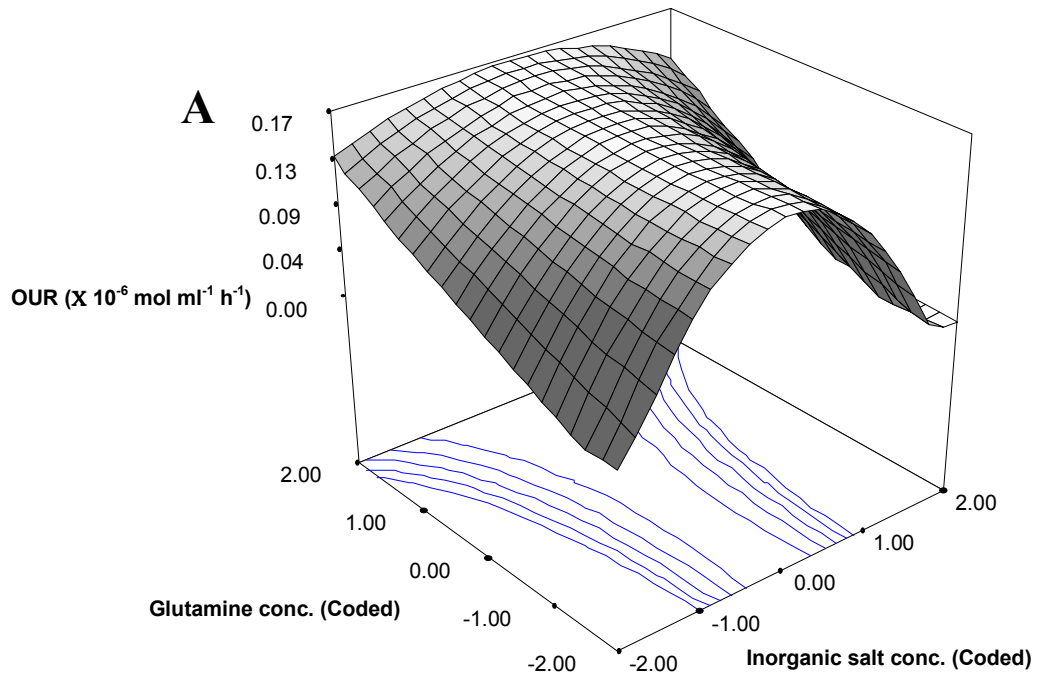
where the terms have the same notation as in equation (4.4.3). The significance of each coefficient was estimated by the F-value. In this case  $A$ ,  $A^2$ ,  $B * C$ ,  $A^2 * B$  and  $A * B * C$  are significant model terms. The predicted response of each of the runs from the model is compared with the observed response in Table 4.4.2.

**Table 4.4.3:** ANOVA for the response surface reduced cubic model.

Source		Sum of Squares	Degree of Freedom	Mean Square	F-Value	Prob>F	
Model		0.079	10	$7.887 \times 10^{-3}$	42.20	<0.001	<i>Significant</i>
	A	$2.71 \times 10^{-3}$	1	$2.71 \times 10^{-3}$	14.51	0.0005	<i>Significant</i>
	B	$1.04 \times 10^{-4}$	1	$1.04 \times 10^{-4}$	0.55	0.4611	
	C	$5.95 \times 10^{-5}$	1	$5.95 \times 10^{-5}$	0.32	0.5759	
	A <sup>2</sup>	0.067	1	0.067	357.32	<0.001	<i>Significant</i>
	AB	$2.47 \times 10^{-4}$	1	$2.47 \times 10^{-4}$	1.32	0.2580	
	AC	$5.65 \times 10^{-4}$	1	$5.65 \times 10^{-4}$	3.02	0.0905	
	BC	$1.95 \times 10^{-3}$	1	$1.95 \times 10^{-3}$	10.43	0.0026	<i>Significant</i>
	A <sup>2</sup> B	$1.18 \times 10^{-3}$	1	$1.18 \times 10^{-3}$	6.33	0.0164	<i>Significant</i>
	A <sup>2</sup> C	$6.46 \times 10^{-4}$	1	$6.46 \times 10^{-4}$	3.45	0.0710	
	ABC	$1.09 \times 10^{-3}$	1	$1.09 \times 10^{-3}$	5.81	0.0210	<i>Significant</i>
Residual		$6.92 \times 10^{-3}$	37	$1.87 \times 10^{-4}$			
Lack of fit		$4.13 \times 10^{-4}$	4	$1.03 \times 10^{-4}$	0.52	0.7189	<i>Not Significant</i>
Pure Error		$6.50 \times 10^{-3}$	33	$1.97 \times 10^{-4}$			
Cor Total		0.086	47				

The Model F-Value of 42.20 implies the model is significant. Values of “Prob>F”, probability of failure, less than 0.05 indicate model terms significant.

Response surface plots of two variables, keeping the others constant, are useful to understand the influence of main and interacting effects of the factors. Figure 4.4.3 (A, B & C) shows the response surface plots of the three tested variables. The salt mixture exerts the most effect on the rates with no dramatic effects seen by the variation in glucose and glutamine concentrations in the concentration range used. The long term effects of these composition ranges are however, not taken into account for this particular set of experimentations.



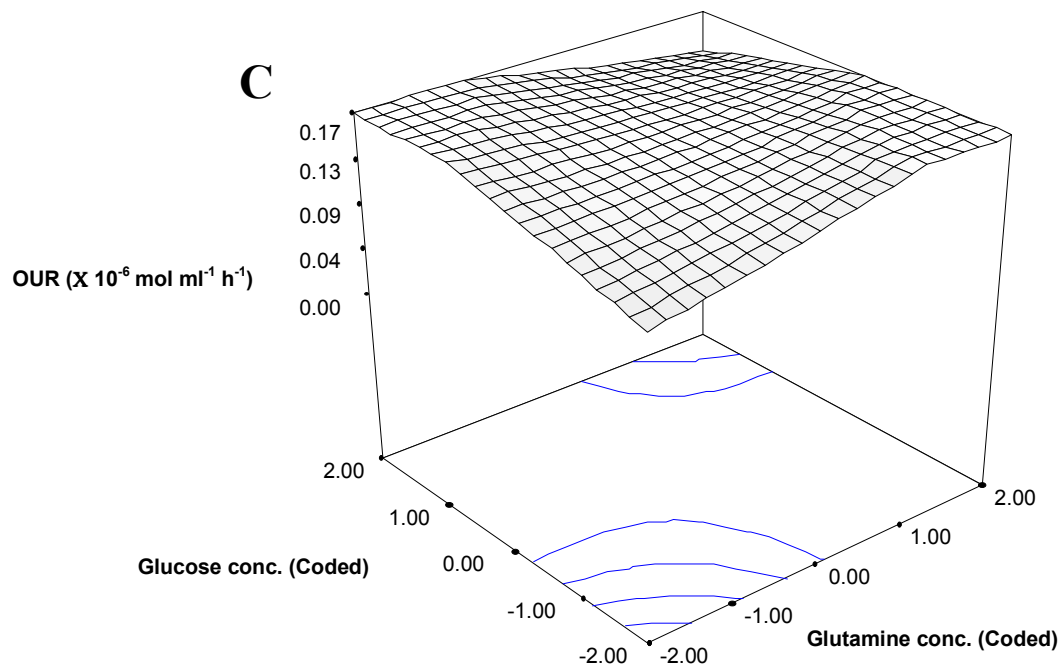


**Figure 4.4.3:** Response surface plot showing effects of media components on the oxygen uptake and hence the culture viability. All other variables are held constant. Concentration levels are specified in Table 4.4.1.

- A) Effect of inorganic salt and glutamine concentrations
- B) Effect of glucose and inorganic salt concentrations
- C) Effect of glucose and glutamine concentrations.

A growth experiment was performed with the optimized medium composition obtained from the regression analysis, and the composition is shown along with its predicted response in Table 4.4.4 and is marked selected.

**Table 4.4.4:** Optimum media compositions obtained from the model (equation 4.4.4).

No.	A-Inorganic salt conc. (%)	B-Glutamine conc. (%)	C-Glucose conc. (%)	Predicted OUR.	Solution
Reduced third order model.					
1	117.3	165.9	41.26	0.20	<u>Selected</u>
2	105.7	142.3	52	0.18	

A growth experiment was also performed with a second optimum given by the analysis to check the validity of the model. The oxygen uptake profiles of the compositions in comparison with the original composition are given in Figure 4.4.5 (A & B). It is seen that the proliferation rate of the cells with the new medium is significantly higher than with the original medium in the initial culture phase thus showing the applicability of the method used. Using OUR for earlier growth phases, e.g. 48 h and 60 h, similar optimum concentrations could be obtained with a standard deviation in the concentration of 10 %.

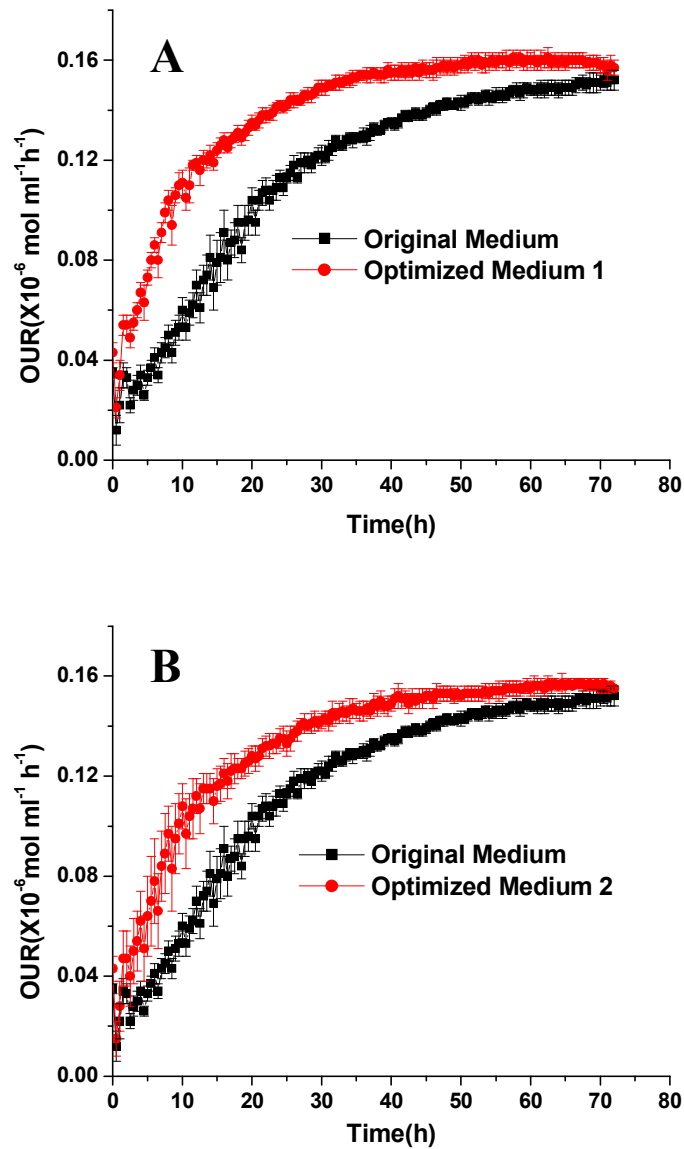


**Figure 4.4.4:** The oxygen uptake profiles of the medium composition obtained from optimization compared with the original composition.

A) Medium formulation with the optimized composition 1 (A=117.3 %, B=166 %, C=41.26 %) compared with the composition (A=100 %, B=100 %, C=100 %)

B) Medium formulation with the optimized composition 1 (A=105.7 %, B=142.3 %, C=52 %) compared with the composition (A=100 %, B=100 %, C=100 %)

#### 4.4.5 Conclusions

The above experiments show that microplates coated with oxygen sensors could be used in the primary step of media optimization. The system is fast, allows high-throughput experiments and measures the metabolic activity of cells. The two major limitations of the method as presented here are: (i) the limited time for growths experiments (<100 h) due to the evaporation from the wells, (ii) the fact that the experiments in the present experimental set-up have to be done in externally buffered media with HEPES. The uneven evaporation of media from the wells of the plates and presence of HEPES could confound the analysis in case of sensitive cell lines. However, both could be overcome by putting the microplate reader into an appropriately humidified chamber with controlled addition of carbon dioxide. Loss of water could also be compensated for by the addition of water after e.g. 80 hours. The method may also be extended by the measurement of the product formed as a secondary output in the statistical analysis. The method is highly cost effective since the amount of media required is very small for each run, a lot of samples can be analyzed at a single go and the oxygen uptake rate measurements are entirely automatic minimizing labor cost. This method seems directly applicable for almost any culture of suspended and probably also attached animal cells which can be grown in microplates and have comparable oxygen uptake rates as the cells used here. This method seems also useful for other purposes as e.g. test of raw materials and conditions of cell stocks which are considered important in mammalian cell production (Hesse and Wagner, 2000) .

A new approach using microtiter plate cultivation with on-line measurement of dissolved oxygen (DO) was applied for medium optimization of mammalian cell culture. Applying dynamic liquid phase balance, oxygen uptake rates were calculated from the DO level and used as an indicator for culture viability. The developed method was successfully applied to optimization of the concentration of glucose, glutamine and inorganic salts for cultivation of a Chinese Hamster Ovary (CHO) cell line. Using a 2<sup>3</sup> full factorial central composite design, the optimum medium composition could be identified in one single run. The developed method exhibits high potential to improve procedures of medium optimization for animal cell cultivation by allowing the investigation of large sets of potentially important variables in short time and with reduced effort.

## 4.5 Cytotoxicity Testing

### 4.5.1 Motivation and theory

Everyday new substances and chemicals are developed using combinatorial chemistry that can synthesize very large number of molecules at about 10,000 varieties of congeners in a stroke, which have the potential to act as drugs or therapeutic agents. These must be screened for potential risk to the health or the environment. The screening includes *in-vivo* and *in-vitro* testing models. However, in recent years the emphasis has been on *in-vitro* testing using human tumors or cell-line models which include primary cells or established cell lines (Davila et al., 1998). In this regard cell proliferation and cytotoxicity assays play a crucial role. Numerous assays are available for these purposes (Mosmann, 1983; Souchier et al., 1995; Jones et al., 2001). These assays are important tools for *in-vitro* testing in pharmaceutical research and their scientific as well as their commercial potential cannot be over-emphasized. Cell viability is usually assessed by membrane integrity (e.g. trypan blue exclusion) and cell proliferation by labeled nucleotide incorporation [e.g. [<sup>3</sup>H]-thymidine), ATP or metabolic markers as MTT, XTT etc (Cunningham, 2001)]. Choosing the right kind of assay for the system to be studied is important and depends on the information sought (Riss and Moravec, 2004). A better understanding is necessary of what each assay measures as the end point, how the measurement correlates with cell viability or proliferation and what are its potential limitations. Also knowledge about changes occurring during different mechanisms of cell death will help deciding which endpoint to choose for a cytotoxicity assay. If the information sought is just the difference in treated and untreated cells with a compound then the choice of assay becomes less complicated. However, for more information on the mechanism of death, the duration of exposure to toxin, the concentration of test compound and thus the choice of assay become critical. The above come into play because of the inherent disadvantage of the assays to measure endpoints. In this part of the thesis a cell proliferation/cytotoxicity assay is reported, which can potentially be useful for eliciting information on mechanisms of cell death, as it is both kinetic and non-destructive to the cells. The assay makes use of 96-well plates with immobilized internally referenced oxygen sensors which permit determination of the respiration rate of the cells for each well of the plate. These rates are known indicators for metabolic activity and can be used to predict the state of growth (Ramirez and Mutharasan, 1990; Eyer et al., 1995; Ducommun et al., 2000; Schoenherr et al., 2000). Earlier reports using oxygen microplates have shown the application and effectiveness of the system

(Wodnicka et al., 2000; Stitt et al., 2002; Hutter and John, 2004; Wittmann et al., 2004). This chapter focuses on the assay methodology of cell proliferation and cytotoxicity testing using oxygen sensor plates. Its distinguishing feature lies in its applications for primary cell cultures (e.g. rat hepatocytes) as well as for adherent and suspension cell lines using flat bottomed and 'U' bottomed well plates. Both adherent and suspension cells can be monitored directly in the plates and harvested for further processing thus requiring no additional procedures or further reagents. It can also be easily adapted for medium to high throughput methods. The assay outcome corresponds well with results of conventional systems presently in use like e.g. MTT. The robustness of the assay was confirmed using the statistical Z'-factor (Zhang et al., 1999).

#### **4.5.2 Cytotoxic compounds**

Compounds used for cytotoxicity assays (Diclofenac, Clozapine, Sodium dodecyl sulfate (SDS), 2-Thiouracil, Tamoxifen and Tranylcpromine) were purchased from Sigma-Aldrich (Taufkirchen, Germany) and the required stocks prepared in an appropriate solvent vehicle. Sodium azide was purchased from Fluka Chemie (Buchs, Switzerland).

#### **4.5.3 Microtiter plate (MTP) growth of cells and cytotoxicity assay**

The cells were grown in the absence of CO<sub>2</sub> incubation thus affecting the bicarbonate buffering of the media. To provide additional buffering capacity, the media was modified by the addition of HEPES buffer. Also the outermost wells of the plate were not used for cultivation and were filled with water to reduce evaporation. All the other wells were used for the experimentation which included the 4 wells for the calibration of the plate. Sterility was ensured during the entire cultivation period by covering the plate with a sterile lid. The growth of cells in these modified conditions was found to be similar to the conditions in CO<sub>2</sub> incubator as shown in the earlier chapter.

##### ***Primary rat hepatocytes:***

For respiration studies freshly prepared hepatocytes were seeded in different concentrations (300 µl per well) in 96-well flat-bottom oxygen-sensor microtiter plates (OP96U) coated with Collagen Type I. The cells were incubated at 37°C in a humidified incubator at 95 % air and 5 % CO<sub>2</sub> and after 1h of attachment the medium was replaced by fresh growth medium. Immediately the plate was placed into a 37 °C temperature controlled fluorescence reader and

read every 30 min. For the studies involving solvents and cytotoxicity, the solvents and compounds were appropriately diluted in culture medium. Cells were seeded at densities of  $2 \times 10^4$  -  $2 \times 10^5$  cells mL<sup>-1</sup> and allowed to attach. The overlaying medium was then removed from the cells and 300  $\mu$ l of the diluted test solutions was added in triplicates with the plates being read every 30 min. For cytotoxicity assays the plate was read for a period of 6 hours and an MTT assay was performed simultaneously for the corresponding.

#### ***Cell lines:***

To determine the oxygen profile, Caco-2 cells were seeded in Oxoplates at different cell densities. Similar conditions as above were used. Before application of the compounds, Caco-2 cells were incubated for 16-20 h at 37°C in a humidified incubator at 95 % air and 5 % CO<sub>2</sub>. The compounds were diluted in culture medium and added to the cells in triplicate after the culture medium was removed.

For suspension cells the inoculum cultivations were made using medium with 35 mM HEPES in spinner flasks with CO<sub>2</sub> incubation. Cells in growth phase were harvested and equal volume (containing equal no. of viable cells) was transferred to 1.5 ml tubes, centrifuged and re-suspended in media, containing different concentrations of the substance to be tested, to give a final viable cell concentration of  $1 \times 10^5$ -  $2 \times 10^5$  cells/ml. This ensured that the final viable cell concentration inoculated was the same. 200  $\mu$ l of these were transferred to the wells of the microplate in triplicates, covered with lid and cultivated in the fluorescence reader at 37°C and 660 rpm (orbital) with a shaking diameter of 2 mm. The plate was read every 30 min for the cultivation period. The tested substances included tamoxifen and diclofenac for HL60 cells and sodium azide for CHO cells.

#### **4.5.4 Comparison of oxygen uptake rates with MTT assay**

It has been previously shown that the oxygen uptake rate compares well with the conventional assay such as MTT. Figure 4.5.1 shows the linearity between the MTT assay and OUR measurement for a range of  $5 \times 10^5$  cells/ml to  $2 \times 10^6$  cells/ml from sampled CHO cells. The OUR is calculated from the drop observed in dissolved oxygen over a period of 3 hours using Eq.4.3.1 allowing 30 minutes for the system to stabilize. From the Figure it is clear that both results are highly comparable with a R<sup>2</sup> value of 0.98 and thus the OUR measurement could be used in place of the conventional MTT assay.

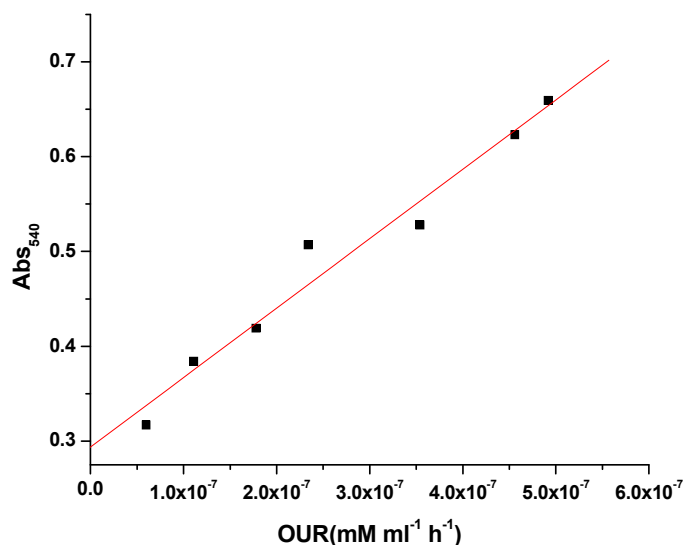


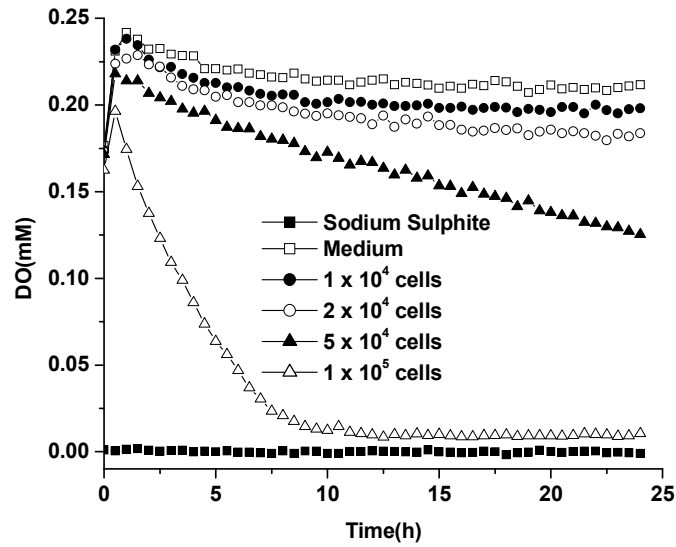
**Figure 4.5.1:** Comparison of MTT assay with OUR measurements of sampled CHO cells.

CHO cells in the range of  $5 \times 10^5$  cells/ml to  $2 \times 10^6$  cells/ml were seeded in sensor coated plates in triplicates and the average uptake rate was calculated from the drop in oxygen noted. Parallel experiment was done for the MTT assay (Abs<sub>540</sub>).

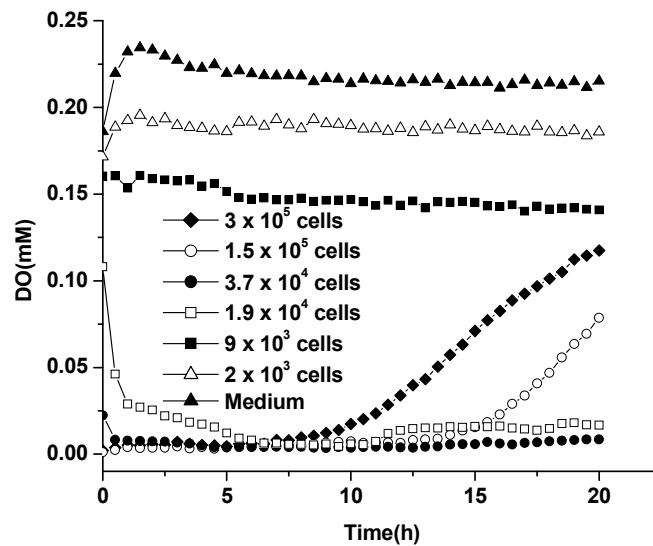
#### 4.5.5 Growth of primary and adherent cells on MTP

The main advantage of the present system is to allow the growth of adherent cells on the flat bottomed plates, which can then be used in cytotoxicity studies. Figure 4.5.2 shows the oxygen profiles of different initial seeding densities of primary rat hepatocytes and Caco-2 cells, an adherent cell line, on the Oxoplates. In the case of the dividing Caco-2 cells, a cell density dependent increase in the respiration rates was observed as tracked by the changes in the dissolved oxygen concentration shown in Figure 4.5.2 (A). Since primary rat hepatocytes are non-dividing cells, other characteristics in the respiration rates were seen for different seeding densities than for Caco-2 cells. For the non-dividing hepatocytes, the seeding of a minimum critical cell concentration is essential for the formation of a monolayer culture which allows the maintaining of the respiratory and metabolic activity of the cells. Figure 4.5.2 (B) shows that small cell concentrations do not result in a decrease of the dissolved oxygen concentration over time. In contrast, seeding concentrations greater than  $1.9 \times 10^4$  cells/well display a very steep decrease of the oxygen concentrations since the critical cell concentration for monolayer formation is reached. From Figure 4.5.2 (B) it can be seen that the respiration rate for adequate cell numbers remain constant at steady state value. The decrease in the respiration rate, as evidenced by an increase in the dissolved oxygen

concentration with time at higher seed densities, might be due to depletion of components from the media as it is seen to be cell density dependent.



(A)



(B)

**Figure 4.5.2:** Dissolved oxygen profiles of different cell densities of primary hepatocytes (A) and CaCo2 cells (B) grown on flat bottomed Oxoplate.

### Effect of solvents on cell viability

New candidate compounds are often poorly soluble in water and have to be solved in solvents like DMSO or Ethanol. For the assay system to be reliable under all conditions, the solvents should not influence or interfere with the system. In order to determine the effects of commonly used solvents on cell viability and the assay system, DMSO and ethanol were tested using primary rat hepatocytes at a concentration generally used (2 %). Triton X, a detergent known to be toxic at the given concentration, was used as a negative control. Figure 4.5.3 gives the respiration profiles in terms of dissolved oxygen concentration showing that the solvents DMSO and ethanol do not have any effect on the system or viability at the given concentration as seen in comparison with control culture. As expected, cells treated with Triton X show no sign of viability as it can be seen from the dissolved oxygen concentration remaining constant at saturation.

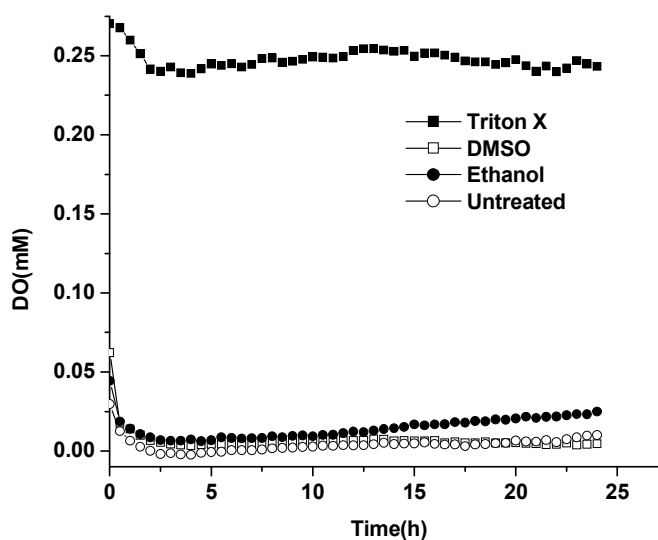


**Figure 4.5.3:** Effect of solvents on primary rat hepatocytes. 2 % Triton X, DMSO and ethanol were used to check their effect on the respiration of the cells.

#### 4.5.6 Cytotoxicity assays and LC<sub>50</sub> determination

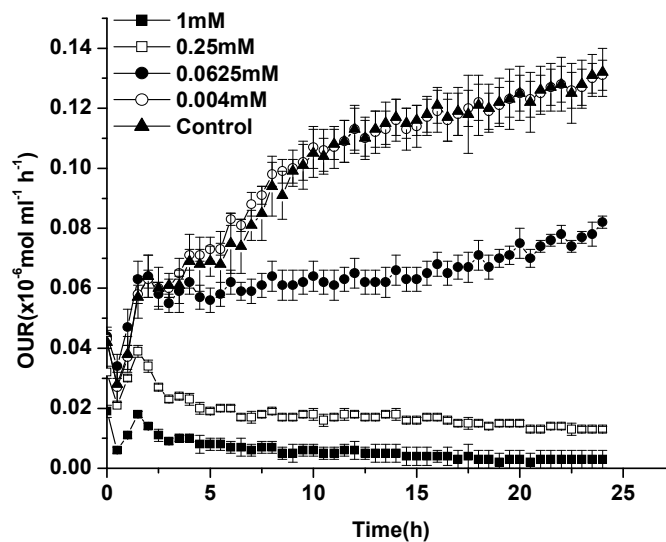
Acute toxic effects (those that occur after a single exposure) of substances are typically measured and defined in terms of the lethal dose 50 (LD<sub>50</sub>) or lethal concentration 50 (LC<sub>50</sub>). The LC<sub>50</sub> is defined as the amount of chemical that when exposed to test animal or cell culture testing systems, will be lethal to fifty percent of the test population. This means that the lower the value of the LD<sub>50</sub> and LC<sub>50</sub> the more toxic the substance and vice versa.

The oxoplates were applied for the detection of cytotoxicity. Sodium azide, a well known toxic agent, was used for the test. CHO cells in suspension were used and the test was carried out in U-bottomed well plates. Figure 4.5.4 shows the oxygen uptake rates of CHO cells, at different concentrations of azide, for a 24 h period. The response of the cells to the compound is clear from the curves and is found to be dose dependent. At higher concentrations of azide (>0.25 mM) the cells do not show any significant oxygen uptake thus indicating loss of viability. At low concentrations there is seemingly no effect on the respiration. These curves are then used to determine the LC<sub>50</sub> of the compound using a four parameter sigmoidal dose-response fit (Origin 6.0, OriginLab Corporation, Northampton, USA).

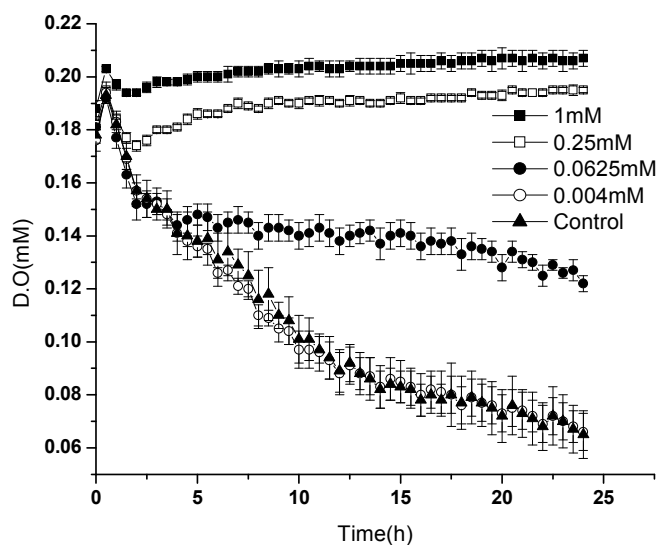
$$Y = Bottom + \frac{(Top - Bottom)}{1 + 10^{(\log LC_{50} - X) * Hillslope}} \quad (4.5.1)$$

where X is the logarithm of concentration and Y is the response; Y starts at Bottom and goes to Top with a sigmoid shape with bottom and top representing the responses of the control and the highest concentration used respectively.

The use of dissolved oxygen concentration as the response would simplify the calculations. We observe that the derivative term of liquid phase oxygen balance equation (4.3.1) does not contribute significantly to the overall observed OUR which is dependent more on the oxygen gradient, thus making it proportional to the dissolved oxygen concentration. Figure 4.5.4(B) shows the dissolved oxygen response of azide on the cells.



(A)

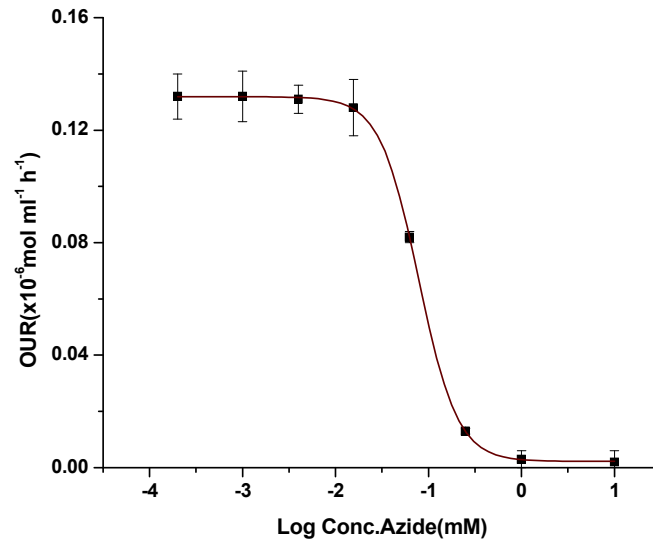


(B)

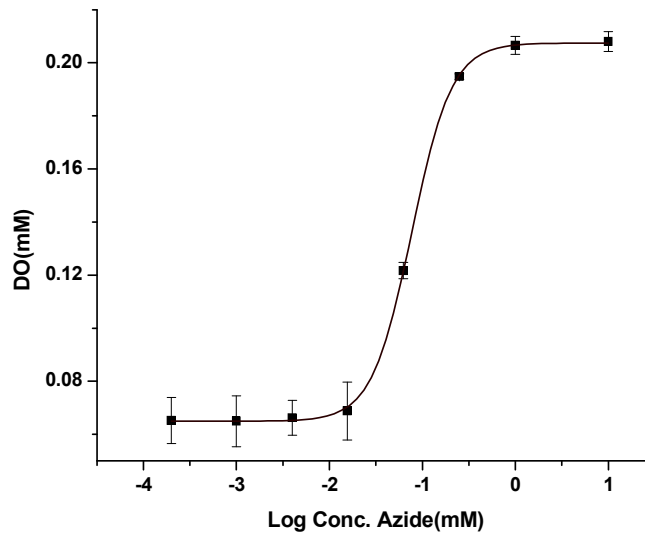
**Figure 4.5.4:** A 24 h cytotoxic assay for Sodium azide using CHO cells done with Oxoplate. The respiration rates calculated with equation (4.3.1) are shown for various concentrations used. All experiments were made in triplicates and the standard deviation is shown.

Figure 4.5.5 compares the azide dose curves for the same with oxygen uptake and, to eliminate calculations, dissolved oxygen taken as the responses. Figure 4.5.5 (A) gives the curve with OUR as response and Figure 4.5.5 (B) with DO for a 24 h period. The  $LC_{50}$  values obtained from both the curves are very similar with a value of 0.078 mM for OUR as response

and 0.077 mM for DO as response. Hence the OUR response could be replaced by DO. This helps to simplify the calculation without affecting the final result.



(A)



(B)

**Figure 4.5.5:** The sodium azide dose response curves with CHO cells comparing the LC 50 obtained with OUR and DO as response at the end of 24h measurement. (A) The dose response curve with OUR as the response giving an LC<sub>50</sub> value of 0.078 mM. (B) The dose response curve with DO as the response giving an LC<sub>50</sub> value of 0.077 mM.

**LC<sub>50</sub> determination of known reference compounds**

Primary hepatocytes from the rat were used to determine the LC<sub>50</sub> values of known reference drugs using the DO response determined via Oxoplates and the classical MTT staining as the parameter for viability. The resulting LC<sub>50</sub> values were compared with values obtained by MTT staining and published values. As shown in Table 4.5.1, the values obtained via the oxygen respiration rate are in good accordance to the values assessed by MTT staining. In addition, the determined LC<sub>50</sub> values are in the same range as published LC<sub>50</sub> values for human hepatocytes (Li et al., 1999). The deviation for tranylcypromin can be due to interspecies differences.

**Table 4.5.1:** LC<sub>50</sub> values for known reference compounds in primary rat or human hepatocytes obtained via different methods for viability detection. The values were determined using triplicates of the concentration and the standard deviation of the resulting oxygen measurements was always found to be ±10 %. LC<sub>50</sub> Literature is from published LC<sub>50</sub> values for human hepatocytes (Li et al., 1999).

<b>Compound</b>	<b>LC<sub>50</sub> (rat, Oxoplate)</b>	<b>LC<sub>50</sub> (rat, MTT)</b>	<b>LC<sub>50</sub> Literature (human, MTT)</b>
Diclofenac	648 µM	537 µM	350 µM
Clozapine	174 µM	211 µM	315 µM
Tranylcypromine	2729 µM	4671 µM	1000 µM
Tamoxifen	72 µM	88 µM	50 µM
2-Thiouracil	> 5000 µM	> 5000 µM	> 1000 µM

#### 4.5.7 Z'-Factor of assay

The robustness of an assay and its reliability is statistically given by the Z'-factor. Z'-factor, the “screening window coefficient” compares the assay’s dynamic range to data variation. The Z'-factor was determined from the cytotoxic assay of azide on CHO cells where 3 wells were plated with the same concentration. The three wells with azide concentration of 1 mM were taken as the negative control and the wells without azide as positive control. The Z'-factor was calculated using the following formula:

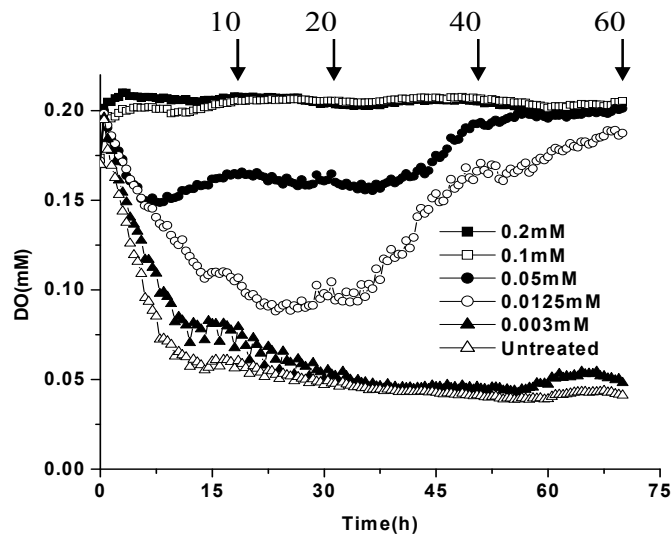
$$Z' = 1 - \frac{(3\sigma_{PC} + 3\sigma_{NC})}{|\mu_{PC} - \mu_{NC}|} \quad (4.5.2)$$

where  $\sigma$  is the standard deviation,  $\mu$  is the mean, *PC* refers to the positive control and *NC* to the negative control.

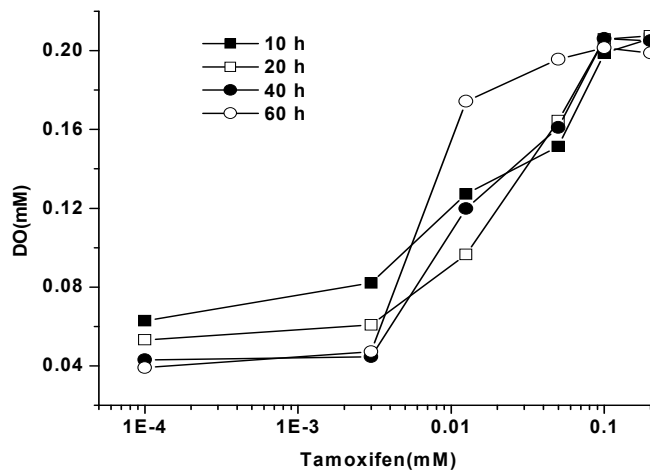
A Z'-factor equal to 1 indicates a perfect assay whereas Z'-factors of above 0.5 indicate excellent assays for cell based systems. Using the above formula, the assay gave a Z'-factor of 0.72 with OUR as the response and 0.74 with DO as the response, showing that the assay system is robust.

#### 4.5.8 Cell death kinetics

The kinetics of cell death was followed by the use of known compounds on HL60 cell line. Figure 4.5.6 shows an example using tamoxifen. Tamoxifen is an anti-estrogen used as adjuvant in therapy following primary treatment for early stage breast cancer. Its mechanism has been attributed to the induction of apoptosis, cell death arrest and accumulation of metabolites (Yao et al., 2001; Brandt et al., 2004). The experiments were carried out for 72 h to determine the effects of the compound. Figure 4.5.6 (A) gives a typical kinetic toxicity curve of tamoxifen on HL60 cells at various concentrations. The curves show unique patterns, thus emphasizing the importance of the endpoint to be chosen along with the effect of concentration. Figure 4.5.6 (B) gives the dose-response at various time points. The  $LC_{50}$  is found to decrease from 0.047 mM at 10 h to 0.007 mM at 60 h thus emphasizing the importance of delayed toxic effects. Since the assay is nondestructive, the cells could be harvested for further analysis.



(A)

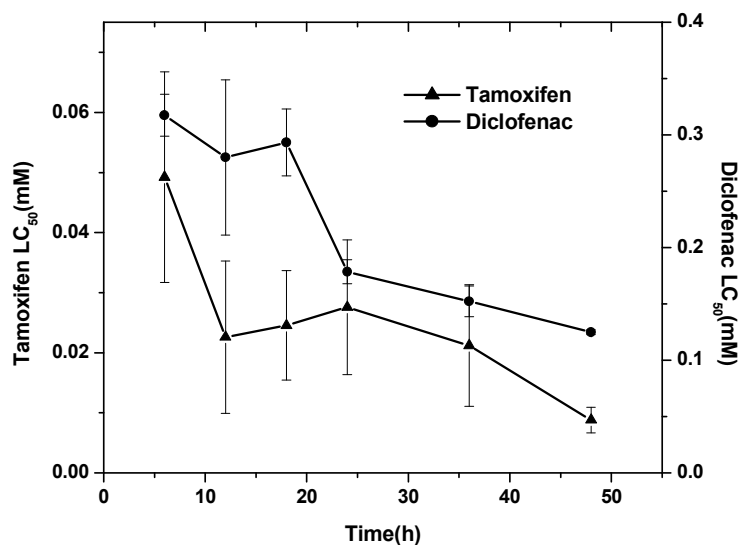


(B)

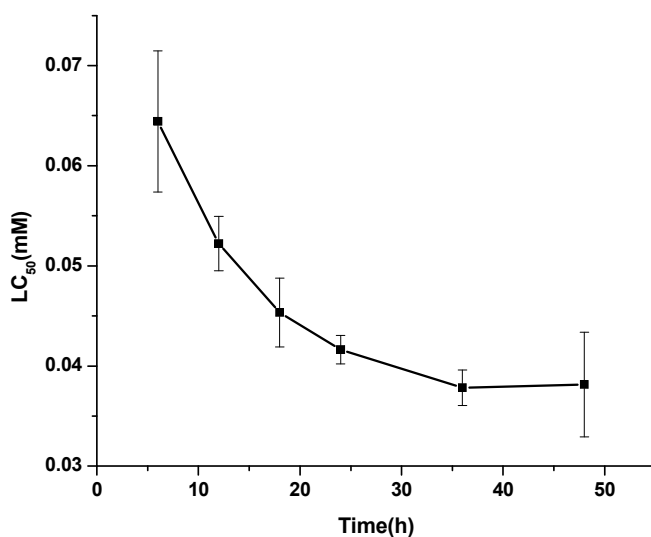
**Figure 4.5.6:** Kinetic dose response of HL60 cells to tamoxifen. (A) The cell death kinetic curve at different concentrations of Tamoxifen with HL60 cell line. (B) The dose response at different time points showing the  $LC_{50}$  shift with respect to time, 0.047 mM at 10 h to 0.007 mM at 60 h calculated using a four parameter sigmoidal dose-response fit.

### **Kinetic Analysis**

The kinetic curves of tamoxifen were compared with those obtained from SDS. While tamoxifen is known to cause cell death by primarily apoptosis followed by secondary necrosis, SDS is a known necrotic agent which causes death by cell wall disruption. The time course of  $LC_{50}$  was followed for both the compounds. The  $LC_{50}$  of tamoxifen decreases from 0.049 mM at 6 h to 0.009 mM at 48 h. As seen from Figure 4.5.7 there is a sudden drop in  $LC_{50}$  from 6 h to 12 h with little change during 12 h to 36 h followed by a drop from 36 h to 48 h, thus indicating different mechanisms of cell death being involved. However, the time course of  $LC_{50}$  with SDS shows no such characteristics, thus indicating a simple death mechanism.



(A)



(B)

**Figure 4.5.7:** Time dependence of the 50 % lethal concentration ( $LC_{50}$ ) of HL60 cells: (A) tamoxifen and diclofenac and (B) SDS. The  $LC_{50}$  was determined using Eq. 4.5.2. Each  $LC_{50}$  value is the average of three parallel respiration measurements. The error bars indicate the standard deviation of these three values.

#### **4.5.9 Conclusions**

This chapter describes an assay system which can be applied to a wide range of cell based systems. The assay is robust, flexible and applicable for medium to high-throughput systems. Its main advantages over other systems are its kinetic nature, the automatic on-line measurement and that the cells can further be processed for any subsequent analysis. We expect this system to be useful to further understand cell death mechanisms and also in drug development and research.

## **5 PHYSIOLOGICAL INVESTIGATIONS ON CHO CELLS**

### **5.1 Introduction**

Metabolic flux analysis has become an important tool in metabolic engineering along with in depth physiological studies and has been extensively used for microorganisms. Its use for mammalian cells has been limited owing to the complexity of the system. However, there are examples for the use of this technique. This has been applied by using material balance techniques, radioactive labeling or stable isotope labeling to measure the fluxes through major pathways or of a particular enzyme. The pre-requisite for the application of this technique is a thorough knowledge about the cellular metabolism to be quantified. In this part of the thesis strategies and methodologies are developed for the generation of data which can later be applied for the quantification of metabolic fluxes in CHO cells. Moreover, a few special physiological studies of the cell line have been carried out.

## 5.2 Review of cellular biochemistry

Metabolism is the overall process through which cells acquire and utilize energy to carry out various cellular functions. Hence it is the complete set of the chemical reactions which occur in the cells. Metabolism consists of catabolism, which represents the breakdown of substrates and biosynthetic precursor substances for the production of energy, and anabolism, which uses this energy to construct components of cells such as proteins and nucleic acids. The chemical reactions of metabolism are organized into metabolic pathways, in which one chemical is transformed into another by a sequence of enzymes. The mammalian cell metabolism is complex which makes its quantitative analysis difficult. Glucose and glutamine are the primary fuels for mammalian cells for the production of energy (Eagle, 1955; Reitzer et al., 1979; Newsholme et al., 1985; Neermann and Wagner, 1996). The cells require the conversion of nutrients to energy, reducing power and biosynthetic precursors for its growth and maintenance. Energy is present in cells in the form of the high energy molecule adenosine 5-triphosphate (ATP), while the reducing power is provided by the reduced form of nicotinamide adenine dinucleotide (NADH) and nicotinamide adenine dinucleotide phosphate (NADPH). Generally, for biosynthesis reactions NADPH is used whereas NADH is used for the production of ATP. Several distinct but linked metabolic pathways are used by cells to breakdown fuel molecules and transfer the energy released for ATP production and for biosynthesis. The catabolism of glucose by way of the glycolysis, pentose phosphate pathway and the citric acid cycle, which is also fed by glutamine, supplies the electrons that produce the energy in form of ATP, required for the cellular processes, in the respiratory chain. These pathways collectively are referred to as the primary or central metabolic pathways. Along with glucose and glutamine, amino acids also play an important role in mammalian metabolism, both in anabolic as well as catabolic pathways, and interact with the central metabolic pathways (Eagle, 1955; Werner and Noe, 1993; Berg et al., 2002). The biochemistry of mammalian cells has been much researched and the principle pathways responsible for the catabolism and anabolism in cellular metabolism are well established (Berg et al., 2002). The mammalian cell biochemistry model considered in this thesis is given in Figure 5.2.1. The individual reactions corresponding to the reaction number are given in the appendix. The model consists of the glycolytic pathway, the pentose phosphate pathway and the tricarboxylic (or citric) acid (TCA) cycle. However, only the reactions that result in a change or contribute to the carbon skeleton of the metabolites are considered. Hence many linear reactions are lumped together as a single reaction. Along with the biochemistry, the

compartmentation of mammalian cells into cytosol and mitochondria is considered in the model.

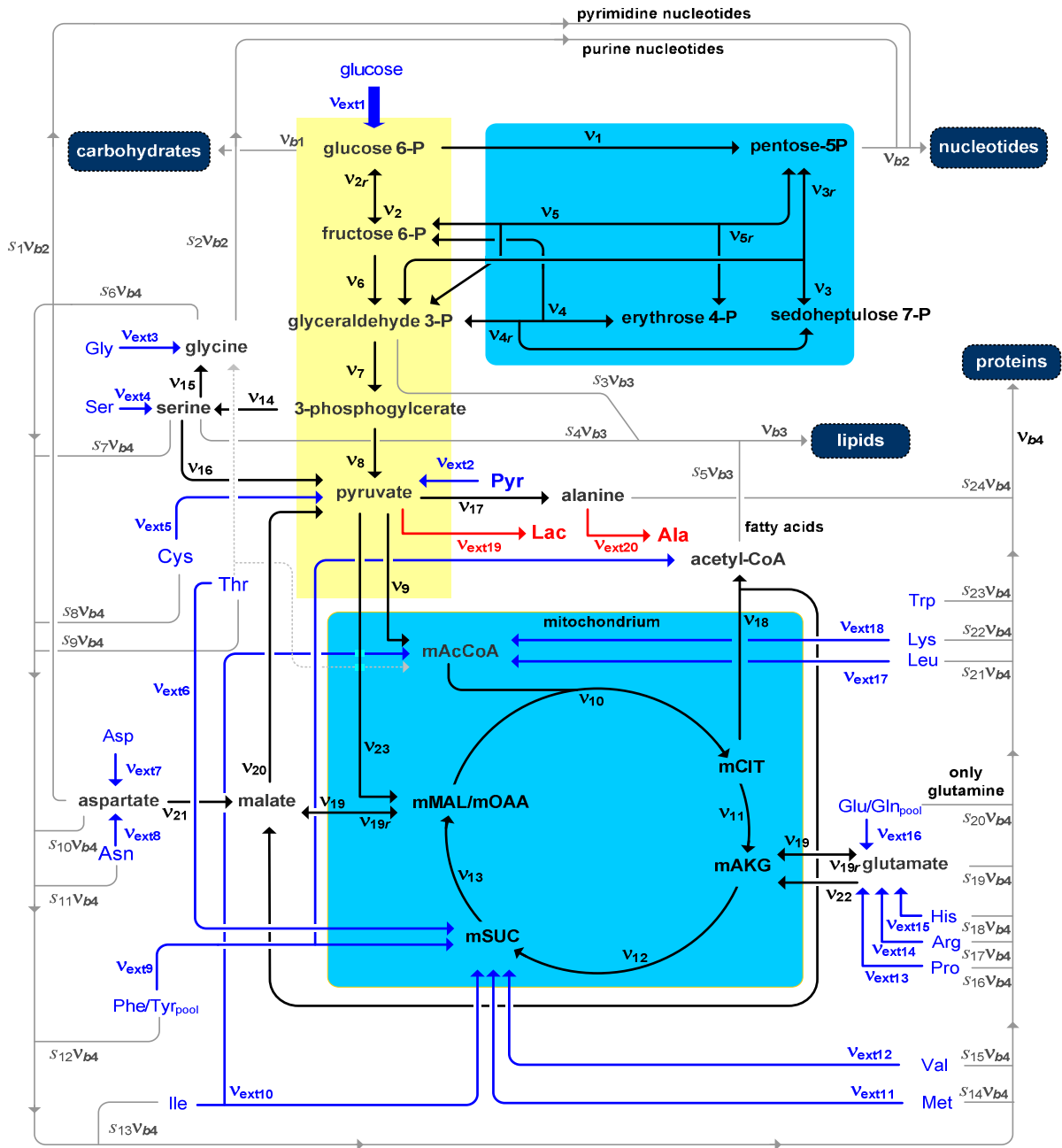
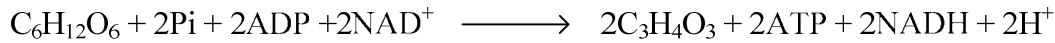


**Figure 5.2.1:** The metabolic model of mammalian cell. (Abbreviations: Pyr pyruvate, Lac lactate, mCit mitochondrial citrate, mMAL mitochondrial malate, mAKG mitochondrial  $\alpha$ -ketoglutarate, mSUC mitochondrial succinate, mOAA mitochondrial oxaloacetate, mAcCoA mitochondrial acetyl-CoA. The amino acids have the standard 3 letter abbreviation)

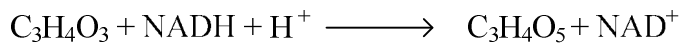
### Glycolysis

Glycolysis is the pathway responsible for the anaerobic catabolism of the 6-carbon glucose to 3-carbon pyruvate for the production of ATP and biosynthetic precursors. In mammalian cells glycolysis occurs in the cytosolic compartment of the cells. The reactions of the glycolysis are given in Table 5.2.1.

The overall reaction of glycolysis is



The pyruvate can either enter the TCA cycle for complete oxidation and production of carbon dioxide and ATP or it can be converted to fermentation products for the regeneration of  $\text{NAD}^+$  and excreted from the cell. In mammalian cells the main waste product formed is lactate catalyzed by the enzyme lactate dehydrogenase. In normal cells the production of lactate occurs only in anaerobic conditions. However, most mammalian cell lines exhibit high rates of anaerobic glycolysis also in the presence of oxygen and thus produce high amounts of lactate.



The glycolytic pathway is controlled by the regulation of the three irreversible reactions catalyzed by hexokinase, phosphofructokinase and pyruvatekinase. However, cultured cells have an altered pattern of regulation which results in a high amount of overflow metabolism resulting in the formation of waste products such as lactate.

In the biochemical model used in this work only the reactions that result in a change of carbon are represented. Hence the reaction of phosphofructokinase forming fructose-1,6-bisphosphate from fructose-6-phosphate is not considered. Moreover, the series of reactions from glyceraldehyde-3-phosphate to pyruvate are lumped into two reactions, the formation of 3-phosphoglycerate from glyceraldehyde-3-phosphate and the conversion of 3-phosphoglycerate to pyruvate.

PHYSIOLOGICAL INVESTIGATIONS ON CHO CELLS

---

**Table 5.2.1:** The reactions of the glycolytic pathway and the enzymes involved [Adapted from Berg et al. (2002)]

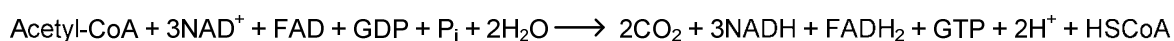
---

Step	Reaction	Enzyme
1	$\text{Glucose} + \text{ATP} \rightarrow \text{glucose 6-phosphate} + \text{ADP} + \text{H}^+$	Hexokinase
2	$\text{Glucose 6-phosphate} \rightleftharpoons \text{fructose 6-phosphate}$	Phosphoglucose isomerase
3	$\text{Fructose 6-phosphate} + \text{ATP} \rightarrow \text{fructose 1,6-bisphosphate} + \text{ADP} + \text{H}^+$	Phosphofructokinase
4	$\text{Fructose 1,6-bisphosphate} \rightleftharpoons \text{dihydroxyacetone phosphate} + \text{glyceraldehyde 3-phosphate}$	Aldolase
5	$\text{Dihydroxyacetone phosphate} \rightleftharpoons \text{glyceraldehyde 3-phosphate}$	Triose phosphate isomerase
6	$\text{Glyceraldehyde 3-phosphate} + \text{P}_i + \text{NAD}^+ \rightleftharpoons \text{1,3-bisphosphoglycerate} + \text{NADH} + \text{H}^+$	Glyceraldehyde 3-phosphate dehydrogenase
7	$\text{1,3-Bisphosphoglycerate} + \text{ADP} \rightleftharpoons \text{3-phosphoglycerate} + \text{ATP}$	Phosphoglycerate kinase
8	$\text{3-Phosphoglycerate} \rightleftharpoons \text{2-phosphoglycerate}$	Phosphoglycerate mutase
9	$\text{2-Phosphoglycerate} \rightleftharpoons \text{phosphoenolpyruvate} + \text{H}_2\text{O}$	Enolase
10	$\text{Phosphoenolpyruvate} + \text{ADP} + \text{H}^+ \rightarrow \text{pyruvate} + \text{ATP}$	Pyruvate kinase

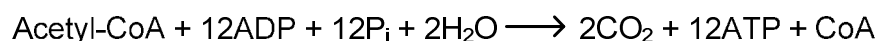
---

**Tricarboxylic acid (TCA) cycle**

The TCA cycle is responsible for the production of reducing equivalents, required for ATP formation, and also for supplying biosynthetic precursors. The reducing equivalents are produced during the oxidation of carbon compounds. The TCA cycle occurs in the mitochondria of eukaryotic cells. Glucose and glutamine are the major energy sources for mammalian cells. The pyruvate produced by the glycolytic pathway from glucose easily enters the matrix of the mitochondria. The pyruvate is then converted to a two-carbon fragment with the loss of the carboxyl group as CO<sub>2</sub> and this two carbon fragment attaches to a coenzyme known as coenzyme-A (CoA) forming acetyl-CoA. This reaction is catalyzed by pyruvate dehydrogenase. A complete turn of the cycle results in the oxidation of the two carbon fragment and formation of reducing equivalents. The reactions of the TCA cycle are given in Table 5.2.2. The net reaction of the TCA cycle for a single turn is given below.



Coupled with the oxidative phosphorylation and with an assumption of P/O ratio of 2.5, the three NADH and one reduced flavin adenine dinucleotide (FADH<sub>2</sub>) can yield a maximum of 9 molecules of ATP (GTP equivalent to ATP)



In addition to the ATP from TCA cycle, glycolysis and the conversion of pyruvate to acetyl-CoA produce an NADH each which can provide another five ATP. Hence the aerobic metabolism is a far more efficient mechanism for energy production than anaerobic metabolism. The TCA cycle is controlled by the NAD<sup>+</sup>/NADH ratio as well as the concentration of intermediates. The TCA cycle is regulated by the activities of the enzymes pyruvate dehydrogenase, citrate synthase, isocitrate dehydrogenase, α-ketoglutarate dehydrogenase and malate dehydrogenase (Berg et al., 2002). In mammalian cells it has been found that glutamine rather than glucose is the primary source of the TCA cycle.

As with the glycolytic pathway only the reactions that result in a change to the carbon skeletons of the metabolites are considered for this work. Hence the metabolites, citrate and isocitrate, succinyl-CoA and succinate, and fumarate and malate are lumped together as seen in Figure 5.2.1.

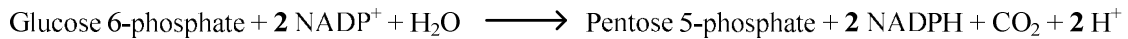
PHYSIOLOGICAL INVESTIGATIONS ON CHO CELLS

**Table 5.2.2:** The reactions of the TCA cycle and the enzymes involved [Adapted from Berg et al. (2002)]

Step	Reaction	Enzyme
1	Acetyl CoA + oxaloacetate + H <sub>2</sub> O → citrate + CoA + H <sup>+</sup>	Citrate synthase
2a	Citrate ⇌ <i>cis</i> -aconitate + H <sub>2</sub> O	Aconitase
2b	<i>cis</i> -Aconitate + H <sub>2</sub> O ⇌ isocitrate	Aconitase
3	Isocitrate + NAD <sup>+</sup> ⇌ α-ketoglutarate + CO <sub>2</sub> + NADH	Isocitrate dehydrogenase
4	α-Ketoglutarate + NAD <sup>+</sup> + CoA ⇌ succinyl CoA + CO <sub>2</sub> + NADH	α-Ketoglutarate dehydrogenase complex
5	Succinyl CoA + P <sub>i</sub> + GDP ⇌ succinate + GTP + CoA	Succinyl CoA synthetase
6	Succinate + FAD (enzyme-bound) ⇌ fumarate + FADH <sub>2</sub> (enzyme-bound)	Succinate dehydrogenase
7	Fumarate + H <sub>2</sub> O ⇌ L-malate	Fumarase
8	L-Malate + NAD <sup>+</sup> ⇌ oxaloacetate + NADH + H <sup>+</sup>	Malate dehydrogenase

**Pentose phosphate pathway (PPP)**

The PPP is responsible for the production of NADPH, and pentose and erythrose carbon units for the biosynthetic requirement of the cell. The pathway consists of an oxidative branch producing NADPH and a non-oxidative branch responsible for the inter-conversion of sugars and connecting the PPP with glycolysis. The reactions are given in Table 5.2.3. The overall reaction of the oxidative branch is given below.



The PPP can operate in different modes depending on the cellular requirement (Berg et al., 2002). In the non-oxidative branch it can interconvert sugars from 3-carbon molecules to 5-, 4- and 7-carbon molecules or it can completely oxidize glucose-6-phosphate to CO<sub>2</sub> for production of NADPH and also contribute to ATP production by converting glucose-6-phosphate to pyruvate. The first step of the oxidative branch by the enzyme glucose 6-phosphate dehydrogenase which is irreversible acts as the main regulatory control for the pathway. The activity of this enzyme is determined by the ratio of NADP<sup>+</sup>/NADPH. The activity of the PPP has been found to be low in mammalian cells, probably due to the slow growth rates of the cells. In the biochemical model considered for this work, both the oxidative and the non-oxidative branch of the pathway are considered.

**Table 5.2.3:** The reactions of the pentose phosphate pathway and the enzymes involved  
 [Adapted from Berg et al. (2002)]

Reaction	Enzyme
<b>Oxidative phase</b>	
Glucose 6-phosphate + NADP <sup>+</sup> → 6-phosphoglucono-δ-lactone + NADPH + H <sup>+</sup>	Glucose 6- phosphate dehydrogenase
6-Phosphoglucono-δ-lactone + H <sub>2</sub> O → 6-phosphogluconate + H <sup>+</sup>	Lactonase
6-Phosphogluconate + NADP <sup>+</sup> → ribulose 5- phosphate + CO <sub>2</sub> + NADPH	6-Phosphogluconate dehydrogenase
<b>Nonoxidative Phase</b>	
Ribulose 5- phosphate ⇌ ribose 5- phosphate	Phosphopentose isomerase
Ribulose 5- phosphate ⇌ xylulose 5- phosphate	Phosphopentose epimerase
Xylulose 5- phosphate + ribose 5- phosphate ⇌ sedoheptulose 7- phosphate + glyceraldehyde 3- phosphate	Transketolase
Sedoheptulose 7- phosphate + glyceraldehyde 3- phosphate ⇌ fructose 6- phosphate + erythrose 4- phosphate	Transaldolase
Xylulose 5- phosphate + erythrose 4- phosphate ⇌ fructose 6- phosphate + glyceraldehyde 3- phosphate	Transketolase

### **Oxidative phosphorylation**

The NADH and FADH<sub>2</sub> produced from the glycolysis and TCA cycle are primarily used to generate energy in form of ATP for the cellular requirement. Oxidative phosphorylation produces ATP from the energy released when the electrons in NADH and FADH<sub>2</sub> are transferred to oxygen. Hence oxygen is essential for this process to occur. In eukaryotes oxidative phosphorylation occurs in the mitochondrial compartment via the electron transport assembly. The electron transport assembly is comprised of a series of protein complexes that catalyze sequential oxidation reduction reactions and are located in the mitochondria. This process is facilitated by a proton carrier in the inner mitochondrial membrane known as ATP synthase. From thermodynamics it is possible to produce 3 ATP from every 2 electrons transferred from NADH to oxygen and 2 ATP from FADH<sub>2</sub> (Berg et al., 2002). However, it has been shown that for every 2 electrons transferred from NADH to oxygen only 2.5 equivalents of ATP are synthesized and 1.5 for FADH<sub>2</sub>. The oxidative phosphorylation is controlled by the availability of ADP. Higher amount of ADP drives the process faster, as the cells require more ATP. The total amount of theoretically possible ATP molecules produced from the complete oxidation of a single molecule of glucose is given in Table 5.2.4. This pathway does not have any effect on the carbon skeleton of the metabolites and hence is not considered in the model.

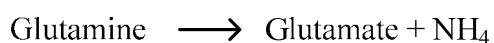
**Table 5.2.4:** The amount of ATP produced from the complete oxidation of a single molecule of glucose [Adapted from Berg et al. (2002)]

Reaction sequence	ATP yield per glucose molecule
<b>Glycolysis: Conversion of glucose into pyruvate (in the cytosol)</b>	
Phosphorylation of glucose	- 1
Phosphorylation of fructose 6-phosphate	- 1
Dephosphorylation of 2 molecules of 1,3-BPG	+ 2
Dephosphorylation of 2 molecules of phosphoenolpyruvate	+ 2
2 molecules of NADH are formed in the oxidation of 2 molecules of glyceraldehyde 3-phosphate	
<b>Conversion of pyruvate into acetyl CoA (inside mitochondria)</b>	
2 molecules of NADH are formed	
<b>Citric acid cycle (inside mitochondria)</b>	
2 molecules of guanosine triphosphate are formed from 2 molecules of succinyl CoA	+ 2
6 molecules of NADH are formed in the oxidation of 2 molecules each of isocitrate, $\alpha$ -ketoglutarate, and malate	
2 molecules of FADH <sub>2</sub> are formed in the oxidation of 2 molecules of succinate	
<b>Oxidative Phosphorylation (inside mitochondria)</b>	
2 molecules of NADH formed in glycolysis; each yields 1.5 molecules of ATP (assuming transport of NADH by the glycerol 3-phosphate shuttle)	+ 3
2 molecules of NADH formed in the oxidative decarboxylation of pyruvate; each yields 2.5 molecules of ATP	+ 5
2 molecules of FADH <sub>2</sub> formed in the citric acid cycle; each yields 1.5 molecules of ATP	+ 3
6 molecules of NADH formed in the citric acid cycle; each yields 2.5 molecules of ATP	+ 15
<b>NET YIELD PER MOLECULE OF GLUCOSE</b>	<b>+ 30</b>

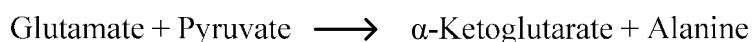
### Metabolism of amino acids

Mammalian cells in tissue culture require a complex mixture of nutrients to grow (Eagle, 1955). Cell culture media typically consists of a mixture of amino acids, vitamins, buffers, salts, essential fatty acids, growth factors etc. Many of these components, especially amino acids and growth factors, interact with the primary pathways and their metabolism needs to be taken into account for a quantitative analysis of the cellular physiology. In the present set of experiments the cells were grown in a media which was chemically defined and contained no peptides or proteins. This simplifies the analysis as only the metabolism of amino acids needs to be taken into consideration. All the amino acids are supplied in the medium and the major utilization of amino acids is for the biosynthesis of proteins. However, a majority of them can also undergo catabolism. The metabolic routes of amino acids and their interaction with the central metabolism are well researched (Berg et al., 2002). A very brief description of their metabolism and interaction with the primary pathways is given below.

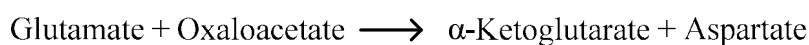
Glutamine is an important metabolic fuel required for the energy production in mammalian cultured cells (Eagle, 1955; Reitzer et al., 1979; Newsholme et al., 1985; Neermann and Wagner, 1996). It is the major nitrogen provider for the cells required for the biosynthesis of nucleotides and other compounds. It is the primary fuel for the TCA cycle. It is linked biochemically with the metabolism of ammonia, glutamate and many other amino acids. The use of glutamine as a substrate for the production of energy takes place via glutaminolysis. The 5-carbon skeleton of glutamine enters the TCA cycle in form of  $\alpha$ -ketoglutarate. Though there are several possible routes for the conversion of glutamine to  $\alpha$ -ketoglutarate it has been found that the primary route is the conversion of glutamine to glutamate via the activity of the mitochondrial enzyme glutaminase (Newsholme et al., 1985).



The glutamate formed can then be converted to  $\alpha$ -ketoglutarate via the activity of the enzymes alanine transaminase,



aspartate transaminase



or glutamate dehydrogenase.



The catabolic pathways of other amino acids such as proline, histidine and arginine all produce glutamate which can then produce  $\alpha$ -ketoglutarate. Serine can be produced from the glycolytic intermediate 3-phosphoglycerate and undergoes catabolism to give glycine and  $\text{N}^5, \text{N}^{10}$ -methylene-tetrahydrofolate (THF). The  $\text{N}^5, \text{N}^{10}$ -methylene-THF acts as a methylene group donor and is involved in many biosynthetic pathways. Serine is also used for the biosynthesis of lipids whereas glycine is utilized for nucleotide biosynthesis. Asparagine is converted to aspartate by the enzyme asparagenase. The TCA cycle intermediates are also supplied by the metabolism of other amino acids. Valine, methionine, tyrosine, phenylalanine, isoleucine and threonine all supply intermediates of the TCA cycle. Leucine, lysine and isoleucine undergo catabolism to produce acetyl-CoA. Aspartate can form oxaloacetate via the action of transaminase and hence can interact with the TCA cycle. Aspartate and glutamate also play a part in the transport of reducing equivalents from the cytoplasm to the mitochondria. All these reactions are considered in the metabolic model to be used for the quantification of metabolic fluxes in the primary network.

### **Anaplerotic reactions**

Anaplerotic reactions are reactions which replenish the pools of metabolic intermediates in the TCA cycle. The TCA cycle along with the formation of the reducing equivalents also functions in biosynthetic processes in which intermediates are removed from the cycle; this necessitates anaplerotic reactions to replenish TCA cycle intermediates to ensure its continued function (Owen et al., 2002). The main anaplerotic reaction is the entry of pyruvate in the TCA cycle after being carboxylated to oxaloacetate via pyruvate carboxylase. The formation of oxaloacetate from aspartate and  $\alpha$ -ketoglutarate from glutamate also serve as anaplerotic reactions. These reactions are shown in Figure 5.2.1 and will be used for further quantitative analysis.

### **Malic enzyme**

Malic enzyme catalyses the formation of pyruvate from the TCA cycle intermediate malate and its activity allows for the complete oxidation of glutamine by removing excess carbon atoms from the TCA cycle (Newsholme et al., 1985). This in turn allows the efficient use of glutamine for the production of ATP.

### **Mitochondrial transport of metabolites**

The mitochondrial membrane is impervious to reducing equivalents and hence special transport shuttles are used for their transport. The most important shuttle for the transport of the equivalents is the aspartate-malate shuttle. The transport occurs with the electrons being carried into the mitochondria via malate which forms oxaloacetate and transferring the electrons for the formation of NADH. This is followed by the transamination of oxaloacetate to give aspartate with the amino group provided by glutamate which forms  $\alpha$ -ketoglutarate. Aspartate is then transported to the cytoplasm where it is converted back to oxaloacetate. The oxaloacetate in the cytoplasm then takes up the electrons from the reducing equivalents and is converted back to malate. This energy rich malate then undergoes the same process forming reducing equivalents in the mitochondria with the formation of oxaloacetate. This results in a continuous carbon exchange between the TCA intermediates with glutamate and aspartate. These reactions are considered in the biochemical model to be used for the determination of carbon fluxes.

The other transport reaction considered in the biochemical model is the transport of citrate out of the mitochondria for the synthesis of fatty acids. Acetyl-CoA is the main precursor for the biosynthesis of fatty acids and the process occurs in the cytosol. However, acetyl-CoA cannot be transported out of the mitochondria. Citrate is transported out of the mitochondria into the cytoplasm where the enzyme citrate lyase converts it to acetyl-CoA and oxaloacetate. The acetyl-CoA formed is used for fatty acid synthesis. Oxaloacetate is converted to malate by the enzyme malate dehydrogenase which is then decarboxylated to pyruvate by the cytosolic malic enzyme.

### **Biomass formation**

The central metabolic pathways provide the precursors required for the synthesis of biomass (cells). The amount of precursors required for the biosynthesis of the major biomass components can be estimated from the composition of the biomass and known biosynthetic metabolic pathways. The major components of biomass are proteins, lipids, nucleotides and carbohydrates. The equations deriving each of the major biomass components along with their average molecular weight are given in the appendix.

## 5.3 Metabolic flux analysis

The growth and maintenance of cells is governed by the operation of complex systems of biochemical reactions. These systems of biochemical reactions are called metabolic networks and involve the action of numerous enzymes along with several regulatory mechanisms. The biochemistry of the mammalian cell along with the various networks/pathways has been explained briefly in the previous section. Metabolic flux analysis (MFA) is a powerful methodology for the determination of intracellular pathway fluxes (reaction rates) through these networks to study cellular physiology. The advantage of MFA is that it provides a quantitative snapshot of the physiological state of the cell. It has been used for information about pathway control (e.g. at branch points), identification of new or alternative pathways, quantifiable changes to normal cellular physiology under conditions of stress or under influence of environmental changes and for strain optimization. It has also emerged as a powerful technique in the field of metabolic engineering (Nielsen, 1998).

### 5.3.1 Methodology

#### Metabolite balancing

Conventional flux analysis of primary metabolic pathways is based on a stoichiometric model and on the measurement of a certain number of extracellular fluxes. The intracellular fluxes are calculated by using a stoichiometric model (metabolic pathway network) for the major intracellular reactions depicting the active metabolism and applying mass balance equations around the metabolites. Reaction kinetics specifies that the intracellular reactions depicting the rate of change of the metabolites be described by sets of differential equations. However, with an assumption of steady state the variation with respect to time tends to zero and thus the whole system is reduced to a set of algebraic equations. The idea of determining the intracellular steady state reaction rates by material balances was first used for a metabolic model of citrate production from glucose (Verhoff and Spradlin, 1976). This method solely relies on the known stoichiometry of a given biochemical reaction network (Varma and Palsson, 1994; Vallino and Stephanopoulos, 2000).

With the knowledge of the metabolic network along with a set of measurable fluxes (the uptake and secretion rates of metabolites along with biomass composition) it is possible to calculate the fluxes through each of the reaction described in the network using matrix algebra

$$r(t) = A \times X(t) \quad (5.3.1)$$

where  $A$  is  $n \times m$  matrix of stoichiometric coefficients of the reactions;  $X(t)$  is  $m$ -dimensional flux vector;  $r(t)$  is  $n$ -dimensional metabolite rate vector. Application of least square method results in solving the system of equation and determination of the intracellular fluxes.

The application of metabolite balance techniques for flux calculation is highly limited (Bonarius et al., 1998; Wiechert, 2001). Linearly dependent reactions such as in metabolic cycle can cause singularity in the network thus making the system underdetermined (Bonarius et al., 1997).

### **Metabolic flux analysis using isotopic tracers**

Metabolic flux analysis by metabolite balancing can be complimented with the inclusion of additional measurement techniques providing more detailed flux information than that embedded in typical extracellular metabolite data. Such information is particularly important for the study of underdetermined systems, which occur when the number of unknown fluxes exceeds the number of available flux measurements and metabolite balances. This is usually the case with highly interconnected networks, networks comprising metabolic cycles and reversible reactions. The basis of such measurement methods is the use of isotope labels as cellular substrates which distribute the label in the metabolites formed based on its metabolism (Wiechert, 2001). Both radioactive and stable isotopes have been applied for the determination of metabolic fluxes (Kelleher, 2001).

With their ease of handling and advances in the analytical techniques such as mass spectrometry (MS) and nuclear magnetic resonance (NMR), stable isotope labeled compounds are becoming the substrates of choice for metabolic studies (Wiechert and de Graaf, 1996; Szyperski, 1998). With experiments performed with isotope enriched substrates and measurement of the fractional enrichment of the isotopes in intracellular and extracellular metabolites, it is possible to apply an additional set of constraints in the stoichiometric model, and a better estimation of the intracellular fluxes may be obtained (Wiechert and de Graaf, 1996). For the measurement of the enrichment, techniques such as MS and NMR have been used. Each system brings with advantages and disadvantages (Szyperski, 1998; Wiechert et

al., 2001). In recent times, gas chromatography mass spectrometry (GC-MS) has emerged as a powerful technique for the measurement of the isotopic enrichment of metabolites due to its high precision, sensitivity and fast measurement (Wittmann and Heinzle, 1999; Wittmann, 2007). A key concept in evaluating the data from GC-MS concept of is that of an isotopomer of a given metabolite. The term isotopomer refers to the different labeling states of a particular metabolite (Malloy et al., 1988; Wiechert, 2001). For example, a metabolite with 'n' carbon atoms can be labeled or unlabeled at each carbon atom position. Thus there can be  $2^n$  different labeling states of this molecule which means that there are  $2^n$  different carbon isotopomers (Wiechert, 2001). GC-MS can resolve single mass isotopomers of a compound differing by the number of labeled atoms and thus allows the measurement of mass isotopomer distributions. The mass isotopomers distribution of a compound can be obtained from the analysis of the ions from the metabolite, which contains the whole isotopic skeleton of the analyte. The mass isotopomers distribution can be used to calculate the average isotopic enrichment of a molecule called the fractional isotope labeling (Wittmann, 2007). The most commonly used stable isotopes for flux calculation involve substrates with  $^{13}\text{C}$  labeling. In these cases, the cells are fed with  $^{13}\text{C}$  labeled substrates, most commonly  $^{13}\text{C}$  labeled glucose. The distribution of the isotope in the monomers of cellular macromolecules, the intracellular and extracellular metabolites of the cells at steady state is then determined using GC-MS. These data combined with metabolite balancing can be used for the calculation of metabolic fluxes by a computer flux model. For determination of the intracellular fluxes, the model should contain all relevant reactions and pathways of the metabolic network being investigated. The model is based not only on the balancing of the metabolites but also on the transfer of the carbon atoms during each of the reactions in the metabolic network (Wiechert and de Graaf, 1996; Wittmann, 2007). For the computation of the fluxes, random initial values for the free fluxes are supplied from which the model calculates the dependent fluxes and the labeling pattern of the metabolites for the supplied fluxes based on the network. Numerical optimization protocols are applied to minimize the difference between the simulated and experimental data. Thus from the 'fit' of these data sets the absolute carbon fluxes throughout the network are obtained (Wiechert and de Graaf, 1996; Wittmann and Heinzle, 1999; Wittmann, 2007). The determination of  $^{13}\text{C}$  labeling patterns in large metabolic networks is a computationally demanding task and various methods are available for their calculation. Few of the methodologies are briefly explained below.

***Atom mapping matrices (AMM)***

The concept of atom mapping matrices (AMM) was introduced for solving the complexities associated with positional isotope labeling or isotopomer distribution (Zupke and Stephanopoulos, 1994). The AMM describe the transfer of the carbon atoms from the reactants to products of every reaction in a metabolic network. Thus the AMM are used to relate the reactant and product isotopomers. The AMM are generated for each reaction in the metabolic network based upon the known biochemistry and do not depend on the network structure. Thus a series of equations are created using the mass balance along with the appropriate AMM and solved iteratively to give the absolute carbon fluxes in the network.

***Isotopomer mapping matrices (IMM)***

Shortly after the concept of metabolite vectors in AMM, the concept of isotopomer distribution vector (IDV) and isotopomer mapping matrices (IMM) were introduced (Schmidt et al., 1997). The IDV's contain mole fractions rather than the fractional enrichment of single atoms of metabolite molecules that are labeled in a specific pattern. Thus, the IDV of a molecule with 'n' carbon has  $2^n$  elements. There are generally one or two reactant molecules and one or two product molecules involved in biological carbon exchange reactions. The isotopomer distribution of the product molecules is determined by the isotopomer distribution of the reactants and the reaction mechanism, which is specified by the AMM's of the particular conversion. Hence, IDV's of the product molecules can be calculated when the AMM's and the reactant IDV's are available. Isotopomers mapping matrices (IMM's) can be constructed to sum up all pairs of reactant isotopomers that produce the respective product isotopomer in all positions of the product IDV. There is one IMM defined for each pair of reactant and product molecules in a biochemical carbon exchange reaction. Using the equations created for a metabolic network, along with the mass balances, the flux analysis can be carried out (Schmidt et al., 1997).

***Isotopomer path tracing***

Isotopomer path tracing identifies paths between *observable* (measurable) isotopomers, many of which are separated by *nonadjacent* (non-measurable) isotope paths. It generates a direct mapping from isotopomer measurements to metabolic fluxes (Forbes et al., 2001).

***Elementary metabolite units***

The elementary metabolite unit (EMU) framework is based on a decomposition method that identifies the minimum amount of information needed to simulate isotopic labeling within a reaction network using the knowledge of atomic transitions occurring in the network reactions. The functional units generated by the decomposition algorithm, called EMU, form the basis for generating system equations that describe the relationship between fluxes and stable isotope measurements (Antoniewicz et al., 2007). EMU are distinct subsets of metabolite atoms as defined by Antoniewicz et al. (2007). A metabolite with 'n' atoms would have  $2^n - 1$  EMU. For example a metabolite with 3 atoms would have 3 EMU of size 1 ( $A_1, A_2, A_3$ ), 3 EMU of size 2 ( $A_{12}, A_{13}, A_{23}$ ) and 1 EMU of size 3 ( $A_{123}$ ). The EMU's in a metabolic network follow two types of reactions, condensation and uni-molecular. The metabolic network is decomposed into EMU reactions and can be solved for intracellular fluxes.

***Cumomer network***

The method of IMM made it possible to simulate all isotopomers distribution for the given set of metabolic fluxes, while the best fit to the experimental distribution pointed to the set compatible with the measured distribution. However, the presence of large exchange fluxes causes severe instability of numerical solution or convergence problems, which restricts the application of this method. This instability can be circumvented by the application of an automatic correction involving the isotopomers pools of certain metabolites (Wittmann and Heinzle, 2001). Another elegant way to overcome the problem of instability is by reformulating isotopomer balance equations into cumomer balance equations (Wiechert et al., 1999). The term cumomer (derived from cumulative isotopomers) designates a sum of isotopomers with fixed positions of label (a 1-cumomer fraction is a sum of the positional enrichments). Thus cumomers are a set of one or more isotopomers that contain a particular labeled fragment. Cumomers are specified using a notation in which 1 indicates a labeled carbon atom, and X indicates an atom that is either labeled or unlabeled. The transformation of the equations in terms of cumomers simplifies the computation and makes it possible to obtain the solution in a single step based on matrix calculus. The equations formulated in terms of cumomer fractions can be solved analytically as a cascade of linear systems, evaluating the cumomer fractions one by one starting from the 0-cumomer fraction. Then the cumomer fractions can be transformed back into isotopomer fractions.

For the present analysis, it will be attempted to create a cumomer network for the metabolic reactions of a mammalian cell. However, the creation of such a network requires a thorough

knowledge of the biochemistry and considerable modeling efforts. In this thesis the required experimentation leading to data required for such an analysis is carried out. Along with this, an investigation into the mammalian biochemistry for an improvement in the network described earlier is also attempted. The modeling efforts for the whole cell metabolic flux analysis of a mammalian cellular system are presently underway (in co-operation with Dr. Tae Hoon Yang, James Brown Cancer Centre, Louisville, USA) but will not be discussed in this thesis.

### **5.3.2 Metabolic flux analysis in mammalian cells**

Traditionally metabolic fluxes have been determined by the use of isotopic-tracers. However, these techniques were earlier generally applied to elucidate the biochemical pathway, rather than its quantification. Examples of the use of tracer substrates for the quantification of carbon fluxes at certain branch points by tracing the fate of the carbon atoms have been provided in a later chapter. To determine the fluxes through primary metabolic pathways the technique of metabolite balancing has been widely used. This methodology requires the measurement of extracellular metabolites only (Varma and Palsson, 1994). By measuring the consumption of given substrate(s) and/or the production of specific end product(s) it is possible, knowing the reactions of the metabolic pathways and assuming a steady-state for the metabolic intermediates, to calculate the fluxes through different pathways as described earlier. This method has been applied frequently in mammalian cell cultures and few of the studies performed are briefly described.

Rat heart metabolism was investigated using material balancing to study the cytosolic-mitochondrial interactions with regard to citric acid cycle intermediates (Safer and Williamson, 1973). Wanders et al. (1983) applied this technique to study the effect of bicarbonate and for the determination of glutamate oxidation in rat liver mitochondria. The effect of dissolved oxygen concentration on the metabolism of a hybridoma cell line was determined by using stoichiometric balancing (Zupke et al., 1995). The metabolism of peptides as substitute for serum in a Chinese hamster ovary cell line was studied using mass balances (Nyberg et al., 1999). The phenomenon of multiple steady states in continuous cultures of mammalian cell cultures was investigated in various studies using metabolic flux analysis by metabolite balancing (Follstad et al., 1999; Europa et al., 2000). Investigations into hepatic metabolism have also been carried out using material balancing techniques (Lee et al., 2000; Arai et al., 2001; Chan et al., 2003b; Chan et al., 2003a). The effects of a

glutamate based media in the absence of glutamine on intracellular fluxes have been studied in the industrially important CHO cell line (Altamirano et al., 2001). A high-throughput methodology based on metabolic flux analysis to screen cellular cultures, to study the effects of toxins, for media optimization etc has been introduced recently (Balcarcel and Clark, 2003). Metabolic differences as described by intracellular fluxes during different physiological states in a hybridoma cell line has also been studied (Gambhir et al., 2003). MFA was instrumental in the identification of a key limitation in the metabolic pathways of HEK-293 cell line which led to an improvement in the glucose and glutamine metabolism by expression of cytosolic pyruvate carboxylase enzyme (Elias et al., 2003). Increase in adenovirus vector production by HEK-293 cells was achieved using strategies developed by investigation of metabolic fluxes (Henry et al., 2005). The metabolism of CHO cell line on galactose for the reduction of overflow metabolism was investigated with MFA (Altamirano et al., 2006).

The above are only few of the many examples for the applications of material balance technique for determination of intracellular fluxes in primary pathways of mammalian cells. Nevertheless this methodology is limited in its usage and fails in situations for the estimation of fluxes in parallel pathways, bidirectional reaction steps, split pathways and in metabolic cycles (Wiechert, 2001). Moreover, frequently the system of equations to be solved is under-determined. Bonarius et al. (1997) described a theoretical constraint based approach for overcoming the above limitations. The most commonly used methodology for the solution of the problems encountered with under-determined system is linear optimization by applying objective functions such as “minimizing the sum of squares of fluxes” , “maximize ATP production” etc (Bonarius et al., 1996; Bonarius et al., 1997). However, it has been seen that the above methodologies do not give exact fluxes and need to be complimented with data from isotopic tracers for the accurate determination of fluxes in cyclic reactions such as those found in the pentose phosphate pathway (Bonarius et al., 1998; Schmidt et al., 1998). Hence most of the studies described above do not consider these pathways in their flux analysis (Paredes et al., 1998; Follstad et al., 1999; Nyberg et al., 1999; Chan et al., 2003b; Chan et al., 2003a). Therefore, even if the analysis of fluxes by material balancing is a useful technique, it is not sufficient to give information about the entire primary central cellular metabolism. For the accurate quantification of cellular fluxes, it is necessary to compliment the stoichiometric balancing of metabolites with isotopic labeling analysis. A few examples for the use of isotopic tracers in mammalian flux analysis are provided in later chapters of the thesis.

## **5.4 Materials and methods**

### **5.4.1 Cell line and culture conditions**

The cell line and culture conditions are similar to the one described in the previous part under materials and methods. Briefly, the Chinese Hamster Ovary (CHO) cell line T-CHO ATIII, obtained from Gesellschaft for Biotechnologische Forschung mbH (Braunschweig, Germany), was used for this research. The cells produce recombinant antithrombin III, which has clinical applications for its coagulation inhibitory activity. The cells are adapted to grow in a protein and peptide free, chemically defined medium (SMIF 6, Life Technologies, Karlsruhe, Germany). The cells were grown in 250 ml spinner flasks placed in a 12 % CO<sub>2</sub> humidified gas controlled incubator at 37°C. The cultures were maintained in growth phase by changing the medium using the serial dilution method.

### **5.4.2 Cell viability assays**

Cells were counted using a Neubauer hemocytometer. Cell concentration and viability were determined using the Trypan Blue exclusion method already described in the previous part.

### **5.4.3 Chemicals**

All chemicals used for media formulation were obtained from Sigma Aldrich and were cell culture grade. Other chemicals were obtained from the following sources: Acros Organics (Geel, Belgium); Merck (Darmstadt, Germany); Aldrich (Steinheim, Germany); Fluka (Buchs, Switzerland). The tracer substrates used were supplied by Cambridge Isotopes, Inc. (Andover, MA).

### **5.4.4 Dry weight determination**

A known volume of culture containing approximately  $1 \times 10^{10}$  cells was taken in replicates. These were centrifuged and concentrated to a volume of about 1 mL and transferred to a pre-weighed 1.5 mL centrifuge tubes. The tubes were then centrifuged, the supernatant removed and the pellet was washed twice with saline (0.9 % NaCl). The weight of the wet pellet in the centrifuge tubes was noted. The tubes were then placed in an 80 °C incubator for 72 h and weighed. The difference in the weight of the tubes with pellet and without pellet along with the number of cells gives the dry weight of the cells.

### 5.4.5 Sampling for analysis

The cells were cultured in media containing labeled substrates. Briefly the cells grown in normal medium were washed twice with the respective substrate deficient media and centrifuged. The cells were then transferred to the media containing the labeled substrates and resuspended. The initial samples were taken after the addition of the media. Hence the initial time represented by time “0” is after the addition of the media. In the experiment with parallel cultures this time varied from 5 minutes to a maximum of 30 minutes.

### 5.4.6 Quantification of extracellular metabolites

The quantification of glucose and lactic acid was done by high pressure liquid chromatography (HPLC) (Kontron Instruments, Neufahrn, Germany) using an Aminex HPX-87H column (300 by 7.8; Biorad, Hercules, CA, USA) at 45°C, with 7 mM H<sub>2</sub>SO<sub>4</sub> as the mobile phase in an isocratic mode and a flow rate of 1 ml min<sup>-1</sup>, and subsequent detection via determination of refraction indexes for Glucose (ERC-7515A, ERC Inc, Alteglofsheim bei Regensburg, Germany) or UV absorption at 210 nm for lactate and pyruvate (HPLC 535, Biotek, Neufahrn, Germany).

The quantification of the amino acids in the cell medium was done with HPLC (Agilent 1100, Agilent, Waldbronn, Germany) as described in Kromer et al. (2005). The cell medium was diluted 1:2 with a solution containing 225 µM of  $\alpha$ -aminobutyric acid (ABU). ABU acts as an internal standard for the quantification. The separation was via a guard cartridge and a Gemini column (Phenomenex, Aschaffenburg, Germany) and was carried out at a flow rate of 1 mL min<sup>-1</sup> at a column temperature of 40°C using 40 mM NaH<sub>2</sub>PO<sub>4</sub> (eluent A, pH 7.8, adjusted with NaOH) as polar phase and an acetonitrile/methanol/water mixture (45/45/10) as non-polar phase (eluent B). The following gradient was applied: Start 0 % B, 40.5min 40.5 % B, 41min 61 % B, 44min 82 % B, 44.5min 100 %B, 47min 0 % B, 2min 0 % B for equilibration. The amino acids are pre-derivatized with *o*-phthaldialdehyde (OPA) and mercaptoethanol (Roth, 1971) subsequently followed by 9-fluorenylmethyl chloroformate (FMOC-Cl) with 3-Mercaptopropionate (0.5 % in 0.5M Bicin) for proline (Schuster, 1988; Haynes et al., 1991). OPA reacts with primary amines in the presence of the thiol compound, to form highly fluorescent isoindole products. However, this does not detect amino acids that exist as secondary amines (e.g. proline). 9-Fluorenylmethyl chloroformate (FMOC-Cl) reacts with both primary and secondary amino acids to form highly fluorescent products. The detection of the amino acids is via a fluorescence detector (Agilent, Waldbronn, Germany) with 340 nm excitation and 450 nm emission for the primary amines and changed at 43.5 minutes to 266

nm excitation and 305 nm emission for the detection of proline. The peaks are manually integrated, and the quantification is done knowing the dilution and the concentration of the internal standard.

**Specific rate calculation:**

The specific rates of metabolites during the exponential phase were calculated using the equation (Zupke et al., 1995):

$$[S]=[S_0]+\frac{q_s \times N_0}{\mu}(e^{\mu t}-1) \tag{5.4.1}$$

where  $q_s$  is the specific rate,  $[S]$  is the measured metabolite conc. ,  $[S_0]$  is the initial conc. ,  $N_0$  is the initial biomass,  $\mu$  is the specific growth rate and  $t$  is the time. Glutamine is hydrolyzed to pyrrolidone-carboxylic acid under cultivation conditions. The rate of glutamine decomposition is first order and calculated to be 0.0037 h<sup>-1</sup>. The actual uptake rate was calculated by using the equation

$$-\frac{d}{dt}(GLN) = k(GLN) + q_{GLN} \cdot X \tag{5.4.2}$$

where  $k$  is the rate constant;  $q_{GLN}$  is actual uptake rate;  $X$  is cell number with  $d/dt(X) = \mu X$  with  $\mu$  being the sp. growth rate.

The equation was fitted with obtained cell growth and glutamine uptake data using the software Berkeley Madonna.

**5.4.7 Gas chromatography-mass spectrometry analysis**

The mass-isotopomers and the fractional carbon labeling (FCL) of the monomers in the cellular macromolecules and the extracellular metabolites were obtained by analyzing the samples using Gas Chromatography-Mass Spectrometry (GC MS) with HP 6890 GC (Hewlett Packard, Palo Alto, CA, USA), equipped with a HP-5MS Column 5 % Phenyl-Methyl-Siloxan- diphenylpolysiloxan; 30 m x 0.251 mm x 0.25 μm, Agilent, Waldbronn, Germany) and Quadrupole- Mass Spectrometer (MS 5973, Agilent, Waldbronn, Germany). Electron Ionization was carried out at 70eV. Carbon mass isotopomer fractions and the fractional labeling of the analyzed samples were calculated from the measured mass distribution of the

derivatized analyte using the method developed by Yang (2006), which is based on earlier work of Wiechert et al. (2001).

### **Extraction and analysis of lactate**

Lactate was extracted from the cellular supernatant using a protocol modified from Suh et al. (1997). Briefly, 100µl of supernatant was acidified with 25µl of conc. HCl. To this 100µl of ethyl acetate was added and thoroughly vortexed for 10-15 min. The organic phase containing lactic acid was then carefully removed and derivatized to its *t*-butyldimethylsilyl (*t*-BDMS) derivative by *N*-Methyl-*N*-(*t*-butyldimethylsilyl)trifluoroacetamide (MTBSTFA, Macherey-Nagel, Dueren, Germany) (Schwenk et al., 1984) by adding an equal amount to the amount of organic phase removed. The mixture was then incubated at 80 °C for 1 h. 1 µl was then injected into the GC MS. The separation was carried out in GC (carrier gas 1 mL min<sup>-1</sup> helium) with the temperature program: Initial column temperature of 100 °C for 1 min, increase of 5 °C min<sup>-1</sup> till 170 °C and then at 30 °C min<sup>-1</sup> till 280 °C with a final holding time of 1 min. The inlet had a temperature of 250 °C and the quadrupole of 280 °C. The total run time was 19.67 min. The ions at 261, 262, 263 and 264 were monitored in the Selected Ion Monitoring (SIM) mode of the MS. The ions contain the carbon backbone of the whole molecule.

### **Extracellular amino acids**

Extracellular amino acids were analyzed by lyophilizing 100µl of either cellular supernatant or the aqueous phase of the lactic acid extraction procedure, and converting them to *t*-BDMS derivative by MTBSTFA (Mawhinney et al., 1986). 50 µL of Dimethylformamid (0.1 % pyridne) was added to the sample along with 50 µL of MTBSTFA and incubated for 1 h at 80 °C. 1 µl was then injected into the GC MS. The separation was carried out in GC (carrier gas 1.1 mL min<sup>-1</sup> helium) with the temperature program: Initial column temperature of 135 °C, increase of 10 °C min<sup>-1</sup> till 325 °C with a final holding time of 1 min. The inlet had a temperature of 320 °C and the quadrupole of 320 °C. The total run time was 20.00 min. In the present experiments where ever possible the aqueous phase of the lactic acid extraction procedure was used. The ions corresponding to the whole carbon backbones of the amino acids were monitored in the SIM mode of the MS.

### **Proteinogenic amino acids**

For the analysis of amino acids from the cell protein, around  $2 \times 10^6$  -  $3 \times 10^6$  of cells were washed twice with PBS. The washed cell pellet was hydrolyzed for 48h with 250µL 6M HCl

at 105°C. The obtained hydrolysate was neutralized (6M NaOH), and freeze-dried. GC/MS analysis of the amino acids was performed after derivatization into the *t*-BDMS derivate with MTBSTFA. 50 µL of dimethylformamid (0.1 % pyridne) was added to the sample along with 50 µL of MTBSTFA and incubated for 1 h at 80 °C. The same conditions as those used for the extracellular amino acids were used in the GC MS analysis.

### **Extraction and analysis fatty acids**

The methyl esters of palmitic acid and stearic acid from cellular samples were monitored in GC-MS. Briefly the fatty acids were extracted in their ester form as follows; to  $2 \times 10^6$  -  $3 \times 10^6$  of the cellular sample was added 500µl of 1:1 Toluene and Methanol along with 10µl of conc. sulphuric acid. This was incubated overnight at 55°C and the organic phase obtained by the addition of 400µl of 0.5M ammonium bicarbonate separated. 1 µl was then injected into the GC MS. The separation was carried out in GC (carrier gas 1 mL min<sup>-1</sup> helium) with the temperature program: Initial column temperature of 150 °C for 5 min, increase of 5 °C min<sup>-1</sup> till 260 °C and then at 30 °C min<sup>-1</sup> till 300 °C with a final holding time of 5 min. The inlet had a temperature of 250 °C and the quadrupole of 280 °C. The total run time was 33.33 min. The ions at 298 till 317 were monitored for stearic acid and from 270 till 288 were monitored for palmitic acid in the Selected Ion Monitoring (SIM) mode of the MS. The ions contain the whole carbon backbone of the molecule.

### **5.4.8 Online monitoring of oxygen in spinner flasks**

#### **Introduction**

The increasing importance of industrial operations based on biochemical engineering has long been recognized. Dissolved oxygen concentration is one of the most important control variables in any aerobic reactor. Oxygen plays an important role in the metabolism of cells and is essential for the oxidative phosphorylation pathway for the production of ATP. It also plays a role in the determination of the redox potential of the cellular medium. The importance of oxygen uptake rates has been stressed in the previous chapter. The metabolism of mammalian cells is highly influenced by the dissolved oxygen concentrations (Zupke et al., 1995). The most commonly used small scale culture devices for mammalian cells are microtiter plates. The transfer characteristics of oxygen in 96-well plates have been discussed in earlier chapters. Mammalian cells in suspension are generally grown in spinner flasks. This is the method of choice for suspension lines including hybridomas, CHO cells and attached lines that have been adapted to growth in suspension. Also attached cell lines can be scaled up with microcarrier beads and grown in spinner flasks. Spinner flasks are either plastic or glass bottles with a central magnetic stirrer shaft and side arms for the addition and removal of cells and medium, and gassing with CO<sub>2</sub> enriched air. Inoculated spinner flasks are placed on a stirrer and incubated under the culture conditions appropriate for the cell line. Commercial spinner flasks are available in the range of 125 ml to 5000 ml. However, the oxygen transfer characteristic in spinner flasks has not been much studied. It has been reported that insect cells undergo oxygen limitation under standard spinner flask cultivation conditions (Annathur et al., 2003). However, the oxygen consumption of mammalian cells is much lower than insect cells and it has been assumed that suspension cells do not undergo oxygen limitation in spinner flasks under normal operating conditions. For metabolic studies, it is essential that the cells undergo normal metabolism without any stress. Hence it is of prime importance that the cells do not undergo oxygen limitation. To test if the cells undergo oxygen limitation in spinner flasks, the spinner flasks were equipped with optical oxygen sensors for on-line monitoring. Moreover the characteristics of oxygen transfer in spinner flasks were studied.

**Spinner flasks with oxygen sensing**

The optical sensing system employed is similar to a system described earlier for shake flask cultures (Wittmann et al., 2003). Briefly the system consists of three parts: (i) an optical sensor spot immobilized on the spinner flask bottom, (ii) a coaster placed below the flask containing an optical fiber, and (iii) a module for data processing and connecting to a PC. The spinner flask with sensor attached to the bottom was supplied by Pre-Sens GmbH (Regensburg, Germany). The sensor was placed in the centre of 250 mL spinner flask to allow uninterrupted rotation of the shaft. The system uses phase modulation technique to determine the luminescent decay time of the O<sub>2</sub> sensor. The decay time is related to the actual dissolved O<sub>2</sub> (DO) by the Stern–Volmer equation (Wittmann et al., 2003). The system uses a two-point calibration with water; zero dissolved oxygen achieved by purging water with nitrogen and 100 % dissolved oxygen achieved by purging water with air. The experiments were carried out in normal culture conditions of CHO cells.

**Characterization of oxygen transfer in spinner flasks**

The volumetric gas-liquid mass transfer coefficient ( $k_{La}$ ) was calculated two different spinner speeds at various volumes using the method described earlier (Wittmann et al., 2003). The speeds used were 40 rpm and 80 rpm. 80 rpm is the maximum speed allowed on the stirrer (Model 104-S, Techne, Staffordshire, United Kingdom). Figure 5.4.1 gives the plot depicting the relationship between various volumes at two different speeds with the gas-liquid mass transfer coefficient. At higher volumes the transfer at both the speeds almost reaches the same values of 0.02 min<sup>-1</sup> thus giving a maximum oxygen transfer rate of 0.28 mM h<sup>-1</sup>. Considering an average specific oxygen uptake rate of  $2 \times 10^{-13}$  mol (O<sub>2</sub>) cell<sup>-1</sup> h<sup>-1</sup> and average cell density of  $1 \times 10^6$  cells mL<sup>-1</sup>, this maximum transfer rate would be just enough to avoid oxygen limitation. However, in exponential phase of cell growth, the specific oxygen uptake rates of cells are much higher and hence the use of large volumes is not recommended for cell culture in spinner flasks.

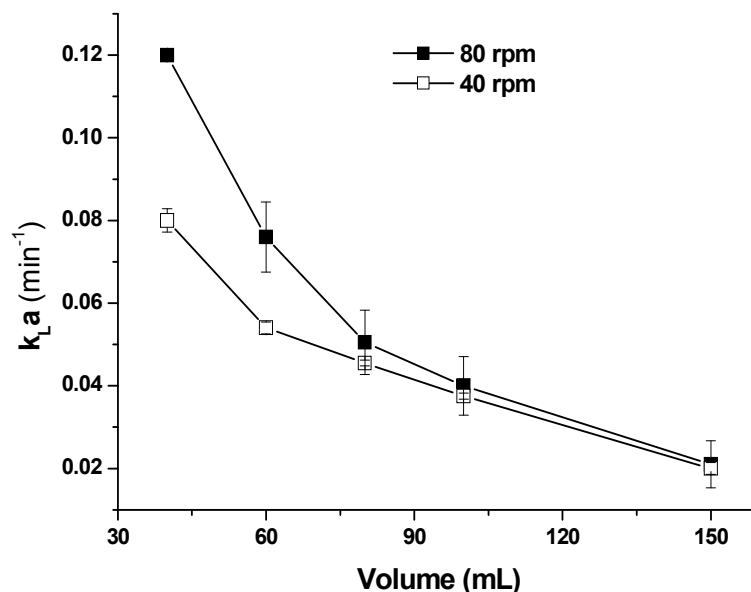


**Figure 5.4.1:** The relationship between the volumetric gas-liquid mass transfer coefficient ( $k_L a$ ) and volume at two different speeds. The  $k_L a$  was calculated by dynamic method using gas-liquid mass transfer equation after removal of oxygen from water by nitrogen, followed by flushing the air space with air.

Another interesting facet about cellular growth in spinner flasks is the use of the side arm. The main purpose of these arms is for the removal of cells or addition of media. These side arms are usually provided with screw caps, and it is recommended to grow the cells without closing them tightly to avoid oxygen limitation. It was decided to investigate the influence of the number of turns the screw cap of the side arms is open on the oxygen transfer. The number of turns the caps takes to fully close was counted. Oxygen transfer characteristic was determined for the flask with no caps, flask with half opened caps and flask whose caps were turned only once after closing the cap completely. The flask was filled with 60 mL water and oxygen removed by purging with nitrogen, placed into the incubator on the stirrer with 80 rpm with the desired rotation of cap and the rise of oxygen monitored. Figure 5.4.2 gives the rise of oxygen under the three conditions. It is seen that the rise is the fastest in the case where there are no caps, and slowest in flask with a single turn. The  $k_L a$  values of the above conditions are not determined since the air space was not flushed with air.

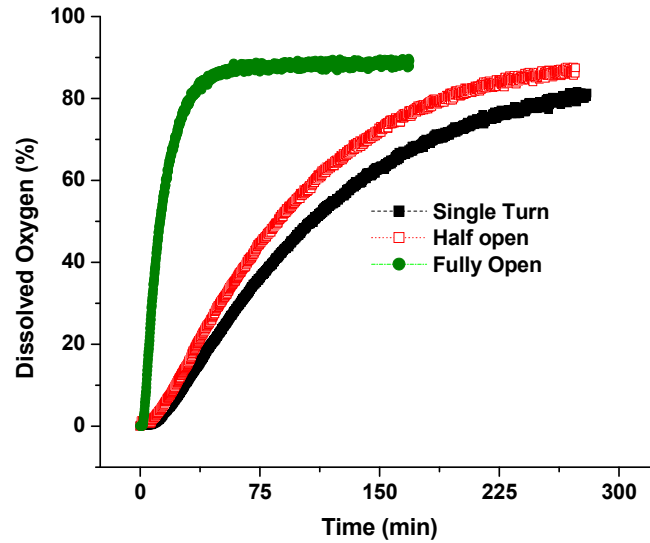


**Figure 5.4.2:** The influence of the turns of the screw caps on the side arm of the spinner flasks on the transfer of oxygen. Flask with no caps (fully open), flask with half opened caps (half open) and flask whose caps were turned only once after closing the cap completely (single turn) were investigated.

#### Online monitoring of cell growth

Cells were grown in the spinner flasks with a volume of 60 mL and at a stirrer speed of 80 rpm. Cells were inoculated at a density of  $2 \times 10^5$  cells mL<sup>-1</sup> and monitored for 190 h. Figure 5.4.3 gives the online profile for the cultivation for 190 h. It is seen that there is a rise in the dissolved oxygen concentration from 150 h probably indicating that the cells start to die during this phase.

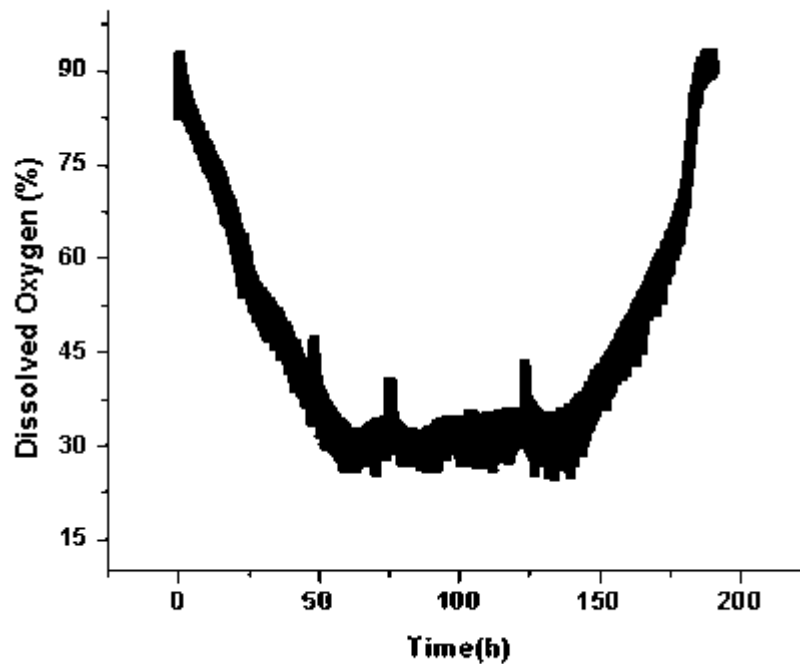


**Figure 5.4.3:** Online monitoring of dissolved oxygen with spinner flasks equipped with optical oxygen sensor. The cells were grown in a 60 mL volume at 80 rpm.

A second experiment was carried out where parallel cultures were grown, one in the normal media and the other in a modified medium where the concentrations of glucose and glutamine had been halved. Additionally samples were taken during the cell growth to determine the cell density. Figure 5.4.4 gives the oxygen consumption of both the cell cultures along with the growth curve. It is seen that the oxygen consumptions are very similar as are the growth curves. Moreover, none of the culture goes into oxygen limitation. However, the process of sampling disturbs the measurements indicated by a rise in the dissolved oxygen concentration after the sampling. Nonetheless the oxygen concentrations reach equilibrium after some time. Hence it was seen that under normal cell culture conditions, the cells do not undergo oxygen limitation when grown in spinner flasks. This system of oxygen monitoring can be later applied for the determination of oxygen uptake rates and also for online process monitoring.

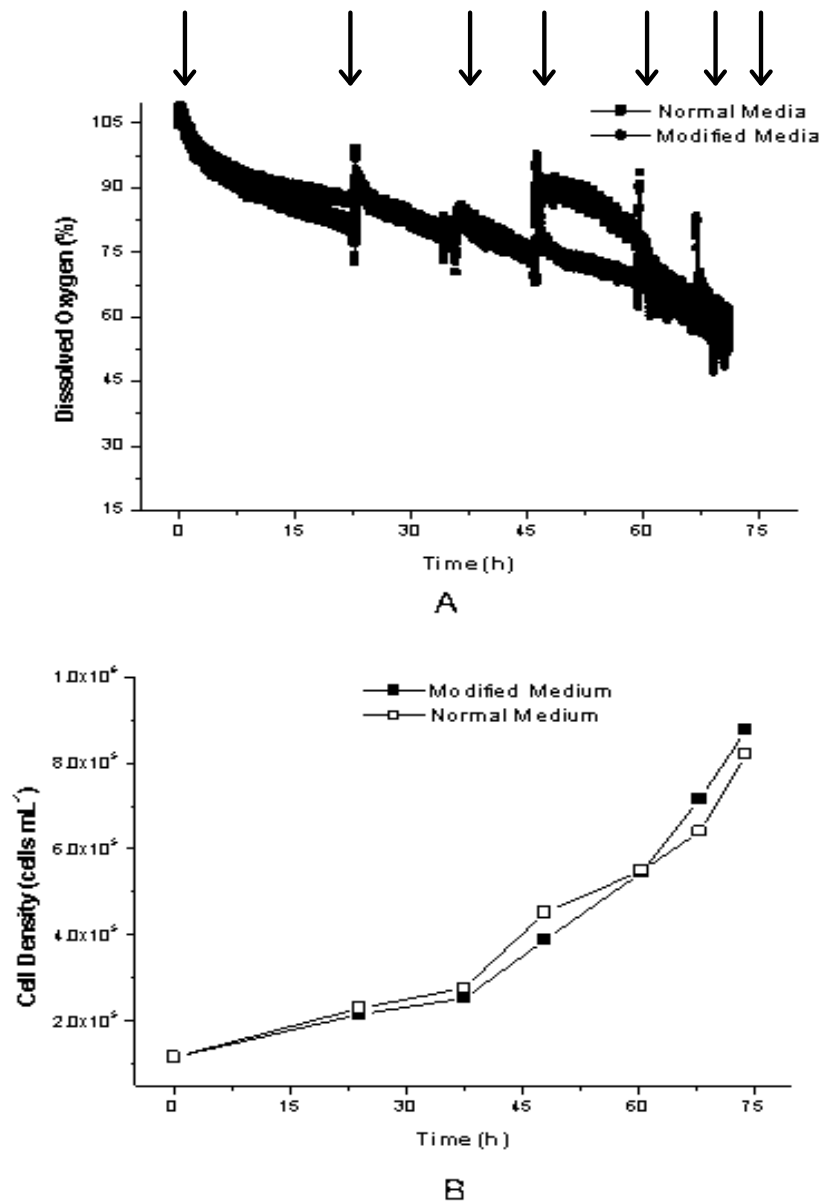


**Figure 5.4.4:** (A) Online monitoring of dissolved oxygen with spinner flasks equipped with optical oxygen sensor for parallel cell cultures. (B) The growth curve of the two cultures. The cell density was determined with trypan blue method. The cells were grown in a 60 mL volume at 80 rpm. The modified medium indicates medium with half the concentration of glucose and glutamine as in the normal medium. The sampling is indicated by arrows.

## **5.5 Investigative physiological studies on CHO cell**

### **5.5.1 Theory**

Consideration of the metabolism of cell is an important parameter in the optimization of industrial processes. However, many industrial processes using mammalian cells often run on suboptimal conditions, mainly due to the lack of understanding of the complex mammalian metabolism and the inability to quantify the metabolism. A brief overview of the mammalian cell biochemistry and the usage of metabolic flux analysis to quantify central metabolic pathway fluxes are provided in the previous chapters. Industrially important mammalian cells have been the focus of many investigations and the effects of various parameters on their physiology have been determined (Hu et al., 1987; Miller et al., 1987; Newland et al., 1990; Ozturk and Palsson, 1990a; Ozturk and Palsson, 1990b; Franek and Dolnikova, 1991; Ozturk and Palsson, 1991; Ronning et al., 1991; Fitzpatrick et al., 1993; Hansen and Emborg, 1994a; Hansen and Emborg, 1994b; Jeong and Wang, 1994; Haggstrom et al., 1996; Neermann and Wagner, 1996; Miller et al., 2000).

Metabolism consists of anabolism, which is the building up of monomers for macromolecular synthesis and catabolism, which is the breakdown of substrates for energy generation. Glucose and glutamine are the primary energy sources for the cells. Both these substrates are broken down to provide cellular energy. Neermann and Wagner (1996) studied the metabolism of glucose and glutamine in various cell lines and their distribution in different pathways. Glutamine entering the TCA cycle was found to be the major energy source for cells whereas the majority of glucose was utilized by glycolysis to form lactate. Along with these two substrates, amino acids play an important role, both in anabolic as well as catabolic pathways. Eagle (1959) studied the metabolism of amino acids in cellular tissue culture and was able to identify essential and non-essential amino acids requirements for cells. Many essential amino acids enter the primary metabolism and break down to provide cellular energy. These pathways have been discussed in the previous chapter on cellular biochemistry. However, every cell line has individual characteristics and has to be studied independently due to variations in its individual physiology and inherent instability (Kromenaker and Srienc, 1994; Wurm, 2004). In this chapter an attempt is made to investigate the cellular physiology and to quantify metabolic fluxes of the CHO cells, with a special emphasis on the metabolism of amino acids.

## 5.5.2 [U-<sup>13</sup>C]Glucose studies of metabolism

### 5.5.2.1 Motivation

Malignant cells display uncontrolled rates of cellular proliferation and require an increased supply of precursor amino acids to support key biosynthetic pathways. Amino acids interact with glucose metabolism both as carbon substrates and by recycling glucose carbon, e.g. alanine and glutamine. The amino acids essential for mammalian cell growth have been determined earlier (Eagle, 1955; Eagle, 1959). However, the requirements and metabolism of individual cell lines vary and depend on numerous extraneous factors; most importantly the cultivation conditions and media used. Generally media are supplemented with serum, proteins or peptides to support growth. However, the present industrial trend is to develop and use chemically defined media because of safety and the control they offer over process conditions. Since the media used in these particular experiments is chemically defined with no protein or peptides, it was necessary and essential to determine the cellular amino acid metabolism.

Carbon labeling experiments offer an elegant way of determining the anabolic or catabolic pathways followed by metabolites. There is a constant interchange of atoms between metabolites in a cell. Thus a labeled metabolite can contribute its label to other metabolites depending on the atom interaction. In such a case, a substrate with labeled atoms should distribute its label to the metabolites it is involved in formation. Hence the anabolic metabolites from a culture grown in fully carbon labeled glucose should show carbon labeling. Using mass spectrometric analysis of the metabolites to determine their labeling along with their uptake rates can thus provide initial information whether a particular metabolite is anabolic or catabolic in nature. This information can be then incorporated to appropriately design strategies to reduce the complexity of the model for the cell biochemistry and to further assist in flux calculations.

### 5.5.2.2 [U-<sup>13</sup>C]Glucose culture and anabolic amino acids

#### *Cell culture with [U-<sup>13</sup>C]glucose*

Exponentially growing cells in normal media were washed with medium without glucose twice and transferred to medium where normal glucose was replaced with [U-<sup>13</sup>C]glucose. The cells were grown till exponential phase and transferred to fresh [U-<sup>13</sup>C]glucose medium after washing twice with glucose free medium. This transfer of cells was done thrice to check if there is a possibility of reaching isotopic steady state in proteinogenic amino acids.

Supernatant samples for analysis were taken at regular interval and cellular samples were taken at the end of every cultivation cycle for macromolecular analysis.

***Cell growth characteristics***

The cell growth of all the four cultures is given in Figure 5.5.1 (A). As seen from the Figure all the growth cycles showed similar growth patterns. The specific growth rates are given in Table 5.5.1. The four cultures showed comparable growth.

The uptake of extracellular glucose along with the production of lactate is shown in Figure 5.5.1 (B). As seen, the production and excretion followed similar patterns. Table 5.5.1 gives the rates of the metabolites. With the exception of the last culture, all show comparable rate patterns. The profile of glutamine, the other major energy source besides glucose is given in Figure 5.5.1 (C). Due to the hydrolysis of glutamine, its initial concentration is found to reduce in subsequent cultures, with it approaching limiting proportions in the final culture. The difference in the rates in the final culture is probably due to the limitation of glutamine, which in turn makes to cell reduce the overflow metabolism as seen from a reduced lactate to glucose ratio.

**Table 5.5.1:** Growth rate and uptake rates for glucose and lactate during the 4 cycles of cultivation

	<b>Growth rate (h<sup>-1</sup>)</b>	<b>Glucose Uptake (10<sup>-3</sup> mM/ 10<sup>6</sup>cells h)</b>	<b>Lactate Production (10<sup>-3</sup> mM/ 10<sup>6</sup>cells h)</b>
<b>1st Medium</b>	0.025	0.4275	0.655
<b>2nd Medium</b>	0.03	0.393	0.618
<b>3rd Medium</b>	0.033	0.4455	0.6237
<b>4th Medium</b>	0.03	0.318	0.417

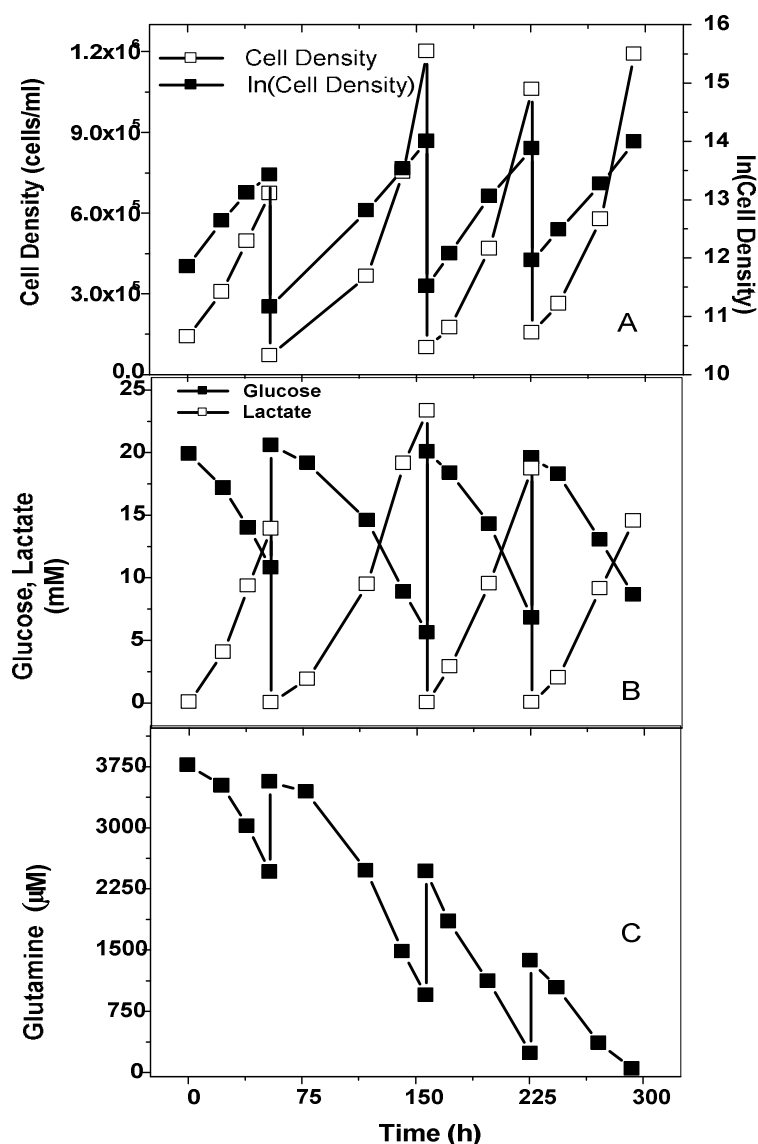


**Figure 5.5.1:** (A) Cell growth of CHO cells during 4 cycles of cultivation. The medium was replaced at time 54 h, 157 h and 226 h. (B) Glucose and lactate profiles during the 4 cultivation cycles for the same cultures shown in Figure 5.5.1 (A). (C) Glutamine profile during the four cultivation cycles for the same cultures shown in Figure 5.5.1 (A).

In the case of amino acids, few did not show linear relationship to glucose consumption rate e.g. aspartate and glutamate. Due to this, only the metabolic quotients on glucose (difference of final and initial concentration) were considered. Figure 5.5.2 depicts the comparative metabolic quotients of the amino acids. Among the amino acids, only aspartate, glutamate, alanine and glycine showed production whereas all the others were consumed.

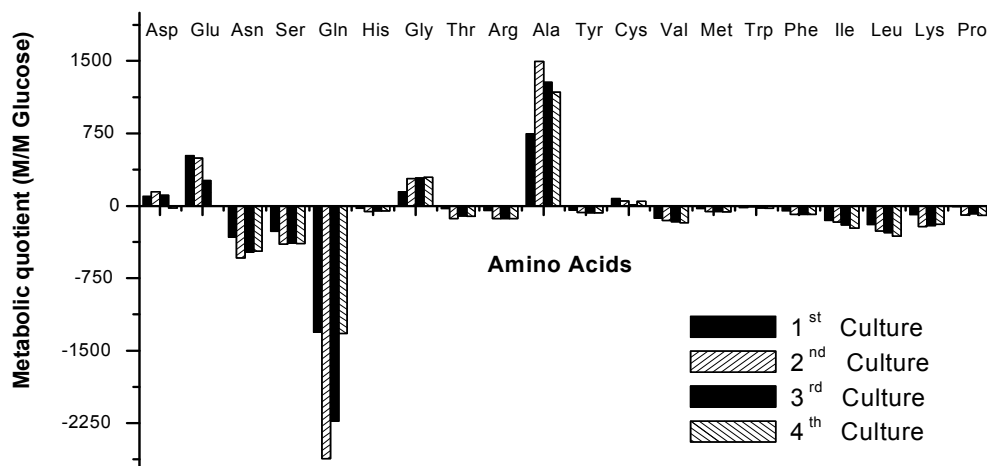


**Figure 5.5.2:** Metabolic quotients of amino acids at the end of each of the four cultivations shown in Figure 5.5.1

Data from the four cultures were combined and the interdependency of the variables was determined by several plots (Figure 5.5.3 A, B & C). The metabolite concentrations were plotted against the corresponding glucose concentrations and a few were also plotted against each other. Yields were determined from the plots using linear regression at two distinct growth phases, at high glucose and at lower glucose concentrations and are shown in Table 5.5.2. The goodness of fit represented by the regression coefficient ( $R^2$ ) is given in the bracket. Except aspartate, glutamate and glutamine all the others show a linear relationship with glucose. Aspartate shows a linear relationship with glutamate probably due to their involvement in the malate - aspartate shuttle. However, aspartate with asparagine, glutamate with glutamine and asparagine with glutamine show no linear relationship. Serine shows a linear relationship with glycine as both the amino acids are related at the biochemical level by the enzyme serine hydroxymethyltransferase. The yields obtained at both the growth phases are comparable for all amino acids showing linear relationships. The non-linear pattern of few amino acids can lead to complications in further analysis and add complexity to further calculations.

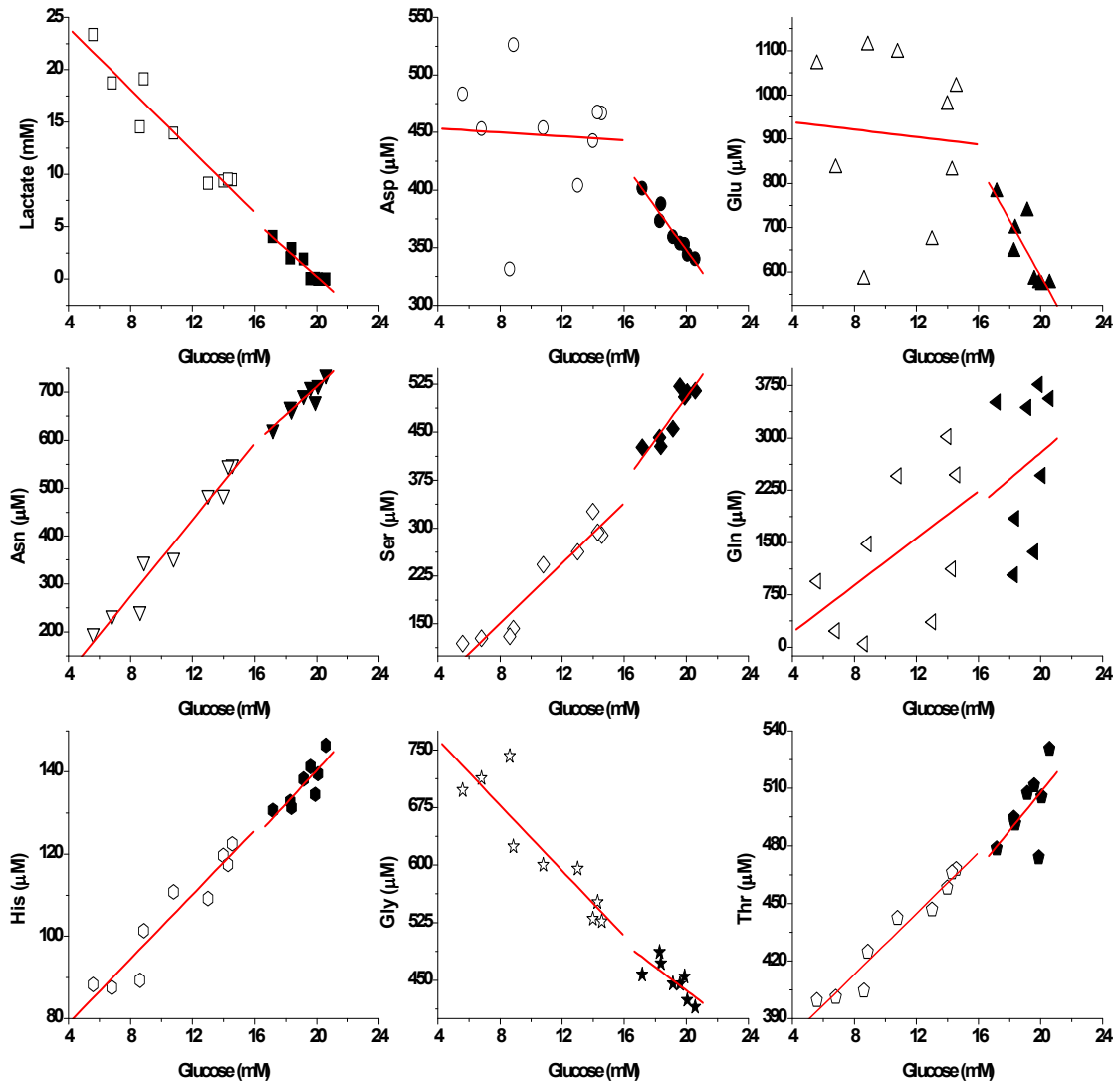


**Figure 5.5.3 (A):** Metabolite concentrations of all the four cultivations plotted against glucose for the four cultures described in Figure 5.5.1. Two separate linear regressions were performed, one for glucose concentrations higher than 15 mM and the other for lower than 15 mM. The closed symbols represent high and the open symbols represent low glucose concentrations.

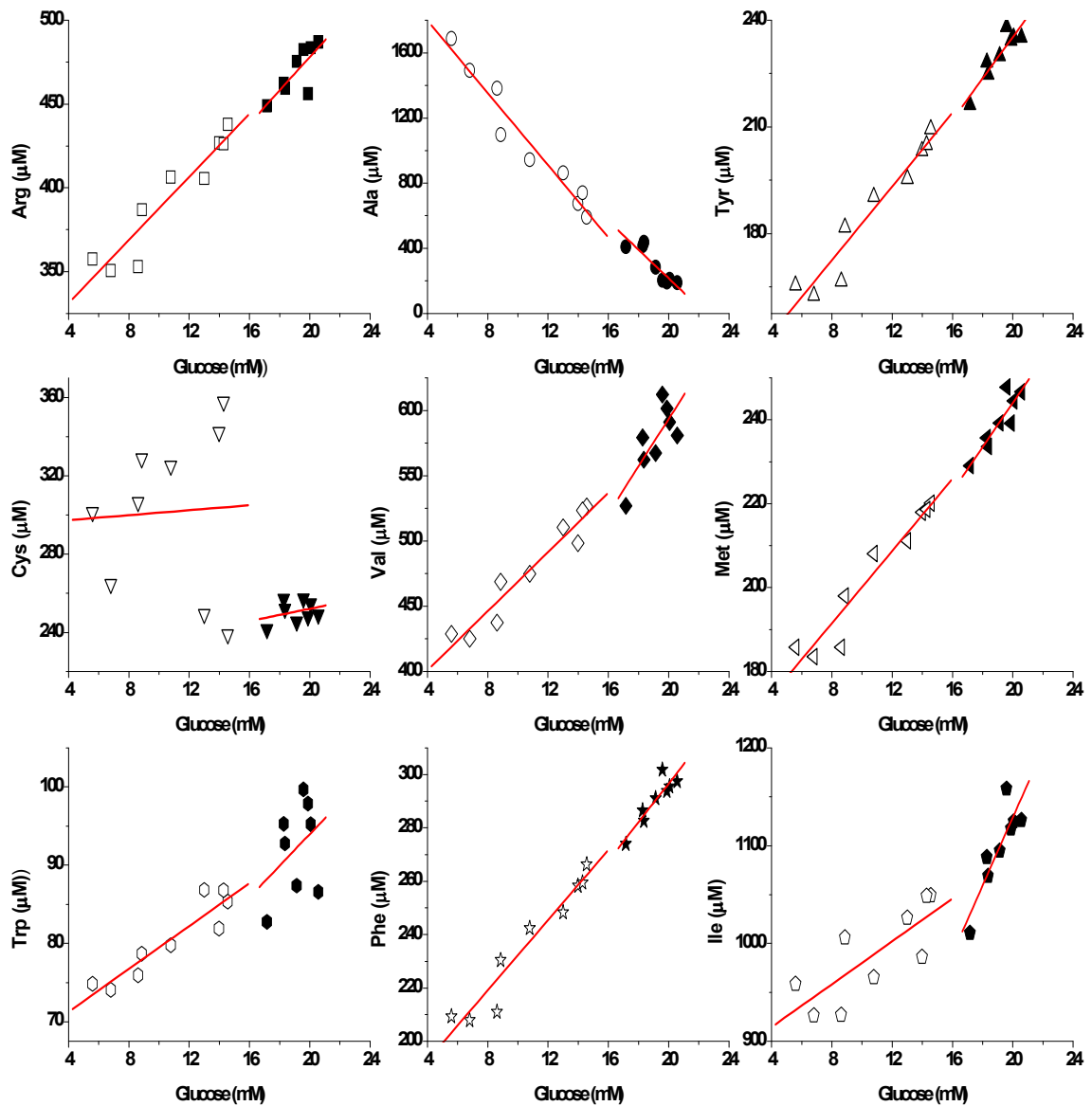


**Figure 5.5.3 (B):** Metabolite concentrations of all the four cultivations plotted against glucose for the four cultures described in Figure 5.5.1. Two separate linear regressions were performed, one for glucose concentrations higher than 15 mM and the other for lower than 15 mM. The closed symbols represent high and the open symbols represent low glucose concentrations.

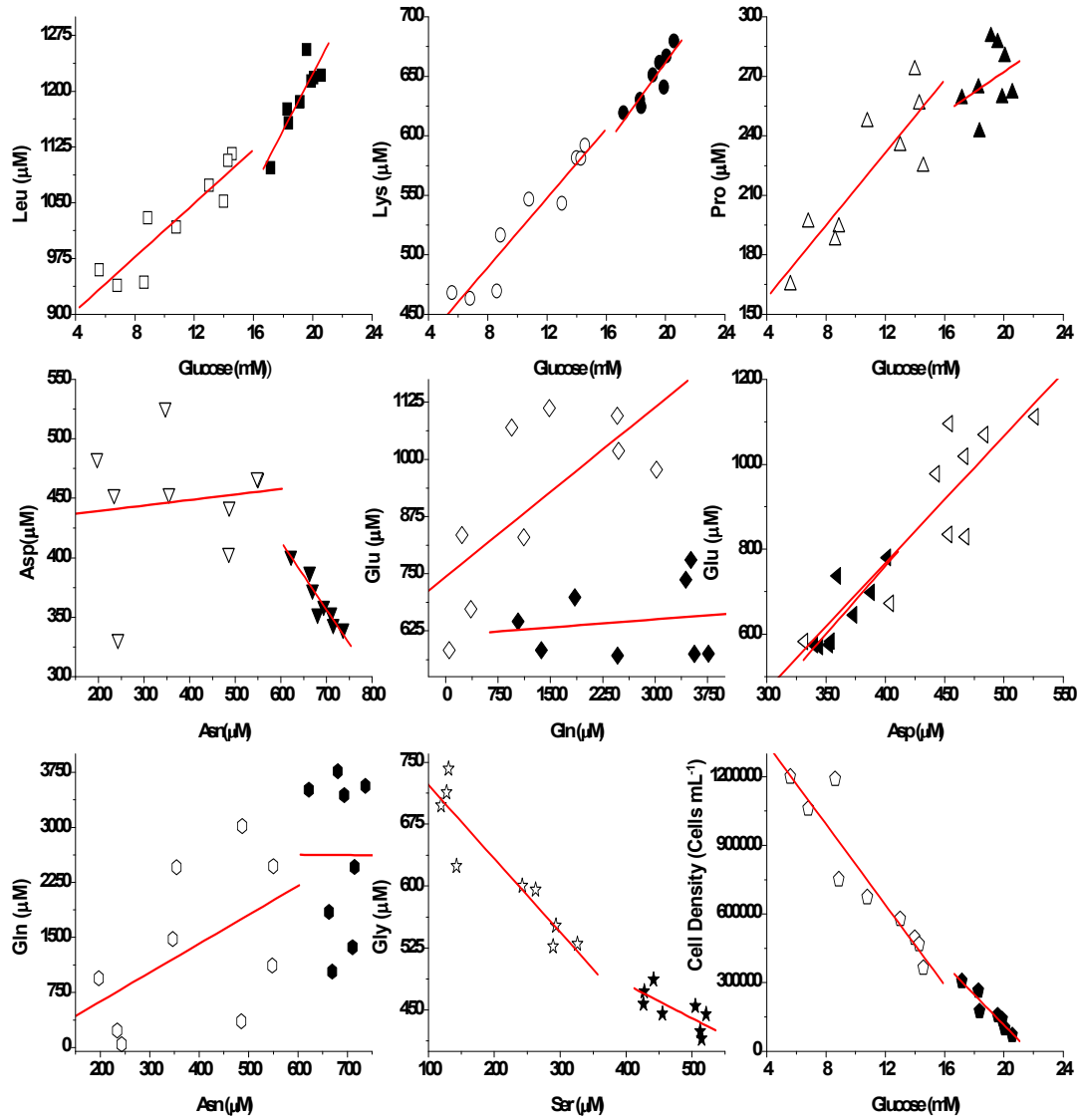


**Figure 5.5.3 (C):** Metabolite concentrations of all the four cultivations plotted against glucose and also a few against each other for the four cultures described in Figure 5.5.1. Two separate linear regressions were performed, one for glucose concentrations higher than 15 mM and the other for lower than 15 mM. The closed symbols represent high and the open symbols represent low glucose concentrations.

**Table 5.5.2:** Yields of the metabolites and cells on glucose at two growth phase with yield 1 at high glucose concentration and yield 2 at lower glucose concentration as represented in the Figure 5.5.3 A, B & C. The goodness of fit ( $R^2$ ) of the linear regression is given in brackets.

<b>Metabolite</b>	<b>Yield 1 (<math>R^2</math>)</b>	<b>Yield 2 (<math>R^2</math>)</b>	<b>Unit</b>
Lactate	-1.3 (0.90)	-1.5 (0.90)	mM/mM Glucose
Asp	-18.7 (0.94)	-0.9 (0.003)	$\mu$ M/mM Glucose
Glu	-62.7 (0.71)	-4.2 (0.006)	$\mu$ M/mM Glucose
Asn	29.6 (0.88)	39.9 (0.95)	$\mu$ M/mM Glucose
Ser	33.4 (0.81)	23.5 (0.91)	$\mu$ M/mM Glucose
Gln	189.9 (0.038)	169.2 (0.28)	$\mu$ M/mM Glucose
His	4.1 (0.70)	3.9 (0.90)	$\mu$ M/mM Glucose
Gly	-15.3 (0.54)	-21.3 (0.81)	$\mu$ M/mM Glucose
Thr	9.9 (0.37)	7.9 (0.94)	$\mu$ M/mM Glucose
Arg	9.9 (0.60)	9.4 (0.89)	$\mu$ M/mM Glucose
Ala	-87.9 (0.81)	-110.9 (0.94)	$\mu$ M/mM Glucose
Tyr	5.8 (0.84)	5.2 (0.93)	$\mu$ M/mM Glucose
Val	10.1 (0.6)	11.3 (0.93)	$\mu$ M/mM Glucose
Met	5.3 (0.81)	4.3 (0.93)	$\mu$ M/mM Glucose
Trp	2.0 (0.14)	1.4 (0.86)	$\mu$ M/mM Glucose
Phe	7.2 (0.82)	6.6 (0.93)	$\mu$ M/mM Glucose
Ile	34.8 (0.77)	11.0 (0.62)	$\mu$ M/mM Glucose
Leu	38.3 (0.79)	18.1 (0.82)	$\mu$ M/mM Glucose
Lys	17.3 (0.81)	14.6 (0.91)	$\mu$ M/mM Glucose
Pro	5.2 (0.13)	9.2 (0.75)	$\mu$ M/mM Glucose
Cells	66.5 (0.90)	88.0 (0.86)	Cells/ $\mu$ M Glucose

***Carbon labeling analysis***

Gas Chromatography- Mass spectrometric (GC-MS) analysis was carried out to determine the mass isotopomers and fractional carbon labeling (FCL) of the samples obtained during the cell cultivation (Wittmann and Heinzle, 1999). The samples were analyzed for the extracellular amino acids, lactate and proteinogenic amino acids. The amino acids which showed  $^{13}\text{C}$  labeling in the extracellular as well as in the proteinogenic samples were alanine, glycine, serine, aspartate and glutamate. This implied that these amino acids were synthesized by the cells. The fractional carbon labeling of the above amino acids in the supernatant with respect to time along with their concentration profile is shown in Figure 5.5.4. Alanine and glycine are secreted in the extracellular medium whereas serine is consumed. Glutamine and aspartate are secreted in the initial phases but consumed during the final phase. Similarly the profile of lactate is also shown in the figure.

It is seen that, with the exception of lactate, none of the others reach a steady state in labeling. All the lactate originating from glucose should have carbon labeling. The fractional carbon labeling of lactate is around 85 %, thus 15 % of lactate comes from carbon sources other than glucose. Since all the amino acids are initially present in the media, they dilute the carbon labeling. Nevertheless, taking into account the initial concentrations of alanine, it is found that an average of 90 % of the alanine over the end of four cultivations is derived from glucose. However, unlike lactate, the fractional labeling of alanine varies with time. The non-steady labeling pattern of other amino acids may be due to their uptake patterns. The pattern of labeling obtained for glutamate is probably influenced by extracellular concentrations of glutamine. Similarly, the labeling of glycine is influenced by serine.

The FCL of proteinogenic amino acids at the end of each growth cycle with comparison to extracellular amino acids is shown in Figure 5.5.5. The lower FCL of proteinogenic amino acids are probably due to the fact that the proteins contain labeling information over the whole growth phase and depend upon their turn over rate. With the exception of alanine and serine, none of the amino acids display steady states in the proteinogenic labeling thus showing that it is difficult to reach isotopic steady states by repetitive cultivations. This further supports the fact that there must be an improvement in the cultivation conditions to reduce the complexity of flux analysis. This was done by modifying the media.

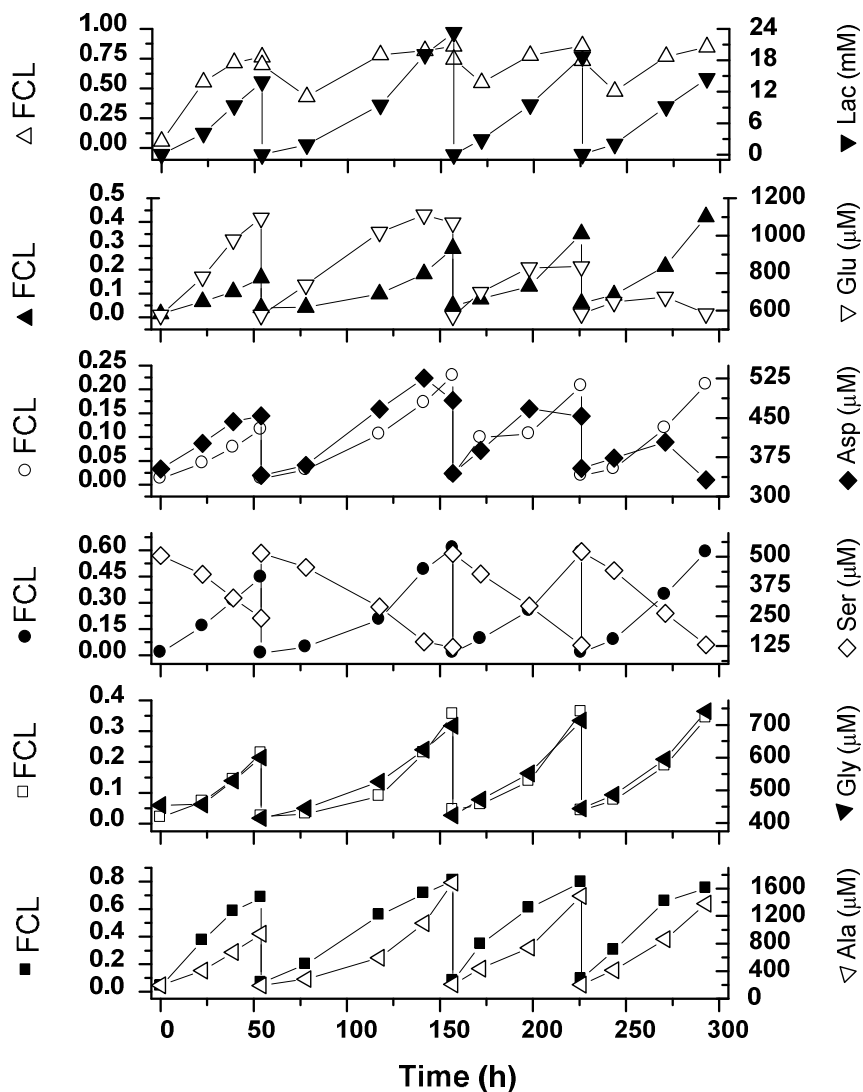


**Figure 5.5.4:** Extracellular metabolite labeling plotted along with extracellular concentration profile for the four cell cultivations in  $[\text{U-}^{13}\text{C}]$ glucose containing media described in Figure 5.5.1. The right axis gives the concentration and the left axis the fractional carbon labeling of the metabolite indicated on the right axis. The sampling procedure is given in material and methods. The initial time “0” refers to the sample after the addition of media to cells.

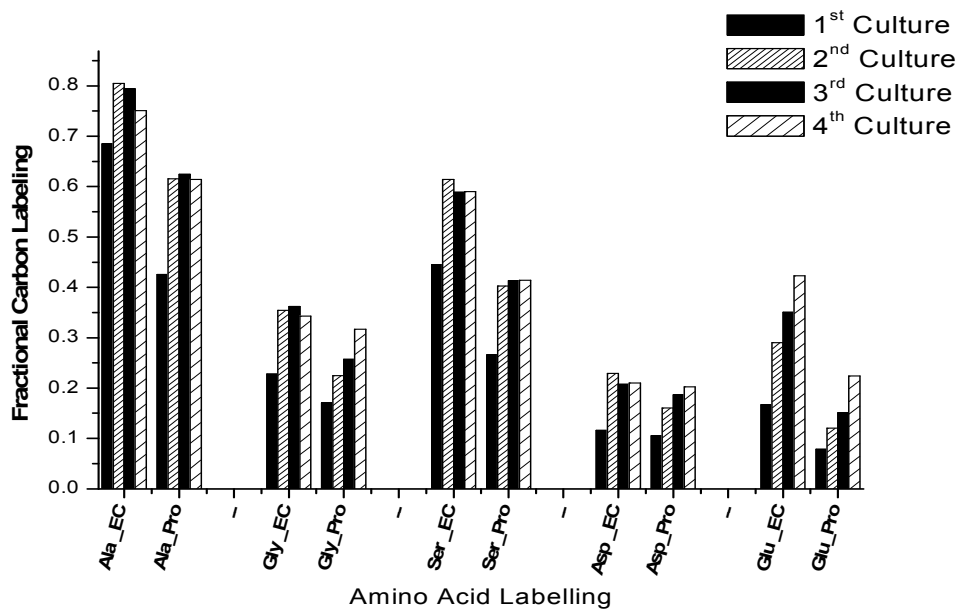


**Figure 5.5.5:** Comparison of FCL from proteinogenic amino acid (Pro) with the extracellular amino acids (EC) at the end of each cycle of cultivation shown in Figure 5.5.1.

### 5.5.2.3 Media optimization for flux calculation

Both essential and non-essential amino acids are required for protein synthesis. The essential amino acids are supplied in the media as they are not synthesized by the cells. Non-essential amino acids, depending on the metabolism can be synthesized by the cell. Generally, most of the cell culture media contain all the 20 amino acids in significant amounts. From the data in the previous section, it is seen that there is a consumption of most amino acids (Asn, Ser, Gln, His, Thr, Arg, Tyr, Cys, Val, Met, Tyr, Phe, Ile, Leu, Lys, Pro) regardless of being essential or non-essential. From the labeling in the proteinogenic amino acids as well as in the extracellular media of cells grown in [U-<sup>13</sup>C]glucose, it can be seen that although most of them are catabolic few of the non-essential amino acids though consumed are also anabolic. From the yield and labeling data, amino acids like Asp, Glu, Ser, Gly and Ala are found to be anabolic. However, the fact that the amino acids aspartic acid, glutamic acid and serine are consumed, and also found to have labeling in the extracellular medium leads to the conclusion that there is continuous exchange between the intracellular and extracellular metabolites. This exchange can lead to problems in the calculation of fluxes.

#### *Cell growth in amino acid depleted media*

To study if the cells can potentially show similar growth with the reduction or removal of the above components, the media was altered and the cell growth monitored. The cells were grown in media containing a progressive decrease of the above labeled amino acids (**LAA**: Asp, Glu, Ser, Gly and Ala). Thus a series of media were prepared containing 50 %, 10 % and 1 % of the normal amounts of LAA. Also a media with none of the above amino acids was prepared. Figure 5.5.6 (A) shows the series of growth curves in the various media. The initial cell density used for the normal media, 50 % and 10 % was different from the initial cell density used for 1 % and media without LAA since the cell growth were performed separately in two sets of experiments. Figure 5.5.6 (B) shows the specific growth rate of the cells in the various media. As seen from the figure, the growth rate is very similar in all the media. Since the cells also grow in the amino acid deficient medium it can be deduced that they are able to produce the amino acids required for their biosynthetic needs. Hence further experiments were conducted using the media without the LAA (i.e. Asp, Glu, Ser, Gly and Ala).

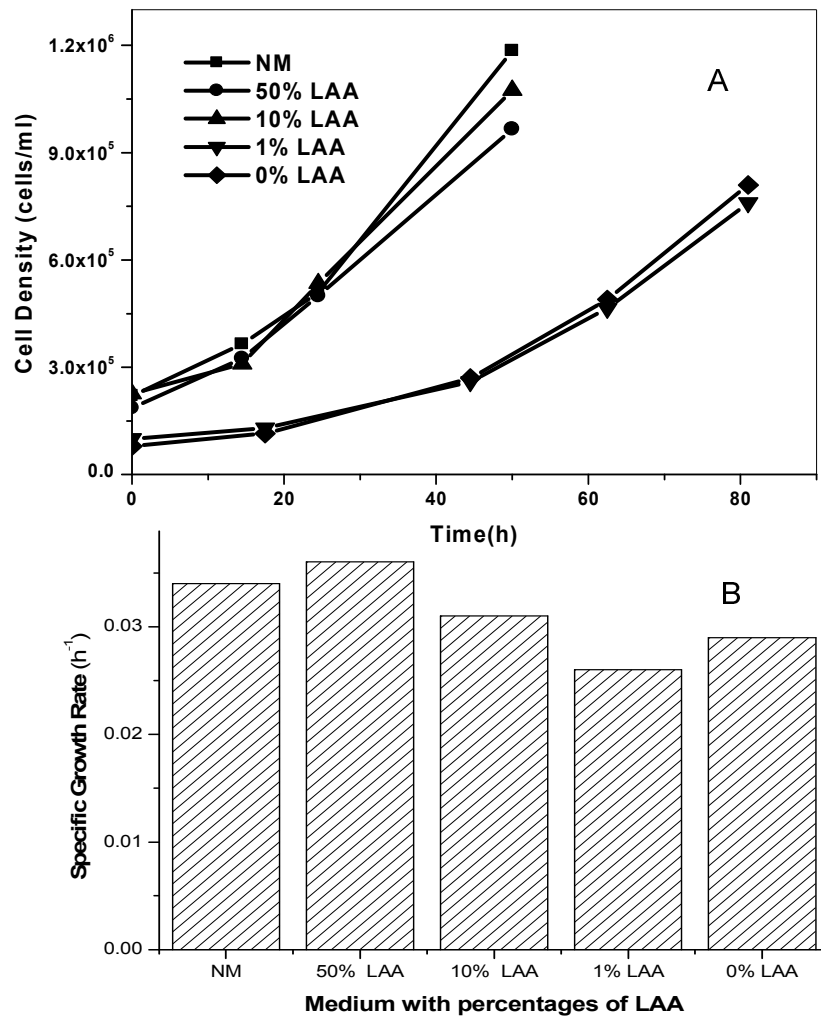


**Figure 5.5.6:** (A) Comparison of cell growth with reduced levels of the labeled amino acids (LAA: Asp, Glu, Ser, Gly and Ala) in media. (B) Growth rates of CHO cells with reduced levels of the labeled amino acids (LAA) in media.

### *Cell growth characteristics with modified media*

The cells were grown in the modified medium containing [U-<sup>13</sup>C]glucose and without the LAA's in parallel with cells grown in normal media, i.e. one containing all the amino acids. On reaching the exponential phase the cells were transferred to fresh medium after washing twice with no glucose containing medium. Thus the cells were grown for two batch cycles in the spinner flasks. Figure 5.5.7 (A) shows the comparison of growth between the modified medium with normal medium. The cells show similar growth pattern and the growth rates are comparable for the growth in modified media and that in the normal media; 0.027 h<sup>-1</sup> and 0.028 h<sup>-1</sup> for the first culture and 0.031 h<sup>-1</sup> and 0.031 h<sup>-1</sup> for the second culture, respectively. Figure 5.5.7 (B) compares glucose, lactate and pyruvate profiles. The average lactate to glucose ratio (mol/mol) for cells grown in the modified medium (1.84) is higher than for that grown in normal medium (1.54) and also corresponds to higher lactate yield. The corresponding specific rates are given in Table 5.5.3 and found to be higher in the modified medium. The uptake rates of glutamine and asparagine were also found to be slightly higher in the modified medium. This is possibly due to the absence of aspartate and glutamate in the medium. However, there was a decrease in the alanine yield compared to the normal media.

**Table 5.5.3:** Comparison of uptake and production rates for glucose, lactate, asparagine, glutamine and alanine in the normal media with the modified media, i.e. [U-<sup>13</sup>C]glucose supplied media without LAA.

		Glucose (10 <sup>-3</sup> mM 10 <sup>6</sup> Cells <sup>-1</sup> h <sup>-1</sup> )	Lactate (10 <sup>-3</sup> mM 10 <sup>6</sup> Cells <sup>-1</sup> h <sup>-1</sup> )	Gln (10 <sup>-3</sup> μM 10 <sup>6</sup> Cells <sup>-1</sup> h <sup>-1</sup> )	Asn (10 <sup>-3</sup> μM 10 <sup>6</sup> Cells <sup>-1</sup> h <sup>-1</sup> )	Ala (10 <sup>-3</sup> μM 10 <sup>6</sup> Cells <sup>-1</sup> h <sup>-1</sup> )
Normal Media	1 <sup>st</sup> Culture	-0.23	0.33	-76.02	-13.67	34.79
	2 <sup>nd</sup> Culture	-0.18	0.26	-64.46	-10.91	30.62
U <sup>13</sup> C <sub>6</sub> Media	1 <sup>st</sup> Culture	-0.29	0.48	-86.43	-15.00	32.21
	2 <sup>nd</sup> Culture	-0.25	0.38	-70.33	-13.42	29.09

The most interesting aspect was the extracellular concentration of aspartate and glutamate as seen in Figure 5.5.8 (A). In the medium, the said amino acids were first produced and then consumed towards the end of the cultivation phase. Viewing the extracellular concentration profiles of asparagine and glutamine [Figure 5.5.8 (B)] along with that of aspartate and glutamate, it is seen that the uptake of aspartate and glutamate correspond to the low levels of asparagine and glutamine present in the medium during the end of the cultivation phase. Thus the consumption might be related to the depletion of the above amino acids.

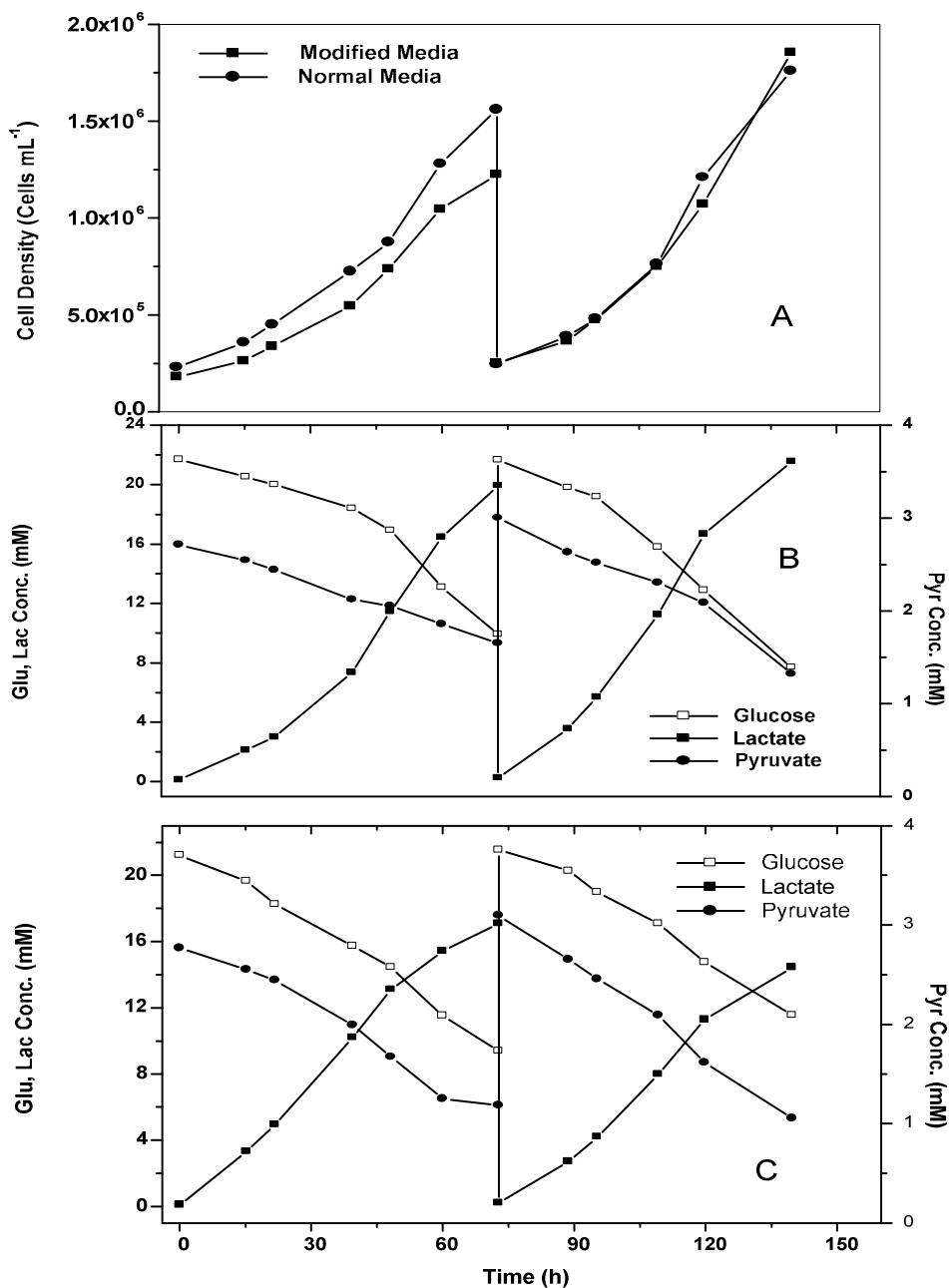


**Figure 5.5.7:** (A) Comparison of cell growth of CHO cells in modified media with [U-<sup>13</sup>C]glucose and original media during two cultivation cycles. (B) Glucose, lactate and pyruvate profiles during the 2 cultivation cycles of CHO cells in modified media with [U-<sup>13</sup>C]glucose. (C) Glucose, lactate and pyruvate profiles during the 2 cultivation cycles of CHO cells in original media

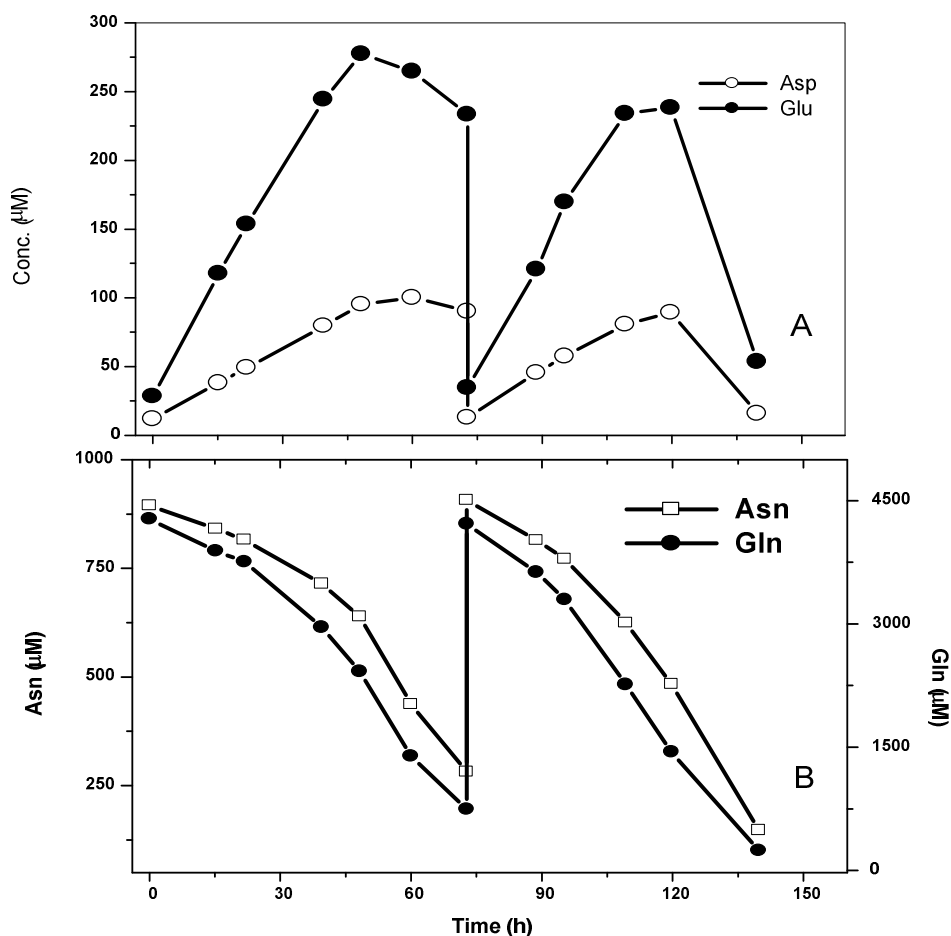


**Figure 5.5.8:** (A) Aspartate and glutamate profiles during the 2 cultivation cycles of CHO cells in modified media with  $[\text{U-}^{13}\text{C}]$ glucose showing their consumption during the latter stages of growth. (B) Asparagine and glutamine profiles during the 2 cultivation cycles of CHO cells in modified media with  $[\text{U-}^{13}\text{C}]$ glucose.

Similar to the previous section, the metabolite concentrations were plotted against the corresponding glucose concentrations and also against each other (Figure 5.5.9). The plots of serine, glycine, aspartate and glutamate show two distinct phases. At high glucose concentration the linear regression on the plot of aspartate with asparagine and glutamate with glutamine gives a positive slope whereas at low glucose it gives a negative slope [Figure 5.5.9(C)]. This is due to the consumption as aspartate and glutamate towards the end of the cultivation whereas glutamine and asparagine are continuously consumed. In the normal medium, serine was consumed and glycine was produced whereas in the modified medium both serine and glycine were found to be secreted in the medium initially and then consumed at the end of the cultivation. The secretion and consumption pattern of the two amino acids are found to be related as seen from the plot of serine against glycine [Figure 5.5.9(C)]. Yields

were determined from the plots using linear regression at two distinct growth phases, at high glucose concentration and at lower glucose concentrations and are shown in Table 5.5.4. Similar to their plots, the yields of aspartate, glutamate, serine and glycine show two distinct phases due to their uptake at the end of the cultivation. This pattern might be due to the limitation of asparagine and glutamine towards the end of the batch cultivation. This is also seen in the yield of lactate, where the overflow metabolism is reduced significantly. Looking at the cellular yield, it is clearly seen that there is efficient utilization of glucose resulting in a significantly higher yield of cells.

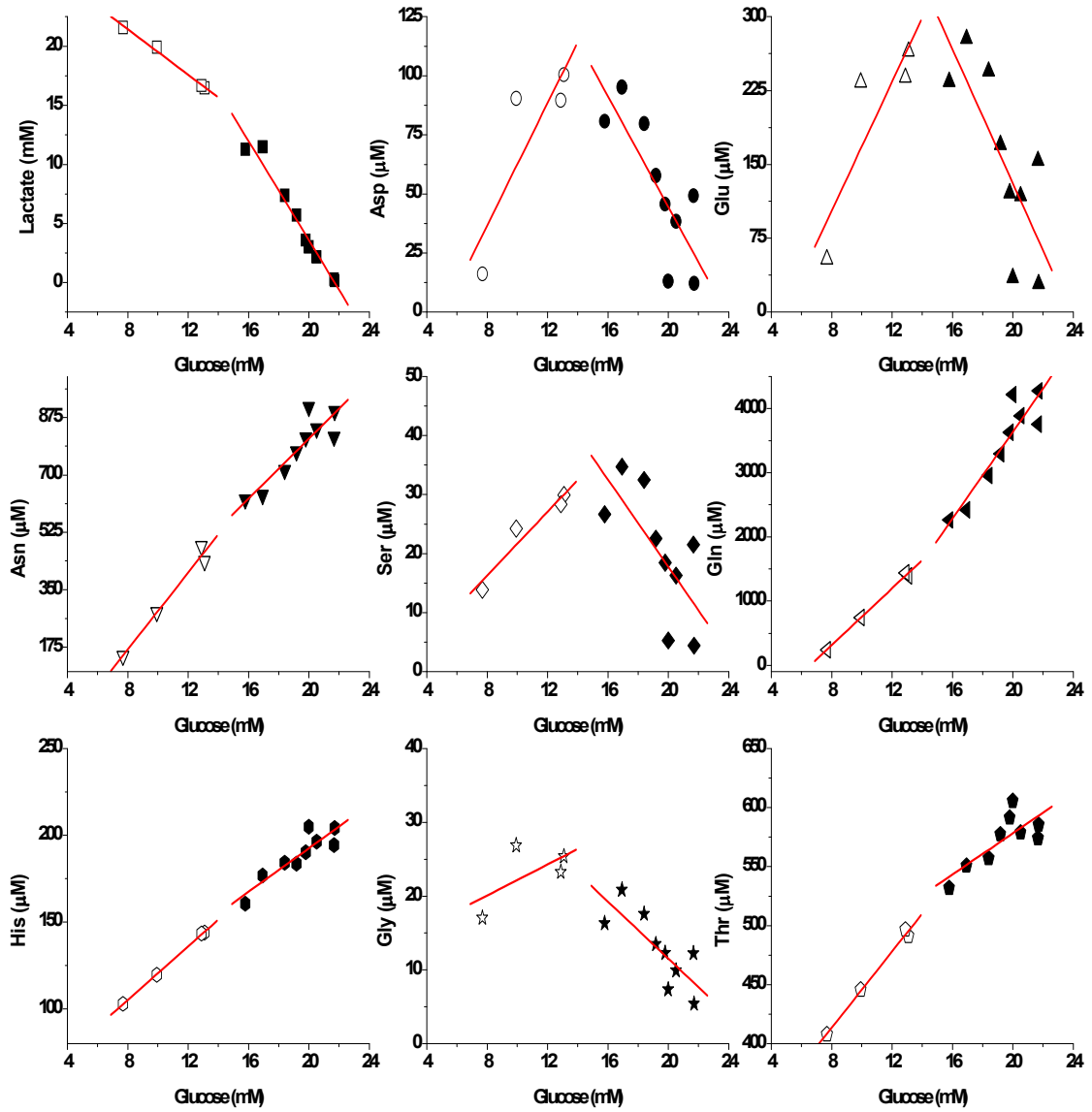


**Figure 5.5.9 (A):** Metabolite concentrations of the two cultivations in modified medium described in Figure 5.5.8 plotted against glucose. Two separate linear regressions were performed, one for glucose concentrations higher than 15 mM and the other for lower than 15 mM. The closed markers indicate the concentrations at high glucose concentration whereas the open symbols indicate low glucose concentration.

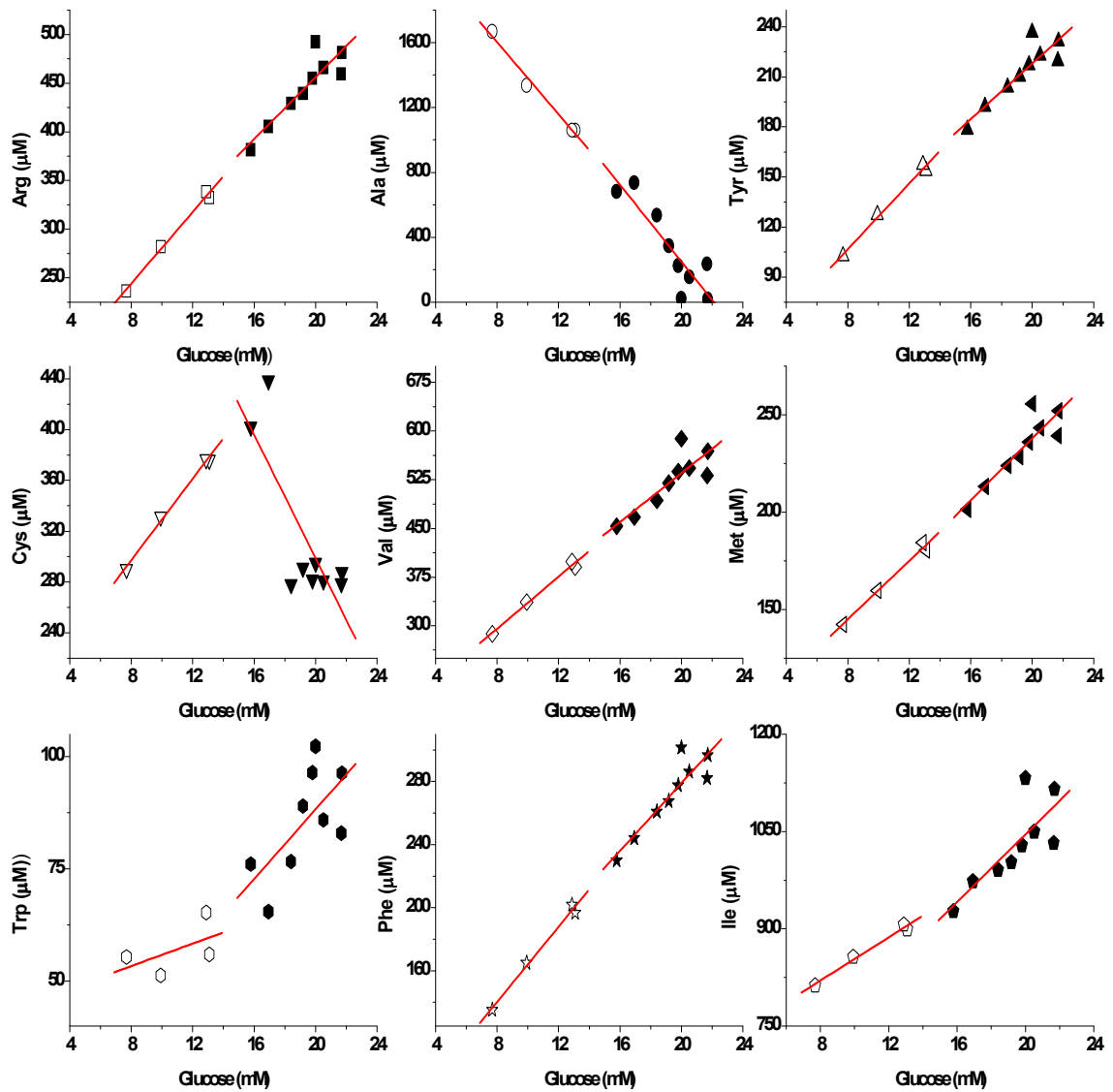


**Figure 5.5.9 (B):** Metabolite concentrations of the two cultivations in modified medium described in Figure 5.5.8 plotted against glucose. Two separate linear regressions were performed, one for glucose concentrations higher than 15  $\text{mM}$  and the other for lower than 15  $\text{mM}$ . The closed markers indicate the concentrations at high glucose concentration whereas the open symbols indicate low glucose concentration.

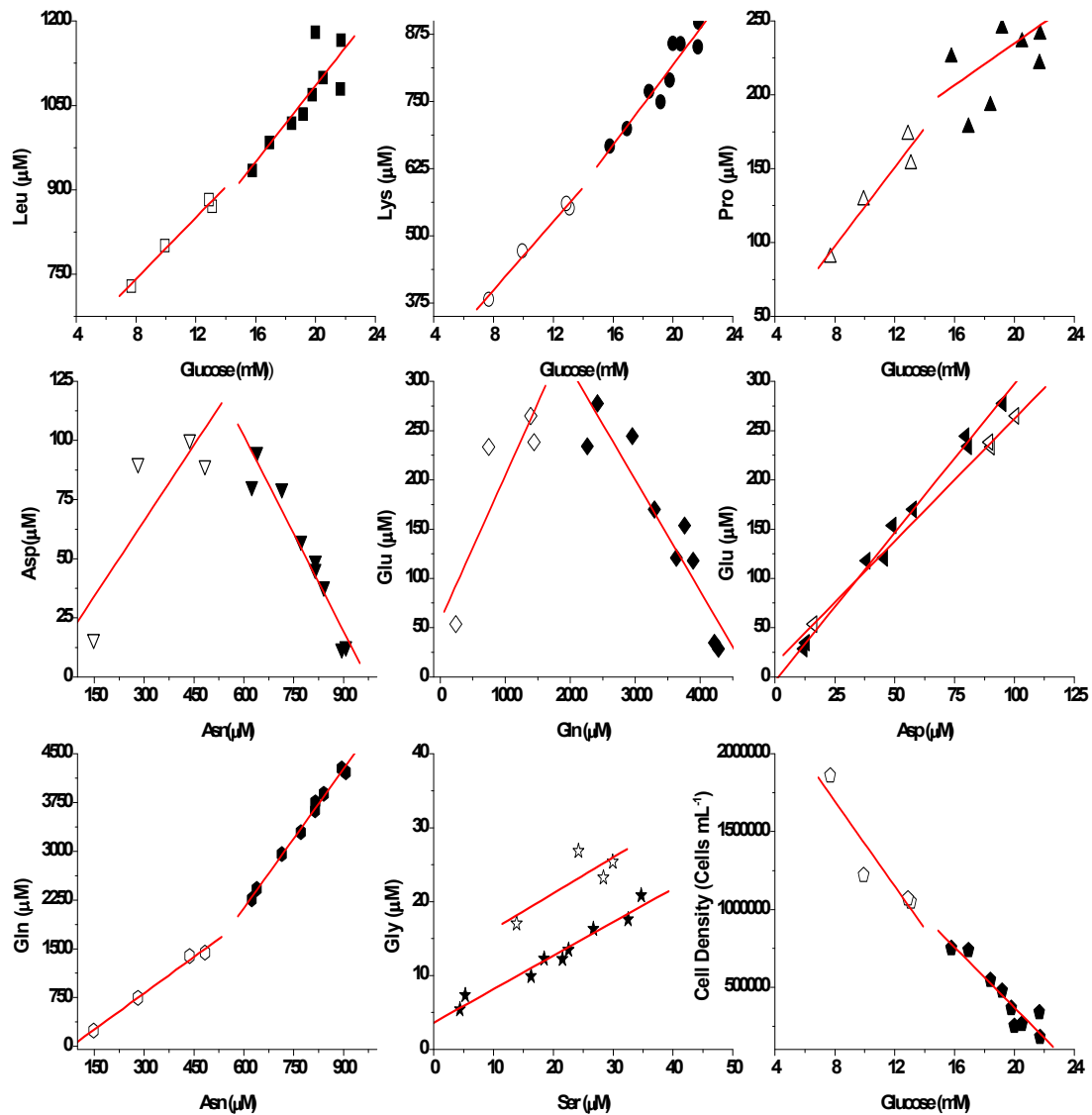


**Figure 5.5.9 (C)** Metabolite concentrations of the two cultivations in modified medium described in Figure 5.5.8 plotted against each other. Two separate linear regressions were performed, one for glucose concentrations higher than 15 mM and the other for lower than 15 mM. The closed markers indicate the concentrations at high glucose concentration whereas the open symbols indicate low glucose concentration.

**Table 5.5.4:** Yields of the metabolites and cells on glucose at two growth phase with yield 1 at high glucose concentration and yield 2 at lower glucose concentration as represented in the Figure 5.5.9 A, B & C. The goodness of fit ( $R^2$ ) of the linear regression is given in brackets.

<b>Metabolite</b>	<b>Yield 1 (<math>R^2</math>)</b>	<b>Yield 2 (<math>R^2</math>)</b>	<b>Unit</b>
Lactate	-2.1 (0.98)	-1.0 (0.99)	mM/mM Glucose
Asp	-11.7 (0.80)	12.9 (0.85)	$\mu$ M/mM Glucose
Glu	-34.1 (0.77)	32.8 (0.87)	$\mu$ M/mM Glucose
Asn	45.7 (0.89)	58.6 (0.99)	$\mu$ M/mM Glucose
Ser	-3.7 (0.69)	2.7 (0.96)	$\mu$ M/mM Glucose
Gln	338.4 (0.92)	221.1 (0.99)	$\mu$ M/mM Glucose
His	6.3 (0.90)	7.7 (0.99)	$\mu$ M/mM Glucose
Gly	-1.9 (0.79)	1.1 (0.63)	$\mu$ M/mM Glucose
Thr	8.8 (0.78)	16.1 (0.99)	$\mu$ M/mM Glucose
Arg	16.0 (0.9)	18.4 (0.99)	$\mu$ M/mM Glucose
Ala	-118.6 (0.89)	-111.0 (0.99)	$\mu$ M/mM Glucose
Tyr	8.3 (0.90)	9.9 (0.99)	$\mu$ M/mM Glucose
Val	18.9 (0.85)	20.0 (0.99)	$\mu$ M/mM Glucose
Met	7.9 (0.90)	7.5 (0.99)	$\mu$ M/mM Glucose
Trp	3.9 (0.66)	1.3 (0.54)	$\mu$ M/mM Glucose
Phe	10.7 (0.91)	11.9 (0.99)	$\mu$ M/mM Glucose
Ile	26.0 (0.80)	16.6 (0.99)	$\mu$ M/mM Glucose
Leu	33.9 (0.86)	27.3 (0.99)	$\mu$ M/mM Glucose
Lys	37.1 (0.95)	31.9 (0.99)	$\mu$ M/mM Glucose
Pro	7.1 (0.47)	13.3 (0.96)	$\mu$ M/mM Glucose
Cells	97.1 (0.93)	13.6 (0.92)	Cells/ $\mu$ M Glucose

***Carbon labeling analysis***

Similar to previous section, GC-MS analysis was carried out to determine the mass isotopomers and fractional carbon labeling (FCL) of the samples obtained during the cell cultivation. The profiles of the metabolites substrates are shown in Figure 5.5.10. In contrast to the previous medium, with the exception of aspartate and glutamate all the metabolites approach steady state in the modified medium. This is clearly a marked improvement above the previous medium since it reduces the complexity of the biochemical model.

The fractional carbon labeling of lactate is around 80 % and 17 % of lactate comes from carbon sources other than glucose. Fully labeled lactate forms 75 % of the total lactate and thus the rest of the labeling (7 %) must be derived from the formation of pyruvate from the TCA cycle. Serine has a fully labeled fraction of 88 %, since the production of serine is mostly in the top part of the glycolysis. Around 5 % of serine is found to be formed from non-labeled carbon sources. In comparison, glycine, which is derived from serine, has a fractional labeling of 81 % and with 17 % unlabeled fraction. This might be due to the intracellular partitioning of glycine and serine metabolism or due to other metabolic pathways related to the anabolism of these amino acids. There is evidence that the major fraction of glycine originates from the mitochondrial pool of serine in CHO cells (Narkewicz et al., 1996). The labeling of alanine is only 70 % compared to the 80 % of lactate. Thus there is an increased non-glucose production of alanine. This is in contrast to the earlier medium where the glucose produced alanine was higher than lactate. Of the above, 60 % is fully labeled and therefore 10 % of alanine is originating from the TCA cycle. This might support the theory of the presence of two pyruvate pools in mammalian cells (Peuhkurinen et al., 1983). The pattern of labeling obtained for glutamate and aspartate is influenced by extracellular concentrations of glutamine and asparagine, respectively. Studying the mass isotopomers of aspartic acid; 15 % is  $^{13}\text{C}_3$  and, 20 % of each are the  $^{13}\text{C}_2$  and  $^{13}\text{C}_1$  isotopomers. It implies that pyruvate enters the TCA cycle via both, the pyruvate carboxylase and the pyruvate dehydrogenase routes.  $^{13}\text{C}_3$  aspartate is derived from  $^{13}\text{C}_3$  oxaloacetate which in turn is formed via the pyruvate carboxylase route without the loss of carbon atoms.  $^{13}\text{C}_2$  and  $^{13}\text{C}_1$  aspartate are formed when there is a loss of carbon atoms from pyruvate via the pyruvate dehydrogenase route.

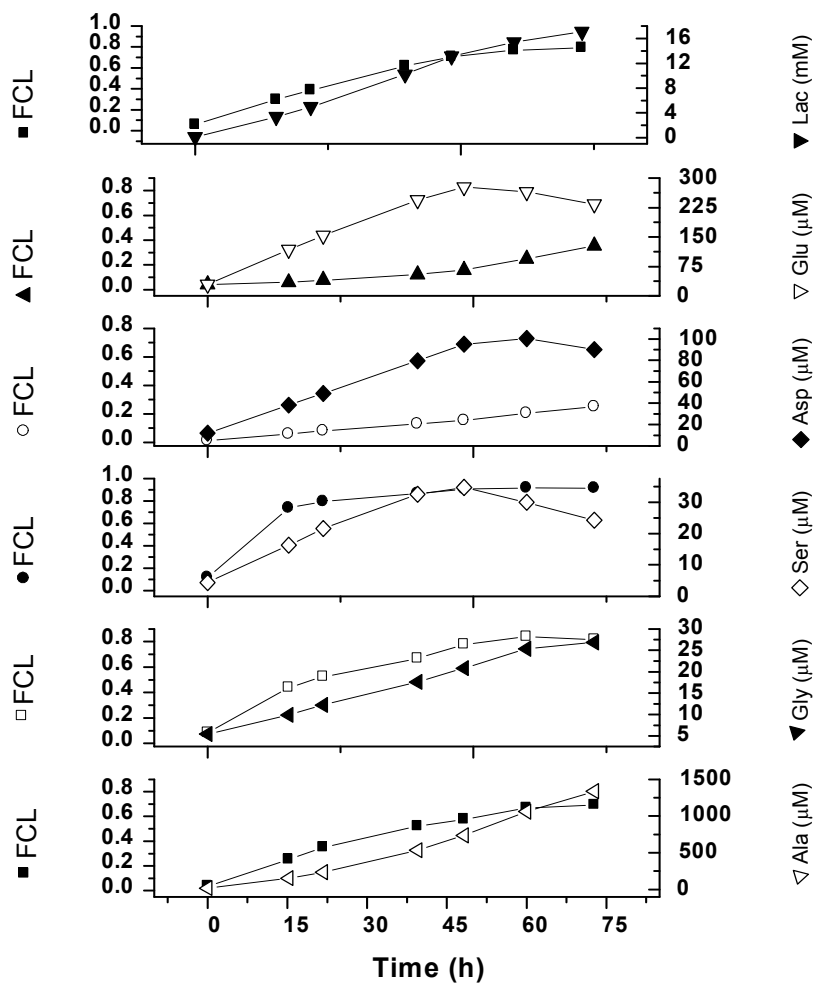


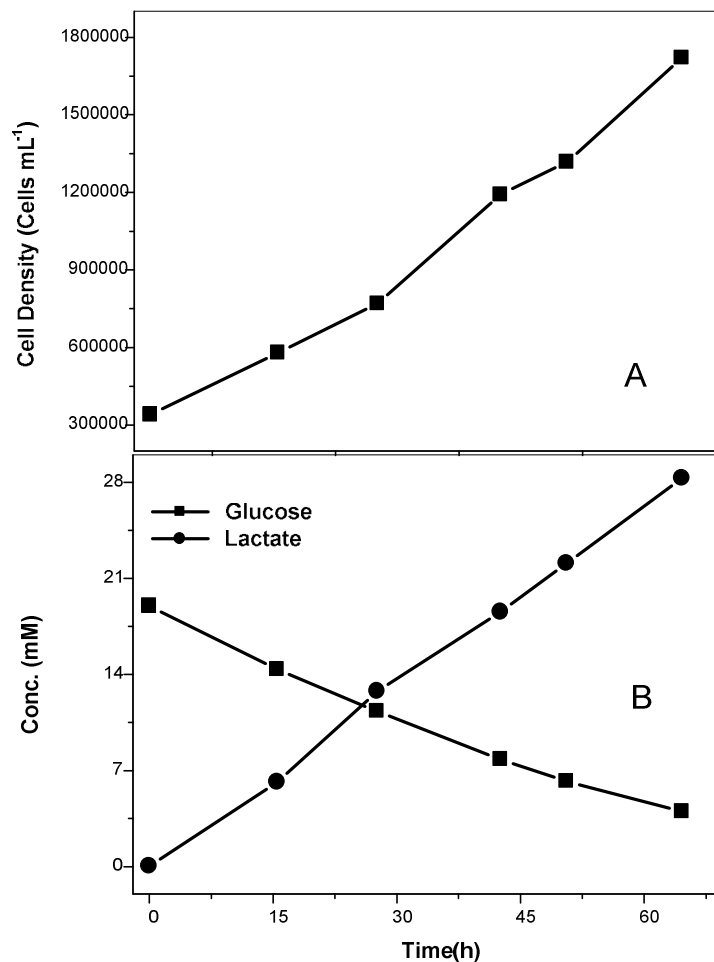
**Figure 5.5.10:** Extracellular substrate labeling plotted along with extracellular concentration profile during the cell growth. The right axis gives the concentration and the left axis the fractional carbon labeling of the metabolite indicated on the right axis. The sampling procedure is given in material and methods. The initial time “0” refers to the sample after the addition of media to cells.

#### **5.5.2.4 [U-<sup>13</sup>C]Glucose study with optimized media**

The media, in which the cells were grown without the anabolic amino acids, though an improvement, nevertheless had the shortcoming of glutamine and asparagine limitation, which was probably responsible for the consumption of aspartate, glutamine and serine towards the end of the batch cultivation. This meant that for the prevention of the consumption, the cells would have to be harvested at a much earlier time point. This would lead to fewer cells to be available for analysis. However, in this case, it was decided to try to supplement the media with an increased amount of asparagine and glutamine. This was done to see if the actual consumption of the few anabolic amino acids were indeed due to the limitation and if the said consumption could be prevented by the use of this strategy. To achieve this, the concentrations of asparagine and glutamine were increased by half their original concentrations in the media.

#### ***Cell growth characteristics for optimized media***

The cells were grown in the medium supplemented with increased amount of asparagine and glutamine containing [U-<sup>13</sup>C]glucose. The cell growth is shown in Figure 5.5.11 (A) and has a specific growth rate of 0.026 h<sup>-1</sup> which is very similar to the growth rates obtained earlier. The glucose and lactate show similar profiles as in earlier media [Figure 5.5.11 (B)] and the lactate to glucose ratio is 1.72, which is normal under the conditions. Thus the cells show normal physiology with regard to growth in the new media.



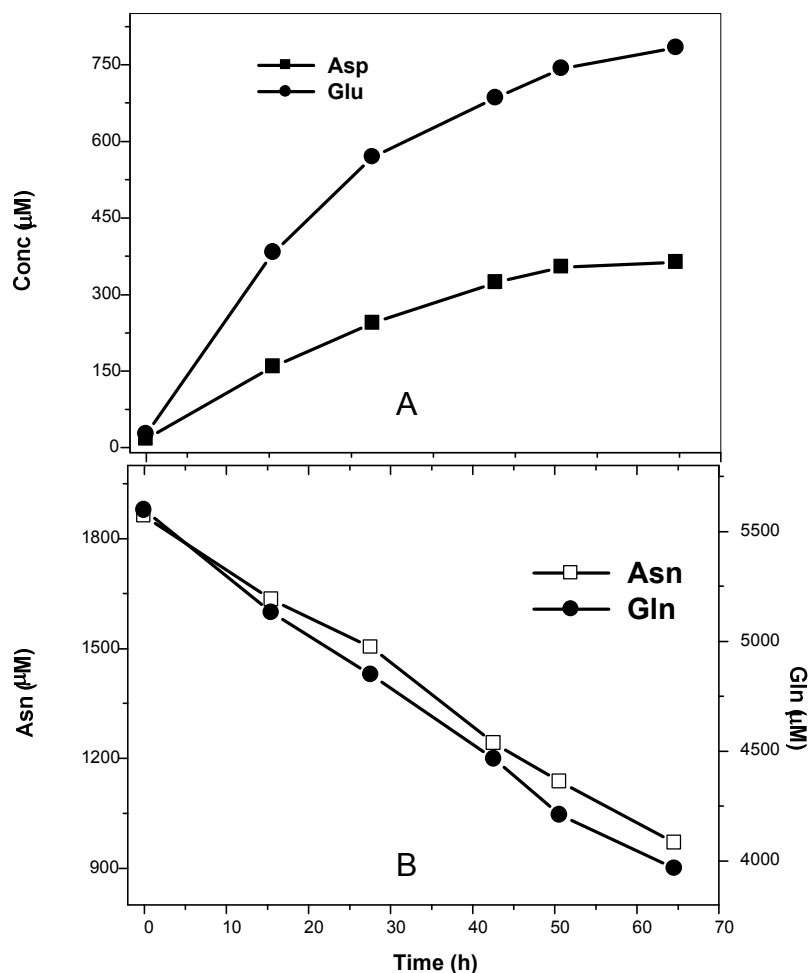
**Figure 5.5.11:** (A) Cell growth of CHO cells in optimized media with [U-<sup>13</sup>C]glucose. (B) Glucose and lactate profiles of CHO cell growth in optimized media.

Table 5.5.5 shows the specific rates of the major metabolites. There is an increase in the rates of both lactate and glucose compared to the rates shown in Table 5.5.3 for the previous medium. The metabolism of glutamine and asparagine are inter-related (Mancuso et al., 1998). In comparison to the previous media, glutamine consumption is decreased and asparagine is increased. However, the precise reasons for this have to be further investigated. Also the production of alanine is higher. This might be due to increased metabolism of the amino acids via the TCA cycle leading to the production of alanine from pyruvate.

**Table 5.5.5:** Uptake and production rates for glucose, lactate, asparagine, glutamine and alanine in the optimized media:

Glucose ( $10^{-3}$ mM $10^6$ Cells $^{-1}$ h $^{-1}$ )	Lactate ( $10^{-3}$ mM $10^6$ Cells $^{-1}$ h $^{-1}$ )	Gln ( $10^{-3}$ $\mu$ M $10^6$ Cells $^{-1}$ h $^{-1}$ )	Asn ( $10^{-3}$ $\mu$ M $10^6$ Cells $^{-1}$ h $^{-1}$ )	Ala ( $10^{-3}$ $\mu$ M $10^6$ Cells $^{-1}$ h $^{-1}$ )
-0.37	0.63	-44.7	-23.4	87.5

The concentrations of asparagine and glutamine along with asparatate and glutamate are shown in Figure 5.5.12. There is no limitation of glutamine and asparagine and also no consumption of glutamate and asparatate. This implies that the strategy of using increased concentration of asparagine and glutamine is successful to avoid the re-consumption. This is also seen in the case of serine which shows no consumption at the end, unlike in the previous media.



**Figure 5.5.12:** (A) Aspartate and glutamate consumption profiles of CHO cells in optimized media with  $[U-^{13}C]$ glucose. (B) Asparagine and glutamine consumption profiles of CHO cells in optimized media with  $[U-^{13}C]$ glucose.

Plots of the metabolites were made as in the previous sections and are shown in Figure 5.5.13. Unlike in the other media, the amino acids showed consistent behavior with regard to their uptake or secretion. Aspartate, glutamate, serine, glycine and alanine were secreted while the rest were consumed. The formation of glycine was found to be higher during the later stages of growth. For a comparison with the previous media, the growth was assumed to be in two phases; one at high glucose concentration and the other at lower glucose concentration. Since, there was only a single sample point above the concentration of 15 mM of glucose; 10 mM was taken as the cut off point. Linear regression was performed on the two phases and is shown in the figure. Table 5.5.6 shows the yields of the various metabolites on glucose at the two phases. The value in the bracket indicates the regression coefficient. The regression at the second phase could not be calculated because only two points are available for each metabolite. It is seen that at later phases, there is an excess of lactate production going up to a lactate to glucose ratio of 2.24. This is in complete contrast to the results obtained with the earlier media, where there was a reduction in the overflow metabolism due to decreased amounts of glucose. The possible explanation might be the presence of excess glutamine in the media since the metabolism of glutamine and glucose have been found to be complimentary except at low concentrations (Ljunggren and Haggstrom, 1992; Jeong and Wang, 1994; Neermann and Wagner, 1996). This is also seen in the previous medium where there is a reduction in the glutamine yield corresponding with reduction in the overflow metabolism. Also, the biomass yield is reduced due to the excess consumption of glucose.

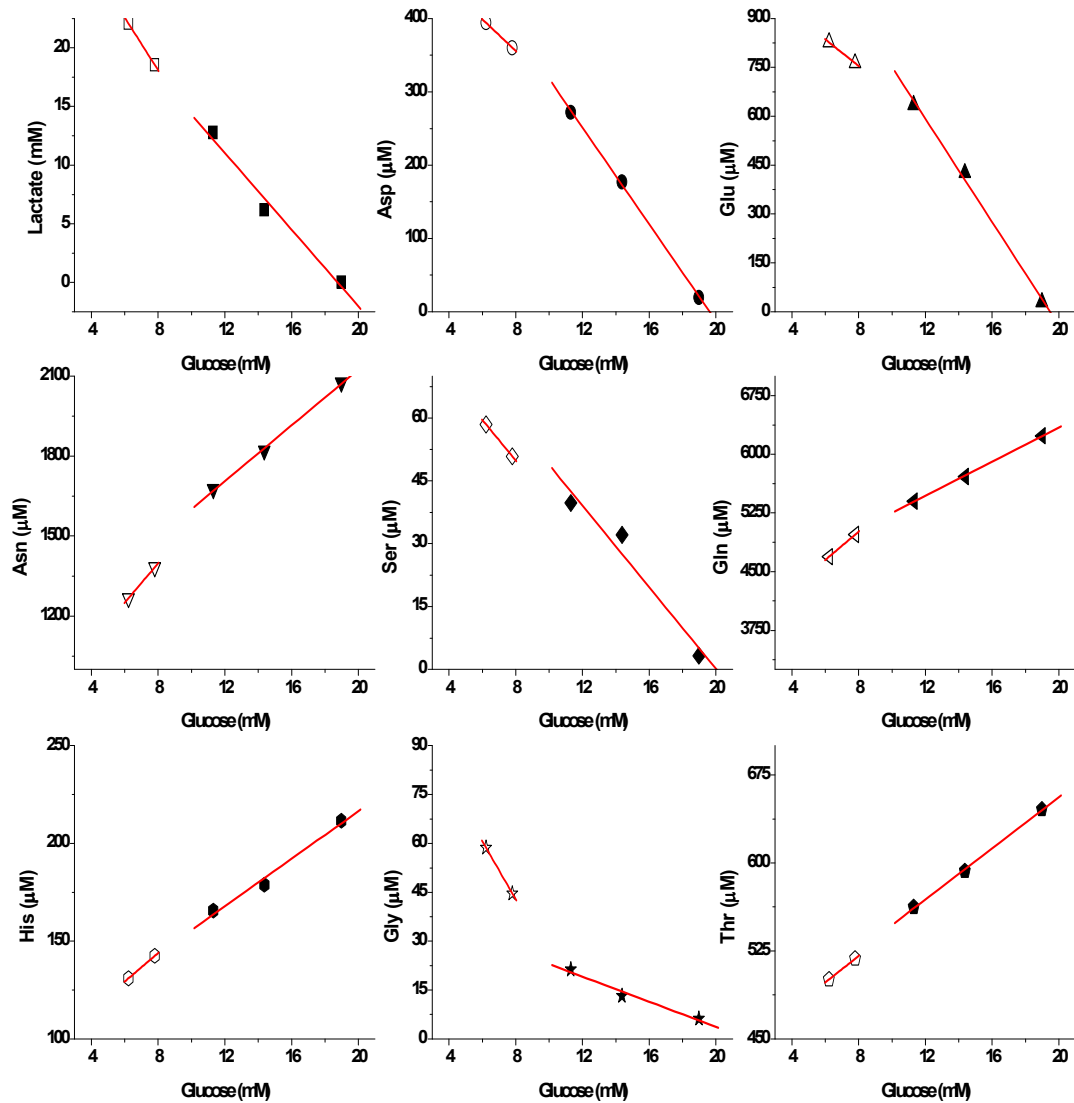


**Figure 5.5.13 (A):** Metabolite concentrations of the cell cultivation plotted against glucose. Two separate linear regressions were performed, one for glucose concentrations higher than 10 mM and the other for lower than 10 mM. The closed markers indicate the concentrations at high glucose concentration whereas the open symbols indicate low glucose concentration.

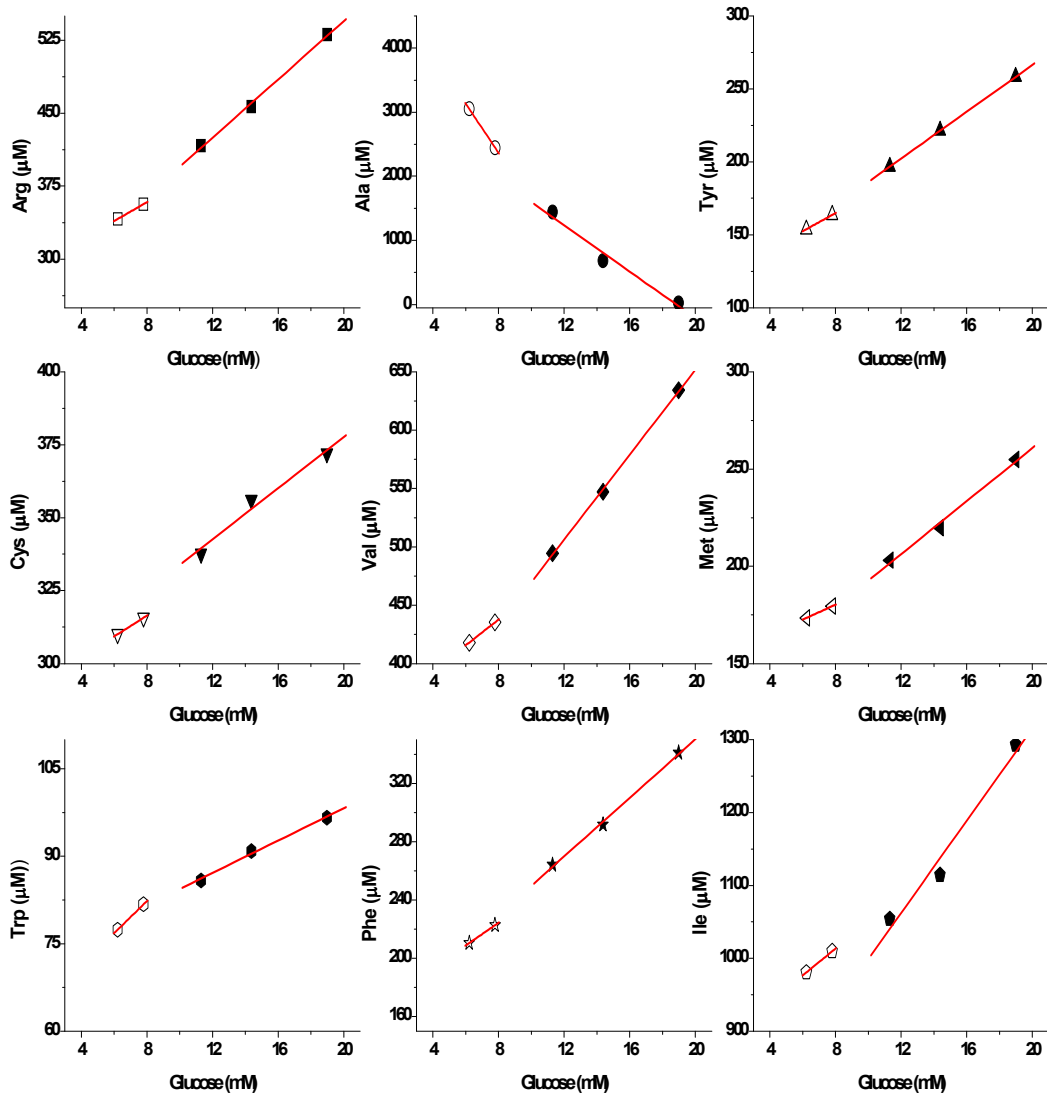


**Figure 5.5.13 (B):** Metabolite plotted against glucose. Two separate linear regressions were performed, one for glucose concentrations higher than 10  $\text{mM}$  and the other for lower than 10  $\text{mM}$ . The closed markers indicate the concentrations at high glucose concentration whereas the open symbols indicate low glucose concentration.

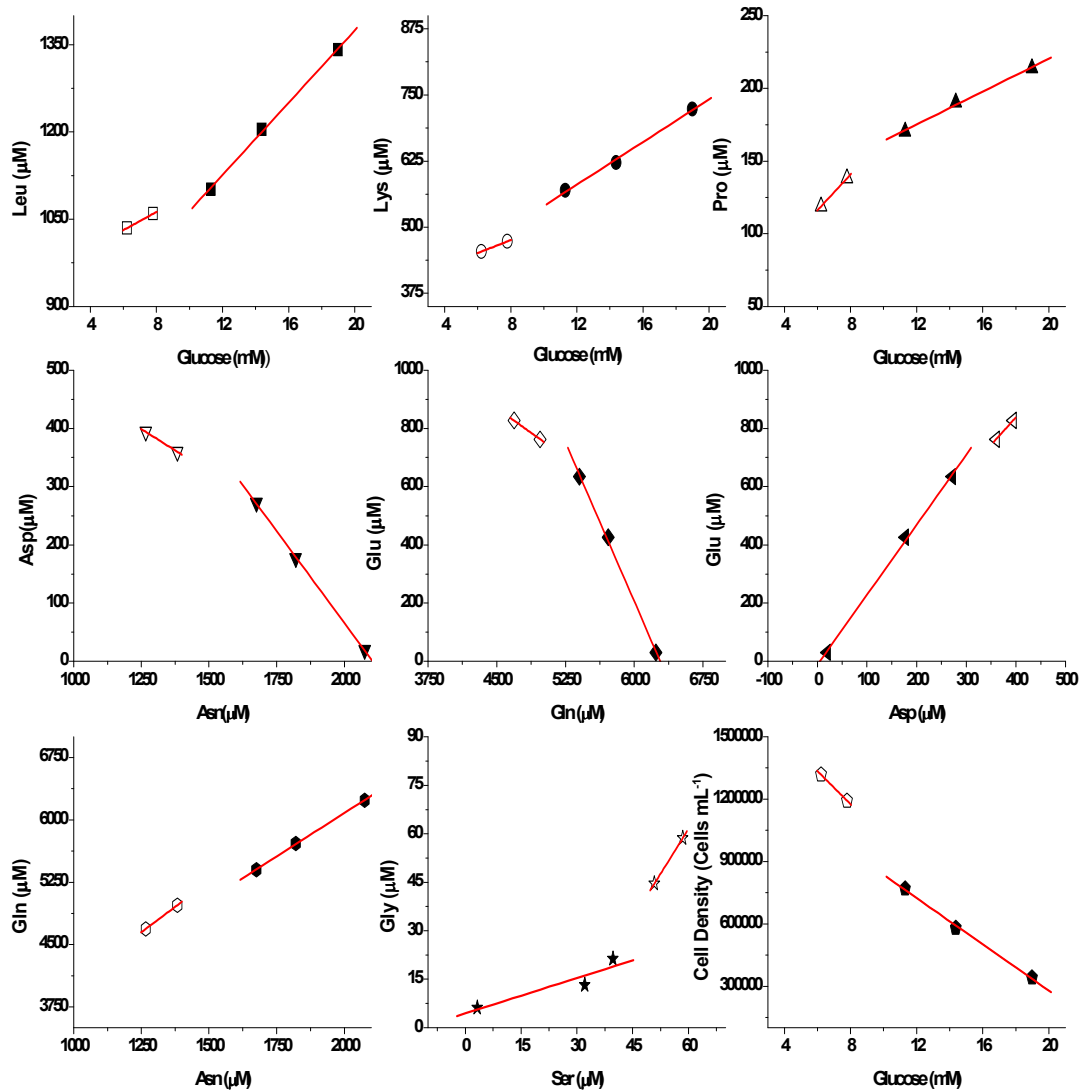


**Figure 5.5.13 (C):** Metabolite concentrations plotted against each other. Two separate linear regressions were performed, one for glucose concentrations higher than 10 mM and the other for lower than 10 mM. The closed markers indicate the concentrations at high glucose concentration whereas the open symbols indicate low glucose concentration.

**Table 5.5.6:** Yields of the metabolites and cells on glucose at two growth phase with yield 1 at high glucose concentration and yield 2 at lower glucose concentration as represented in the Figure 5.5.13 A, B & C. The regression coefficient ( $R^2$ ) of the linear regression is given in brackets. The regression coefficient of yield 2 could not be calculated because only two measurements were available for this phase.

Metabolite	Yield 1 ( $R^2$ )	Yield 2 ( $R^2$ )	Unit
Lactate	-1.6 (0.99)	-2.2	mM/mM Glucose
Asp	-33.0 (0.99)	-21.6	$\mu$ M/mM Glucose
Glu	-79.3 (0.99)	-40.8	$\mu$ M/mM Glucose
Asn	52.3 (0.99)	73.8	$\mu$ M/mM Glucose
Ser	-4.9 (0.97)	-4.8	$\mu$ M/mM Glucose
Gln	109.2 (0.99)	180.8	$\mu$ M/mM Glucose
His	6.1 (0.99)	7.3	$\mu$ M/mM Glucose
Gly	-1.9 (0.98)	-8.9	$\mu$ M/mM Glucose
Thr	10.9 (0.99)	11.3	$\mu$ M/mM Glucose
Arg	15.0 (0.99)	9.7	$\mu$ M/mM Glucose
Ala	-181.0 (0.98)	-383.3	$\mu$ M/mM Glucose
Tyr	8.0 (0.99)	6.3	$\mu$ M/mM Glucose
Val	18.2 (0.98)	11.0	$\mu$ M/mM Glucose
Met	6.8 (0.99)	3.9	$\mu$ M/mM Glucose
Trp	1.4 (0.99)	2.8	$\mu$ M/mM Glucose
Phe	10.1 (0.99)	7.8	$\mu$ M/mM Glucose
Ile	31.7 (0.98)	18.4	$\mu$ M/mM Glucose
Leu	31.1 (0.99)	15.7	$\mu$ M/mM Glucose
Lys	20.2 (0.99)	12.2	$\mu$ M/mM Glucose
Pro	5.7 (0.99)	12.3	$\mu$ M/mM Glucose
Cells	55.6 (0.99)	79.6	Cells/ $\mu$ M Glucose

***Carbon labeling analysis***

Figure 5.5.14 gives the fractional carbon labeling profile along with the concentrations of the metabolites found to be labeled. All the metabolites show or approach steady state in their fractional labeling. Lactate has a fractional carbon labeling of 80 % which is similar to the labeling obtained in the previous media. 75 % of the lactate is fully labeled and is thus formed directly from the glycolytic pathway. 9 % are either  $^{13}\text{C}_1$  (2 %) or  $^{13}\text{C}_2$  (7 %) isotopomers, implying that they originate from the pyruvate produced from TCA cycle. Compared to the previous media, a lower percentage of serine is found to be fully labeled at 84 % with 5 % being unlabeled. The same percentage of glycine is found to be fully labeled with 12 % being unlabeled. This shows that there might be other sources for glycine production. Fully labeled alanine makes up 66 % of the total with 21 % being unlabeled compared to 14 % in lactate. Thus a higher percentage of alanine is formed from carbon sources other than glucose. 10 % of aspartate is formed via the pyruvate entering TCA cycle via pyruvate carboxylase and 16 % from pyruvate dehydrogenase. The above results indicate a higher amount of amino acid carbon entering the TCA cycle.

This media without the anabolic amino acids and excess concentrations of asparagine and glutamine offers the best possible solution to reduce the complexity of further calculations due to the linear relationship of the metabolites and the approach of steady state in the labeling.

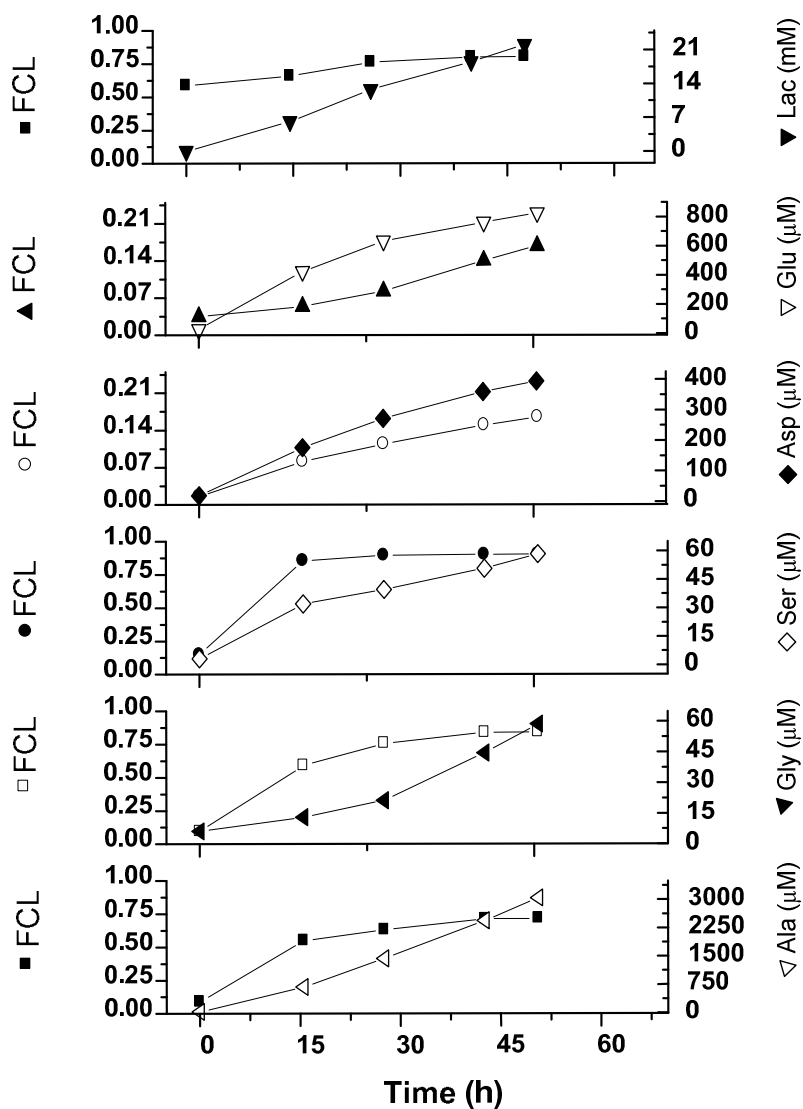


**Figure 5.5.14:** Extracellular substrate labeling plotted along with extracellular concentration. The right axis gives the concentration and the left axis the fractional carbon labeling of the metabolite indicated on the right axis. The sampling procedure is given in material and methods. The initial time “0” refers to the sample after the addition of media to cells.

### 5.5.2.5 Elemental carbon balance for the estimation of carbon dioxide production rate (CPR)

Material balances are routinely used in microbial fermentation. These are determined generally by applying elemental balances on carbon, nitrogen, oxygen, etc. On the other hand because of the complex nutritional requirements, detailed stoichiometric material balances in animal cell culture have been difficult to achieve (Xie and Wang, 1996). Due to the complexities of animal cell metabolism, the elemental balances for animal cell cultivation are a difficult problem to solve. Closing carbon balances in animal cell culture pose a peculiar problem due to the slow growth rates, low specific metabolic rates of such cultures, the low cell densities normally obtained in suspension cultures, and particularly the use of bicarbonate buffers in media (Lovrecz and Gray, 1994; Xiu et al., 1999). This buffer improves the pH control of media incubated in a CO<sub>2</sub> atmosphere and provides cells with carbonate ions that are necessary for the metabolic functions of most cells particularly for the carboxylation reactions. Though theoretically it is possible to replace bicarbonate buffering with other organic buffering systems like HEPES, it is important to maintain sufficient bicarbonate in the medium for nutritional purposes and intracellular pH regulation (Ganz et al., 1989). There are few published reports on closing carbon balances in mammalian cell cultures (Lovrecz and Gray, 1994; Bonarius et al., 1999; Oezemre and Heinzle, 2001) which all require the measurement of the carbon dioxide evolution rate.

Xiu et al. (1999) estimated the carbon dioxide evolution rate by employing an elemental balance around carbon and obtained results similar to those reported in literature. A similar analysis was performed here, by which it was attempted to use the carbon balance to estimate the carbon dioxide evolution rate. Briefly, the methodology involves the calculation of the specific rates of measured components and estimating the carbon input and output. The difference between the input and output gives the carbon dioxide production rate (CPR).

The carbon balance for the culture is given by the equation

$$6q_1 + 5q_2 + q_3 = 3q_4 + 3q_5 + q_6 + q_{CO_2} \quad (5.5.1)$$

where  $q_1$ ,  $q_2$ ,  $q_3$ ,  $q_4$ ,  $q_5$ ,  $q_6$ ,  $q_{CO_2}$  are the specific consumption rates of glucose, glutamine, amino acids and production rates of lactate, alanine, biomass, and CO<sub>2</sub>, respectively.  $q_6$  is the carbon mole specific biomass production rate. The biomass rate is calculated from the biomass equations derived in the earlier section.

The consumption rate for amino acids excluding glutamine and alanine are given by

$$q_3 = \sum C_i q_{AAi} \quad (5.5.2)$$

$C_i$  is the carbon atom number of  $i^{\text{th}}$  amino acid (excluding glutamine and alanine) and  $q_{AAi}$  represents the specific utilization rate of amino acid  $i$ .

Table 5.5.7 gives the specific rates of the major metabolites involved in carbon metabolism. By employing the above method, the CPR of the culture was found to be  $1.85 \times 10^{-13} \text{ mol cell}^{-1} \text{ h}^{-1}$ . This value is in the lower range of the values reported by (Zupke et al., 1995) of  $2 \times 10^{-13} \text{ mol cell}^{-1} \text{ h}^{-1}$  and (Bonarius et al., 1999) of  $2 \sim 5 \times 10^{-13} \text{ mol cell}^{-1} \text{ h}^{-1}$ . The carbon input and output are given in percentage in the Figure 5.5.15. Without considering CPR it was possible to close the carbon balance at 93 %. However, using the above analysis around 7 % of the carbon forms  $\text{CO}_2$  and this value is represented in the figure as difference referring to the difference between input and output elemental carbon.

**Table 5.5.7:** The specific rates of metabolites involved in carbon metabolism for CHO cells grown in the optimized media shown in Figure 5.5.11. The positive sign indicates production and the negative sign indicates consumption of the metabolite.

Metabolite	Specific Rate ( $\text{mol cell}^{-1} \text{ h}^{-1}$ )	Metabolite	Specific Rate ( $\text{mol cell}^{-1} \text{ h}^{-1}$ )
Glucose	$-3.3 \times 10^{-13}$	Cystine	$-1.4 \times 10^{-15}$
Lactate	$5.7 \times 10^{-13}$	Valine	$-5.6 \times 10^{-15}$
Pyruvate	$-1.6 \times 10^{-14}$	Methionine	$-2.1 \times 10^{-15}$
Aspartate	$9.7 \times 10^{-15}$	Tryptophan	$-2.9 \times 10^{-16}$
Glutamate	$2.1 \times 10^{-14}$	Phenylalanine	$-3.4 \times 10^{-15}$
Asparagine	$-2.1 \times 10^{-14}$	Isoleucine	$-5.3 \times 10^{-15}$
Serine	$1.4 \times 10^{-15}$	Leucine	$-8.3 \times 10^{-15}$
Glutamine	$-4.0 \times 10^{-14}$	Lysine	$-7.0 \times 10^{-15}$
Histidine	$-1.9 \times 10^{-15}$	Proline	$-2.5 \times 10^{-15}$
Glycine	$1.4 \times 10^{-15}$	Protein	$5.2 \times 10^{-14}$
Threonine	$-3.4 \times 10^{-15}$	DNA	$4.9 \times 10^{-16}$
Arginine	$-4.9 \times 10^{-15}$	RNA	$1.4 \times 10^{-15}$
Alanine	$7.9 \times 10^{-14}$	Lipids	$8.5 \times 10^{-16}$
Tyrosine	$-2.7 \times 10^{-15}$	Carbohydrates	$3.4 \times 10^{-15}$

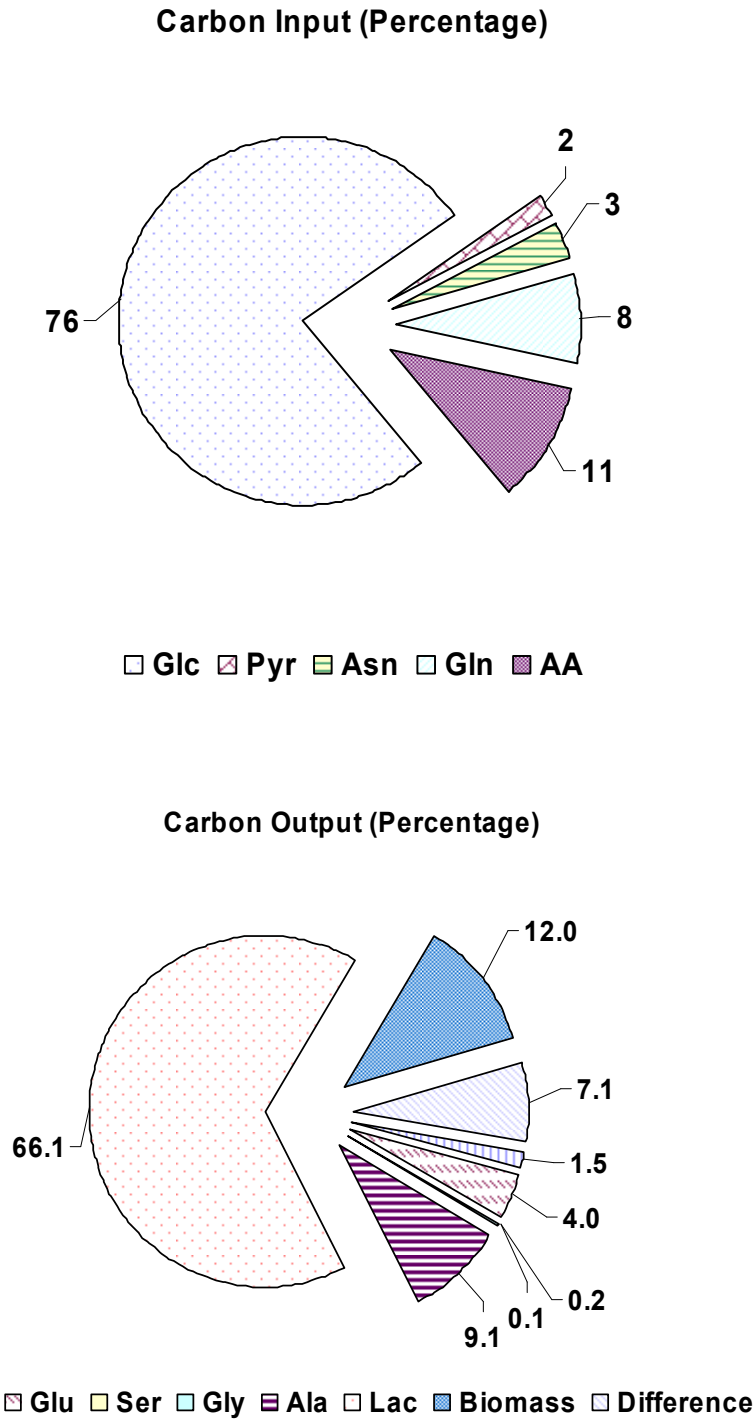


**Figure 5.5.15:** Carbon balance on the cell culture in optimized media described in Figure 5.5.11.

### 5.5.2.6 Conclusions

In this part of the work an attempt was made to understand the physiology of the cells and use this information for the simplification of the model to be used later for the metabolic flux analysis. In this regard considerable progress was achieved towards the goal. From cell culture experiments with [U-<sup>13</sup>C]glucose, the anabolic amino acids were determined. Alanine, serine, glycine, aspartate and glutamate were found to be labeled with <sup>13</sup>C and thus the biosynthetic pathways of these amino acids are active. This was in spite of the fact that the media, as most of the commercially available media, contained these amino acids in significant amounts. To simplify the biochemical model to be used for flux calculation, cells were grown in media with reduced amounts of the above amino acids and also media lacking the amino acids. The cell growth in all the media was similar to the growth in the original media. Thus the cells were able to produce these amino acids in sufficient amounts for their metabolic maintenance. The physiology of cells in the media lacking these amino acids was investigated. It was observed that there was an initial production and a subsequent consumption of the amino acids aspartate, glutamate and serine. This was linked to possible limitation of the amino acids asparagine and glutamine. The above media was modified with an increased concentration of asparagine and glutamine, and cell growth and physiology was investigated. The cell growth was observed to be normal; however, as expected some differences were noted with respect to cell physiology in comparison to the other media. There was no consumption of the anabolic amino acids, and the fractional carbon labeling of the extracellular metabolites was found to approach steady state. A necessary precondition for the exact calculation of carbon metabolic fluxes is the determination of carbon balance. Hence, the carbon balance in the cell culture was determined using which the carbon dioxide evolution rate could be estimated. These results enable us to simplify the model by removing the uptake fluxes of anabolic amino acids, to avoid the exchange of amino acids and to approach a steady state with regard to the fractional carbon labeling. The next part of the work deals with the actual experimentation and data which can be used for the absolute flux quantification.

### 5.5.3 Parallel labeling studies for metabolic studies

#### 5.5.3.1 Motivation and choice of labeling substrates

Isotopic tracers have played an important role in biomedical research since the invention of artificial radioactivity by J.F. Joliot-Curie and Irene Joliot-Curie in Paris in 1934, the production of radioisotopes by cyclotron invented by Ernest O. Lawrence in Berkeley in 1930 and by nuclear reactor demonstrated by Enrico Fermi and co-workers in Rome in 1942. They have been playing a vital role in the growth and development of life science and medicine right from the understanding of the chemistry of the photosynthesis (by Melvin Calvin's Berkeley team using  $^{14}\text{C}$ ) to the development of molecular biology. The most commonly used radioactive isotopes are  $^{14}\text{C}$  and  $^3\text{H}$  (tritium). In parallel to the research using radioisotopes, in the 1930's Schoenheimer and Rittenberg provided the scientific foundation for the development and application of stable isotope techniques in biological research (Young and Ajami, 1999). The use of stable isotopes has increased dramatically with advances in analytical capabilities like NMR and GC-MS. Aspects of metabolism have been investigated employing molecules labeled with  $^2\text{H}$ ,  $^{13}\text{C}$ ,  $^{15}\text{N}$ , and  $^{18}\text{O}$ . At present more than 6000 stable isotope labeled compounds (tracers) are commercially available for use in metabolic studies. Kelleher (2001) has reviewed the usage of tracers in metabolic studies and as a consequence for flux estimation.

Isotopes of carbon offer an elegant method to investigate the central metabolism. Reeds et al. (1997) have reviewed the use of uniform stable isotope labeled substrates for metabolic studies. Isotopomers of glucose have long been and are still the most favored for the investigation of mammalian cellular physiology, since glucose is the primary substrate for cellular metabolism. The use of fully labeled  $[\text{U-}^{13}\text{C}]$ glucose as a substrate to study physiology has been demonstrated in the previous section. Katz and Wood (1960) presented a theoretical consideration of the methods to evaluate metabolic pathways using  $^{14}\text{C}$  glucose. The rates of carbon dioxide evolution from the simultaneous incubation with  $[1\text{-}^{13}\text{C}_1]$  and  $[6\text{-}^{13}\text{C}_1]$ glucose are used to measure the activity of the pentose phosphate shunt (Katz and Wood, 1963; Mancuso et al., 1994; Bonarius et al., 1998).  $[1\text{-}^{13}\text{C}_1]$ Glucose has been used to determine the metabolic flux rates in a simplified network depicting the central metabolic pathway of C6 glioma cells (Portais et al., 1993). Longenecker and Williams (1980) quantified the type-L pentose phosphate cycle in hepatocytes using  $[2\text{-}^{14}\text{C}_1]$  and  $[5\text{-}^{14}\text{C}_1]$  glucose.  $[1,2\text{-}^{13}\text{C}_2]$ Glucose has been applied to quantify the oxidative pentose-phosphate activity along with anaplerosis and rate of macromolecule synthesis (Lee et al., 1998; Boren

et al., 2003). Ross et al. (1994) found [1,6-<sup>13</sup>C<sub>2</sub> 6,6-<sup>2</sup>H<sub>2</sub>]glucose a better substrate to quantify pentose phosphate activity in a single incubation when compared to [1,5,6-<sup>13</sup>C<sub>3</sub>]glucose and [6-<sup>13</sup>C 1,6,6-<sup>2</sup>H<sub>3</sub>]glucose. Schrader et al. (1993) applied [2-<sup>13</sup>C<sub>1</sub>]glucose to study the pentose phosphate shunt activity and also fluxes through phosphofructokinase, the 2,3-diphosphoglycerate bypass, and phosphoglycerate kinase in erythrocytes. Sibson et al. (2001) demonstrated the use of [2-<sup>13</sup>C<sub>1</sub>] and [5-<sup>13</sup>C<sub>1</sub>]glucose to study the glutamate cycling, anaplerosis and TCA cycle flux in cerebral cortex.

Amino acids labeled at their carbon positions have been also used to study the metabolism of mammalian cells. Fully radio-labeled [U-<sup>14</sup>C]glutamine was used by Reitzer et al. (1979) to show that glutamine oxidation and not glycolysis is the major energy source in cultured cells. Piva and McEvoy-Bowe (1998) studied the oxidation of glutamine in truncated TCA cycle of cultured cervical cancer (HeLa) cells using [U-<sup>14</sup>C]glutamine. Sharfstein et al. (1994) used [3-<sup>13</sup>C<sub>1</sub>] glutamine to study the primary metabolism in a hybridoma cell line. Harper et al. (1984) have reviewed the metabolism of branched chained amino acids (isoleucine, leucine and valine) and the role played by isotopes for their elucidation. Glutamate and aspartate play an important role as neurotransmitters and hence many studies on their metabolism in neurons and glial cells have been performed using labeled isotopes (Snyder et al., 1973; Man et al., 1987; Erecinska and Silver, 1990). Olsen et al. (1943) were the first to investigate the metabolism of glycine using stable isotopes. Narkewicz et al. (1996) used stable isotope labeled serine and glycine to study the intracellular partitioning of their metabolism. House et al. (2001) investigated threonine catabolism in rat hepatocytes using [1-<sup>14</sup>C<sub>1</sub>]threonine. Along with sugars and amino acids, other carbon substrates have also been used to study certain aspects of metabolism. Kelleher et al. (1987) used <sup>14</sup>C labeled citrate, succinate and pyruvate for the metabolic investigation of the TCA cycle. [U-<sup>13</sup>C]Pyruvate and [U-<sup>13</sup>C]acetate have been used for the studies of the TCA cycle (Fernandez and Des Rosiers, 1995). Cruz et al. (2001) used labels of pyruvate and glucose to determine the intracellular compartmentation of pyruvate.

The above are only few of the numerous examples involving labeled substrates. A detailed review of the applications of isotope labels and methods in biological research can be found in Berliner and Robitaille (1998) and Wolfe and Chinkes (2004).

A fact that stands out from the examples given above is that the complexity of the mammalian physiology requires multiple complimentary investigations by utilizing various different substrates to determine the metabolism. In the case of the central metabolism, this complexity is also induced by the fact that the carbon requirement of the cells is not fulfilled by a single

(e.g. glucose in case of many bacteria) but by many carbon substrates (e.g. glucose, amino acids, pyruvate etc) entering the metabolic pathway. Quantitative analysis of the whole cell metabolism in mammalian cells is thus an arduous task. In earlier chapter, the methodology of metabolic flux analysis for the quantitative analysis of cellular physiology has been explained. Also, the application of this methodology for mammalian cell culture and the shortcomings of the methods employed have been discussed. In this chapter, the application of parallel cell cultures with different labeled substrates for flux calculations is shown.

The culture media of the mammalian cells is composed of many carbon containing substrates, which are taken up by the cells and participate in the central metabolism. The previous chapter described the optimization of the media with a view to reduce the complexity in the calculation of metabolic fluxes. This involved the elimination of substrates which are simultaneous both catabolic and anabolic in nature. To accurately quantify the fluxes of the metabolic pathways, the knowledge of the contribution of individual carbon substrates to the central metabolism is essential. In this regard, we employ a strategy of parallel cell cultivations with differently labeled substrates. The labeling data along with the uptake and production rates of the main metabolites will then be utilized for the calculation of fluxes. Along with the quantification, it is also important to gain an insight into the metabolism. In order to carry out the analysis, the choice of substrates to be labeled and the position of labeling are of prime importance. An ideal situation would be to carry out labeling experiments with all carbon substrates labeled at various different positions. This, however, would not be feasible as among other pitfalls it would be expensive, time consuming and would lead to redundant data sets. Studying the biochemistry and the network to be quantified makes the choice of labeled substrates simpler. Also, the simultaneous use of two labeled substrate in the same culture leads to the possibility of gaining a more informative insight into the metabolism.

The isotopic substrates used in this study and the information they could provide are listed below.

### **[1-<sup>13</sup>C<sub>1</sub>]Glucose and [U-<sup>13</sup>C]glutamine**

[1-<sup>13</sup>C<sub>1</sub>]Glucose is a widely used substrate to quantify fluxes in microbial cultures particularly providing information about glycolysis-PPP splitting (Wittmann and Heinzle, 1999; Wittmann, 2007). Glutamine is the major energy source in cultured cells (Reitzer et al., 1979), and its metabolism has been investigated using labeled substrates as explained earlier. The use

of the simultaneous application of these substrates would help to quantify among others, the pentose phosphate activity, the TCA cycle, and anaplerotic fluxes.

### **[1-<sup>13</sup>C<sub>1</sub>]Glucose and [U-<sup>13</sup>C]threonine**

The carbon chain of threonine is converted to succinyl-CoA, which feeds directly into the citric acid cycle. This was long thought to be the only active catabolic mechanism of threonine present in mammalian cells. However, in recent literature this has been contradicted. The oxidation of threonine can be broadly classified glycine dependent and glycine independent (House et al., 2001). One of the pathways produces glycine and acetyl-CoA, and the other pathway produces succinyl-CoA. To study the contribution of each mechanism to the central metabolism, [U-<sup>13</sup>C]threonine is used as one of the substrates along with [1-<sup>13</sup>C<sub>1</sub>]glucose.

### **[1,2-<sup>13</sup>C<sub>2</sub>]Glucose**

The advantage of using [1,2-<sup>13</sup>C<sub>2</sub>]glucose has been explained earlier. The oxidative pentose-phosphate activity along with anaplerosis and rate of macromolecule synthesis can be estimated.

### **[3-<sup>13</sup>C<sub>1</sub>]Pyruvate**

Peuhkurinen et al. (1983), Cruz et al. (2001) and Zwingmann et al. (2001) have reported the presence of intracellular cytosolic compartmentation of pyruvate. [3-<sup>13</sup>C<sub>1</sub>]Pyruvate is used in this study to investigate the compartmentation and also the contribution from extracellular pyruvate to the central metabolism. [3-<sup>13</sup>C<sub>1</sub>]Pyruvate would enter the TCA cycle as singly labeled acetyl-CoA losing a carbon atom as CO<sub>2</sub>. Alanine and lactate formed from extracellular [3-<sup>13</sup>C<sub>1</sub>]pyruvate would be singly labeled whereas that from the glycolysis would be unlabeled. The recycled pyruvate would be a mixture of unlabeled, single, double and fully labeled molecules. The labeling patterns of lactate and alanine along with the data from the other cultures help to investigate the pyruvate compartmentation.

### **5.5.3.2 Parallel cell growth and carbon labeling**

The results obtained from the parallel culture with multiple labeled substrates are discussed below. In the first part the general comparison of growth and physiology is described. The growth characteristics of individual experiments are discussed in the second part. The third part gives an overall comparative view of the whole cell metabolism and physiology from all the four cultures with emphasis on the metabolic pathways.

#### **Comparison of growth in the four cultures**

The cells were grown in parallel in the media with the labeled substrates, i.e. [1-<sup>13</sup>C<sub>1</sub>]glucose and [U-<sup>13</sup>C]glutamine, [1-<sup>13</sup>C<sub>1</sub>]glucose and [U-<sup>13</sup>C]threonine, [1,2-<sup>13</sup>C<sub>2</sub>]glucose, and [3-<sup>13</sup>C<sub>1</sub>]pyruvate. The cell growth of all the four cultures is given in Figure 5.6.1. The cells show similar growth patterns and growth rates. The lactate and glucose concentration profiles of the cultures are shown in Figure 5.6.2. Table 5.6.1 also gives the specific rates of glucose uptake and lactate production in the four cultures. The starting concentration of glucose in the four cultures is different and is possibly responsible for the slight differences in the rates, with the cultures having a higher starting concentration showing a higher uptake. The concentration of glucose in cultures containing [1-<sup>13</sup>C<sub>1</sub>]glucose is lower than that of the other two cultures. This phenomenon has also been observed in other cell lines (Neermann and Wagner, 1996).

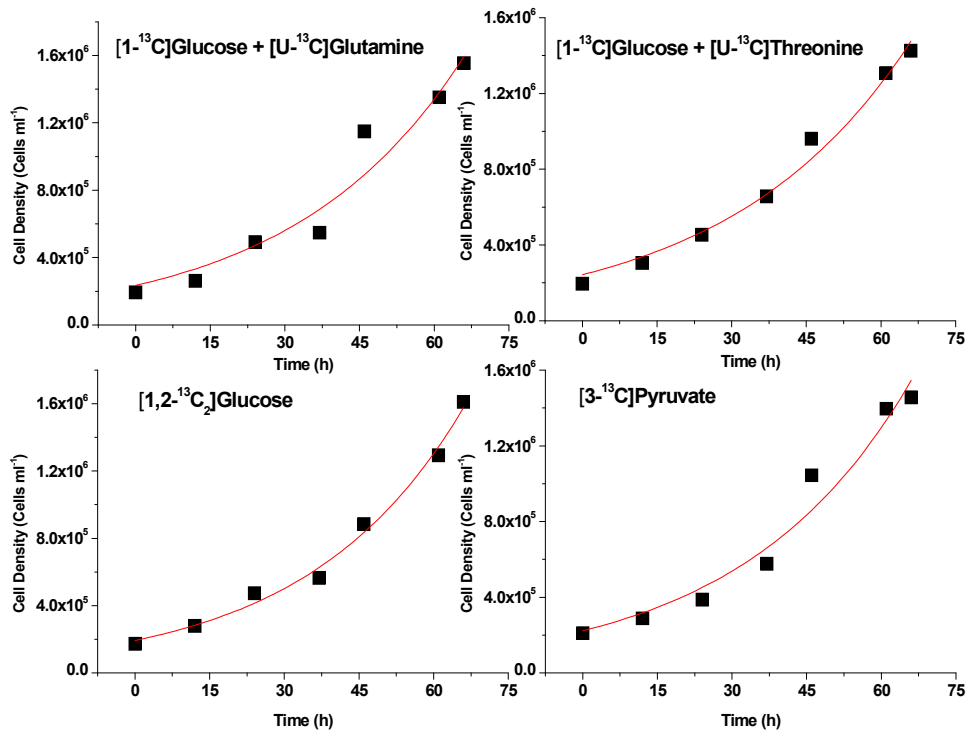


**Figure 5.6.1:** Cell growth of CHO cells in four parallel cultures with different isotopic labeled substrates. The isotopic labels used in the culture are depicted on top of each graph.

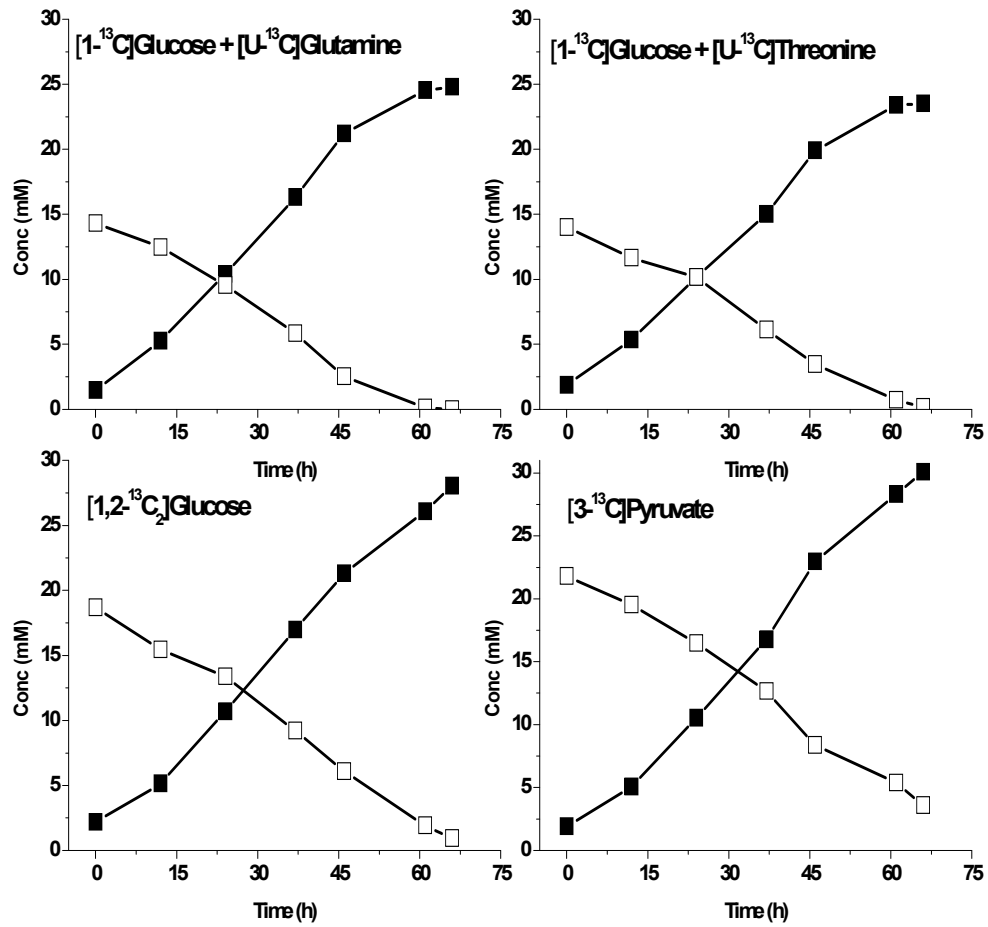


**Figure 5.6.2:** The glucose and lactate concentration profiles during cell growth in four parallel cultures of CHO cells with different isotopic labeled substrates. The isotopic labels used in the culture are depicted on top of each graph. The open symbols represent glucose and the closed symbols represent lactate.

**Table 5.6.1:** Growth rate, glucose uptake and lactate production for the parallel cell cultures using different labels

Labeled isotopes used in culture	Growth rate (h <sup>-1</sup> )	Glucose Uptake (× 10 <sup>-9</sup> Mol cell <sup>-1</sup> day <sup>-1</sup> )	Lactate Production (× 10 <sup>-8</sup> Mol cell <sup>-1</sup> day <sup>-1</sup> )	Lactate/Glucose (Mol/Mol)
[1- <sup>13</sup> C <sub>1</sub> ]Glc + [U- <sup>13</sup> C]Gln	0.033	8.06	1.31	1.63
[1- <sup>13</sup> C <sub>1</sub> ]Glc + [U- <sup>13</sup> C]Thr	0.031	8.11	1.27	1.57
[1,2- <sup>13</sup> C <sub>2</sub> ]Glc	0.033	9.49	1.38	1.45
[3- <sup>13</sup> C <sub>1</sub> ]Pyr	0.032	10.9	1.68	1.54
<b>Mean</b>	<b>0.032</b>	<b>9.14</b>	<b>1.41</b>	<b>1.55</b>
<b>Standard Deviation</b>	0.001	1.35	0.186	0.07
<b>Standard Deviation (%)</b>	<b>2.97</b>	<b>14.74</b>	<b>13.17</b>	<b>4.59</b>

### Growth and isotope labeling characteristics of individual cultures

#### *[1-<sup>13</sup>C<sub>1</sub>]Glucose and [U-<sup>13</sup>C]glutamine*

Similar to the previous section, the interdependency of the different metabolites in the cultures was determined by plotting their concentrations against the corresponding glucose concentration. A few of the metabolites were plotted against each other. Figure 5.6.3 (A, B and C) gives the plots of the culture with [1-<sup>13</sup>C<sub>1</sub>]glucose and [U-<sup>13</sup>C]glutamine. Most of these plots show linear relationship as expected due to the use of the optimized media. There is a consumption of serine during the end of the cultivation subsequent to its production during the initial phases. This is most probably due to the lower amount of glucose present in the media during this phase. This leads to the non-linear relationship between serine and glucose as seen in Figure 5.6.3 (A), and between serine and glycine seen in Figure 5.6.3 (C). Aspartate and glutamate are not consumed during the end of the cultivation even in the presence of low amounts of glucose in the media. This probably is due to asparagine and glutamine feeding the TCA cycle in sufficient amounts to satisfy the biosynthetic requirement of the cells for aspartate and glutamate. This is in contrast to serine, which is consumed during the end phase, thus the biosynthetic need of serine is supplied directly from glucose. Glycine, whose biosynthesis is linked to serine, shows no consumption in contrast to serine. This might possibly be due to serine being an important gluconeogenic substrate converting readily to pyruvate via serine hydratase. Other reason might be the degradation of threonine to produce glycine.

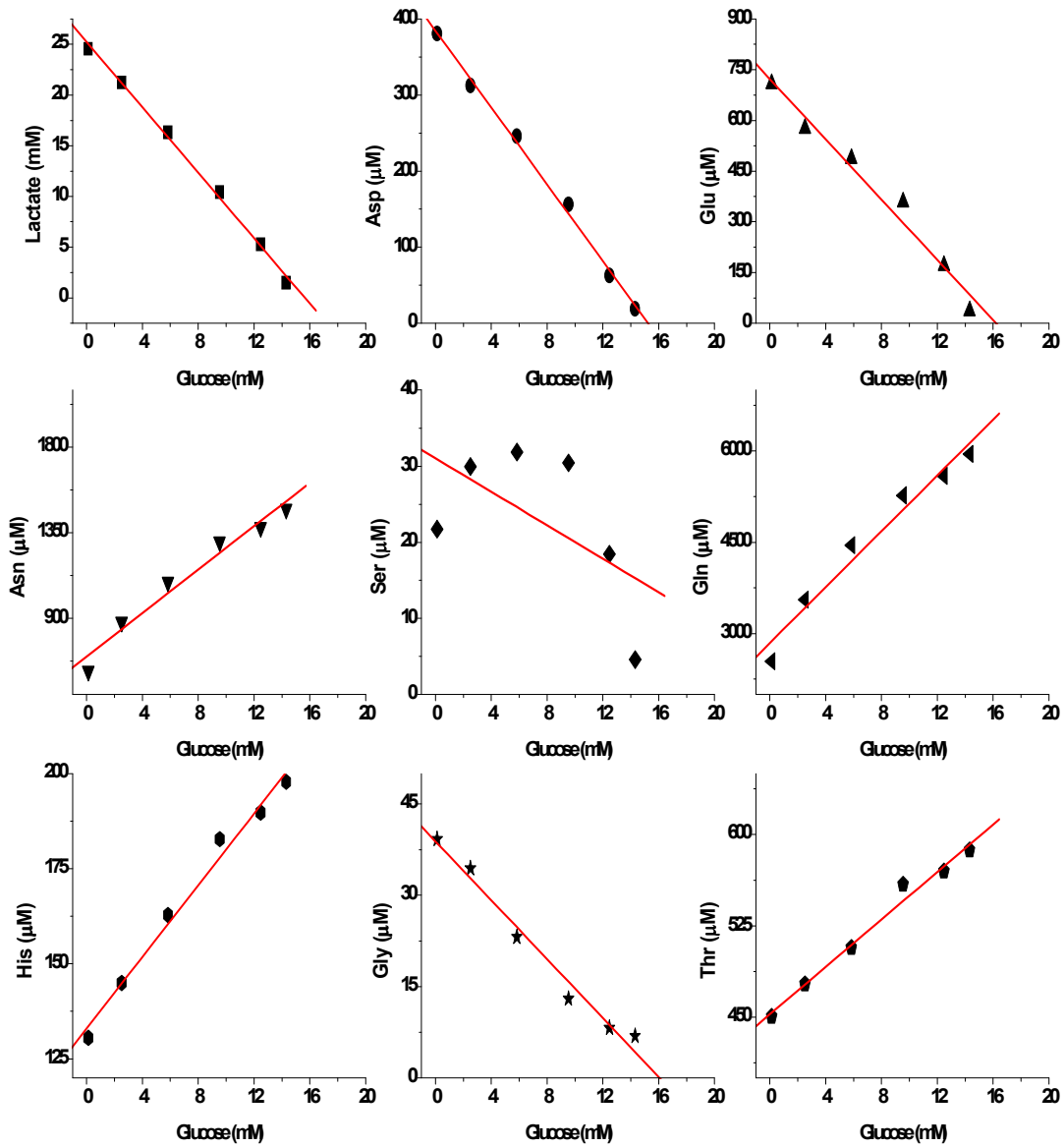


**Figure 5.6.3 (A):** Metabolite concentrations of the cultivation using  $[1-^{13}\text{C}_1]\text{glucose} + [\text{U}-^{13}\text{C}]\text{glutamine}$  isotopic label plotted against glucose for the culture described in Figure 5.6.1. Linear regression was performed on each of the metabolite.

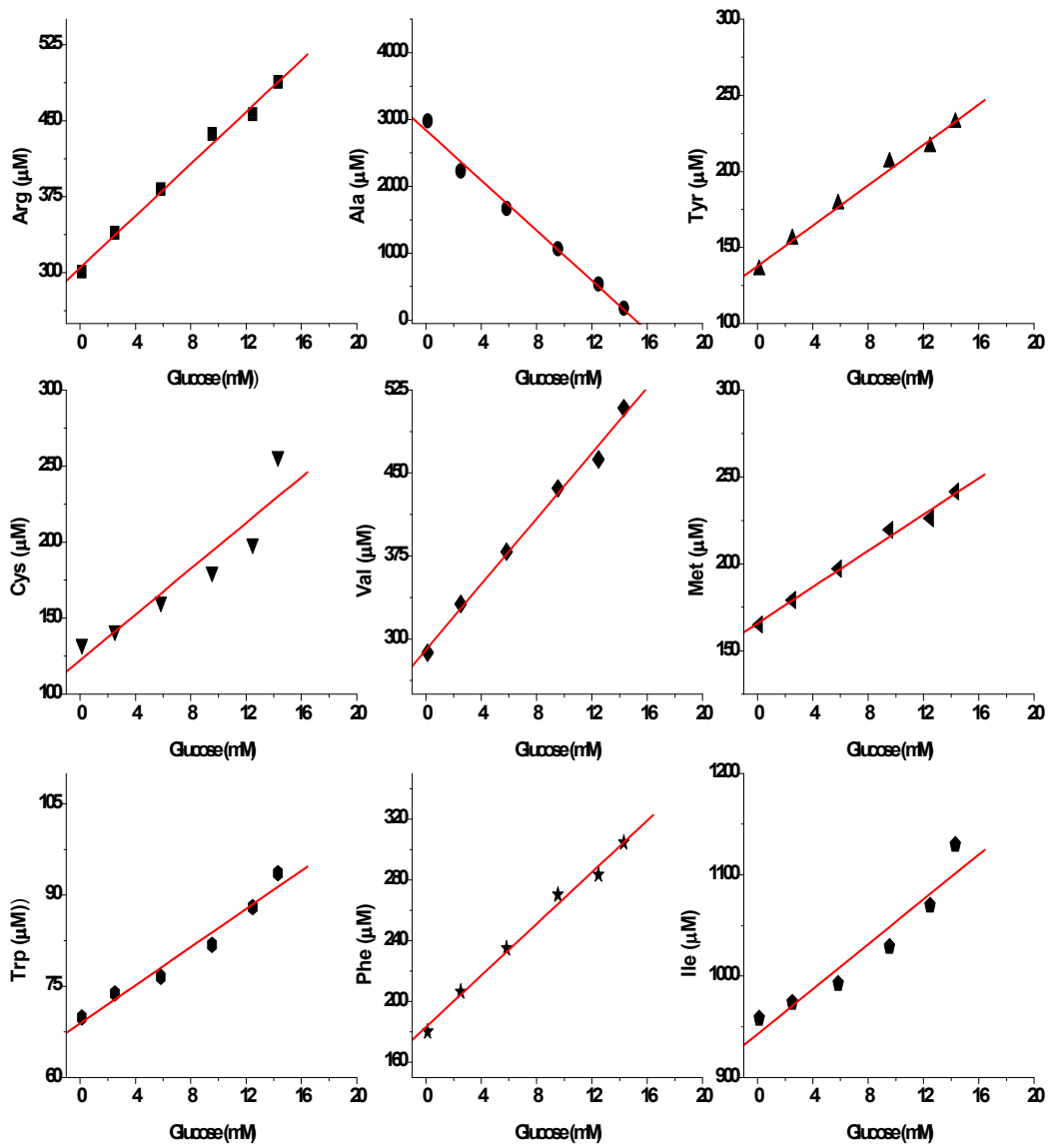


**Figure 5.6.3 (B):** Metabolite concentrations of the cultivation using  $[1-^{13}\text{C}]$ glucose +  $[\text{U}-^{13}\text{C}]$ glutamine isotopic label plotted against glucose for the culture described in Figure 5.6.1. Linear regression was performed on each of the metabolite.

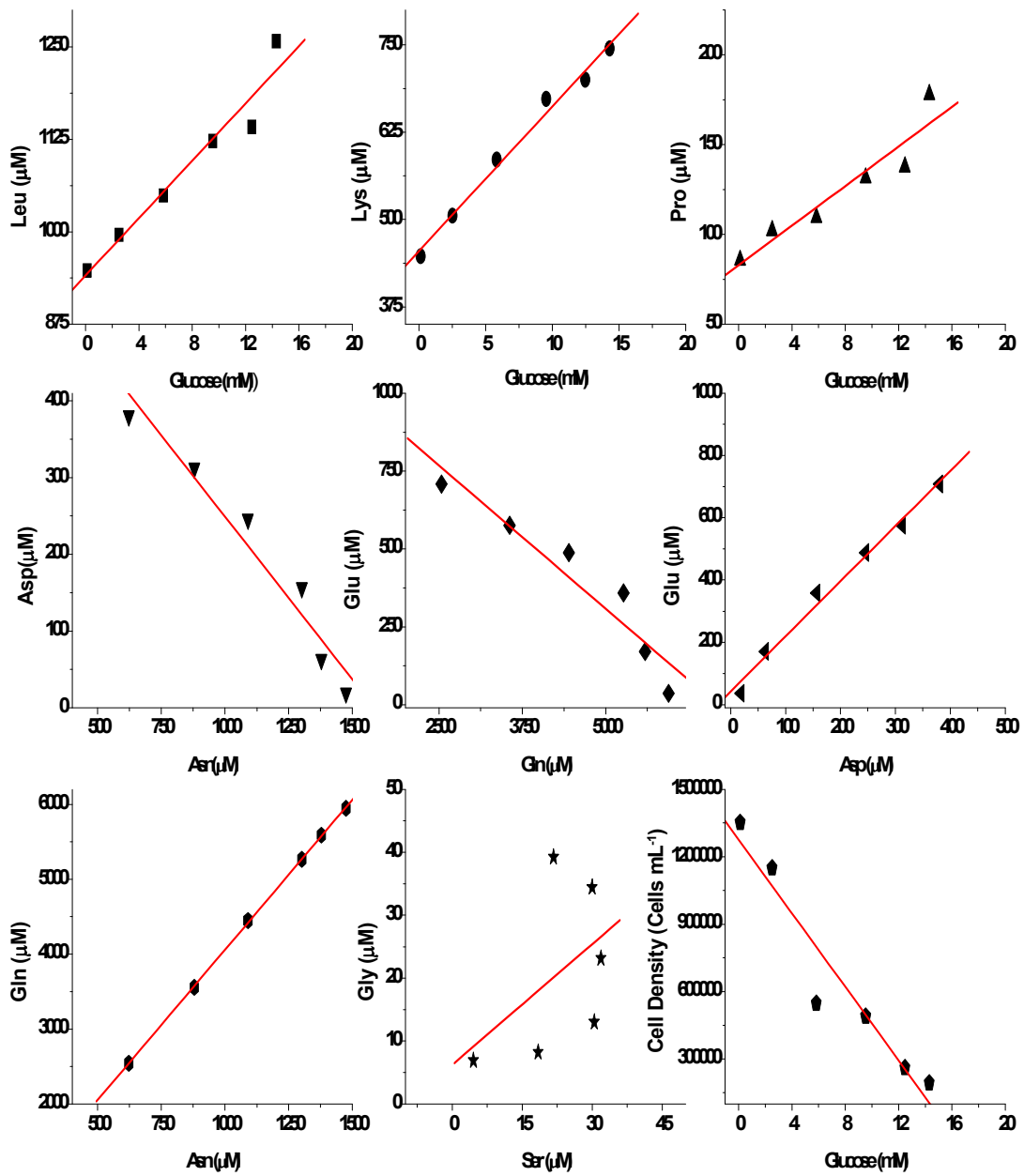


**Figure 5.6.3 (C):** Metabolite concentrations of the cultivation using  $[1-^{13}\text{C}_1]\text{glucose} + [\text{U}-^{13}\text{C}]\text{glutamine}$  isotopic label plotted against glucose and also a few against each other for the culture described in Figure 5.6.1. Linear regression was performed on each of the metabolite.

Gas chromatographic mass spectrometric analysis was carried out to determine the mass isotopomers and fractional carbon labeling (FCL) of the samples obtained during the cell cultivation using [1-<sup>13</sup>C<sub>1</sub>]glucose and [U-<sup>13</sup>C]glutamine. Similar to the previous section, the samples were analyzed for the extracellular amino acids and lactate, and the fractional carbon labeling of the amino acids and lactate in the culture supernatant with respect to time along with their concentration profile is shown in Figure 5.6.4. The final fractional carbon labeling of lactate is 0.19 and that of alanine is 0.21. Looking at the mass isotopomers, single labeled lactate makes up 39 % and fully labeled lactate 5 % as compared to alanine in which the single labeled species makes up 36 % and the fully labeled 7 %. In addition the doubly labeled species of alanine has a higher labeling (3 %) compared to lactate (2 %). Thus the amount of alanine formed from the carbon of the TCA cycle is higher than the amount of lactate formed. This is also seen in the culture using [U-<sup>13</sup>C]glucose in the previous section, where the amount of alanine formed is higher than the amount of lactate formed from carbon sources other than glucose. The fractional labeling of glycine reaches a maximum of 0.12 (measured at 24 h) before reaching a final fractional labeling of 0.06. At 24 h the single labeled species makes up for 12 % and fully labeled species at 6 % compared with 6 % and 3 % for the singly and fully labeled species at the end of the cultivation respectively. The final fractional labeling of serine is 0.18 with 37 % being the single labeled species and 6 % making up double (4 %) and fully labeled (2 %) serine. The decrease in the fractional labeling during the end of cultivation is probably due to the consumption of serine which might lead to exchange fluxes. This is explained in detail in the later part. Fully labeled glutamate makes up 56 % of the total glutamate produced with a final fractional labeling of 0.76. The <sup>13</sup>C<sub>3</sub> fraction makes up 12 % and the <sup>13</sup>C<sub>4</sub> makes up 10 %. The <sup>13</sup>C<sub>1</sub> and <sup>13</sup>C<sub>2</sub> fractions are 7 % each respectively. Aspartate has a final fractional labeling of 0.37. The fully labeled fraction is 23 % whereas the unlabeled fraction is around 50 %. The <sup>13</sup>C<sub>1</sub>, <sup>13</sup>C<sub>2</sub> and <sup>13</sup>C<sub>3</sub> make up 9 % each respectively. The fully labeled glutamate is probably mostly formed from fully labeled glutamine due to the glutaminase activity. However, the presence of other labeled forms of glutamate and also the presence of labeled aspartate indicate high glutamate dehydrogenase activity for the entry of glutamate into the TCA cycle and aspartate transaminase/malate dehydrogenase for the aspartate-malate shuttle.

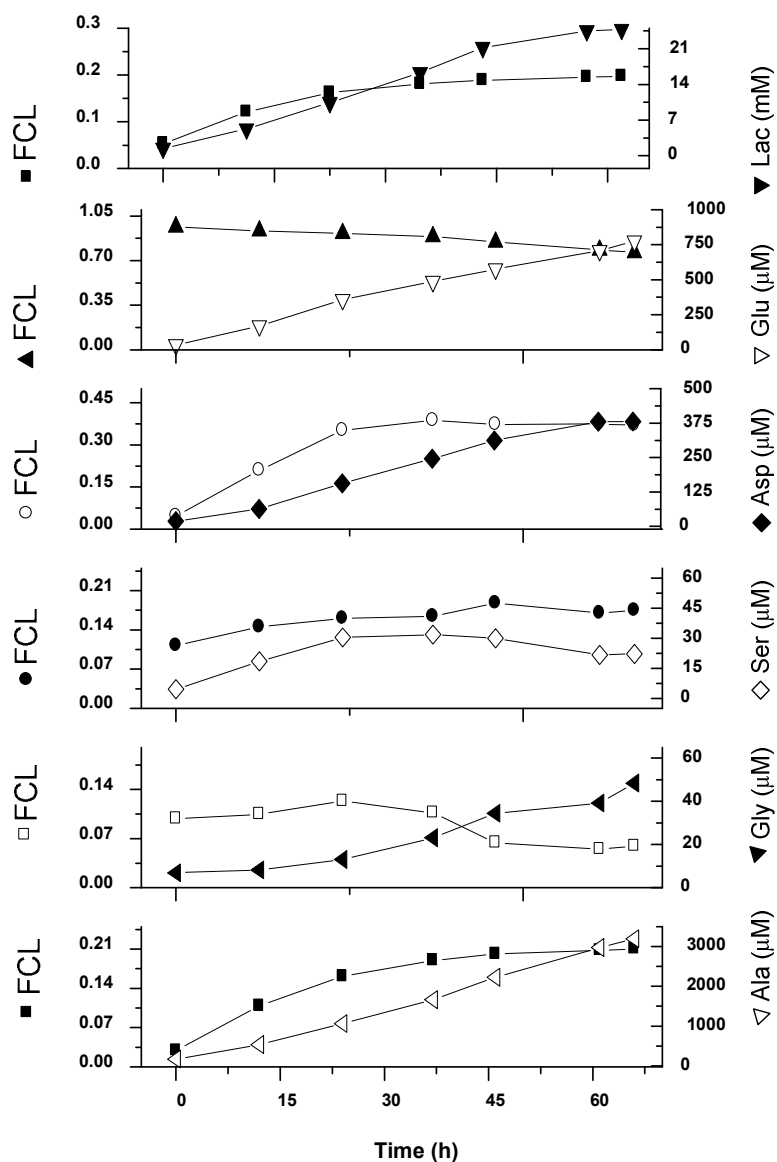


**Figure 5.5.4:** Extracellular metabolite labeling plotted along with extracellular concentration profile for the cultivation using  $[1-^{13}\text{C}_1]\text{glucose} + [\text{U}-^{13}\text{C}]\text{glutamine}$  containing media described in Figure 5.5.1. The right axis gives the concentration and the left axis the fractional carbon labeling of the metabolite indicated on the right axis. The sampling procedure is given in material and methods. The initial time “0” refers to the sample after the addition of media to cells.

***[1-<sup>13</sup>C<sub>1</sub>]Glucose and [U-<sup>13</sup>C]threonine***

The plots showing the interdependency of the metabolites in the culture with [1-<sup>13</sup>C<sub>1</sub>]glucose and [U-<sup>13</sup>C]threonine show very similar patterns to the cultures with [1-<sup>13</sup>C<sub>1</sub>]glucose and [U-<sup>13</sup>C]glutamine [Figure 5.6.4 (A), (B) and (C)]. The relationship between the metabolites has been explained earlier. There is a linear relationship between most of the metabolites. The non-linear relationship of serine is due to its consumption at the end of the cultivation phase in the presence of low concentrations of glucose.

The extracellular samples of the cultivation with [1-<sup>13</sup>C<sub>1</sub>]glucose and [U-<sup>13</sup>C]threonine were analyzed for the amino acids and lactate, and the fractional carbon labeling of the amino acids and lactate in the supernatant with respect to time along with their concentration profile is shown in Figure 5.6.5. Lactate reaches a higher final fractional carbon labeling (0.14) than alanine (0.13). The major labeled isotopomer in both the metabolites is the singly labeled species making up 38 % in lactate and 35 % in alanine. 62 % of alanine is unlabeled compared to 60 % of lactate offering further evidence that higher percentage of alanine is produced compared to lactate from TCA cycle. Glycine has a high fractional labeling of 0.16 (at 24h) and reaches a final carbon labeling of 0.06. The single labeled species makes up for 12 % and fully labeled species at 10 % at 24h and drops down to 6 % and 3 % for the singly and fully labeled species respectively at the end of the cultivation. The fractional carbon labeling of serine reaches 0.15 at the end of cultivation from a high of 0.28. The fully labeled species of serine drops down to 0.3 % from a high of 21 % at the start of the cultivation. The fractional labeling of aspartate and glutamate is 0.04 and 0.06 respectively. 19 % of the glutamate and 14 % of aspartate is single labeled. This supports the fact that there is a high degree of activity of glutamate dehydrogenase and aspartate transaminase/malate dehydrogenase.

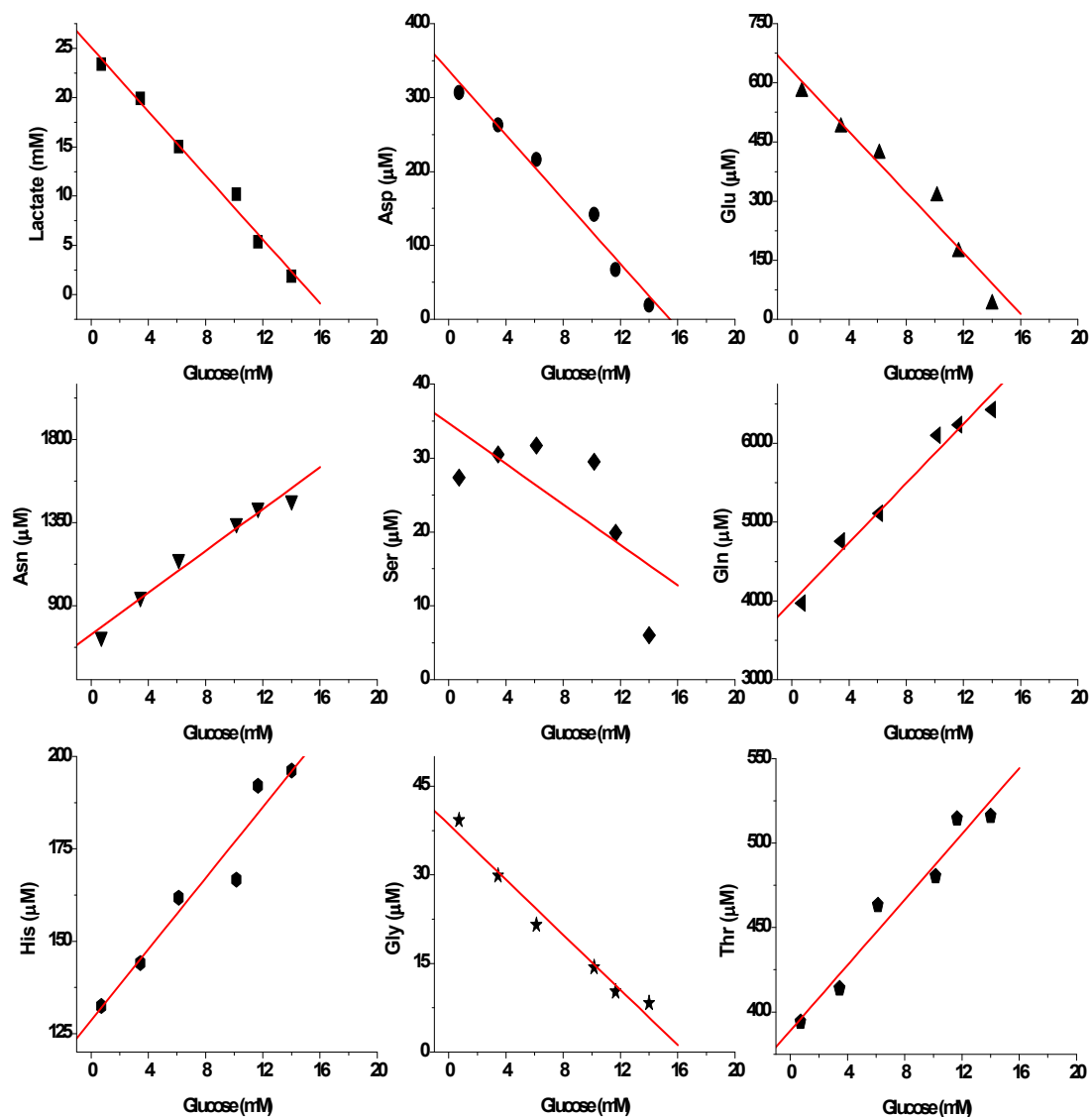


**Figure 5.6.4 (A):** Metabolite concentrations of the cultivation using  $[1-^{13}\text{C}]$ glucose +  $[U-^{13}\text{C}]$ threonine isotopic label plotted against glucose for the culture described in Figure 5.6.1. Linear regression was performed on each of the metabolite.

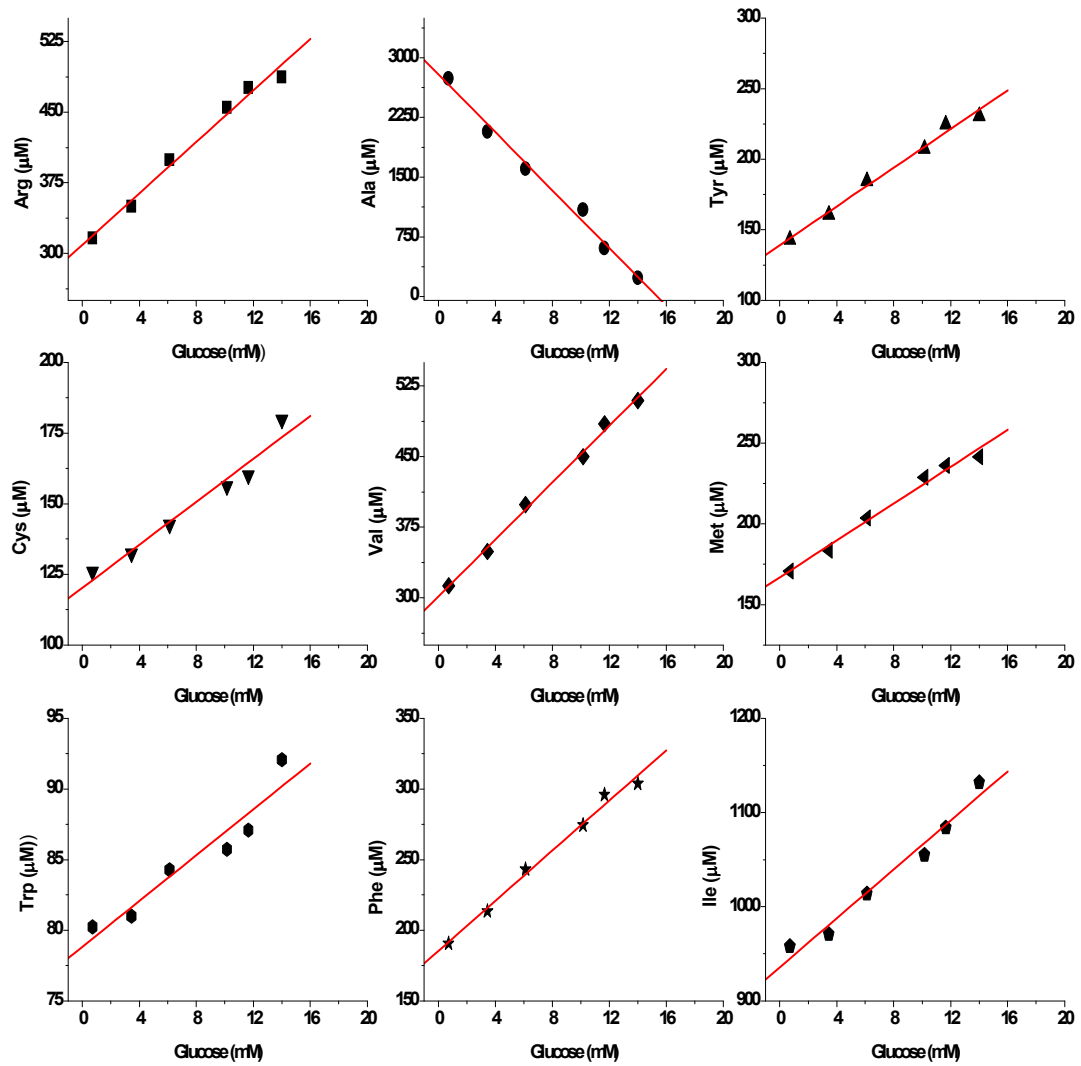


**Figure 5.6.4 (B):** Metabolite concentrations of the cultivation using  $[1-^{13}\text{C}]$ glucose +  $[\text{U}-^{13}\text{C}]$ threonine isotopic label plotted against glucose for the culture described in Figure 5.6.1. Linear regression was performed on each of the metabolite.

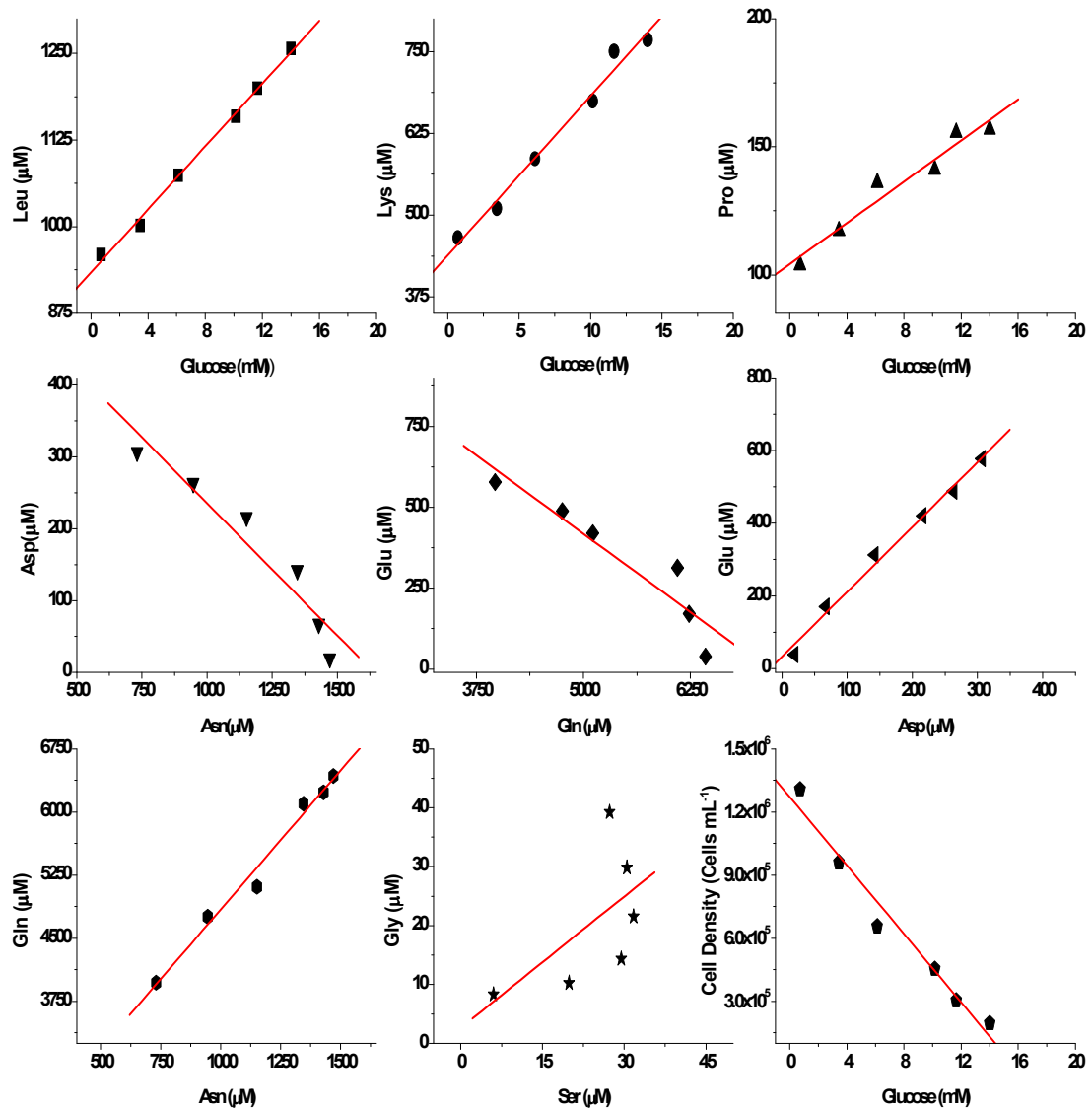


**Figure 5.6.4 (C):** Metabolite concentrations of the cultivation using  $[1-^{13}\text{C}_1]\text{glucose} + [\text{U}-^{13}\text{C}]\text{threonine}$  isotopic label plotted against glucose and also a few against each other for the culture described in Figure 5.6.1. Linear regression was performed on each of the metabolite.

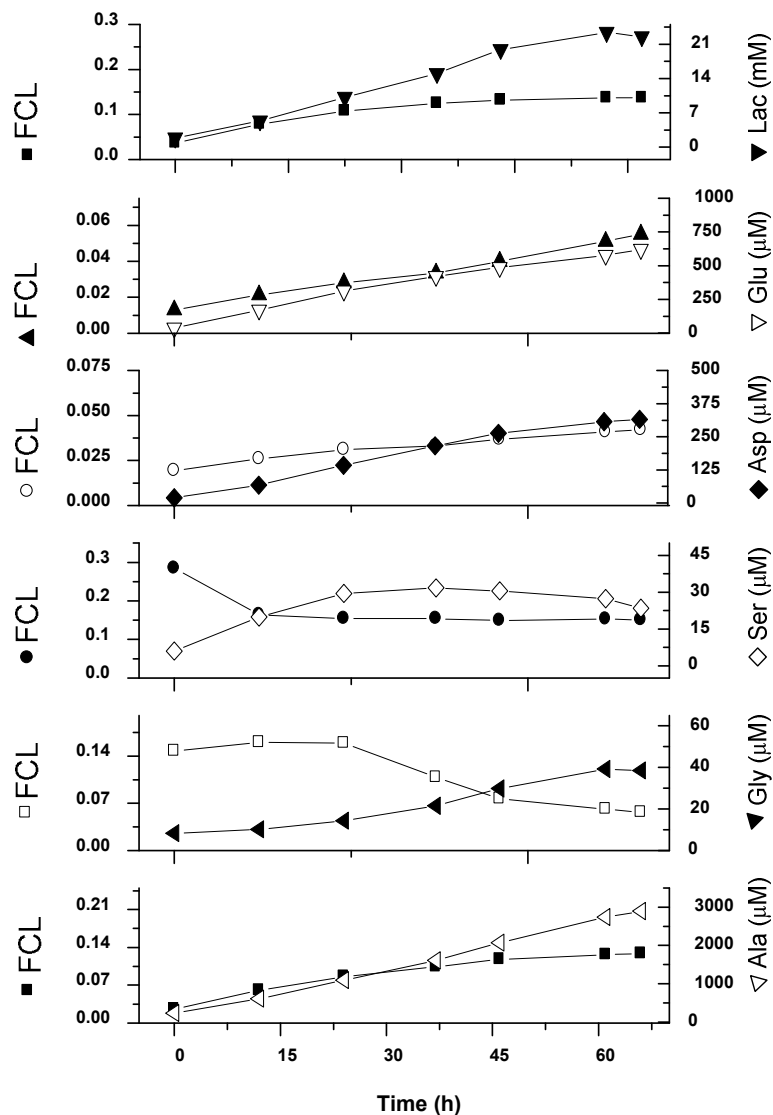
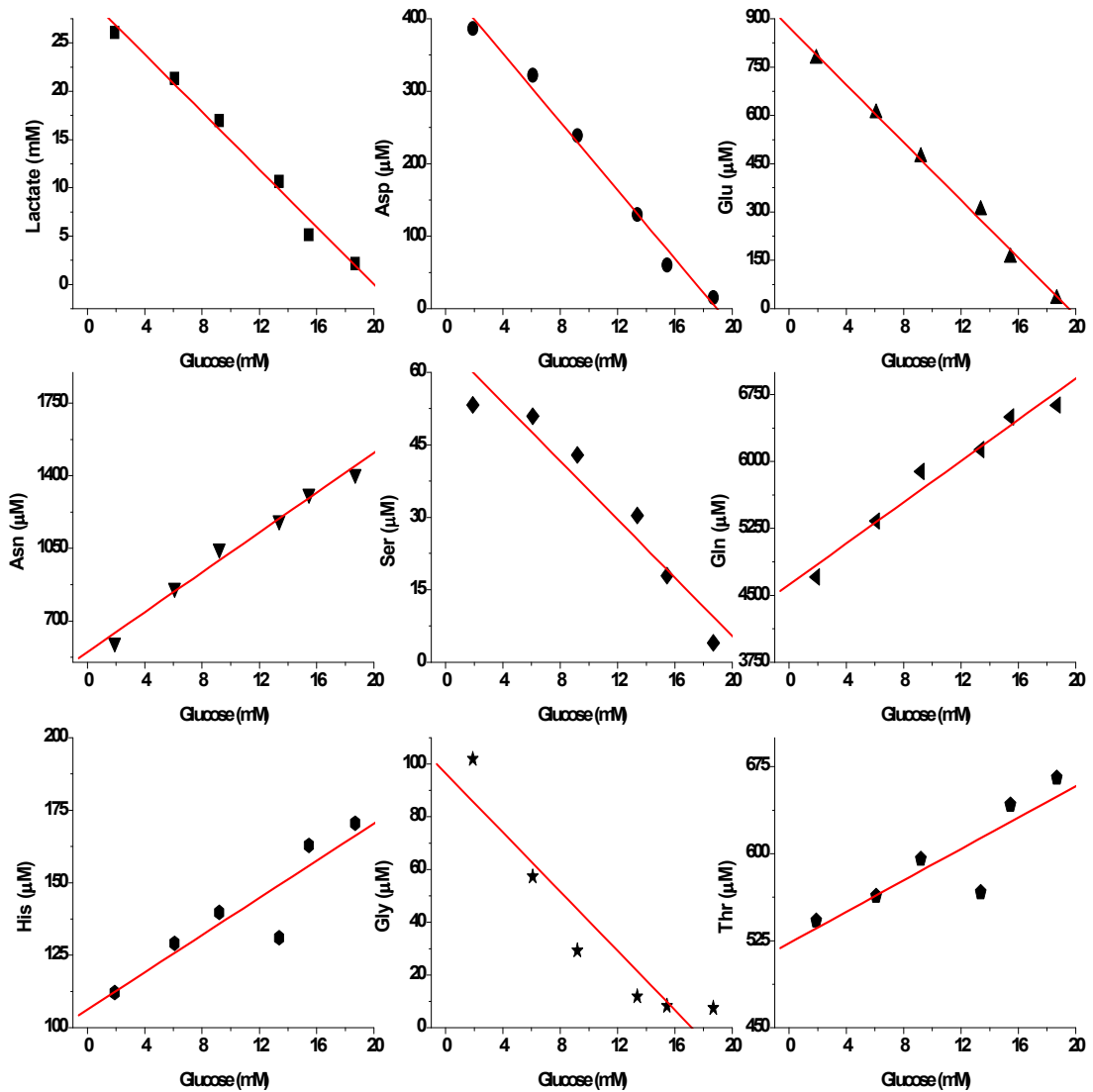


**Figure 5.6.5:** Extracellular metabolite labeling plotted along with extracellular concentration profile for the cultivation using  $[1-^{13}\text{C}_1]\text{glucose} + [\text{U}-^{13}\text{C}]\text{threonine}$  containing media described in Figure 5.6.1. The right axis gives the concentration and the left axis the fractional carbon labeling of the metabolite indicated on the right axis. The sampling procedure is given in material and methods. The initial time “0” refers to the sample after the addition of media to cells.

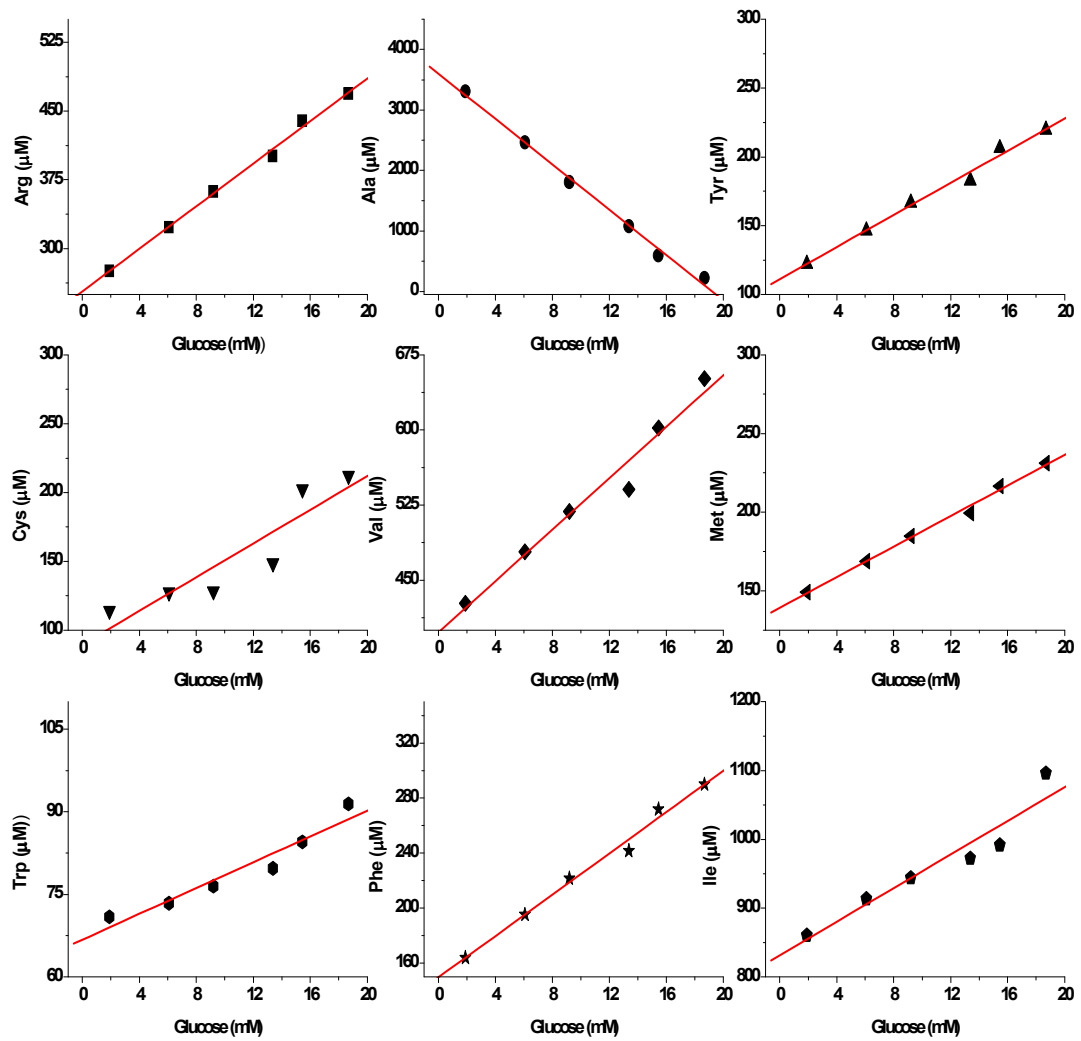
***[1,2-<sup>13</sup>C<sub>2</sub>]Glucose***

Figure 5.6.6 (A, B and C) gives the plots of the metabolite interdependency of the culture with [1,2-<sup>13</sup>C<sub>2</sub>]glucose. All the metabolites show linear relationship with glucose. There is no consumption of serine during the end of the cultivation unlike the previous culture because of the availability of sufficient glucose. The yield of glycine increases dramatically towards the end of the cultivation compared to the previous two cultures. The most probable reason might be the continual production of serine in the presence of glucose.

The fractional carbon labeling of the amino acids and lactate in the supernatant with respect to time along with their concentration profile is shown in Figure 5.6.7. Lactate has a final fractional carbon labeling of 0.27 with 36 % being <sup>13</sup>C<sub>2</sub> species and 5 % being <sup>13</sup>C<sub>1</sub> labeled. 32 % of the alanine concentration is <sup>13</sup>C<sub>2</sub> and 6 % being <sup>13</sup>C<sub>1</sub> with a final fractional carbon labeling of 0.24. In contrast to the previous culture, the fractional labeling of glycine increases with time, and it has a final fractional labeling of 0.23. 41 % of the final glycine is made up of <sup>13</sup>C<sub>1</sub> species. Serine reaches a final FCL of 0.3 with 22 % of <sup>13</sup>C<sub>1</sub> and 32 % of <sup>13</sup>C<sub>2</sub> serine. Aspartate and glutamate have a FCL of 0.08 and 0.1 respectively at the end of cultivation with <sup>13</sup>C<sub>2</sub> being the major contributor of the <sup>13</sup>C isotope in both the amino acids (9 % for aspartate and 13 % for glutamate).



**Figure 5.6.6 (A):** Metabolite concentrations of the cultivation using  $[1,2-^{13}\text{C}_2]$ glucose isotopic label plotted against glucose for the culture described in Figure 5.6.1. Linear regression was performed on each of the metabolite.



**Figure 5.6.6 (B):** Metabolite concentrations of the cultivation using  $[1,2-^{13}\text{C}_2]$ glucose isotopic label plotted against glucose for the culture described in Figure 5.6.1. Linear regression was performed on each of the metabolite.

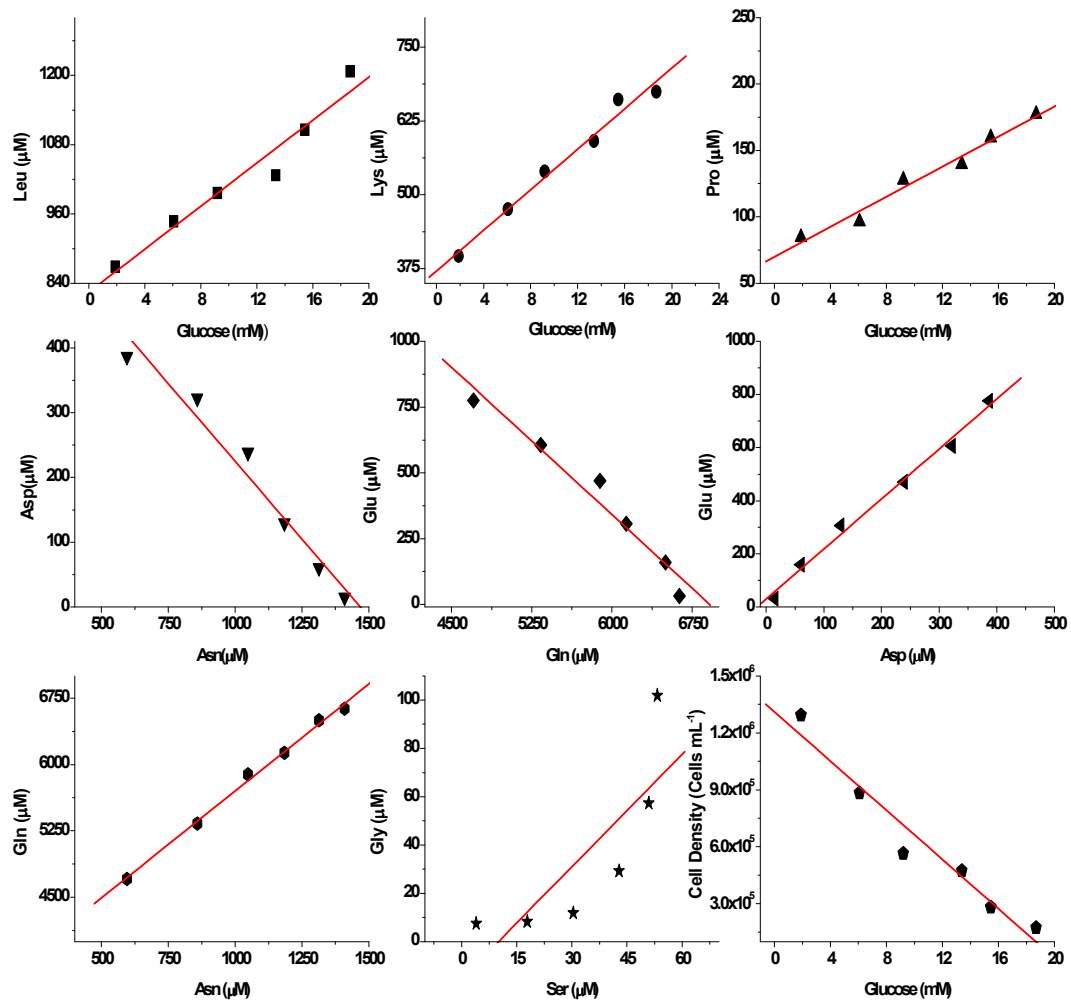


**Figure 5.6.6 (C):** Metabolite concentrations of the cultivation using [1,2-<sup>13</sup>C<sub>2</sub>]glucose isotopic label plotted against glucose and also a few against each other for the culture described in Figure 5.6.1. Linear regression was performed on each of the metabolite.

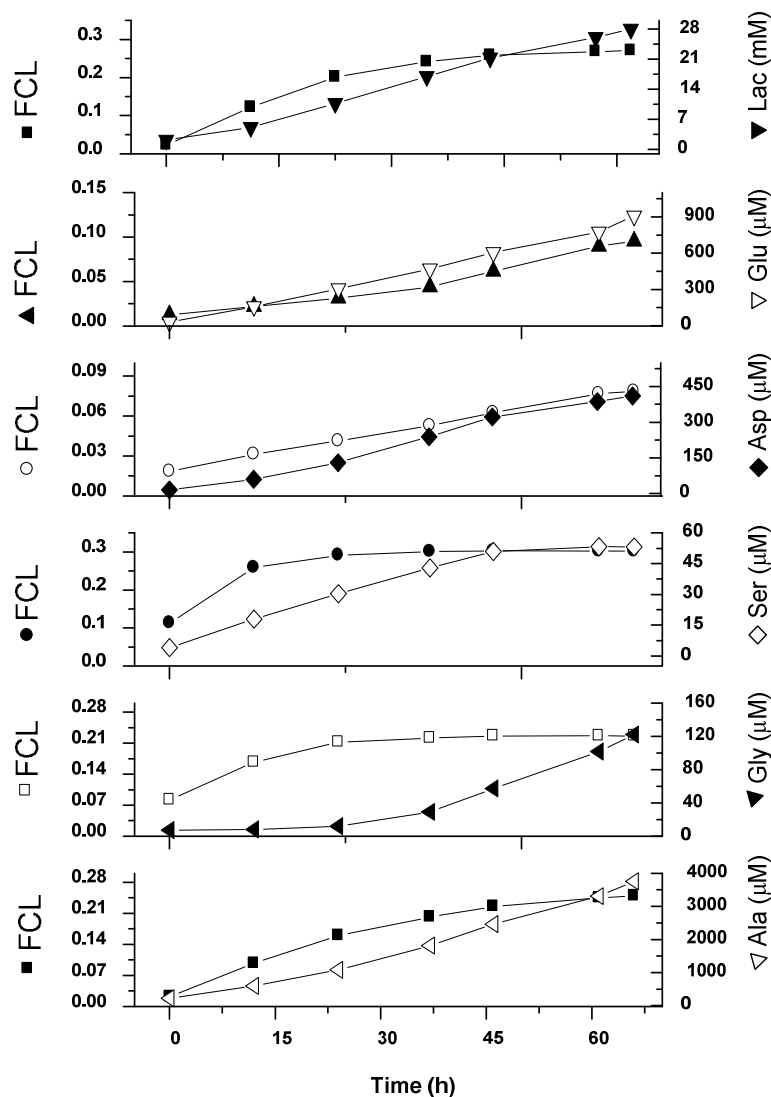


**Figure 5.6.7:** Extracellular metabolite labeling plotted along with extracellular concentration profile for the cultivation using  $[1,2-^{13}\text{C}_2]$ glucose containing media described in Figure 5.6.1. The right axis gives the concentration and the left axis the fractional carbon labeling of the metabolite indicated on the right axis. The sampling procedure is given in material and methods. The initial time “0” refers to the sample after the addition of media to cells.

***[3-<sup>13</sup>C<sub>1</sub>]Pyruvate***

The interdependency of the metabolites in the culture with [3-<sup>13</sup>C<sub>1</sub>]pyruvate is shown in Figure 5.7.7 (A, B & C). The linear relationships shown are similar to the culture with 1,2 <sup>13</sup>C<sub>2</sub> glucose.

Figure 5.6.9 shows the fractional carbon labeling of the amino acids and lactate in the supernatant with respect to time along with their concentration profile. The fractional carbon labeling of lactate at the end of 12 h is 0.13 and decreases to 0.03 at the end of the cultivation. Similarly, alanine has a fractional labeling of 0.11 at the end of 12 h and 0.04 at the end of the cultivation. 35 % <sup>13</sup>C<sub>1</sub> lactate is present at 12 h with 8 % at the end and in case of alanine it drops from 32 % <sup>13</sup>C<sub>1</sub> alanine at 12 h to 11 % the end of the cultivation. Glycine has 15 % <sup>13</sup>C<sub>1</sub> and 5 % fully labeled species at 24 h decreasing to 5 % <sup>13</sup>C<sub>1</sub> and 0.3 % <sup>13</sup>C<sub>2</sub> at the end of cultivation. The fractional labeling also shows a decrease from 0.12 at 24 h to 0.03 at the end of cultivation. Serine follows a similar pattern with the <sup>13</sup>C<sub>1</sub> being 8 % at 12 h to 4 % at the end. The fractional labeling of serine is lower than glycine being 0.02, in contrast to the three previous cultures where serine had higher fractional carbon labeling. Aspartate and glutamate show similar final fractional labeling of 0.02. The <sup>13</sup>C<sub>1</sub> fraction makes up 7 % of the final aspartate and 10 % of the final glutamate.

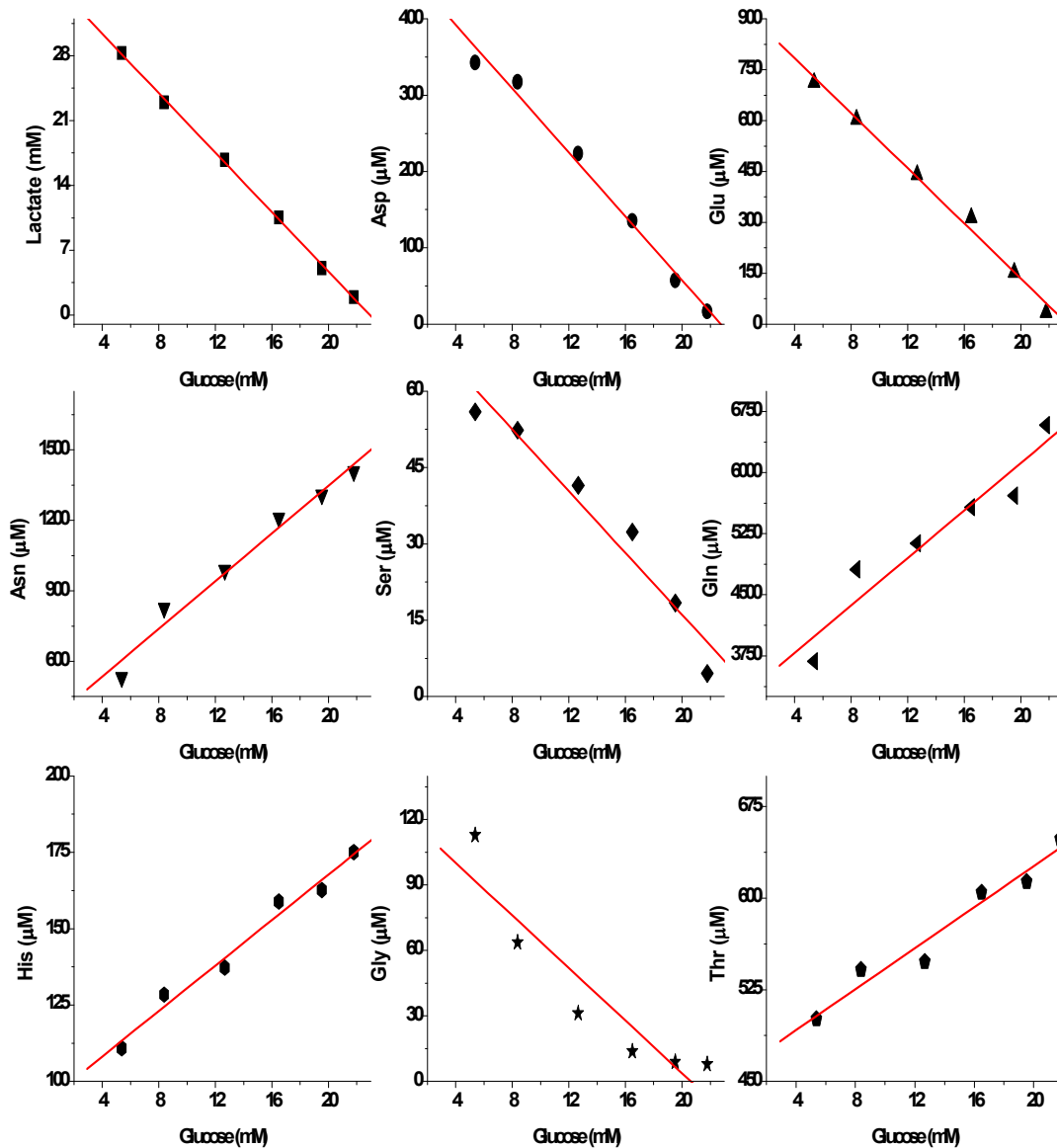


**Figure 5.6.8 (A):** Metabolite concentrations of the cultivation using  $[3-^{13}\text{C}_1]$ pyruvate isotopic label plotted against glucose for the culture described in Figure 5.6.1. Linear regression was performed on each of the metabolite.

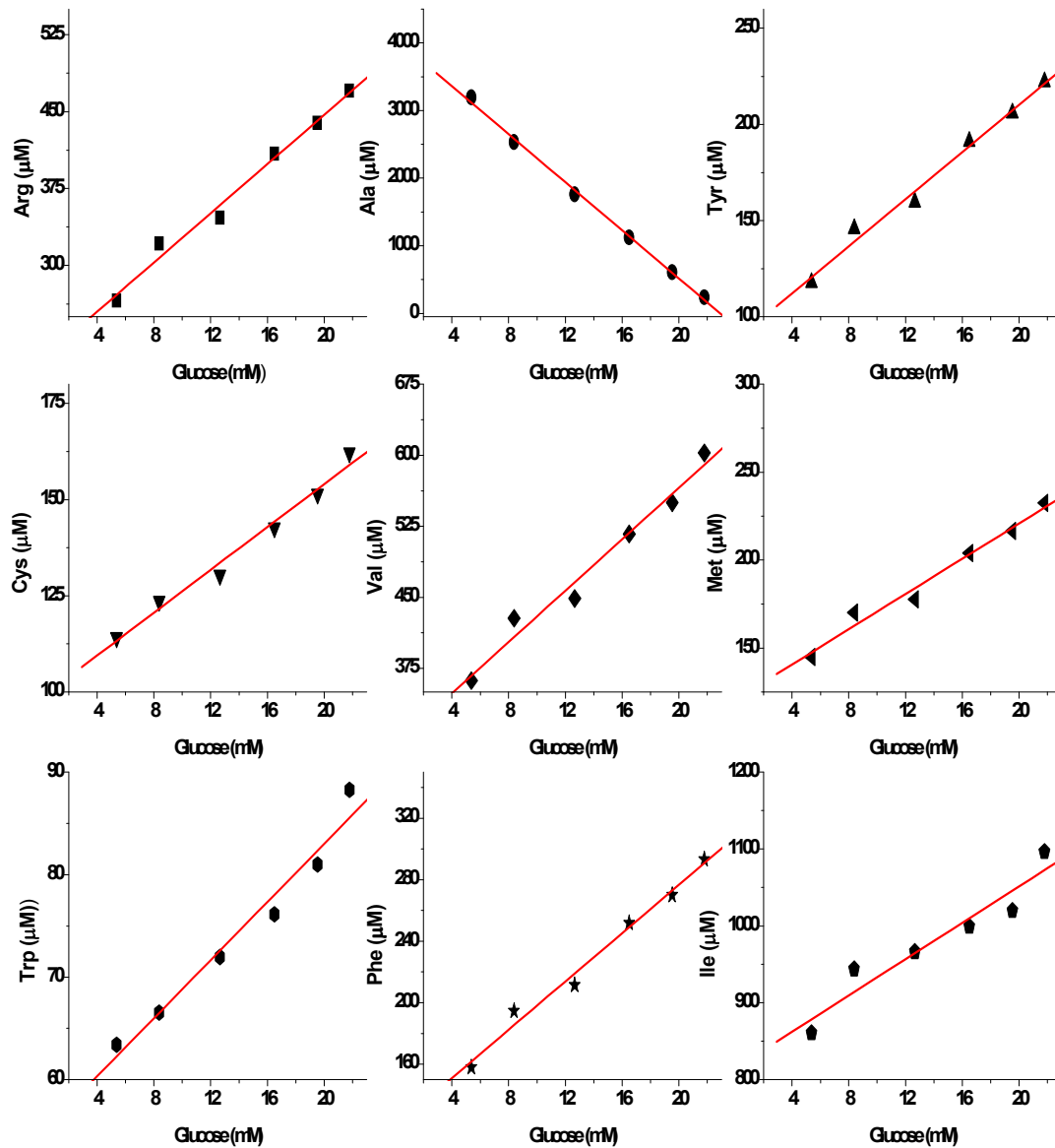


**Figure 5.6.8 (B):** Metabolite concentrations of the cultivation using  $[3-^{13}\text{C}_1]$ pyruvate isotopic label plotted against glucose for the culture described in Figure 5.6.1. Linear regression was performed on each of the metabolite.

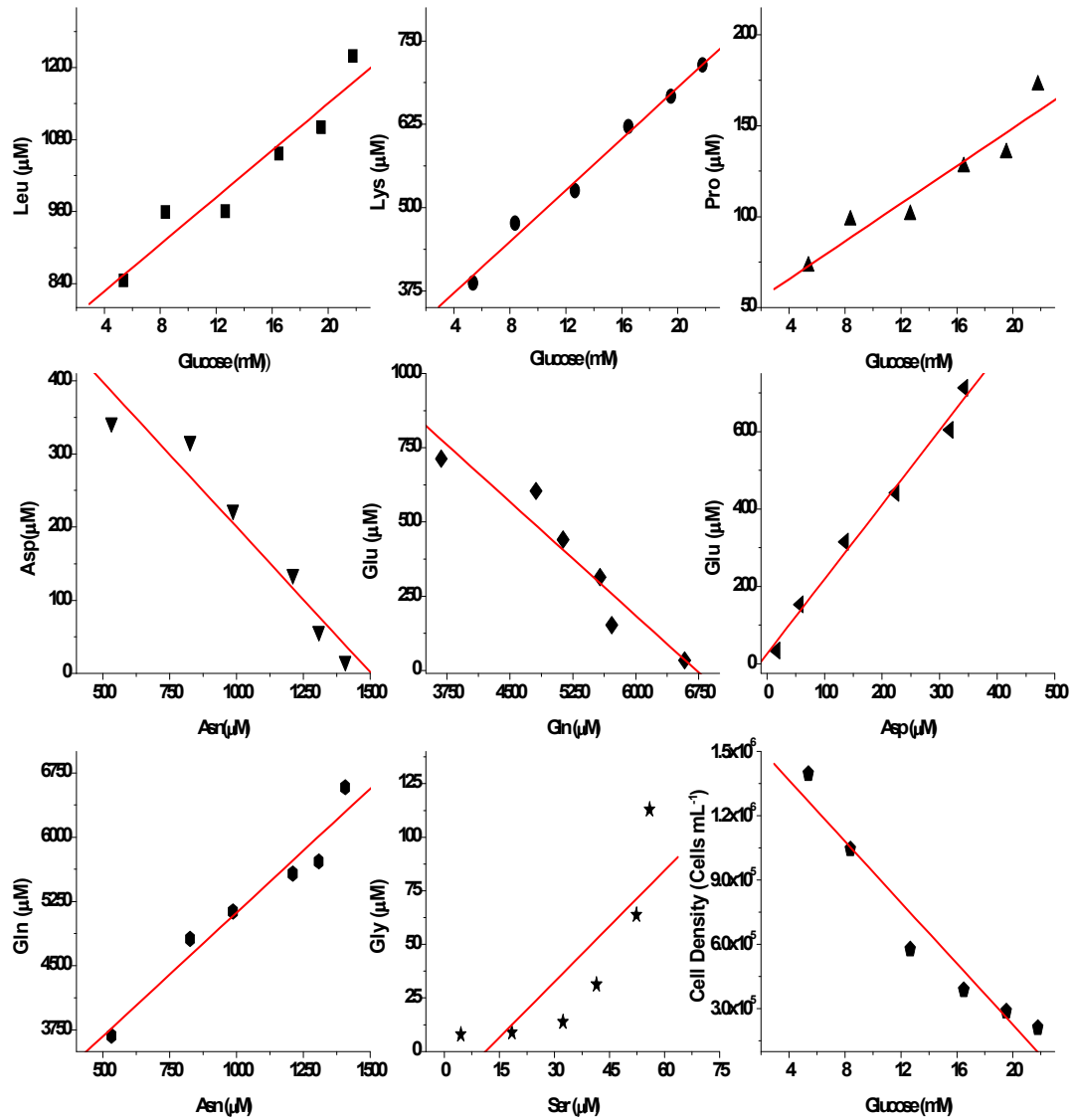


**Figure 5.6.8 (C):** Metabolite concentrations of the cultivation using  $[3-^{13}\text{C}_1]$ pyruvate isotopic label plotted against glucose and also a few against each other for the culture described in Figure 5.6.1. Linear regression was performed on each of the metabolite.

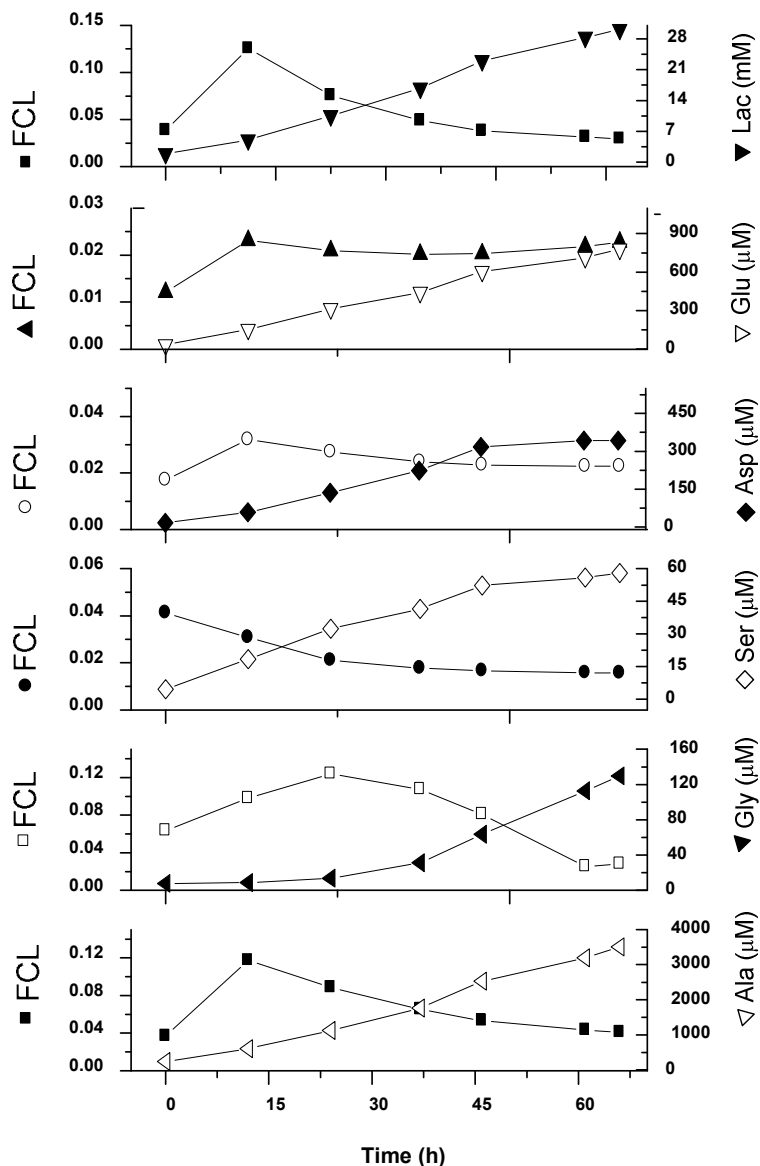


**Figure 5.6.9:** Extracellular metabolite labeling plotted along with extracellular concentration profile for the cultivation using  $[3-^{13}\text{C}_1]$ pyruvate containing media described in Figure 5.6.1. The right axis gives the concentration and the left axis the fractional carbon labeling of the metabolite indicated on the right axis. The sampling procedure is given in material and methods. The initial time “0” refers to the sample after the addition of media to cells.

### 5.5.3.3 Examination of metabolic pathways

#### Specific rate of metabolites

The data from the four cultivations were compared to get a relatively complete picture of the metabolism. The specific rate of production and consumption of the metabolites for the four cultures along with the mean and standard deviation over the whole culture is given in Table 5.6.2. The cell cultures with [1,2-<sup>13</sup>C<sub>2</sub>]glucose and [3-<sup>13</sup>C<sub>1</sub>]pyruvate show high specific rates for glucose consumption and lactate production compared to the other cultures. This is due to the presence of higher concentration of glucose in these two cultures compared to the other two cultures. The lactate to glucose (L/G) (M/M) ratio of all the four cultures over the whole cultivation ranges from 1.45 for the culture with [1,2-<sup>13</sup>C<sub>2</sub>]glucose to 1.62 for the culture with [1-<sup>13</sup>C<sub>1</sub>]glucose and [U-<sup>13</sup>C]glutamine. However, these ratios do not show specific relationship to the specific rate of glucose uptake. Nevertheless the higher L/G ratio of the culture with [1-<sup>13</sup>C<sub>1</sub>]glucose and [U-<sup>13</sup>C]glutamine shows a higher specific uptake of glutamine, in comparison to the culture with [1,2-<sup>13</sup>C<sub>2</sub>]glucose. Hence the entry of a higher amount of glutamine in the TCA cycle probably redirects the glucose to the overflow metabolism. Also seen is that the specific rate of lactate and alanine formation show a linear relationship. This is due to the fact that both these metabolites are derived from pyruvate. In the cultivations with [1-<sup>13</sup>C<sub>1</sub>]glucose + [U-<sup>13</sup>C]glutamine and [1-<sup>13</sup>C<sub>1</sub>]glucose + [U-<sup>13</sup>C]threonine, it is seen that there is a consumption of serine towards the end of the culture time. This is most probably due to the reduction in the concentration of glucose available in the media. The cultures with [1,2-<sup>13</sup>C<sub>2</sub>]glucose and [3-<sup>13</sup>C<sub>1</sub>]pyruvate do not show this phenomenon of serine consumption and thus the highest deviation is shown by the metabolites glycine and serine for the four cultures. However, the specific rates of the two sets of cultures are highly comparable. The other metabolites don't show this high deviation.

PHYSIOLOGICAL INVESTIGATIONS ON CHO CELLS

**Table 5.6.2:** Specific rates of uptake and production of metabolites in the parallel cell cultures using different isotopic labels. Negative values indicate uptake while positive values indicate production.

Metabolite	$1^{13}\text{C-Glc} + \text{U}^{13}\text{C-Gln}$ (mol cell <sup>-1</sup> h <sup>-1</sup> )	$1^{13}\text{C-Glc} + \text{U}^{13}\text{C-Thr}$ (mol cell <sup>-1</sup> h <sup>-1</sup> )	$1,2^{13}\text{C-Glc}$ (mol cell <sup>-1</sup> h <sup>-1</sup> )	$3^{13}\text{C-Pyr}$ (mol cell <sup>-1</sup> h <sup>-1</sup> )	Mean	S.D	S.D (%)
<b>Anabolic Metabolites</b>							
Lactate	$1.3 \times 10^{-08}$	$1.3 \times 10^{-08}$	$1.4 \times 10^{-08}$	$1.7 \times 10^{-08}$	<b><math>1.4 \times 10^{-08}</math></b>	$1.9 \times 10^{-09}$	13
Alanine	$1.7 \times 10^{-09}$	$1.6 \times 10^{-09}$	$1.9 \times 10^{-09}$	$2.0 \times 10^{-09}$	<b><math>1.8 \times 10^{-09}</math></b>	$1.8 \times 10^{-10}$	10
Aspartate	$2.0 \times 10^{-10}$	$1.7 \times 10^{-10}$	$2.1 \times 10^{-10}$	$2.0 \times 10^{-10}$	<b><math>2.0 \times 10^{-10}</math></b>	$1.6 \times 10^{-11}$	8
Glutamate	$4.2 \times 10^{-10}$	$3.4 \times 10^{-10}$	$4.7 \times 10^{-10}$	$4.5 \times 10^{-10}$	<b><math>4.2 \times 10^{-10}</math></b>	$5.6 \times 10^{-11}$	13
Serine	$10.0 \times 10^{-12}$	$1.0 \times 10^{-11}$	$2.6 \times 10^{-11}$	$3.2 \times 10^{-11}$	<b><math>2.0 \times 10^{-11}</math></b>	$1.1 \times 10^{-11}$	57
Glycine	$2.3 \times 10^{-11}$	$1.8 \times 10^{-11}$	$6.1 \times 10^{-11}$	$7.3 \times 10^{-11}$	<b><math>4.4 \times 10^{-11}</math></b>	$2.7 \times 10^{-11}$	62
<b>Catabolic Metabolites</b>							
Glucose	$-8.1 \times 10^{-09}$	$-8.1 \times 10^{-09}$	$-9.5 \times 10^{-09}$	$-1.1 \times 10^{-08}$	<b><math>-9.1 \times 10^{-09}</math></b>	$1.3 \times 10^{-09}$	14
Pyruvate	$-1.8 \times 10^{-10}$	$-1.0 \times 10^{-10}$	$-1.8 \times 10^{-10}$	$-1.6 \times 10^{-10}$	<b><math>-1.6 \times 10^{-10}</math></b>	$3.5 \times 10^{-11}$	22
Glutamine	$-2.1 \times 10^{-09}$	$-1.7 \times 10^{-09}$	$-1.1 \times 10^{-09}$	$-1.9 \times 10^{-09}$	<b><math>-1.7 \times 10^{-09}</math></b>	$4.3 \times 10^{-10}$	24
Asparagine	$-5.3 \times 10^{-10}$	$-4.9 \times 10^{-10}$	$-4.7 \times 10^{-10}$	$-5.7 \times 10^{-10}$	<b><math>-5.2 \times 10^{-10}</math></b>	$4.7 \times 10^{-11}$	9
Histidine	$-4.6 \times 10^{-11}$	$-4.2 \times 10^{-11}$	$-3.2 \times 10^{-11}$	$-4.0 \times 10^{-11}$	<b><math>-4.0 \times 10^{-11}</math></b>	$6.0 \times 10^{-12}$	15
Threonine	$-9.2 \times 10^{-11}$	$-8.3 \times 10^{-11}$	$-6.7 \times 10^{-11}$	$-9.3 \times 10^{-11}$	<b><math>-8.4 \times 10^{-11}</math></b>	$1.2 \times 10^{-11}$	14
Arginine	$-1.1 \times 10^{-10}$	$-1.1 \times 10^{-10}$	$-1.0 \times 10^{-10}$	$-1.3 \times 10^{-10}$	<b><math>-1.1 \times 10^{-10}</math></b>	$1.0 \times 10^{-11}$	9
Tyrosine	$-6.0 \times 10^{-11}$	$-5.7 \times 10^{-11}$	$-5.3 \times 10^{-11}$	$-6.6 \times 10^{-11}$	<b><math>-5.9 \times 10^{-11}</math></b>	$5.4 \times 10^{-12}$	9
Cysteine	$-7.0 \times 10^{-11}$	$-3.4 \times 10^{-11}$	$-3.0 \times 10^{-11}$	$-3.1 \times 10^{-11}$	<b><math>-4.1 \times 10^{-11}</math></b>	$2.0 \times 10^{-11}$	47
Valine	$-1.4 \times 10^{-10}$	$-1.3 \times 10^{-10}$	$-1.3 \times 10^{-10}$	$-1.5 \times 10^{-10}$	<b><math>-1.3 \times 10^{-10}</math></b>	$1.2 \times 10^{-11}$	9
Methionine	$-4.6 \times 10^{-11}$	$-4.7 \times 10^{-11}$	$-4.5 \times 10^{-11}$	$-5.5 \times 10^{-11}$	<b><math>-4.8 \times 10^{-11}</math></b>	$4.7 \times 10^{-12}$	10
Tryptophan	$-1.6 \times 10^{-11}$	$-1.3 \times 10^{-11}$	$-1.3 \times 10^{-11}$	$-1.6 \times 10^{-11}$	<b><math>-1.4 \times 10^{-11}</math></b>	$1.6 \times 10^{-12}$	11
Phenylalanine	$-7.7 \times 10^{-11}$	$-7.4 \times 10^{-11}$	$-6.8 \times 10^{-11}$	$-8.5 \times 10^{-11}$	<b><math>-7.6 \times 10^{-11}</math></b>	$7.2 \times 10^{-12}$	10
Isoleucine	$-1.2 \times 10^{-10}$	$-1.2 \times 10^{-10}$	$-1.1 \times 10^{-10}$	$-1.5 \times 10^{-10}$	<b><math>-1.2 \times 10^{-10}</math></b>	$1.4 \times 10^{-11}$	12
Leucine	$-2.0 \times 10^{-10}$	$-2.0 \times 10^{-10}$	$-1.8 \times 10^{-10}$	$-2.3 \times 10^{-10}$	<b><math>-2.0 \times 10^{-10}</math></b>	$2.2 \times 10^{-11}$	11
Lysine	$-1.8 \times 10^{-10}$	$-2.0 \times 10^{-10}$	$-1.5 \times 10^{-10}$	$-2.0 \times 10^{-10}$	<b><math>-1.8 \times 10^{-10}</math></b>	$2.4 \times 10^{-11}$	13
Proline	$-5.5 \times 10^{-11}$	$-3.6 \times 10^{-11}$	$-5.1 \times 10^{-11}$	$-6.3 \times 10^{-11}$	<b><math>-5.1 \times 10^{-11}</math></b>	$1.1 \times 10^{-11}$	22

**Metabolic quotient of metabolites**

Due to the consumption of serine at the end of the cultivation, the metabolic quotient on glucose for the cultures was calculated only during their exponential growth phases. For the first set of two cultures i.e. with [1-<sup>13</sup>C<sub>1</sub>]glucose plus [U-<sup>13</sup>C]glutamine and with [1-<sup>13</sup>C<sub>1</sub>]glucose plus [U-<sup>13</sup>C]threonine, the quotients were calculated from the initial time (time 0) to the cultivation time of 37h. For the other set i.e. with [1,2-<sup>13</sup>C<sub>2</sub>]glucose and [3-<sup>13</sup>C<sub>1</sub>]pyruvate, the time chosen for the quotient calculation was from 12 h to 46 h. The quotients were calculated using three separate methods of calculation. The first method used the difference of the concentrations of the metabolites and glucose. In the second method the concentration profile of the metabolite and glucose was smoothed by spline fitting using MATLAB and then calculating the difference of the concentrations from the spline curve. The third method used the slope of each time point on the concentration-time curves of the metabolite and glucose to provide the quotient. Table 5.6.3 gives the mean quotients on glucose calculated for the four cultures using the three methods and also the cumulative average and deviation. With the exception of glycine, none of the metabolites show major deviations. However, with regard to glycine, the cultivation set with [1-<sup>13</sup>C<sub>1</sub>]glucose plus [U-<sup>13</sup>C]glutamine and [1-<sup>13</sup>C<sub>1</sub>]glucose plus [U-<sup>13</sup>C]threonine show comparable quotients and also the cultivation set with [1,2-<sup>13</sup>C<sub>2</sub>]glucose and [3-<sup>13</sup>C<sub>1</sub>]pyruvate. The production of glycine is lower in the cultivations with low concentration of glucose. Unlike their production rates, alanine and lactate do not display a linear relationship with respect to their yields from glucose. This shows that though both these metabolites are formed from the same precursor, i.e. pyruvate but the source of the precursor is not solely glucose. The metabolic quotients of the branched chain amino acids are higher in the cultures with lower glucose, i.e. [1-<sup>13</sup>C<sub>1</sub>]glucose plus [U-<sup>13</sup>C]glutamine and [1-<sup>13</sup>C<sub>1</sub>]glucose plus [U-<sup>13</sup>C]threonine. Again this might be to feed the TCA cycle due to the lower amount of glucose present and this is also seen with the quotients of glutamine. Moreover, the catabolism of branched chain amino acids is a rich provider of reducing equivalents and, due to the lower uptake of glucose in these media, probably provides the equivalents for energy production. The metabolic quotient of glutamate is also higher in the cultures with lower glucose due to the higher uptake of glutamine. Since the growth rate of the four cultures is comparable, the cellular components show very low deviation. These metabolic quotients and the labeling data would form the basis for the quantification of the whole cell metabolism using the technique of metabolic flux analysis.

PHYSIOLOGICAL INVESTIGATIONS ON CHO CELLS

**Table 5.6.3:** The metabolic quotient on glucose of the metabolites in the parallel cell cultures with different isotopic labels. Negative values indicate uptake while positive values indicate production. The biomass quotients are calculated using the biomass equations.

METABOLITE	$[1-^{13}\text{C}_1]\text{Glc} + [\text{U}-^{13}\text{C}]\text{Gln}$ (M/M)		$[1-^{13}\text{C}_1]\text{Glc} + [\text{U}-^{13}\text{C}]\text{Thr}$ (M/M)		$[1,2-^{13}\text{C}_2]\text{Glc}$ (M/M)		$[3-^{13}\text{C}_1]\text{Pyr}$ (M/M)		Cumulative (M/M)		
	Mean	Std.Dev	Mean	Std.Dev	Mean	Std.Dev	Mean	Std.Dev	Mean	Std.Dev	% Deviation
<b>Anabolic Metabolites</b>											
Lactate	1.763	0.058	1.861	0.056	1.686	0.157	1.664	0.034	1.744	0.089	5
Alanine	0.177	0.003	0.192	0.010	0.198	0.007	0.184	0.011	0.188	0.009	5
Glutamate	0.055	0.004	0.054	0.005	0.047	0.004	0.041	0.001	0.049	0.006	13
Aspartate	0.027	0.000	0.028	0.002	0.027	0.001	0.024	0.001	0.026	0.002	6
Glycine	0.002	0.000	0.002	0.000	0.005	0.001	0.006	0.001	0.004	0.002	54
Serine	0.003	0.001	0.004	0.001	0.003	0.001	0.003	0.000	0.003	0.000	7
<b>Catabolic Metabolites</b>											
Glutamine	-0.175	0.005	-0.147	0.011	-0.126	0.011	-0.106	0.024	-0.139	0.030	21
Asparagene	-0.045	0.001	-0.042	0.005	-0.049	0.002	-0.048	0.005	-0.046	0.003	7
Arginine	-0.012	0.001	-0.011	0.001	-0.013	0.001	-0.011	0.001	-0.012	0.001	5
Cysteine	-0.006	0.001	-0.005	0.000	-0.003	0.001	-0.003	0.000	-0.004	0.001	32
Histidine	-0.004	0.000	-0.006	0.001	-0.004	0.000	-0.003	0.000	-0.004	0.001	27
Isoleucine	-0.017	0.003	-0.016	0.001	-0.008	0.001	-0.008	0.001	-0.012	0.005	38
Leucine	-0.025	0.006	-0.024	0.000	-0.018	0.003	-0.015	0.001	-0.020	0.005	25
Lysine	-0.019	0.000	-0.026	0.001	-0.020	0.002	-0.018	0.001	-0.021	0.003	17
Methionine	-0.005	0.000	-0.005	0.000	-0.005	0.000	-0.004	0.000	-0.005	0.000	7
Phenylalanine	-0.008	0.000	-0.008	0.001	-0.008	0.001	-0.007	0.000	-0.008	0.000	6
Proline	-0.004	0.001	-0.004	0.000	-0.006	0.001	-0.004	0.000	-0.004	0.001	31
Threonine	-0.009	0.000	-0.009	0.001	-0.008	0.001	-0.007	0.001	-0.008	0.001	9
Tryptophan	-0.001	0.000	-0.001	0.000	-0.001	0.000	-0.001	0.000	-0.001	0.000	33
Tyrosine	-0.006	0.000	-0.007	0.000	-0.006	0.001	-0.006	0.000	-0.006	0.000	5
Valine	-0.015	0.001	-0.015	0.000	-0.013	0.002	-0.012	0.001	-0.014	0.002	11
<b>Biomass</b>											
Cells (g/mM)	0.018	0.004	0.020	0.002	0.021	0.002	0.022	0.003	0.020	0.002	9
Protein	0.117	0.025	0.133	0.010	0.135	0.013	0.145	0.020	0.132	0.012	9
DNA	0.001	0.000	0.001	0.000	0.001	0.000	0.001	0.000	0.001	0.000	9
RNA	0.021	0.004	0.024	0.002	0.024	0.002	0.026	0.004	0.024	0.002	9
Lipids	0.002	0.000	0.002	0.000	0.002	0.000	0.002	0.000	0.002	0.000	9
Carbohydrate	0.008	0.002	0.009	0.001	0.009	0.001	0.010	0.001	0.009	0.001	9

**Pyruvate metabolism**

In the biochemical network described in the earlier section, the cellular compartmentation into cytosol and mitochondria has been considered. Pyruvate has been assumed to be of a single pool in the cytosol entering the mitochondria as acetyl-CoA. It is known that eukaryotic cells have two pyruvate pools, one cytosolic and the other mitochondrial. However, since the transport of pyruvate into the mitochondria through the mitochondrial membrane takes place via the pyruvate carrier in exchange of a hydroxyl group (Lanoue and Schoolwerth, 1979), the assumption of a single pyruvate pool seemed to be justified. In the biochemical network, the formation of alanine and lactate, the two major products of overflow metabolism, was assumed to be from the single cytosolic pyruvate pool since there would be no difference in the labeling patterns. But the mass isotopomer and the fractional carbon labeling data obtained for lactate and alanine in the four cultivations could not be explained with the assumption of a single pyruvate pool. For example the fractional labeling of lactate in the cell cultivation with  $[1-^{13}\text{C}_1]\text{glucose}$  plus  $[\text{U}-^{13}\text{C}]\text{glutamine}$  was found to be lower than that of alanine. Assuming a single pool would give both the metabolites the same fractional labeling. In microbial systems, alanine can be formed by the catabolism of aspartate. However, this would give alanine a lower fractional carbon labeling than lactate. Considering a model in which there are only two pyruvate pools, one mitochondrial and the other cytosolic, with alanine being formed from the mitochondrial pool would give lactate a higher fractional labeling which is contrary to the data obtained. Carbon isotopic kinetic effects have not been demonstrated in the activity of lactate dehydrogenase. However, if present, the kinetic effects of isotope would still not explain the labeling obtained in a satisfactory manner. Peuhkurinen et al. (1983), Bouzier et al. (1998) and Zwingmann et al. (2001) have previously postulated the existence of two cytosolic and one mitochondrial pools of pyruvate associated with mammalian cells. The metabolic model of Peuhkurinen et al. (1983) obtained using data from incubation of perfused rats with  $[1-^{14}\text{C}_1]\text{pyruvate}$  or  $[1-^{14}\text{C}_1]\text{lactate}$  showed one of the cytosolic pool as 'glycolytic', being associated more closely with glycolysis, while the other 'peripheral' pool which communicates more closely with extracellular pyruvate than with cellular lactate. However, the above scheme also fails to explain the labeling patterns of alanine and lactate obtained in the four cultivations as seen in Table 5.6.4.

The concept of cytosolic compartmentation of metabolites in cells is a matter of debate and has been mathematically contradicted (Barros and Martinez, 2007). However, the possible basis for the presence of two pyruvate pools might have to do with the concept of metabolic channeling in pathway. Channeling of metabolites in a reaction sequence is the phenomenon

of the transfer of the reaction product of one enzyme to the next enzyme as its substrate without equilibrating with bulk solution (Ovadi, 1991). Association of glycolytic enzymes into multi-enzyme complexes or “metabolons” has been proposed as a mechanism to control glycolytic flux (Fothergillgilmore and Michels, 1993). Though highly debated, the association of glycolytic enzymes with the cytoskeleton of the cells has been demonstrated in a number of mammalian cells and tissues (al-Habori, 1995). Recently there has been biochemical and biophysical evidence that there exists a glycolytic enzyme complex on the cytoplasmic surface of the human RBC membrane (Campanella et al., 2005) and that the glycolytic enzymes are localized on fibrous sheaths in mouse spermatozoa (Krisfalusi et al., 2006). Substrate or metabolite channeling refers to the restricted diffusion or direct transfer of intermediates which can occur between active sites of sequential enzymes. Metabolic control theory has shown that flux control coefficients for enzymes of channeled pathways are usually larger than those in the corresponding non-channeled pathway and hence channeling plays a substantial role in the regulatory mechanism of pathways (Kholodenko et al., 1994). Though the concept of channeling has been around for quite a long time, there seems to have been no association made between the phenomena of multiple cytosolic compartmentation of pyruvate with that of channeling.

A possible biochemical network for the metabolism of pyruvate which explains the labeling as seen in the experiments is shown in Figure 5.6.10. The network shown is a modified version of the model proposed by Peuhkurinen et al. (1983). In the model, there are two cytosolic pools of pyruvate and a single mitochondrial pool of pyruvate. One of the cytosolic pools, depicted as pyruvate pool 1 in the figure, is derived from the glycolytic complex by channeling and accounts for the major production of lactate. This pool has only limited exchange with other metabolites except from glycolysis. The second cytosolic pool of pyruvate depicted as pyruvate pool 2 is associated with the first pool of pyruvate as well as the mitochondrial pool of pyruvate. This pyruvate pool 2 is fed by the extracellular pyruvate and by recycled pyruvate from either the malate shunt or synthesis of fatty acids. It is probable that pyruvate produced from glycolysis by free glycolytic enzymes/isoenzymes might also contribute to this pool. The mitochondrial pyruvate pool is depicted as pyruvate pool 3. The pyruvate pool 2 and pyruvate pool 3 produce alanine. The above model is derived by taking into account the isotopomer and carbon labeling data of alanine and lactate obtained by the cell growth in different labeled substrates.

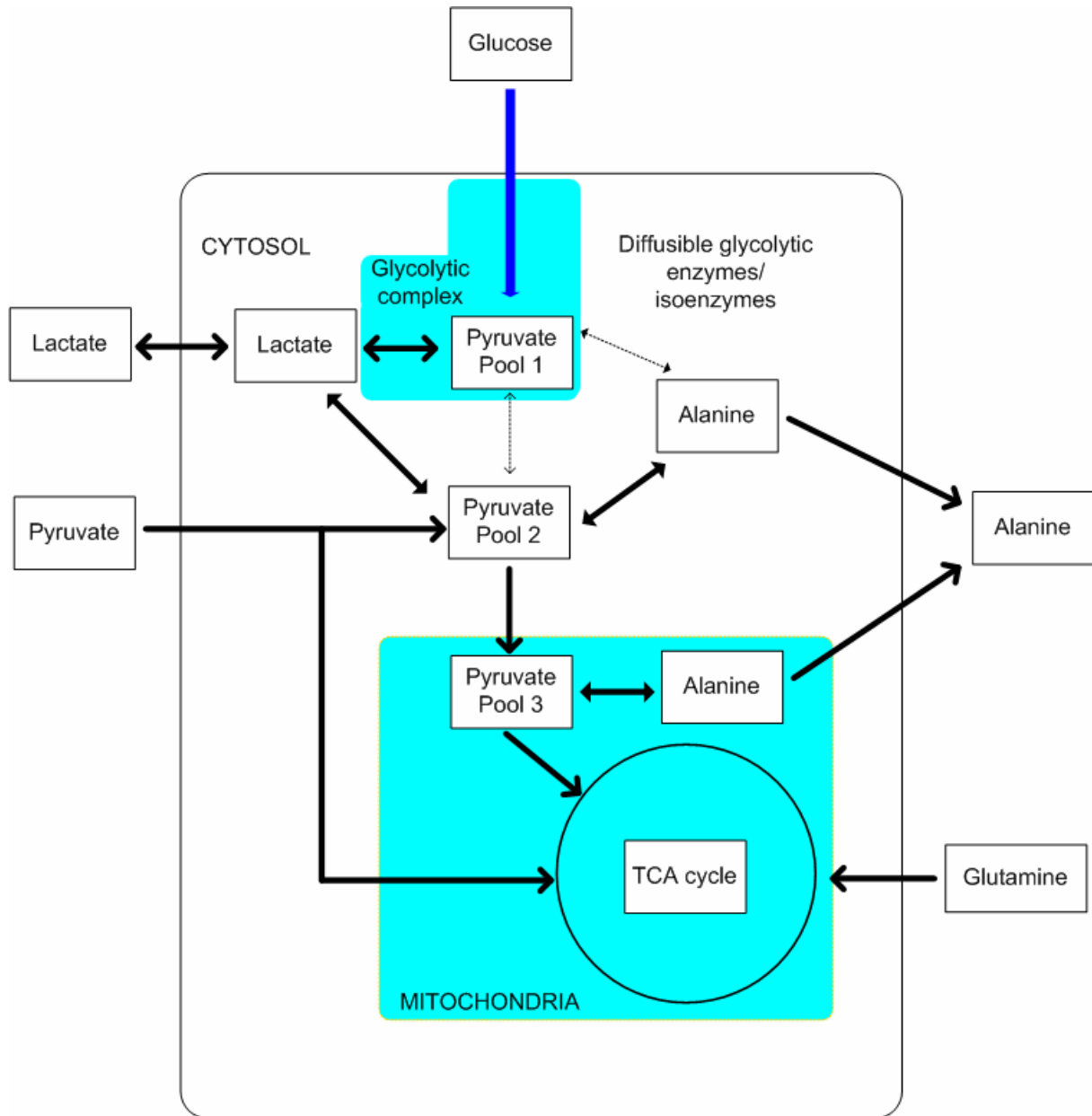


**Figure 5.6.10:** The proposed model for pyruvate compartmentation and metabolism. The model is modified form of the model put forward by Peuhkurinen et al. (1983). The thick arrows depict high flux.

The fractional labeling of alanine was found to be higher in the cultivation of CHO cells in media containing [1-<sup>13</sup>C<sub>1</sub>]glucose plus [U-<sup>13</sup>C]glutamine. Looking at the mass isotopomers, alanine has a higher percentage of <sup>13</sup>C<sub>2</sub> and fully labeled fraction at 3 % and 7 % respectively compared to lactate which has 2 % of doubly labeled and 5 % of fully labeled. Nevertheless lactate has a higher percentage of single labeled species at 39 % compared to 37 % of alanine. Hence it is seen that the alanine contains a higher percentage of labeled carbon obtained from TCA cycle supplied by fully labeled glutamine compared to lactate. In the experiment with [1-<sup>13</sup>C<sub>1</sub>]glucose plus [U-<sup>13</sup>C]threonine, the fractional labeling of lactate is higher than that of alanine. This is due to threonine not being metabolized as highly as glutamine to feed into the TCA cycle. However, the mass isotopomers of unlabeled and <sup>13</sup>C<sub>2</sub> species are higher in alanine in comparison to lactate. The data from the cultivation with [1,2-<sup>13</sup>C<sub>2</sub>]glucose also supports the model of two cytosolic pyruvate pools with one being also fed from the TCA cycle, with the unlabeled and <sup>13</sup>C<sub>1</sub> fraction being higher in alanine compared to lactate, since these isotopomers would also be derived from TCA cycle. The feeding of the pyruvate pool 2 with extracellular pyruvate is conclusively proved with the labeling and isotopomers data from the growth of cells in media containing [3-<sup>13</sup>C<sub>1</sub>]pyruvate. Alanine contains 12 % <sup>13</sup>C<sub>1</sub> fraction compared to 9 % of lactate with a higher carbon fractional labeling of 0.04. The experiments with [U-<sup>13</sup>C]glucose in the previous section offer further support to the model described above.

Hence, it is likely that the two cytosolic pyruvate pools are actually of dynamic nature differentiated by the channeling. The first cytosolic pyruvate pool is mostly derived from the pyruvate kinase and the major part of it is then directly channeled to the lactate dehydrogenase (LDH). The proposed glycolytic complex is shown in Figure 5.6.11. It has been shown that there exists two major isoforms of lactate dehydrogenase. One of the isoforms LDH-5 favors anaerobic oxidation, while the other isoform LDH-1 favors aerobic oxidation (Koukourakis et al., 2003). Hence it is probable that the LDH-5 isoform is associated with the glycolytic complex. It is also likely that the glycolytic enzymes or their isoenzymes would also exist in free form in the cytoplasm. The second cytosolic pyruvate pool is a mix of the part from the glycolysis and of the pyruvate derived from the TCA cycle, and undergoes further metabolism. Hence for the purpose of quantitative metabolic studies the assumption of a single pyruvate pool is not justified, furthermore the common approach of considering two pyruvate pools, one mitochondrial and the other cytosolic, seems to be misleading. A better quantitative picture would emerge when three pools of pyruvate are considered.

PHYSIOLOGICAL INVESTIGATIONS ON CHO CELLS

**Table 5.6.4:** Time course of the mass isotopomers with the fractional carbon labeling (FCL) of extracellular lactate and alanine in the four parallel cultures, with different isotopic labeled substrates. m+0, m+1, m+2 and m+3 indicate the unlabeled, single, double and fully labeled isotopomers respectively. The sampling procedure is given in material and methods. The initial time “0” refers to the sample after the addition of media to cells.

LACTATE						ALANINE					
<b>[1-<sup>13</sup>C<sub>1</sub>]Glucose plus [U-<sup>13</sup>C]Glutamine</b>											
Time (h)	m + 00	m + 01	m + 02	m + 03	FCL	Time (h)	m + 00	m + 01	m + 02	m + 03	FCL
0	0.869	0.109	0.016	0.006	0.053	0	0.923	0.071	0.000	0.005	0.029
12	0.721	0.218	0.036	0.024	0.121	12	0.759	0.191	0.015	0.036	0.109
24	0.616	0.318	0.028	0.038	0.162	24	0.649	0.272	0.022	0.056	0.162
37	0.565	0.369	0.022	0.043	0.181	37	0.588	0.320	0.027	0.065	0.190
46	0.545	0.387	0.024	0.044	0.189	46	0.558	0.346	0.031	0.065	0.201
61	0.535	0.391	0.026	0.048	0.195	61	0.539	0.364	0.033	0.065	0.208
<b>[1-<sup>13</sup>C<sub>1</sub>]Glucose plus [U-<sup>13</sup>C]threonine</b>											
0	0.902	0.087	0.011	0.000	0.036	0	0.927	0.070	0.002	0.001	0.026
12	0.775	0.216	0.009	0.000	0.078	12	0.824	0.172	0.004	0.000	0.060
24	0.686	0.305	0.010	0.000	0.108	24	0.747	0.247	0.006	0.000	0.086
37	0.635	0.355	0.010	0.000	0.125	37	0.696	0.297	0.007	0.000	0.104
46	0.614	0.377	0.010	0.000	0.132	46	0.659	0.328	0.012	0.000	0.118
61	0.601	0.388	0.011	0.000	0.137	61	0.634	0.353	0.013	0.000	0.126
<b>[1,2-<sup>13</sup>C<sub>2</sub>]Glucose</b>											
0	0.947	0.036	0.016	0.000	0.023	0	0.943	0.051	0.004	0.003	0.022
12	0.800	0.039	0.157	0.004	0.122	12	0.831	0.051	0.113	0.005	0.097
24	0.680	0.043	0.270	0.007	0.201	24	0.735	0.058	0.200	0.007	0.160
37	0.619	0.046	0.327	0.008	0.242	37	0.673	0.059	0.258	0.009	0.202
46	0.594	0.048	0.347	0.011	0.258	46	0.637	0.062	0.289	0.012	0.225
61	0.578	0.051	0.358	0.013	0.268	61	0.610	0.061	0.317	0.013	0.244
<b>[3-<sup>13</sup>C<sub>1</sub>]Pyruvate</b>											
0	0.894	0.095	0.010	0.000	0.039	0	0.897	0.098	0.003	0.002	0.037
12	0.638	0.348	0.014	0.000	0.125	12	0.660	0.329	0.010	0.001	0.117
24	0.781	0.212	0.008	0.000	0.076	24	0.742	0.250	0.007	0.001	0.089
37	0.858	0.138	0.004	0.000	0.049	37	0.809	0.186	0.005	0.000	0.065
46	0.889	0.108	0.003	0.000	0.038	46	0.845	0.151	0.004	0.000	0.053
61	0.908	0.091	0.002	0.000	0.031	61	0.873	0.123	0.003	0.000	0.043

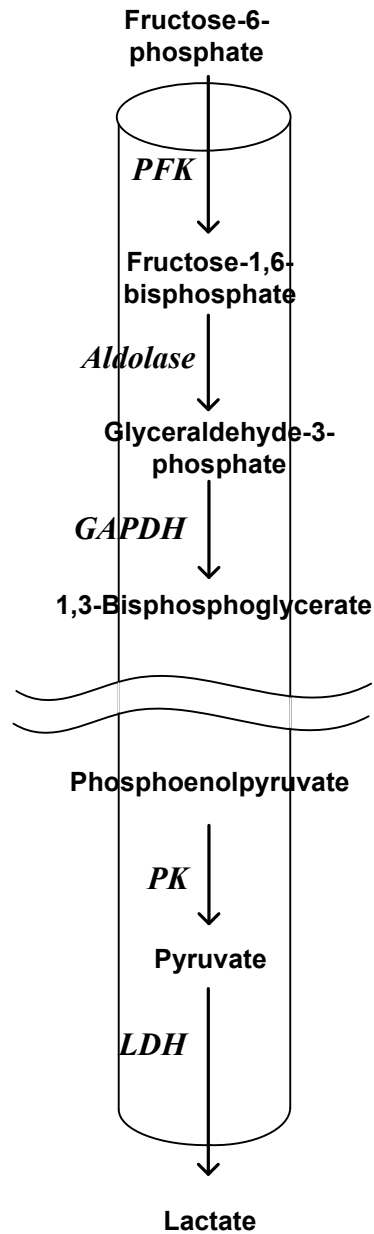


**Figure 5.6.11:** The proposed glycolytic channeling for pyruvate compartmentation and metabolism based on the glycolytic complex detected in human erythrocytes by Campanella et al. 2005 . (Abbreviations: PFK Phosphofruktokinase, GAPDH glyceraldehyde-3-PO<sub>4</sub>-dehydrogenase, PK Pyruvate kinase, LDH Lactate dehydrogenase)

**Glycine-serine metabolism**

The metabolism of serine and glycine are linked biochemically by the enzyme serine hydroxymethyltransferase. This enzyme catalyses the reversible reaction involving the transfer of the hydroxymethyl group from serine to the cofactor tetrahydrofolate (THF), producing glycine and N<sup>5</sup>,N<sup>10</sup>-methylene-THF. The biosynthesis of serine occurs from the glycolytic intermediate 3-phosphoglycerate. Serine can also form pyruvate, the reaction catalyzed by the enzyme serine dehydratase. Serine and glycine are both important precursors for the formation of cellular components in addition to proteins. Serine is involved in the formation of lipids while glycine in the formation of nucleotides. Serine also acts as an important donor of hydroxymethyl group. Both these amino acids can be synthesized by the cells and the cells can be grown in media without these amino acids as shown earlier. In the metabolic network described earlier, all the above mentioned reactions are considered. However, the carbon labeling and the isotopomers data obtained for these two amino acids from the parallel cultures with multiple labeled substrates could not be explained with the metabolic reactions described. The labeling patterns of serine and glycine obtained in the four cultivations are shown in Table 5.6.5. Considering the data obtained from the cultivation of cells with [1-<sup>13</sup>C<sub>1</sub>]glucose plus [U-<sup>13</sup>C]glutamine, serine shows a final carbon fractional labeling of 0.17 compared to 0.05 of glycine. This lower amount of labeling in glycine is due to the formation of unlabeled glycine from [3-<sup>13</sup>C<sub>1</sub>]serine derived from [1-<sup>13</sup>C<sub>1</sub>]glucose. Nevertheless 6 % of the glycine is made up of <sup>13</sup>C<sub>1</sub> species and 3 % by fully labeled. During the early phases of the growth, at the end of 24 h of culture these values are higher with a fractional labeling of 0.12 and, the <sup>13</sup>C<sub>1</sub> and fully labeled species making up 12 % and 6 % respectively. These values drop down to the final values given in Table 5.6.5. Considering the metabolic reactions in the network described earlier these labeling patterns cannot be explained. The presence of high amounts of labeled glycine at the beginning of the culture indicates a precursor other than serine and also rules out the possibility of active gluconeogenesis. Furthermore since [U-<sup>13</sup>C]glutamine is one of the substrates used in the culture, this probably indicates a source derived from the TCA cycle.

PHYSIOLOGICAL INVESTIGATIONS ON CHO CELLS

**Table 5.6.5:** Time course of the mass isotopomers with the fractional carbon labeling (FCL) of extracellular serine and glycine in the four parallel cultures, with different isotopic labeled substrates. m+0, m+1, m+2 and m+3 indicate mass isotopomers. The sampling procedure is given in material and methods. The initial time “0” refers to the sample after the addition of media to cells.

GLYCINE					SERINE					
<b>[1-<sup>13</sup>C<sub>1</sub>]Glucose plus [U-<sup>13</sup>C]glutamine</b>										
Time (h)	m + 00	m + 01	m + 02	FCL	Time (h)	m + 00	m + 01	m + 02	m + 03	FCL
0	0.841	0.122	0.037	0.098	0	0.758	0.183	0.023	0.036	0.112
12	0.833	0.123	0.043	0.105	12	0.588	0.392	0.014	0.006	0.145
24	0.819	0.115	0.066	0.123	24	0.552	0.423	0.018	0.008	0.160
37	0.846	0.094	0.060	0.107	37	0.540	0.433	0.019	0.007	0.164
46	0.905	0.063	0.033	0.064	46	0.512	0.431	0.040	0.017	0.188
61	0.916	0.059	0.025	0.055	61	0.547	0.411	0.028	0.014	0.170
<b>[1-<sup>13</sup>C<sub>1</sub>]Glucose plus [U-<sup>13</sup>C]threonine</b>										
0	0.803	0.099	0.098	0.147	0	0.605	0.155	0.023	0.218	0.285
12	0.775	0.128	0.096	0.160	12	0.588	0.365	0.014	0.033	0.164
24	0.778	0.125	0.097	0.159	24	0.572	0.404	0.012	0.011	0.154
37	0.848	0.086	0.066	0.109	37	0.559	0.424	0.012	0.005	0.154
46	0.890	0.066	0.044	0.077	46	0.576	0.406	0.012	0.006	0.149
61	0.910	0.058	0.032	0.061	61	0.559	0.425	0.013	0.003	0.153
<b>[1,2-<sup>13</sup>C<sub>2</sub>]Glucose</b>										
0	0.861	0.114	0.025	0.082	0	0.800	0.073	0.114	0.013	0.114
12	0.691	0.284	0.025	0.167	12	0.576	0.083	0.329	0.012	0.259
24	0.601	0.374	0.025	0.212	24	0.522	0.094	0.372	0.012	0.291
37	0.579	0.401	0.021	0.221	37	0.489	0.132	0.367	0.012	0.301
46	0.568	0.411	0.020	0.226	46	0.468	0.168	0.350	0.014	0.303
61	0.569	0.409	0.022	0.227	61	0.450	0.209	0.326	0.015	0.302
<b>[3-<sup>13</sup>C<sub>1</sub>]Pyruvate</b>										
0	0.885	0.104	0.012	0.063	0	0.902	0.082	0.007	0.009	0.041
12	0.843	0.118	0.039	0.098	12	0.914	0.081	0.003	0.002	0.031
24	0.800	0.153	0.047	0.124	24	0.941	0.056	0.002	0.001	0.021
37	0.815	0.155	0.030	0.107	37	0.950	0.048	0.001	0.001	0.018
46	0.855	0.129	0.016	0.081	46	0.952	0.046	0.002	0.000	0.017
61	0.953	0.044	0.004	0.025	61	0.954	0.044	0.001	0.000	0.016

The glyoxylate cycle is catalyzed by two unique enzymes, isocitrate lyase and malate synthase of which isocitrate lyase, catalyses the formation of glyoxylate from isocitrate and the second enzyme, malate synthase, catalyses the conversion of acetyl-CoA from glyoxylate. However, glyoxylate can also be converted to glycine by the enzyme glyoxylate aminotransferase. This metabolic pathway was earlier thought to be operative in only the cells of higher plants and some unicellular organisms. However, it has been shown recently that this pathway is active in many of the mammalian tissues (Davis and Goodman, 1992; Vandenbosch et al., 1992). Considering the glyoxylate pathway in the metabolism of CHO cells could provide an explanation of the labeling data observed. In the culture with [1-<sup>13</sup>C<sub>1</sub>]glucose plus [U-<sup>13</sup>C]glutamine, glycine would show fractions of <sup>13</sup>C<sub>1</sub> and fully labeled species as these would come from the TCA cycle intermediate isocitrate.

However, it is seen that the fractions of <sup>13</sup>C<sub>1</sub> are comparably higher than the fully labeled fraction. Since [U-<sup>13</sup>C]glutamine is used as a substrate, this should not be the case. Rather we should observe the fully labeled fraction to be higher than the single labeled fraction if the glyoxylate pathway were the only other pathway active for the formation of glycine. The other possibility of glycine biosynthesis is the glycine cleavage system. This reaction has been found to be reversible in mammalian systems (Kikuchi, 1973). The reversible glycine cleavage produces glycine from CO<sub>2</sub> and N<sup>5</sup>,N<sup>10</sup>-methylene-THF. The N<sup>5</sup>,N<sup>10</sup>-methylene-THF would be produced from the action of serine hydroxymethyltransferase on serine and would thus be labeled. This would lead to the formation of <sup>13</sup>C<sub>1</sub> glycine.

Another biosynthetic pathway for the formation of glycine is from the catabolism of threonine. The amino acid threonine has potentially three catabolic pathways via threonine dehydrogenase, threonine aldolase and threonine dehydratase. Two of these pathways via threonine dehydrogenase and threonine aldolase lead to the formation of glycine. In the majority of the previous works dealing with metabolic fluxes (Sharfstein et al., 1994; Altamirano et al., 2001; Gambhir et al., 2003), only the catabolism of threonine via threonine dehydratase to alpha-ketobutyrate leading to succinyl-CoA has been considered. This is also the case in the network described in the earlier section. However, there is evidence that the other pathways of threonine are also active in mammalian cells (House et al., 2001). From the data of the culture with [1-<sup>13</sup>C<sub>1</sub>]glucose plus [U-<sup>13</sup>C]threonine we see that at the end of 24 h, around 10 % of the glycine is made up of fully labeled fraction compared to 1 % of serine. If this glycine fraction was from the TCA cycle intermediate isocitrate, then the culture with [1-<sup>13</sup>C<sub>1</sub>]glucose plus [U-<sup>13</sup>C]glutamine would have shown a higher percentage, since glutamine is metabolized at a higher rate in the TCA cycle than threonine. Furthermore, the glycine

cleavage system would provide  $^{13}\text{C}_1$  glycine. Thus part of the fully labeled fraction is derived from the metabolism of threonine. Glycine also shows 12 % of  $^{13}\text{C}_1$  fraction at the end of 24 h. This fraction is derived from the TCA cycle, which is fed by  $[1-^{13}\text{C}_1]$ glucose, and the glycine cleavage system. However, these fractions reduce to 3 % of fully labeled and 6 % of  $^{13}\text{C}_1$  species at the end of the cultivation. This shows that the glyoxylate cycle and the reversible glycine cleavage system are probably active at a higher rate during the initial phases of growth for the production of glycine. This follows to reason since the cells are grown in a glycine and serine deficient media. In the absence of its direct precursor, i.e. serine, in sufficient amounts, the requirement of glycine for the cells during the early part of the cell growth is probably partly supplied by the two alternative pathways. Nevertheless this is the first reported indirect evidence for the activity of glyoxylate cycle in CHO cells and further biochemical studies such as enzymatic assays need to be done to confirm this. Recently the hepatic glyoxylate pathway was reconstructed into CHO cells as these cells were thought to lack the glyoxylate cycle, which was evidenced by a lack of expression of the glyoxylate pathway enzymes in CHO cells (Behnam et al., 2006). However, in the said study, the media used contained serum, glycine and serine. It might be probable that the expression of the glyoxylate pathway enzymes is regulated by the extracellular media composition. It has been shown that in rat liver the glyoxylate cycle enzymes can be induced by starvation (Popov et al., 1996). It is seen that in the above experiments, the highest activity of the glyoxylate cycle is at the start of the culture when there is no glycine and serine present in the media.

Fractions of  $^{13}\text{C}_2$  and fully labeled species of serine are seen in the culture of both the cultivations with  $[1-^{13}\text{C}_1]$ glucose plus  $[\text{U}-^{13}\text{C}]$ glutamine and  $[1-^{13}\text{C}_1]$ glucose plus  $[\text{U}-^{13}\text{C}]$ threonine. The possible explanation of this would be the conversion of glycine to serine via hydroxymethyltransferase. The fully labeled fraction would occur when the labeled  $\text{N}^5, \text{N}^{10}$ -methylene-THF released by serine during the conversion of serine to glycine reacts again with fully labeled glycine to give fully labeled serine. The above labeling patterns can also be explained if we consider the activity of serine hydratase for the formation of serine from pyruvate. However, this enzyme is known to act on serine to form pyruvate and its reversibility in mammalian systems has not been documented. In the cultivations with  $[3-^{13}\text{C}_1]$ pyruvate, 15 % of glycine is  $^{13}\text{C}_1$  fraction compared to 5 % of serine. If serine was formed from pyruvate, this fraction would be higher in comparison to glycine. There is a decrease in the fractional carbon labeling of serine at the end of the cultivations in cultures with  $[1-^{13}\text{C}_1]$ glucose plus  $[\text{U}-^{13}\text{C}]$ glutamine and  $[1-^{13}\text{C}_1]$ glucose plus  $[\text{U}-^{13}\text{C}]$ threonine. Serine is an important gluconeogenic substrate and can be converted to pyruvate via serine

hydratase. The decrease in the fractional carbon labeling can be explained by the formation of serine from glycine and simultaneous consumption leading to extracellular exchange of serine. With the above observations, Figure 5.6.12 gives the possible pathways of serine and glycine in CHO cells.

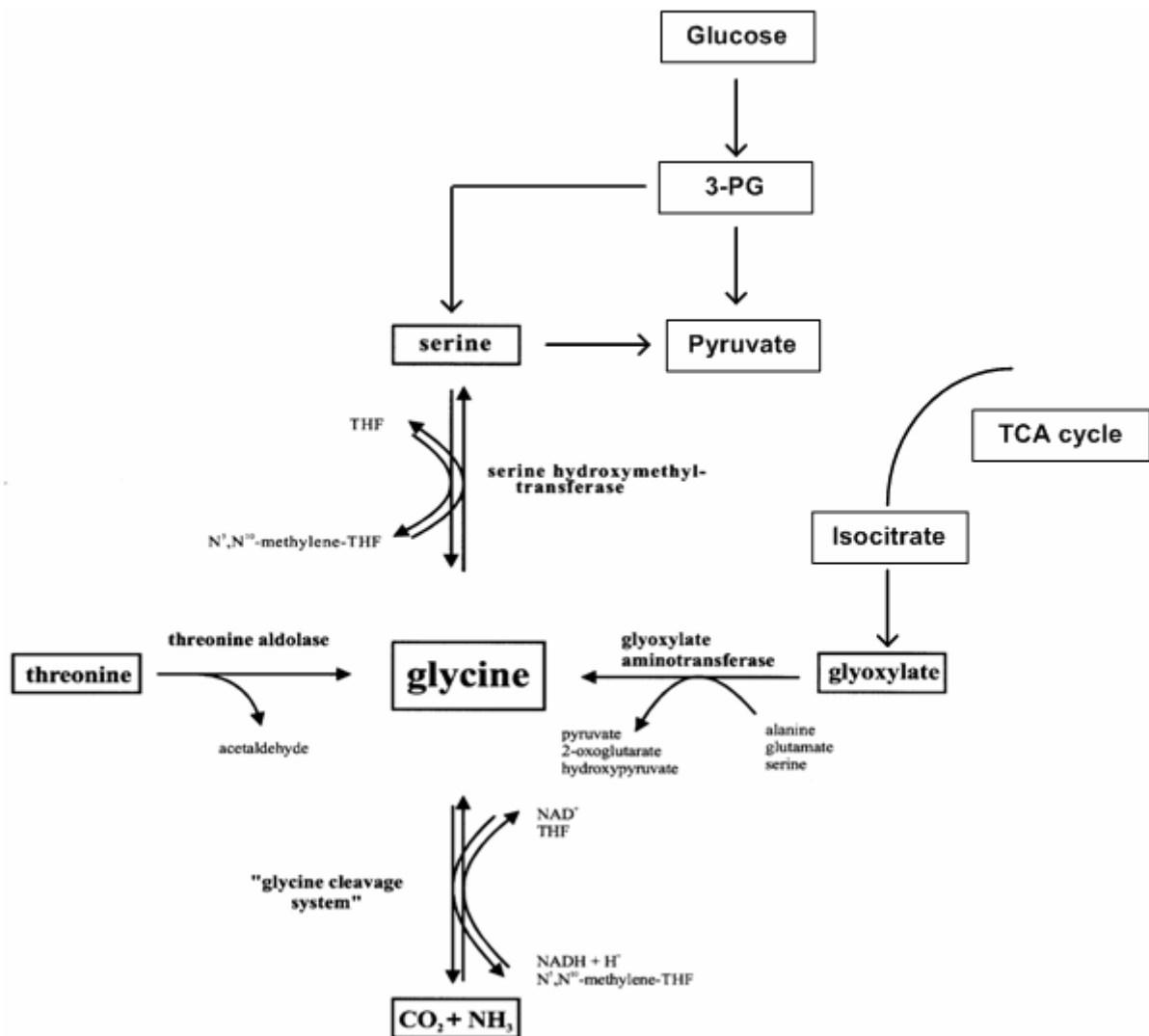


**Figure 5.6.11:** The proposed serine and glycine metabolic pathways operational in CHO cells.

**Glycolysis**

As described earlier, the lactate to glucose (M/M) ratio of all the four cultures over the whole cultivation ranges from 1.45 for the culture with [1,2-<sup>13</sup>C<sub>2</sub>]glucose to 1.62 for the culture with [1-<sup>13</sup>C<sub>1</sub>]glucose and [U-<sup>13</sup>C]glutamine. Thus around 72 % to 82 % of lactate is produced from glycolysis. The alanine to glucose (M/M) ratio ranges from 0.2 for the culture with [1-<sup>13</sup>C<sub>1</sub>]glucose and [U-<sup>13</sup>C]glutamine to 0.18 for the culture with [3-<sup>13</sup>C<sub>1</sub>]pyruvate. Hence 82 % to 91 % of glucose is metabolized by overflow metabolism. However, the activity of glycolysis, calculated using the lactate and alanine produced, also includes the activity from the pentose phosphate shunt and the recycle from the TCA cycle.

**Pentose-phosphate pathway**

The rate of oxidative pentose phosphate relative to glycolytic flux can be estimated from the culture of [1,2-<sup>13</sup>C<sub>2</sub>]glucose. <sup>13</sup>C<sub>2</sub> Lactate originates from glucose that is converted to lactate directly by glycolysis, whereas <sup>13</sup>C<sub>1</sub> lactate originates from glucose metabolized by direct oxidation via the oxidative steps of the pentose phosphate pathways and then recycled to glycolysis via the non-oxidative pentose cycle. From these results, we can predict pentose cycle flux relative to the glycolytic flux, and it is calculated using the <sup>13</sup>C<sub>1</sub>/<sup>13</sup>C<sub>2</sub> ratio in lactate (Lee et al., 1998; Boren et al., 2003). From this it is found that the pentose phosphate activity is 4.5 % of the glycolytic activity. This value is similar to the values reported for hybridomas (4 %) (Sharfstein et al., 1994). However, this would be the maximum of the pentose-phosphate activity. The actual value would be lower since the <sup>13</sup>C<sub>1</sub> and <sup>13</sup>C<sub>2</sub> label would be diluted by the pyruvate recycled from the TCA cycle and also the non-oxidative branch of pentose phosphate cycle.

**Tri-carboxylic acid cycle**

The tri-carboxylic acid (TCA) cycle is fed mainly by pyruvate derived from glucose and glutamine. Using simple balances with the activity of the glycolysis and the overflow metabolism, it is seen that 9 % (by [1-<sup>13</sup>C<sub>1</sub>]glucose and [U-<sup>13</sup>C]glutamine experiment) to 18 % (by [1,2-<sup>13</sup>C<sub>2</sub>]glucose experiment) of the glucose from the four cultures feeds into the TCA cycle. The rate of glutamine uptake relative to glucose uptake ranges from 12 % of the glucose flux for the culture with [1,2-<sup>13</sup>C<sub>2</sub>]glucose to 26 % for the culture with [1-<sup>13</sup>C<sub>1</sub>]glucose and [U-<sup>13</sup>C]glutamine. Hence the flux of glutamine into the TCA cycle is dependent on the flux of pyruvate, with a lower flux of pyruvate into the TCA cycle indicating a higher flux from glutamine. This is contrary to the data observed with the specific

rates. A higher specific rate of glucose uptake implies a higher glutamine uptake. However, from the data it seems that the flux of pyruvate into TCA cycle controls the rate of glutamine uptake. This has also been shown to work in reverse, where the overflow metabolism of a myeloma cell line was reduced in a glutamine limited culture (Ljunggren and Haggstrom, 1992).

### **Aspartate-malate shuttle**

Glutamate and aspartate are non-essential amino acids and thus play an important role in cellular central metabolism. The first reaction of amino acid breakdown is transamination which produces glutamate from alpha-ketoglutarate. Moreover, glutamine, the major provider of energy to the cellular metabolism, is broken down to glutamate by glutaminase in the mitochondria. Glutamate can be transported across the mitochondria via two carriers. One carrier catalyses electroneutral exchange between glutamate and hydroxyl ions, and the other carrier catalyses an obligatory coupled exchange between external glutamate and intramitochondrial aspartate. The biochemical function of the glutamate/OH-antiporter is thought to be the provision of glutamate for the production of ammonia via glutamate dehydrogenase, which is exclusively located in the mitochondria. Glutamate entering on the glutamate/aspartate antiporter is necessarily transaminated with intramitochondrial oxaloacetate to form aspartate and  $\alpha$ -ketoglutarate, and is hence not available to the glutamate dehydrogenase (Bradford and McGivan, 1973). The mitochondrial aspartate is produced due to the activity of the aspartate-malate shuttle (Figure 5.6.12). For the movement of reducing equivalents (NADH) from the cytoplasm to the mitochondria the malate/aspartate shuttle is the principal mechanism. In the mitochondria the electrons of NADH can be coupled to ATP production during the process of oxidative phosphorylation. The electrons are "carried" into the mitochondria in the form of malate. Cytoplasmic malate dehydrogenase (MDH) reduces oxaloacetate to malate while oxidizing NADH to  $\text{NAD}^+$ . Malate then enters the mitochondria where the reverse reaction is carried out by mitochondrial MDH. Movement of mitochondrial oxaloacetate to the cytoplasm to maintain this cycle requires it be transaminated to aspartate with the amino group being donated by glutamate. The aspartate then leaves the mitochondria and enters the cytoplasm. The deamination of glutamate generates  $\alpha$ -ketoglutarate in the mitochondria which is transported readily to cytoplasm with the entry of malate. Since both glutamate and aspartate interact freely with the TCA cycle intermediates and can be transported out of the mitochondria, they exhibit labeling when isotopically labeled substrates are used for cell growth. The activity of the aspartate-malate shuttle has been assumed to be

low and hence many previous studies concerning quantitative metabolism have neglected to take this shuttle into account (Zupke et al., 1995; Follstad et al., 1999; Bonarius et al., 2001). The mass isotopomers with the fractional carbon labeling of aspartate and glutamine are given in Table 5.6.6. The data from the culture with  $[1-^{13}\text{C}_1]\text{glucose}$  plus  $[\text{U}-^{13}\text{C}]\text{glutamine}$  would provide clues to the activity of this shuttle. Since glutamine is the primary substrate in the TCA cycle, the glutamate supplying the TCA cycle would be fully labeled in the above culture. Aspartate can be formed from the deamination of asparagine and also from the TCA cycle intermediate oxaloacetate during the shuttle. Since oxaloacetate would be carrying the isotopic label from the TCA cycle, the isotopic labeling of aspartate would give the relative activity of the shuttle. From the labeling data of the culture medium, it is seen that aspartate has a final fractional carbon labeling of 0.37 and 49 % of it is unlabeled. Hence 51 % of aspartate carries isotopic labeling, and thus comes from oxaloacetate. This value gives the minimum activity of the shuttle. In reality this would be higher, since the aspartate pool in exchange with glutamate would be diluted from the aspartate produced from asparagine. This minimum value represents around 2 % of the total glucose flux and around 6 % of the glutamine flux entering the metabolism in the culture with  $[1-^{13}\text{C}_1]\text{glucose}$  plus  $[\text{U}-^{13}\text{C}]\text{glutamine}$ .

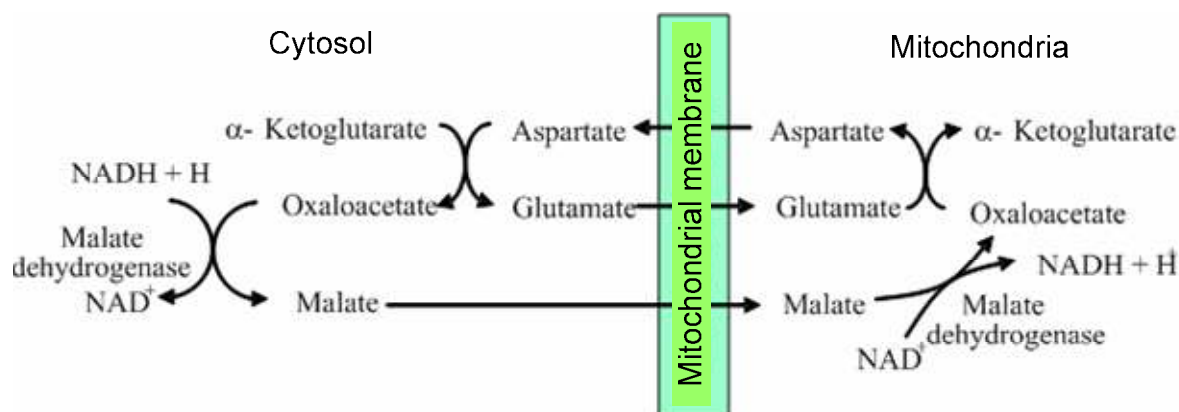


**Figure 5.6.12:** The malate-aspartate shuttle system in mammalian cells for the transport of reducing equivalents to the mitochondria.

PHYSIOLOGICAL INVESTIGATIONS ON CHO CELLS

**Table 5.6.6:** Time course of the mass isotopomers with the fractional carbon labeling (FCL) of extracellular aspartate and glutamate in the four parallel cultures, with different isotopic labeled substrates. m+0, m+1, m+2, m+3, m+4 and m+5 indicate labeled mass isotopomers. The sampling procedure is given in material and methods. The initial time “0” refers to the sample after the addition of media to cells.

ASPARTATE							GLUTAMATE							
<b>[1-<sup>13</sup>C<sub>1</sub>]Glucose plus [U-<sup>13</sup>C]glutamine</b>														
Time (h)	m + 00	m + 01	m + 02	m + 03	m + 04	FCL	Time (h)	m + 00	m + 01	m + 02	m + 03	m + 04	m + 05	FCL
0	0.91	0.05	0.01	0.01	0.02	0.05	0	0.02	0.00	0.00	0.01	0.06	0.92	0.97
12	0.71	0.06	0.04	0.05	0.14	0.21	12	0.02	0.01	0.01	0.03	0.06	0.86	0.93
24	0.55	0.07	0.06	0.08	0.24	0.35	24	0.03	0.02	0.02	0.05	0.07	0.82	0.91
37	0.50	0.07	0.07	0.09	0.27	0.39	37	0.03	0.03	0.03	0.07	0.08	0.77	0.89
46	0.51	0.08	0.07	0.09	0.25	0.37	46	0.04	0.04	0.04	0.09	0.09	0.70	0.85
61	0.49	0.09	0.08	0.09	0.24	0.37	61	0.06	0.07	0.06	0.12	0.10	0.60	0.78
<b>[1-<sup>13</sup>C<sub>1</sub>]Glucose plus [U-<sup>13</sup>C]threonine</b>														
0	0.94	0.05	0.00	0.00	0.00	0.02	0	0.94	0.06	0.00	0.00	0.00	0.00	0.01
12	0.91	0.08	0.01	0.00	0.00	0.03	12	0.90	0.09	0.01	0.00	0.00	0.00	0.02
24	0.89	0.10	0.01	0.00	0.00	0.03	24	0.88	0.11	0.01	0.00	0.00	0.00	0.03
37	0.88	0.11	0.01	0.00	0.00	0.03	37	0.85	0.13	0.02	0.00	0.00	0.00	0.03
46	0.87	0.12	0.01	0.00	0.00	0.04	46	0.83	0.15	0.02	0.00	0.00	0.00	0.04
61	0.85	0.13	0.01	0.00	0.00	0.04	61	0.78	0.18	0.03	0.00	0.00	0.00	0.05
<b>[1,2-<sup>13</sup>C<sub>2</sub>]glucose</b>														
0	0.94	0.05	0.00	0.00	0.00	0.02	0	0.94	0.06	0.00	0.00	0.00	0.00	0.01
12	0.91	0.05	0.03	0.00	0.00	0.03	12	0.92	0.06	0.02	0.00	0.00	0.00	0.02
24	0.89	0.05	0.05	0.00	0.00	0.04	24	0.90	0.06	0.04	0.00	0.00	0.00	0.03
37	0.87	0.06	0.06	0.01	0.00	0.05	37	0.87	0.06	0.06	0.01	0.00	0.00	0.04
46	0.85	0.06	0.08	0.01	0.00	0.06	46	0.83	0.07	0.09	0.01	0.01	0.00	0.06
61	0.82	0.07	0.09	0.01	0.00	0.08	61	0.76	0.08	0.12	0.02	0.01	0.00	0.09
<b>[3-<sup>13</sup>C<sub>1</sub>]Pyruvate</b>														
0	0.94	0.05	0.00	0.00	0.00	0.02	0	0.94	0.05	0.00	0.00	0.00	0.00	0.01
12	0.89	0.10	0.01	0.00	0.00	0.03	12	0.90	0.09	0.01	0.00	0.00	0.00	0.02
24	0.90	0.09	0.01	0.00	0.00	0.03	24	0.91	0.09	0.01	0.00	0.00	0.00	0.02
37	0.91	0.08	0.01	0.00	0.00	0.02	37	0.91	0.08	0.01	0.00	0.00	0.00	0.02
46	0.92	0.08	0.01	0.00	0.00	0.02	46	0.91	0.09	0.01	0.00	0.00	0.00	0.02
61	0.92	0.08	0.01	0.00	0.00	0.02	61	0.90	0.09	0.01	0.00	0.00	0.00	0.02

**Malate shunt**

The recycle from the TCA cycle to pyruvate occurs through malate shunt. This occurs via phosphoenolpyruvate carboxykinase or the malic enzyme. The data from the culture with [1-<sup>13</sup>C<sub>1</sub>]glucose and [U-<sup>13</sup>C]glutamine should give an indication for the recycle. The <sup>13</sup>C<sub>2</sub> and fully labeled fractions of alanine and lactate must be solely derived from pyruvate derived from malate. This value is found to be 10 % of the alanine and 8 % of lactate formed. This value represents the minimum of the recycle, since the catabolism of other amino acids and the entry of pyruvate into the TCA cycle would contribute unlabeled and <sup>13</sup>C<sub>1</sub> fraction to the shunt.

**Modified metabolic model**

The analysis of the above data particularly dealing with the pyruvate and glycine-serine metabolism led to an alteration in the metabolic model presented earlier. The new metabolic model (Figure 5.6.13) incorporated the metabolism involving the multiple pyruvate pools and also the various pathways of glycine and serine metabolism. The glycolytic enzymes are membrane bound and the metabolites of glycolysis in this model are channeled as shown in the figure. However, this model does not take into account the possibility of the presence of cytosolic glycolytic enzymes which might contribute pyruvate to the second pyruvate pool. The role of pentose phosphate pathway is also unclear. The low activity of the PPP might be due to its linkage with the low amounts of free diffusible metabolites of the glycolytic pathway. The labeling of <sup>13</sup>C<sub>1</sub> serine is higher than <sup>13</sup>C<sub>1</sub> alanine in the culture with [1-<sup>13</sup>C<sub>1</sub>]glucose and [U-<sup>13</sup>C]glutamine. However, the lower labeling of alanine at <sup>13</sup>C<sub>1</sub> might be due to the dilution of pyruvate. In the model the serine is assumed to be derived from the glycolytic complex though there is no clear evidence for this. The reactions for the model are given in the appendix.



#### 5.5.3.4 Conclusions

Parallel experiments were conducted using multiple substrates for investigating and quantifying the metabolism of CHO cells. The labels used were [1-<sup>13</sup>C<sub>1</sub>]glucose and [U-<sup>13</sup>C]glutamine, [1-<sup>13</sup>C<sub>1</sub>]glucose and [U-<sup>13</sup>C]threonine, [1,2-<sup>13</sup>C<sub>2</sub>]glucose, and [3-<sup>13</sup>C<sub>1</sub>]pyruvate. These labels were pre-selected for the optimal flux quantification. Using the methodology described above, many significant facets of metabolism were determined. There was evidence of intracellular cytosolic compartmentation of pyruvate. It is likely that the intracellular cytosolic pools of pyruvate might be linked to metabolite channeling. The direct transfer of the product from one enzyme to the subsequent without free diffusion increases the efficiency of the pathway. It is known that immortal cells show a high degree of glycolysis. The relatively low activity of the other pathways might be associated with the channeling of metabolites. Also, immortal cells are known to survive in hypoxia conditions due to the high activity of anaerobic glycolysis. It has also been proposed that the assembly of the glycolytic enzymes on the membrane might account for the compartmentalization of the ATP formed, without being released into the cytoplasm for the utilization in ion pumps (Campanella et al., 2005). The channeling of substrates in the glycolysis might be linked to the survival of immortal cells under hypoxia conditions.

A model of the pyruvate compartmentation within the cells, with three pyruvate pools which can explain the labeling obtained in the extracellular lactate and alanine is proposed. One of the pools is linked to the metabolite channel via the glycolytic complex. The second pool derives from the free glycolysis as well as the recycling of pyruvate via the malate shunt. The extracellular pyruvate also feeds into this pool. The third pyruvate pool is located in the mitochondria.

The investigations into the glycine-serine metabolism revealed indirect evidence for the activity of the glyoxylate cycle in CHO cells. The reversible glycine cleavage system also showed high activity. However, these pathways were found to be active only during the beginning of the culture where there was a starvation of serine and glycine. Furthermore relative fluxes of aspartate-malate shuttle, glycolysis, citric acid cycle and malate shunt were determined. It is seen that the flux of glutamine into the TCA cycle is probably controlled by the flux of pyruvate into the citric acid cycle. Moreover, at lower glucose concentrations, the uptake of branched chain amino acids was increased. There is a significant amount of malate shunt feeding into the pyruvate probably for the complete oxidation of glutamine feeding into the TCA cycle.

Hence, labeling with multiple substrates with parallel experiments offers the best possible solution for not only the complete quantification of the mammalian cell metabolism but also for a deeper understanding of the various metabolic pathways. The metabolic quotients and the labeling data obtained from the above cell cultivations can be later used for the quantification of whole cell metabolic pathway fluxes. However, this requires considerable modeling efforts which are presently underway. The quantification of these fluxes is therefore beyond the scope of this thesis.

## 6 CONCLUSIONS

Along with their rising importance for the production of biologicals, mammalian cells are routinely used now a day's for medical and biochemical research. However, the culturing of these cells as well as the biochemical aspects related to mammalian cells is complex when compared to other microorganisms. Hence new methods are needed for their cultivation as well as physiological studies. Part of the work carried out in this thesis was the development of methods for high throughput applications using innovative 96-well microplates equipped with optical sensors for oxygen monitoring. The innovative 96-well microplates were used for respiration measurements, medium optimization and *in vitro* cytotoxicity testing. The value of  $k_L a$  volumetric liquid phase mass transfer coefficient was determined for the 96-well microtiter plates at the desired shaking rates. From the  $k_L a$ , the respiration rates of the cellular culture in each of the well could be calculated. This method of respiration rate calculation was then applied for process optimization by using them for cellular medium optimization. For medium optimization a large number of experiments could be done in a single run and on a single microplate thus reducing the cost, time and effort generally required for this process. The system can also be used as a substitute for presently available viability assays such as MTT and therefore be used for cytotoxicity testing. An *in vitro* cytotoxicity assay using these plates was developed. The assay developed is robust, flexible and applicable for medium to high-throughput systems. Its main advantages over other cytotoxicity assays are its kinetic nature, the automatic on-line measurement and that the cells can further be processed for any subsequent analysis.

The second part of this thesis dealt with development of methods for the quantitative physiological studies of CHO cells with the help of metabolic flux analysis. Quantification of metabolites was done by HPLC and the isotopic labeling was analyzed using GC-MS. The cellular media used for the culture of cells was optimized to simplify the calculation of these fluxes by determining the anabolic and catabolic metabolites using [U-<sup>13</sup>C]glucose. Parallel experiments were performed with various different labeled substrates for the generation of data to be utilized for metabolic flux calculation. Using the labeling data obtained from alanine and lactate, a model for the metabolism of the key intermediate metabolite pyruvate is proposed. The model takes into account the present theory of cytosolic compartmentation of pyruvate and proposes the channeling of the glycolytic pathway in a glycolytic complex. Moreover, the data from the labeling of glycine and serine offered new insights into their

## CONCLUSIONS

---

metabolism. It was seen that the glycine cleavage system was operating in the reverse and also that the glyoxylate pathway was active. This is the first reported indirect evidence for the activity of the glyoxylate cycle in CHO cells. A modified metabolic model was proposed incorporating the deductions arrived using the labeling data. Furthermore relative fluxes were calculated for the major pathways in CHO cells. It was seen that the flux of glutamine into the TCA cycle is controlled by the flux of pyruvate into the cycle. However, the absolute fluxes for the whole cellular metabolism were not calculated in this work. Work is presently underway for these calculations using the data generated by the experiments performed in this thesis.

## 7 OUTLOOK

Mammalian cells are widely applied for biochemical and medical research and for the manufacture of biologically relevant proteins. Both of these applications require a thorough knowledge about the cellular physiology. Another major application of mammalian cells is in drug testing. Although the human genome project is yielding clues to thousands of new targets for drug development, selecting suitable targets is not easy and requires a systematic approach. Nevertheless “intelligent drug design”, whose targets include enzymes and receptors, appears not to include the idea that what cells are supposed to do is metabolism and the major thing drugs are supposed to do is to alter the metabolism (Cornish-Bowden and Cardenas, 2003). In reality, the final information on the true performance of a new drug can only be derived from a clinical trial program. However, the capacity to test new treatment in patients is limited in comparison with the great number of promising new drugs. For safety reasons and for optimizing the chance of finding new active drugs, a lot of information needs to be collected during the pre-clinical stage of development of the drug.

Early definitions of metabolic engineering were posed in terms of cell (or whole organism) improvement by genetic changes, often based on recombinant DNA methods. However, this view is changing fast. A drug is essentially an agent for metabolic engineering- by inhibiting or activating a particular protein or pathway. Metabolic engineers are therefore well prepared to consider basic strategies for attaining desired phenotype by exposing biological systems to particular agents and also to collect information about their action on metabolism (Bailey, 2001). Metabolic flux analysis has become an important tool in metabolic engineering and has been extensively used for microorganisms. It allows the quantification of important fluxes in the central metabolism of an organism (Wiechert and de Graaf, 1996). Its use for mammalian cells has been limited owing to the complexity of the system. However, there are examples for the use of this technique. This has been applied by using material balance techniques, radioactive labeling or stable isotope labeling to measure the fluxes through major pathways or of a particular enzyme. Material balancing techniques have been applied to study the metabolism of CHO, hybridoma and other cell lines as explained earlier. The effects of drugs on metabolism have been studied by the use of isotopes. The metabolic effects of sulphonylureas, bacitracin and tocotrienols on isolated rat hepatocytes were determined by using radiolabeled substrates by enzymatic flux determination (Agius et al., 1983; Judd et al., 1992; Parker et al., 1993). Stable isotope labeled glucose and butyrate has been used to study

## OUTLOOK

---

the regulation of tumor cell proliferation and differentiation by metabolic pathway analysis (Boren et al., 2003). Astrocytes metabolism under the influence of external components have also been studied using isotopes (Yu et al., 1983; Hassel and Sonnewald, 2002). Thus this methodology can principally be used for the determination of drug actions.

The majority of anti-cancer drugs act as cytotoxic agents. The effect of cytotoxic drugs on cellular metabolism has not been a major field of research. But some knowledge is available. For example the drug paclitaxal has been reported to inhibit the respiratory chain in rat hepatocytes (Manzano et al., 1996) and doxorubicin has a stimulating effect on the respiration (Ganey et al., 1988). The metabolic effect of cytotoxic agents at sub-lethal doses might provide an answer to their mode of action and cell regulation. For example the sub-lethal dose of activated complement has been seen to increase rat lymphocyte glutamine utilization suggesting that glutamine metabolism is important for cell defense (Bacurau et al., 2002). However, the metabolic effects of many cytotoxic drugs, especially at the sub-lethal doses, are unknown. The effect of these drugs at sub-lethal doses if combined with flux analysis techniques might suggest their possible mode of action and might also be used as a reference for predictive toxicology.

In the above work the use of material balance technique in combination with stable isotope labeling to quantify the intracellular fluxes has been shown to be a powerful methodology. However, for the method to be truly effective the use of different multiple labeled substrates are essential. For the future perspective, cytotoxic drugs could be applied at sub-lethal doses and multiple stable isotope labeled substrates could be used to quantify intracellular fluxes in the cells using simple metabolic models with the application of GC/MS, HPLC and enzymatic assay data. These could be compared with the control cells to see changes in the labeling and flux patterns of the metabolites to determine the metabolic effects of the drug on the primary metabolic pathway.

The use of 96-well microtiter plates with oxygen sensor would complement this effort as to reduce the cost of labeled substrates used due to the low volume. Additionally it would provide a high throughput environment where experiments with multiple isotopic labels could be carried out in parallel with a single plate. The sensor coated plates would also provide additional information on the oxygen uptake rate. The additional advantage would be the use of these plates for the determination of sub-lethal concentrations of drugs. Recently microplates have been used to metabolically screen rapamycin-treated hybridomas using a simple metabolic model based on metabolite balancing (Balcarcel and Clark, 2003). The use of multiple labeled substrates would provide a more in-depth look at the metabolism under the

influence of different environmental stress, such as drugs, media components etc. The method of flux analysis in combination with sensor coated microplates could be thus used to reduce the time and cost associated with drug development. Moreover it could acts as a predictor for the metabolic effects of drugs.

From the market approval of the first therapeutic protein to be produced from mammalian cells (human tissue plasminogen activator) in 1986, mammalian cells now account for the production of 70 % of all market approved therapeutic protein (Wurm, 2004). Initial development of production processes for mammalian cell culture was focused on reactor development and manipulation of process parameters. The reactor technology for many of the large-scale cell culture has now settled on the standard stirred-tank reactor as the technology of choice (Chu and Robinson, 2001). However, challenges such as adapting cells to suspension culture, development of animal-product free media, control of product quality, control of carbon dioxide concentration and minimizing the risk of contamination in large scale culture remain. Interest in the metabolism and physiology of mammalian cells in culture arises from the belief that high cell concentration and productivity is primarily limited by the accumulation of inhibitory factors. Although factors such as accumulation of lactate and ammonium play a significant inhibitory role, other factors such as osmolality of the media and also the composition contribute to the inhibition of growth and thus affect productivity (Hu and Aunins, 1997). Hence, investigation into the physiological effects of different factors is of significant importance to increase product yield. Also the effect of genetic modifications as well as the efficiency of various gene transfer vectors on expression levels of the required product in mammalian cells requires a thorough physiological study. Metabolic flux analysis can play an important role in this regard. The methods developed in this work for metabolic flux analysis along with high throughput cultivation methods can provide important clues for increasing the productivity of the cells in large scale cultures.

---

## 8 REFERENCES

### [A]

- Adinarayana, K. and Ellaiah, P. (2002) Response surface optimization of the critical medium components for the production of alkaline protease by a newly isolated *Bacillus* sp. *J Pharm Pharm Sci* 5, 272-8.
- Agius, L., Wilding, C. and Alberti, K.G. (1983) Metabolic effects of bacitracin in isolated rat hepatocytes. *Biochem J* 216, 369-75.
- al-Habori, M. (1995) Microcompartmentation, metabolic channeling and carbohydrate metabolism. *Int J Biochem Cell Biol* 27, 123-32.
- Altamirano, C., Illanes, A., Becerra, S., Cairo, J.J. and Godia, F. (2006) Considerations on the lactate consumption by CHO cells in the presence of galactose. *J Biotechnol* 125, 547-56.
- Altamirano, C., Illanes, A., Casablancas, A., Gamez, X., Cairo, J.J. and Godia, C. (2001) Analysis of CHO cells metabolic redistribution in a glutamate-based defined medium in continuous culture. *Biotechnol Prog* 17, 1032-41.
- Annathur, G.V., Pierce, J.L., Combs, R.G., Rathore, A.S., Banerjee, A. and Steinmeyer, D.E. (2003) Improvements in spinner-flask designs for insect-cell suspension culture. *Biotechnol Appl Biochem* 38, 15-8.
- Antoniewicz, M.R., Kelleher, J.K. and Stephanopoulos, G. (2007) Elementary metabolite units (EMU): A novel framework for modeling isotopic distributions. *Metab Eng* 9, 68-86.
- Arai, K., Lee, K., Berthiaume, F., Tompkins, R.G. and Yarmush, M.L. (2001) Intrahepatic amino acid and glucose metabolism in a D-galactosamine-induced rat liver failure model. *Hepatology* 34, 360-71.

### [B]

- Bacurau, R.F., O'Toole, C.E., Newsholme, P. and Costa Rosa, L.F. (2002) Sub-lethal concentrations of activated complement increase rat lymphocyte glutamine utilization and oxidation while lethal concentrations cause death by a mechanism involving ATP depletion. *Cell Biochem Funct* 20, 183-90.
- Bailey, J.E. (2001) Reflections on the scope and the future of metabolic engineering and its connections to functional genomics and drug discovery. *Metab Eng* 3, 111-4.
- Balcarcel, R.R. and Clark, L.M. (2003) Metabolic screening of mammalian cell cultures using well-plates. *Biotechnol Prog* 19, 98-108.

## REFERENCES

---

- Barros, L.F. and Martinez, C. (2007) An enquiry into metabolite domains. *Biophysical Journal* 92, 3878-3884.
- Behnam, J.T., Williams, E.L., Brink, S., Rumsby, G. and Danpure, C.J. (2006) Reconstruction of human hepatocyte glyoxylate metabolic pathways in stably transformed Chinese-hamster ovary cells. *Biochem J* 394, 409-16.
- Berg, J., Tymoczko, J. and Stryer, L. (2002) *Biochemistry*. W.H. Freeman and Company.
- Berliner, J.L. and Robitaille, P. (1998) *In vivo Carbon-13 NMR*, Vol. 15. Springer, USA.
- Bonarius, H.P., Houtman, J., Schmid, G., de Gooijer, C. and Tramper, J. (1999) Error analysis of metabolic-rate measurements in mammalian-cell culture by carbon and nitrogen balances. *Cytotechnology* 29, 167-176.
- Bonarius, H.P., Ozemre, A., Timmerarends, B., Skrabal, P., Tramper, J., Schmid, G. and Heinzle, E. (2001) Metabolic-flux analysis of continuously cultured hybridoma cells using  $(^{13}\text{C})\text{CO}_2$  mass spectrometry in combination with  $(^{13}\text{C})$ -lactate nuclear magnetic resonance spectroscopy and metabolite balancing. *Biotechnol Bioeng* 74, 528-38.
- Bonarius, H.P., Timmerarends, B., de Gooijer, C.D. and Tramper, J. (1998) Metabolite-balancing techniques vs.  $^{13}\text{C}$  tracer experiments to determine metabolic fluxes in hybridoma cells. *Biotechnol Bioeng* 58, 258-62.
- Bonarius, H.P.J., Hatzimanikatis, V., Meesters, K.P.H., deGooijer, C.D., Schmid, G. and Tramper, J. (1996) Metabolic flux analysis of hybridoma cells in different culture media using mass balances. *Biotechnol Bioeng* 50, 299-318.
- Bonarius, H.P.J., Schmid, G. and Tramper, J. (1997) Flux analysis of underdetermined metabolic networks: The quest for the missing constraints. *Trends Biotechnol* 15, 308-314.
- Boren, J., Lee, W.N., Bassilian, S., Centelles, J.J., Lim, S., Ahmed, S., Boros, L.G. and Cascante, M. (2003) The stable isotope-based dynamic metabolic profile of butyrate-induced HT29 cell differentiation. *J Biol Chem* 278, 28395-402.
- Bouzier, A.K., Goodwin, R., de Gannes, F.M., Valeins, H., Voisin, P., Canioni, P. and Merle, M. (1998) Compartmentation of lactate and glucose metabolism in C6 glioma cells. A  $^{13}\text{C}$  and  $^1\text{H}$  NMR study. *J Biol Chem* 273, 27162-9.
- Bradford, N.M. and McGivan, J.D. (1973) Quantitative Characteristics of Glutamate Transport in Rat-Liver Mitochondria. *Biochem J* 134, 1023-1029.

## REFERENCES

---

Brandt, S., Heller, H., Schuster, K.D. and Grote, J. (2004) Tamoxifen induces suppression of cell viability and apoptosis in the human hepatoblastoma cell line HepG2 via down-regulation of telomerase activity. *Liver Int* 24, 46-54.

### [C]

Campanella, M.E., Chu, H.Y. and Low, P.S. (2005) Assembly and regulation of a glycolytic enzyme complex on the human erythrocyte membrane. *Proceedings of the National Academy of Sciences of the United States of America* 102, 2402-2407.

Castro, P.M., Hayter, P.M., Ison, A.P. and Bull, A.T. (1992) Application of a statistical design to the optimization of culture medium for recombinant interferon-gamma production by Chinese hamster ovary cells. *Appl Microbiol Biotechnol* 38, 84-90.

Chan, C., Berthiaume, F., Lee, K. and Yarmush, M.L. (2003a) Metabolic flux analysis of cultured hepatocytes exposed to plasma. *Biotechnol Bioeng* 81, 33-49.

Chan, C., Berthiaume, F., Lee, K. and Yarmush, M.L. (2003b) Metabolic flux analysis of hepatocyte function in hormone- and amino acid-supplemented plasma. *Metab Eng* 5, 1-15.

Chu, L. and Robinson, D.K. (2001) Industrial choices for protein production by large-scale cell culture. *Curr Opin Biotechnol* 12, 180-7.

Chun, C., Heineken, K., Szeto, D., Ryll, T., Chamow, S. and Chung, J.D. (2003) Application of factorial design to accelerate identification of CHO growth factor requirements. *Biotechnol Prog* 19, 52-7.

Cornish-Bowden, A. and Cardenas, M.L. (2003) Metabolic analysis in drug design. *C R Biol* 326, 509-15.

Cruz, F., Villalba, M., Garcia-Espinosa, M.A., Ballesteros, P., Bogonez, E., Satrustegui, J. and Cerdan, S. (2001) Intracellular compartmentation of pyruvate in primary cultures of cortical neurons as detected by C-13 NMR spectroscopy with multiple C-13 labels. *Journal of Neuroscience Research* 66, 771-781.

Cunningham, B.A. (2001) A Growing Issue: Cell Proliferation Assays. *The Scientist* 15, 26.

### [D]

Davila, J.C., Rodriguez, R.J., Melchert, R.B. and Acosta, D., Jr. (1998) Predictive value of in vitro model systems in toxicology. *Annu Rev Pharmacol Toxicol* 38, 63-96.

Davis, W.L. and Goodman, D.B.P. (1992) Evidence for the Glyoxylate Cycle in Human Liver. *Anatomical Record* 234, 461-468.

## REFERENCES

---

Ducommun, P., Ruffieux, P., Furter, M., Marison, I. and von Stockar, U. (2000) A new method for on-line measurement of the volumetric oxygen uptake rate in membrane aerated animal cell cultures. *J Biotechnol* 78, 139-47.

### [E]

Eagle, H. (1955) Nutrition needs of mammalian cells in tissue culture. *Science* 122, 501-14.

Eagle, H. (1959) Amino acid metabolism in mammalian cell cultures. *Science* 130, 432-7.

Elias, C.B., Carpentier, E., Durocher, Y., Bisson, L., Wagner, R. and Kamen, A. (2003) Improving glucose and gluamiue metabolism of human HEK 293 and *Trchoplusia ni* insect cells engineered to express a cytosolic pyruvate carboxylase enzyme. *Biotechnol Prog* 19, 90-97.

Erecinska, M. and Silver, I.A. (1990) Metabolism and role of glutamate in mammalian brain. *Prog Neurobiol* 35, 245-96.

Ertola, R.J., Giulietti, A.M. and Castillo, F.J. (1995) Design, formulation, and optimization of media. *Bioprocess Technol* 21, 89-137.

Europa, A.F., Gambhir, A., Fu, P.C. and Hu, W.S. (2000) Multiple steady states with distinct cellular metabolism in continuous culture of mammalian cells. *Biotechnol Bioeng* 67, 25-34.

Eyer, K., Oeggerli, A. and Heinzle, E. (1995) Online gas analysis in animal cell cultivation: II. Methods for oxygen uptake rate estimation and its application to controlled feeding of glutamine. *Biotechnol. Bioeng* 45, 54-62.

### [F]

Fernandez, C.A. and Des Rosiers, C. (1995) Modeling of liver citric acid cycle and gluconeogenesis based on <sup>13</sup>C mass isotopomer distribution analysis of intermediates. *J Biol Chem* 270, 10037-42.

Fitzpatrick, L., Jenkins, H.A. and Butler, M. (1993) Glucose and glutamine metabolism of a murine B-lymphocyte hybridoma grown in batch culture. *Appl Biochem Biotechnol* 43, 93-116.

Follstad, B.D., Balcarcel, R.R., Stephanopoulos, G. and Wang, D.I. (1999) Metabolic flux analysis of hybridoma continuous culture steady state multiplicity. *Biotechnol Bioeng* 63, 675-83.

Forbes, N.S., Clark, D.S. and Blanch, H.W. (2001) Using isotopomer path tracing to quantify metabolic fluxes in pathway models containing reversible reactions. *Biotechnol Bioeng* 74, 196-211.

## REFERENCES

---

Fothergillgilmore, L.A. and Michels, P.A.M. (1993) Evolution of Glycolysis. Progress in Biophysics & Molecular Biology 59, 105-235.

Franek, F. and Dolnikova, J. (1991) Hybridoma growth and monoclonal antibody production in iron-rich protein-free medium: effect of nutrient concentration. Cytotechnology 7, 33-8.

### [G]

Gambhir, A., Korke, R., Lee, J., Fu, P.C., Europa, A. and Hu, W.S. (2003) Analysis of cellular metabolism of hybridoma cells at distinct physiological states. J Biosci Bioeng 95, 317-27.

Ganey, P.E., Kauffman, F.C. and Thurman, R.G. (1988) Oxygen-Dependent Hepatotoxicity Due to Doxorubicin - Role of Reducing Equivalent Supply in Perfused Rat-Liver. Molecular Pharmacology 34, 695-701.

Ganz, M.B., Boyarsky, G., Sterzel, R.B. and Boron, W.F. (1989) Arginine vasopressin enhances pHi regulation in the presence of HCO<sub>3</sub><sup>-</sup> by stimulating three acid-base transport systems. Nature 337, 648-51.

### [H]

Haggstrom, L., Ljunggren, J. and Ohman, L. (1996) Metabolic engineering of animal cells. Ann N Y Acad Sci 782, 40-52.

Hansen, H.A. and Emborg, C. (1994a) Extra- and intracellular amino acid concentrations in continuous Chinese hamster ovary cell culture. Appl Microbiol Biotechnol 41, 560-4.

Hansen, H.A. and Emborg, C. (1994b) Influence of ammonium on growth, metabolism, and productivity of a continuous suspension Chinese hamster ovary cell culture. Biotechnol Prog 10, 121-4.

Harper, A.E., Miller, R.H. and Block, K.P. (1984) Branched-chain amino acid metabolism. Annu Rev Nutr 4, 409-54.

Hassel, B. and Sonnewald, U. (2002) Effects of potassium and glutamine on metabolism of glucose in astrocytes. Neurochem Res 27, 167-71.

Haynes, P.A., Sheumack, D., Greig, L.G., Kibby, J. and Redmond, J.W. (1991) Applications of automated amino acid analysis using 9-fluorenylmethyl chloroformate. J Chromatogr 588, 107-14.

Henry, O., Perrier, M. and Kamen, A. (2005) Metabolic flux analysis of HEK-293 cells in perfusion cultures for the production of adenoviral vectors. Metab Eng 7, 467-76.

Hermann, R., Lehmann, M. and Buchs, J. (2003) Characterization of gas-liquid mass transfer phenomena in microtiter plates. Biotechnol Bioeng 81, 178-86.

## REFERENCES

---

- Hertzberg, R.P. and Pope, A.J. (2000) High-throughput screening: new technology for the 21st century. *Curr Opin Chem Biol* 4, 445-51.
- Hesse, F. and Wagner, R. (2000) Developments and improvements in the manufacturing of human therapeutics with mammalian cell cultures. *Trends Biotechnol* 18, 173-80.
- House, J.D., Hall, B.N. and Brosnan, J.T. (2001) Threonine metabolism in isolated rat hepatocytes. *Am J Physiol Endocrinol Metab* 281, E1300-7.
- Hsie, A.W. and Schenley, R.L. (1983) Utilization of Chinese hamster cells in vitro and in vivo in genetic toxicology: a multiphasic approach. *Environ Mutagen* 5, 733-44.
- Hu, W.S. and Aunins, J.G. (1997) Large-scale mammalian cell culture. *Curr Opin Biotechnol* 8, 148-53.
- Hu, W.S., Dodge, T.C., Frame, K.K. and Himes, V.B. (1987) Effect of glucose on the cultivation of mammalian cells. *Dev Biol Stand* 66, 279-90.
- Hutter, B. and John, G.T. (2004) Evaluation of OxoPlate for real-time assessment of antibacterial activities. *Curr Microbiol* 48, 57-61.
- Hynes, J., Floyd, S., Soini, A.E., O'Connor, R. and Papkovsky, D.B. (2003) Fluorescence-based cell viability screening assays using water-soluble oxygen probes. *J Biomol Screen* 8, 264-72.
- [J]**
- Jeong, Y. and Wang, S.S. (1994) Role of glutamine in hybridoma cell culture: Effects on cell growth, antibody production, and cell metabolism. *Enzyme Microb Technol* 17, 47-55.
- John, G.T., Klimant, I., Wittmann, C. and Heinzle, E. (2003) Integrated optical sensing of dissolved oxygen in microtiter plates: a novel tool for microbial cultivation. *Biotechnol Bioeng* 81, 829-36.
- Jones, L.J., Gray, M., Yue, S.T., Haugland, R.P. and Singer, V.L. (2001) Sensitive determination of cell number using the CyQUANT cell proliferation assay. *J Immunol Methods* 254, 85-98.
- Judd, R.L., Kunjathoor, V.V., Pillai, U.A., Ferguson, P.W. and Medon, P.J. (1992) Effect of tolbutamide and glyburide on pyruvate kinase flux in isolated rat hepatocytes. *Life Sci* 50, PL203-8.
- [K]**
- Katz, J. and Wood, H.G. (1960) The use of glucose-C14 for the evaluation of the pathways of glucose metabolism. *J Biol Chem* 235, 2165-77.
- Katz, J. and Wood, H.G. (1963) The use of C14O2 yields from glucose-1- and -6-C14 for the evaluation of the pathways of glucose metabolism. *J Biol Chem* 238, 517-23.

## REFERENCES

---

- Kelleher, J.K. (2001) Flux estimation using isotopic tracers: Common ground for metabolic physiology and metabolic engineering. *Metab Eng* 3, 100-110.
- Kelleher, J.K., Bryan, B.M., Mallet, R.T., Holleran, A.L., Murphy, A.N. and Fiskum, G. (1987) Analysis of Tricarboxylic Acid-Cycle Metabolism of Hepatoma-Cells by Comparison of (Co<sup>2</sup>)C-14 Ratios. *Biochem J* 246, 633-639.
- Kholodenko, B.N., Cascante, M. and Westerhoff, H.V. (1994) Control-Theory of Metabolic Channeling. *Mol Cell Biochem* 133, 313-331.
- Kikuchi, G. (1973) The glycine cleavage system: composition, reaction mechanism, and physiological significance. *Mol Cell Biochem* 1, 169-87.
- Kimura, R. and Miller, W.M. (1996) Effects of elevated pCO<sub>2</sub> and/or osmolality on the growth and recombinant tPA production of CHO cells. *Biotechnol Bioeng* 52, 152-160.
- Koukourakis, M.I., Giatromanolaki, A. and Sivridis, E. (2003) Lactate dehydrogenase isoenzymes 1 and 5: differential expression by neoplastic and stromal cells in non-small cell lung cancer and other epithelial malignant tumors. *Tumour Biol* 24, 199-202.
- Krisfalusi, M., Miki, K., Magyar, P.L. and O'Brien, D.A. (2006) Multiple glycolytic enzymes are tightly bound to the fibrous sheath of mouse spermatozoa. *Biology of Reproduction* 75, 270-278.
- Kromenaker, S.J. and Srienc, F. (1994) Stability of producer hybridoma cell lines after cell sorting: a case study. *Biotechnol Prog* 10, 299-307.
- Kromer, J.O., Fritz, M., Heinzle, E. and Wittmann, C. (2005) In vivo quantification of intracellular amino acids and intermediates of the methionine pathway in *Corynebacterium glutamicum*. *Anal Biochem* 340, 171-3.
- [L]**
- Lanoue, K.F. and Schoolwerth, A.C. (1979) Metabolite Transport in Mitochondria. *Annual Review of Biochemistry* 48, 871-922.
- Lee, G.M., Kim, E.J., Kim, N.S., Yoon, S.K., Ahn, Y.H. and Song, J.Y. (1999) Development of a serum-free medium for the production of erythropoietin by suspension culture of recombinant Chinese hamster ovary cells using a statistical design. *J Biotechnol* 69, 85-93.
- Lee, K., Berthiaume, F., Stephanopoulos, G.N., Yarmush, D.M. and Yarmush, M.L. (2000) Metabolic flux analysis of postburn hepatic hypermetabolism. *Metab Eng* 2, 312-27.

## REFERENCES

---

- Lee, W.N., Boros, L.G., Puigjaner, J., Bassilian, S., Lim, S. and Cascante, M. (1998) Mass isotopomer study of the nonoxidative pathways of the pentose cycle with [1,2-<sup>13</sup>C<sub>2</sub>]glucose. *Am J Physiol* 274, E843-51.
- Li, A.P., Lu, C., Brent, J.A., Pham, C., Fackett, A., Ruegg, C.E. and Silber, P.M. (1999) Cryopreserved human hepatocytes: characterization of drug-metabolizing enzyme activities and applications in higher throughput screening assays for hepatotoxicity, metabolic stability, and drug-drug interaction potential. *Chem Biol Interact* 121, 17-35.
- Ljunggren, J. and Haggstrom, L. (1992) Glutamine limited fed-batch culture reduces the overflow metabolism of amino acids in myeloma cells. *Cytotechnology* 8, 45-56.
- Longenecker, J.P. and Williams, J.F. (1980) Quantitative Measurement of the Type-L Pentose-Phosphate Cycle with [2-C-<sup>14</sup>] Glucose and [5-C-<sup>14</sup>-Labeled] Glucose in Isolated Hepatocytes. *Biochem J* 188, 859-865.
- Lovrecz, G. and Gray, P. (1994) Use of on-line gas analysis to monitor recombinant mammalian cell cultures. *Cytotechnology* 14, 167-75.
- Malloy, C.R., Sherry, A.D. and Jeffrey, F.M.H. (1988) Evaluation of Carbon Flux and Substrate Selection through Alternate Pathways Involving the Citric-Acid Cycle of the Heart by C-<sup>13</sup> Nmr-Spectroscopy. *J Biol Chem* 263, 6964-6971.
- [M]**
- Man, E.H., Fisher, G.H., Payan, I.L., Cadilla-Perezrios, R., Garcia, N.M., Chemburkar, R., Arends, G. and Frey, W.H., 2nd. (1987) D-aspartate in human brain. *J Neurochem* 48, 510-5.
- Mancuso, A., Sharfstein, S.T., Fernandez, E.J., Clark, D.S. and Blanch, H.W. (1998) Effect of extracellular glutamine concentration on primary and secondary metabolism of a murine hybridoma: an in vivo <sup>13</sup>C nuclear magnetic resonance study. *Biotechnol Bioeng* 57, 172-86.
- Mancuso, A., Sharfstein, S.T., Tucker, N.S., Clark, D.S. and Blanch, H.W. (1994) Examination of Primary Metabolic Pathways in a Murine Hybridoma with Carbon-<sup>13</sup> Nuclear Magnetic Resonance Spectroscopy. *Biotechnol Bioeng* 44, 563-585.
- Manzano, A., Roig, T., Bermudez, J. and Bartrons, R. (1996) Effects of taxol on isolated rat hepatocyte metabolism. *Am J Physiol* 271, C1957-62.
- Massart, D.L., Vandeginste, B.G.M., Buydens, L.M.C., De Jong, S., Lewi, P.J. and Smeyers-Verbeke, J. (1997) *Handbook of Chemometrics and Qualimetrics : Part A*. Elsevier Science B.V, The Netherlands.

## REFERENCES

---

- Mawhinney, T.P., Robinett, R.S., Atalay, A. and Madson, M.A. (1986) Analysis of amino acids as their tert.-butyldimethylsilyl derivatives by gas-liquid chromatography and mass spectrometry. *J Chromatogr* 358, 231-42.
- Miller, W.M., Blanch, H.W. and Wilke, C.R. (2000) A kinetic analysis of hybridoma growth and metabolism in batch and continuous suspension culture: effect of nutrient concentration, dilution rate, and pH. Reprinted from *Biotechnology and Bioengineering*, Vol. 32, Pp 947-965 (1988). *Biotechnol Bioeng* 67, 853-71.
- Miller, W.M., Wilke, C.R. and Blanch, H.W. (1987) Effects of dissolved oxygen concentration on hybridoma growth and metabolism in continuous culture. *J Cell Physiol* 132, 524-30.
- Morris, C., Griffiths, J.B., Warburton, S., West, C.M.L., Al-Rubeai, M., Clarke, J.B., Simone, F. and Doyle, A. (1997) *Core techniques*. J.Wiley and Sons, Cambridge.
- Mosmann, T. (1983) Rapid colorimetric assay for cellular growth and survival: application to proliferation and cytotoxicity assays. *J Immunol Methods* 65, 55-63.
- [N]
- Narkewicz, M.R., Sauls, S.D., Tjoa, S.S., Teng, C. and Fennessey, P.V. (1996) Evidence for intracellular partitioning of serine and glycine metabolism in Chinese hamster ovary cells. *Biochem J* 313 ( Pt 3), 991-6.
- Neermann, J. and Wagner, R. (1996) Comparative analysis of glucose and glutamine metabolism in transformed mammalian cell lines, insect and primary liver cells. *J Cell Physiol* 166, 152-69.
- Newland, M., Greenfield, P.F. and Reid, S. (1990) Hybridoma growth limitations: the roles of energy metabolism and ammonia production. *Cytotechnology* 3, 215-29.
- Newsholme, E.A., Crabtree, B. and Ardawi, M.S. (1985) The role of high rates of glycolysis and glutamine utilization in rapidly dividing cells. *Biosci Rep* 5, 393-400.
- Nielsen, J. (1998) *Metabolic engineering: Techniques for analysis of targets for genetic manipulations*. *Biotechnol Bioeng* 58, 125-132.
- Nussler, A.K., Wang, A., Neuhaus, P., Fischer, J., Yuan, J., Liu, L., Zeilinger, K., Gerlach, J., Arnold, P.J. and Albrecht, W. (2001) The suitability of hepatocyte culture models to study various aspects of drug metabolism. *Altex* 18, 91-101.
- Nyberg, G.B., Balcarcel, R.R., Follstad, B.D., Stephanopoulos, G. and Wang, D.I. (1999) Metabolism of peptide amino acids by Chinese hamster ovary cells grown in a complex medium. *Biotechnol Bioeng* 62, 324-35.

## REFERENCES

---

### [O]

- Oezemre, A. and Heinzle, E. (2001) Measurement of oxygen uptake and carbon dioxide production rates of mammalian cells using membrane mass spectrometry. *Cytotechnology* 37, 153-162.
- Olsen, N.S., Hemingway, A. and Nier, A.O. (1943) The metabolism of glycine I. Studies with the stable isotope of carbon. *J Biol Chem* 148, 611-617.
- O'Riordan, T.C., Buckley, D., Ogurtsov, V., O'Connor, R. and Papkovsky, D.B. (2000) A cell viability assay based on monitoring respiration by optical oxygen sensing. *Anal Biochem* 278, 221-7.
- Ovadi, J. (1991) Physiological significance of metabolic channelling. *J Theor Biol* 152, 1-22.
- Owen, O.E., Kalhan, S.C. and Hanson, R.W. (2002) The key role of anaplerosis and cataplerosis for citric acid cycle function. *J Biol Chem* 277, 30409-12.
- Ozturk, S.S. and Palsson, B.O. (1990a) Effect of initial cell density on hybridoma growth, metabolism, and monoclonal antibody production. *J Biotechnol* 16, 259-78.
- Ozturk, S.S. and Palsson, B.O. (1990b) Effects of dissolved oxygen on hybridoma cell growth, metabolism, and antibody production kinetics in continuous culture. *Biotechnol Prog* 6, 437-46.
- Ozturk, S.S. and Palsson, B.O. (1991) Growth, metabolic, and antibody production kinetics of hybridoma cell culture: 1. Analysis of data from controlled batch reactors. *Biotechnol Prog* 7, 471-80.

### [P]

- Palmqvist, E., Grage, H., Meinander, N.Q. and Hahn-Hagerdal, B. (1999) Main and interaction effects of acetic acid, furfural, and p-hydroxybenzoic acid on growth and ethanol productivity of yeasts. *Biotechnol Bioeng* 63, 46-55.
- Paredes, C., Sanfeliu, A., Cardenas, F., Cairo, J.J. and Godia, F. (1998) Estimation of the intracellular fluxes for a hybridoma cell line by material balances. *Enzyme and Microbial Technology* 23, 187-198.
- Parker, R.A., Pearce, B.C., Clark, R.W., Gordon, D.A. and Wright, J.J. (1993) Tocotrienols regulate cholesterol production in mammalian cells by post-transcriptional suppression of 3-hydroxy-3-methylglutaryl-coenzyme A reductase. *J Biol Chem* 268, 11230-8.
- Peuhkurinen, K.J., Hiltunen, J.K. and Hassinen, I.E. (1983) Metabolic compartmentation of pyruvate in the isolated perfused rat heart. *Biochem J* 210, 193-8.
- Piva, T.J. and McEvoy-Bowe, E. (1998) Oxidation of glutamine in HeLa cells: Role and control of truncated TCA cycles in tumour mitochondria. *J Cell Biochem* 68, 213-225.

## REFERENCES

---

Popov, V.N., Igamberdiev, A.U., Schnarrenberger, C. and Volvenkin, S.V. (1996) Induction of glyoxylate cycle enzymes in rat liver upon food starvation. *Febs Letters* 390, 258-260.

Portais, J.C., Schuster, R., Merle, M. and Canioni, P. (1993) Metabolic Flux Determination in C6 Glioma-Cells Using C-13 Distribution Upon [1-C-13]Glucose Incubation. *Eur J Biochem* 217, 457-468.

Puck, T.T., Cieciura, S.J. and Robinson, A. (1958) Genetics of somatic mammalian cells. III. Long-term cultivation of euploid cells from human and animal subjects. *J Exp Med* 108, 945-56.

### [R]

Ramirez, O.T. and Mutharasan, R. (1990) Cell cycle- and growth phase dependent variations in size distribution, antibody productivity, and oxygen demand in hybridoma cultures. *Biotechnol Bioeng* 36, 839-848.

Reeds, P.J., Berthold, H.K., Boza, J.J., Burrin, D.G., Jahoor, F., Jaksic, T., Klein, P.D., Keshen, T., Miller, R., Stoll, B. and Wykes, L.J. (1997) Integration of amino acid and carbon intermediary metabolism: studies with uniformly labeled tracers and mass isotopomer analysis. *Eur J Pediatr* 156, S50-S58.

Reitzer, L.J., Wice, B.M. and Kennell, D. (1979) Evidence that glutamine, not sugar, is the major energy source for cultured HeLa cells. *J Biol Chem* 254, 2669-76.

Riss, T.L. and Moravec, R.A. (2004) Use of multiple assay endpoints to investigate the effects of incubation time, dose of toxin, and plating density in cell-based cytotoxicity assays. *Assay Drug Dev Technol* 2, 51-62.

Ronning, O.W., Schartum, M., Winsnes, A. and Lindberg, G. (1991) Growth limitation in hybridoma cell cultures: the role of inhibitory or toxic metabolites. *Cytotechnology* 7, 15-24.

Ross, B.D., Kingsley, P.B. and Ben-Yoseph, O. (1994) Measurement of pentose phosphate-pathway activity in a single incubation with [1,6-13C2,6,6-2H2]glucose. *Biochem J* 302 ( Pt 1), 31-8.

Roth, M. (1971) Fluorescence reaction for amino acids. *Anal Chem* 43, 880-2.

### [S]

Safer, B. and Williamson, J.R. (1973) Mitochondrial-cytosolic interactions in perfused rat heart. Role of coupled transamination in repletion of citric acid cycle intermediates. *J Biol Chem* 248, 2570-9.

## REFERENCES

---

- Schmidt, K., Carlsen, M., Nielsen, J. and Villadsen, J. (1997) Modeling isotopomer distributions in biochemical networks using isotopomer mapping matrices. *Biotechnol Bioeng* 55, 831-840.
- Schmidt, K., Marx, A., de Graaf, A.A., Wiechert, W., Sahm, H., Nielsen, J. and Villadsen, J. (1998)  $^{13}\text{C}$  tracer experiments and metabolite balancing for metabolic flux analysis: comparing two approaches. *Biotechnol Bioeng* 58, 254-7.
- Schoenherr, I., Stapp, T. and Ryll, T. (2000) A comparison of different methods to determine the end of exponential growth in CHO cell cultures for optimization of scale-up. *Biotechnol Prog* 16, 815-21.
- Schrader, M.C., Eskey, C.J., Simplaceanu, V. and Ho, C. (1993) A carbon-13 nuclear magnetic resonance investigation of the metabolic fluxes associated with glucose metabolism in human erythrocytes. *Biochim Biophys Acta* 1182, 162-78.
- Schuster, R. (1988) Determination of amino acids in biological, pharmaceutical, plant and food samples by automated precolumn derivatization and high-performance liquid chromatography. *J Chromatogr* 431, 271-84.
- Schwenk, W.F., Berg, P.J., Beaufre, B., Miles, J.M. and Haymond, M.W. (1984) Use of *t*-butyldimethylsilylation in the gas chromatographic/mass spectrometric analysis of physiologic compounds found in plasma using electron-impact ionization. *Anal Biochem* 141, 101-9.
- Seglen, P.O. (1976) Preparation of isolated rat liver cells. *Methods Cell Biol* 13, 29-83.
- Sharfstein, S.T., Tucker, N.S., Mancuso, A., Blanch, H.W. and Clark, D.S. (1994) Quantitative In Vivo Nuclear Magnetic Resonance Studies of Hybridoma Metabolism. *Biotechnol Bioeng* 43, 1059-1074.
- Sibson, N.R., Mason, G.F., Shen, J., Cline, G.W., Herskovits, A.Z., Wall, J.E., Behar, K.L., Rothman, D.L. and Shulman, R.G. (2001) In vivo  $(^{13}\text{C})$  NMR measurement of neurotransmitter glutamate cycling, anaplerosis and TCA cycle flux in rat brain during  $[2-(^{13}\text{C})]$ glucose infusion. *J Neurochem* 76, 975-89.
- Snyder, S.H., Logan, W.J., Bennett, J.P. and Arregui, A. (1973) Amino acids as central nervous transmitters: biochemical studies. *Neurosci Res (N Y)* 5, 131-57.
- Souchier, C., Ffrench, M., Benchaib, M., Catallo, R. and Bryon, P.A. (1995) Methods for cell proliferation analysis by fluorescent image cytometry. *Cytometry* 20, 203-9.
- Stitt, D.T., Nagar, M.S., Haq, T.A. and Timmins, M.R. (2002) Determination of growth rate of microorganisms in broth from oxygen-sensitive fluorescence plate reader measurements. *Biotechniques* 32, 684, 686, 688-9.

## REFERENCES

---

Suh, J.W., Lee, S.H. and Chung, B.C. (1997) GC-MS determination of organic acids with solvent extraction after cation-exchange chromatography. *Clin Chem* 43, 2256-61.

Szyperski, T. (1998) C-13-NMR, MS and metabolic flux balancing in biotechnology research. *Quarterly Reviews of Biophysics* 31, 41-106.

### [T]

Trubel, H. and Barnikol, W.K. (1998) [A new microprocedure for continuous and non-consuming determination of cellular oxygen uptake based on fluorescence quenching]. *Biomed Tech (Berl)* 43, 302-9.

### [V]

Vallino, J.J. and Stephanopoulos, G. (2000) Metabolic flux distributions in *Corynebacterium glutamicum* during growth and lysine overproduction. Reprinted from *Biotechnology and Bioengineering*, Vol. 41, Pp 633-646 (1993). *Biotechnol Bioeng* 67, 872-85.

Vandenbosch, H., Schutgens, R.B.H., Wanders, R.J.A. and Tager, J.M. (1992) Biochemistry of Peroxisomes. *Annu Rev Biochem* 61, 157-197.

Varma, A. and Palsson, B.O. (1994) Metabolic Flux Balancing - Basic Concepts, Scientific and Practical Use. *Bio-Technology* 12, 994-998.

Verhoff, F.H. and Spradlin, J.E. (1976) Mass and energy balance analysis of metabolic pathways applied to citric acid production by *Aspergillus niger*. *Biotechnol Bioeng* 18, 452-32.

### [W]

Wanders, R.J., Meijer, A.J., Groen, A.K. and Tager, J.M. (1983) Bicarbonate and the pathway of glutamate oxidation in isolated rat-liver mitochondria. *Eur J Biochem* 133, 245-54.

Weiss, S., John, G.T., Klimant, I. and Heinzle, E. (2002) Modeling of mixing in 96-well microplates observed with fluorescence indicators. *Biotechnol Prog* 18, 821-30.

Werner, R.G. and Noe, W. (1993) Mammalian cell cultures. Part I: Characterization, morphology and metabolism. *Arzneimittelforschung* 43, 1134-9.

Wiechert, W. (2001) C-13 metabolic flux analysis. *Metab Eng* 3, 195-206.

Wiechert, W. and de Graaf, A.A. (1996) In vivo stationary flux analysis by <sup>13</sup>C labeling experiments. *Adv Biochem Eng Biotechnol* 54, 109-54.

Wiechert, W., Mollney, M., Isermann, N., Wurzel, W. and de Graaf, A.A. (1999) Bidirectional reaction steps in metabolic networks: III. Explicit solution and analysis of isotopomer labeling systems. *Biotechnol Bioeng* 66, 69-85.

Wiechert, W., Mollney, M., Petersen, S. and de Graaf, A.A. (2001) A universal framework for <sup>13</sup>C metabolic flux analysis. *Metab Eng* 3, 265-83.

## REFERENCES

---

- Wittmann, C. (2007) Fluxome analysis using GC-MS. *Microbial Cell Factories* 6, -.
- Wittmann, C. and Heinzle, E. (1999) Mass spectrometry for metabolic flux analysis. *Biotechnol Bioeng* 62, 739-750.
- Wittmann, C. and Heinzle, E. (2001) Modeling and experimental design for metabolic flux analysis of lysine-producing *Corynebacteria* by mass spectrometry. *Metab Eng* 3, 173-91.
- Wittmann, C., Kim, H.M. and Heinzle, E. (2004) Metabolic network analysis of lysine producing *Corynebacterium glutamicum* at a miniaturized scale. *Biotechnol Bioeng* 87, 1-6.
- Wittmann, C., Kim, H.M., John, G. and Heinzle, E. (2003) Characterization and application of an optical sensor for quantification of dissolved O<sub>2</sub> in shake-flasks. *Biotechnol Lett* 25, 377-80.
- Wodnicka, M., Guarino, R.D., Hemperly, J.J., Timmins, M.R., Stitt, D. and Pitner, J.B. (2000) Novel fluorescent technology platform for high throughput cytotoxicity and proliferation assays. *J Biomol Screen* 5, 141-52.
- Wolfe, R.R. and Chinkes, D.L. (2004) *Isotope Tracers in Metabolic Research: Principles and Practice of Kinetic Analysis*. Wiley, UK.
- Wurm, F.M. (2004) Production of recombinant protein therapeutics in cultivated mammalian cells. *Nat Biotechnol* 22, 1393-8.
- [X]**
- Xie, L. and Wang, D.I. (1996) Material Balance Studies on Animal Cell Metabolism Using a Stoichiometrically Based Reaction Network. *Biotechnol Bioeng* 52, 579-590
- Xiu, Z., Deckwer, W.D. and Zeng, A.P. (1999) Estimation of rates of oxygen uptake and carbon dioxide evolution of animal cell culture using material and energy balances. *Cytotechnology* 29, 159-166.
- [Y]**
- Yang, T.H. (2006) In vivo respirometric <sup>13</sup>C flux analysis. In: *Technische Biochemie*. Saarland University, Saarbruecken.
- Yao, D., Zhang, F., Yu, L., Yang, Y., van Breemen, R.B. and Bolton, J.L. (2001) Synthesis and reactivity of potential toxic metabolites of tamoxifen analogues: droloxifene and toremifene o-quinones. *Chem Res Toxicol* 14, 1643-53.
- Young, V.R. and Ajami, A. (1999) The Rudolf Schoenheimer Centenary Lecture. Isotopes in nutrition research. *Proc Nutr Soc* 58, 15-32.

## REFERENCES

---

Yu, A.C., Hertz, E. and Hertz, L. (1983) Effects of barbiturates on energy and intermediary metabolism in cultured astrocytes. *Prog Neuropsychopharmacol Biol Psychiatry* 7, 691-6.

### [Z]

Zhang, J.H., Chung, T.D. and Oldenburg, K.R. (1999) A Simple Statistical Parameter for Use in Evaluation and Validation of High Throughput Screening Assays. *J Biomol Screen* 4, 67-73.

Zupke, C., Sinskey, A.J. and Stephanopoulos, G. (1995) Intracellular flux analysis applied to the effect of dissolved oxygen on hybridomas. *Appl Microbiol Biotechnol* 44, 27-36.

Zupke, C. and Stephanopoulos, G. (1994) Modeling of Isotope Distributions and Intracellular Fluxes in Metabolic Networks Using Atom Mapping Matrices. *Biotechnol Prog* 10, 489-498.

Zwingmann, C., Richter-Landsberg, C. and Leibfritz, D. (2001) <sup>13</sup>C isotopomer analysis of glucose and alanine metabolism reveals cytosolic pyruvate compartmentation as part of energy metabolism in astrocytes. *Glia* 34, 200-12.

## 9 APPENDIX

### 9.1 Symbols and abbreviations

$\mu$	Growth rate
$q_{O_2}$	Specific oxygen uptake rate
<b>AcCoA</b>	Acetyl CoA
<b>ADP</b>	Adenosine diphosphate
<b>AKG</b>	$\alpha$ -Ketoglutarate
<b>ALA</b>	Alanine
<b>ARG</b>	Arginine
<b>ASN</b>	Asparagine
<b>ASP</b>	Aspartic acid
<b>ATP</b>	Adenosine triphosphate
<b>Caco-2</b>	Colonic carcinoma cell line
<b>CHO</b>	Chinese hamster ovary
<b>CIT</b>	Citrate
<b>CYS</b>	Cysteine
<b>DNA</b>	Deoxyribonucleic acid
<b>E4P</b>	Erythrose 4-phosphate
<b>F6P</b>	Fructose 6-phosphate
<b>FAD</b>	Flavin adenine dinucleotide oxidised
<b>FADH</b>	Flavin adenine dinucleotide reduced
<b>FUM</b>	Fumerate
<b>G6P</b>	Glucose 6-phosphate
<b>GAP</b>	Glyceraldehyde 3-phosphate
<b>GLC</b>	Glucose
<b>GLN</b>	Glutamine
<b>GLOX</b>	Glyoxylate
<b>GLU</b>	Glutamic acid
<b>GLY</b>	Glycine
<b>HIS</b>	Histidine
<b>HL-60</b>	Human acute myeloid leukemia
<b>ILE</b>	Isoleucine

## APPENDIX

---

<b>LAC</b>	Lactate
<b>LEU</b>	Leucine
<b>LYS</b>	Lysine
<b>Kla</b>	Volumetric mass transfer coefficient
<b>mAcCoA</b>	Mitochondrial acetyl CoA
<b>mAKG</b>	Mitochondrial $\alpha$ -ketoglutarate
<b>MAL</b>	Malate
<b>mCIT</b>	Mitochondrial citrate
<b>MET</b>	Methionine
<b>mMAL</b>	Mitochondrial malate
<b>mOAA</b>	Mitochondrial oxaloacetate
<b>mPYR</b>	Mitochondrial pyruvate
<b>mSUC</b>	Mitochondrial succinate
<b>MTHF</b>	5,10-Methylenetetrahydrofolate
<b>MTP</b>	Microtiter plate
<b>MTT</b>	3-(4,5-Dimethylthiazol-2-yl)-2,5-diphenyltetrazolium bromide
<b>NAD</b>	Nicotinamide adenine dinucleotide oxidised
<b>NADH</b>	Nicotinamide adenine dinucleotide reduced
<b>NADP</b>	Nicotinamide adenine dinucleotide phosphate oxidised
<b>NADPH</b>	Nicotinamide adenine dinucleotide phosphate reduced
<b>OAA</b>	Oxaloacetate
<b>OUR</b>	Oxygen uptake rate
<b>P5P</b>	Pentose 5-phosphate
<b>PG</b>	Phosphoglycerate
<b>PHE</b>	Phenylalanine
<b>PPP</b>	Pentose phosphate pathway
<b>PRO</b>	Proline
<b>PYR</b>	Pyruvate
<b>RNA</b>	Ribonucleic acid
<b>S7P</b>	Sedoheptulose 7-phosphate
<b>SER</b>	Serine
<b>SUC</b>	Succinate
<b>TCA</b>	Tricarboxylic acid
<b>THF</b>	Tetrahydrofolic acid

## APPENDIX

---

<b>THR</b>	Threonine
<b>TRP</b>	Tryptophan
<b>TYR</b>	Tyrosine
<b>VAL</b>	Valine

## 9.2 Berkeley Madonna program for *kla* determination

{Berkeley Madonna program for calculation of *kla* using microtiter plate with integrated oxygen sensor. Oxygen removed by addition of dithionite. After consumption of dithionite which reacts rapidly with oxygen, oxygen concentration rises again}

DT=0.01  
DTMAX=0.1  
DTOUT=0.1  
TOLERANCE=0.001

KLA=0.001 ; volumetric liquid phase mass transfer coefficient h-1

CLS=100 ; Saturation concentration of Oxygen (%)

init CS=0.5 ; Initial concentration of Dithionite (mM)

k=200 ; Rate constant for dithionite reaction

init CL =0 ; Initial concentration of oxygen

**{Oxygen balance for dithionite oxidation}**

DCLDT=KLA\*(CLS-CL)-k\*CL\*CS

d/dt(CL)=DCLDT

**{Rate equation for dithionite oxidation}**

d/dt(CS)=-k\*CL\*CS

Limit CL>=0

### 9.3 Equations for the biochemical metabolic model in Figure 5.2.1

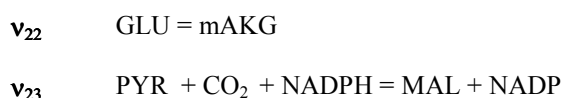
#### Reactions for internal fluxes:

##### Reaction no. Biochemical equation

v <sub>1</sub>	G6P + 2NADP = P5P + 2NADPH + CO <sub>2</sub>
v <sub>2</sub>	G6P = F6P
v <sub>2r</sub>	F6P = G6P
v <sub>3</sub>	2P5P = S7P + GAP
v <sub>3r</sub>	S7P + GAP = 2P5P
v <sub>4</sub>	GAP + S7P = F6P + E4P
v <sub>4r</sub>	F6P + E4P = GAP + S7P
v <sub>5</sub>	E4P + P5P = F6P + GAP
v <sub>5r</sub>	F6P + GAP = E4P + P5P
v <sub>6</sub>	F6P + ATP = ADP + 2GAP
v <sub>7</sub>	GAP + ADP + NAD = PG + ATP + NADH
v <sub>8</sub>	PG + ADP = PYR + ATP
v <sub>9</sub>	PYR = mPYR; PYR + CoA + NAD = mAcCoA + NADH + CO <sub>2</sub>
v <sub>10</sub>	mAcCoA + mOAA + H <sub>2</sub> O = mCIT + CoA
v <sub>11</sub>	mCIT + NAD = mAKG + NADH + CO <sub>2</sub>
v <sub>12</sub>	mAKG + ADP + NAD = mSUC + NADH + CO <sub>2</sub> + ATP
v <sub>13</sub>	FAD + mSUC + H <sub>2</sub> O = FADH + mMAL; mMAL + NAD = mOAA + NADH
v <sub>14</sub>	PG + ADP + NAD = SER + ATP + NADH
v <sub>15</sub>	SER + TTTHF = GLY + MTTHF
v <sub>16</sub>	SER = PYR + NH <sub>4</sub>
v <sub>17</sub>	PYR (+GLU) = ALA (+AKG)
v <sub>18</sub>	mCIT = AcCoA + MAL
v <sub>19</sub>	mMAL + GLU = MAL + mAKG
v <sub>19r</sub>	MAL + mAKG = mMAL + GLU
v <sub>20</sub>	MAL + NADP = PYR + CO <sub>2</sub> + NADPH
v <sub>21</sub>	ASP (+AKG) = MAL (+GLU)

## APPENDIX

---



### **Reactions for external fluxes:**

<b><u>Reaction no.</u></b>	<b><u>Biochemical equation</u></b>
$v_{ext1}$	$GLC + ATP = ADP + G6P$
$v_{ext2}$	$extPYR = PYR$
$v_{ext3}$	$extGLY = GLY$
$v_{ext4}$	$extSER = SER$
$v_{ext5}$	$CYS (+mAKG) = PYR (+GLU)$
$v_{ext6}$	$THR = mSUC$
$v_{ext7}$	$extASP = ASP$
$v_{ext8}$	$ASN = ASP + NH_4$
$v_{ext9}$	$TYR + CoA (+AKG) = mSUC + 2AcCoA + CO_2 (+GLU) \ \& \ PHE + NADPH = TYR + NADP$
$v_{ext10}$	$ILE + ATP + CoA + 3NAD (+AKG) = mSUC + mAcCoA + ADP + 3NADH (+GLU)$
$v_{ext11}$	$MET + 4ATP + 2NAD + 4H_2O (+SER) (+THF) = mSUC + NH_4 + 4ADP + 2NADH (+CYS) (+MTHF)$
$v_{ext12}$	$VAL + 2ATP + COA + 4NAD (+AKG) = mSUC + 2ADP + 4NADH + CO_2 (+GLU)$
$v_{ext13}$	$PRO + 2NAD = GLU + 2NADH$
$v_{ext14}$	$ARG + NAD (+AKG) = GLU + NADH (+GLU)$
$v_{ext15}$	$HIS + THF + NADPH = GLU + MTHF + NADP + 2NH_4$
$v_{ext16}$	$extGLU/GLN \ pool = GLU \ \& \ GLN = GLU + NH_4$
$v_{ext17}$	$LEU + ATP + 2NAD + 3CoA (+mAKG) = 3AcCoA + 2NADH + ADP (+GLU)$
$v_{ext18}$	$LYS + 2CoA + 0.5O_2 + 4NAD (+mAKG) = 2AcCoA + 2CO_2 + NH_4 + 4NADH (+GLU)$
$v_{ext19}$	$PYR + NADH = LAC + NAD$
$v_{ext20}$	$PYR (+GLU) = ALA (+AKG)$

## APPENDIX

---

### Reactions for biomass fluxes:

<u>Reaction</u> <u>no.</u>	<u>Biochemical equation</u>
<b>Vb1</b>	$G6P + 3.5ATP = \mathbf{CARBO} + 3.5ADP$
<b>Vb2</b>	$R5P + (4.67ATP) + 1.24ASP + 0.5GLY + MTHF + (1.76GLN) = \mathbf{RNA} + (4.67ADP) + 0.26FUM + (1.76GLU) + THF$
	$R5P + (4.7ATP) + 1.295ASP + 0.5GLY + 1.29MTHF + (1.41GLN) = \mathbf{DNA} + (4.7ADP) + 1.29THF + (1.41GLU) + 0.205FUM$
<b>Vb3</b>	$0.75\text{ GAP} + 17.8\text{ AcCoA} + 0.193\text{ SER} + 0.375\text{ Choline} + 0.2\text{ Ethanolamine} + 0.036\text{ Inositol} = \mathbf{Lipids}$
<b>Vb4</b>	$0.095ALA + 0.048ASP + 0.039ASN + 0.063ARG + 0.028CYS + 0.052GLN + 0.064GLU + 0.078GLY + 0.022HIS + 0.052ILE + 0.088LEU + 0.089LYS + 0.02MET + 0.021PHE + 0.028PRO + 0.057SER + 0.061THR + 0.006TRP + 0.02TYR + 0.059VAL + 4ATP + 4H_2O = \mathbf{Protein} + 4ADP + 4P_i$

## 9.4 Equations for the biochemical metabolic model in Figure 5.6.13

### Reactions for internal fluxes:

<u>Reaction no.</u>	<u>Biochemical equation</u>
v <sub>1</sub>	G6P + 2NADP = P5P + 2NADPH + CO <sub>2</sub>
v <sub>2</sub>	G6P = F6P
v <sub>2r</sub>	F6P = G6P
v <sub>3</sub>	2P5P = S7P + GAP
v <sub>3r</sub>	S7P + GAP = 2P5P
v <sub>4</sub>	GAP + S7P = F6P + E4P
v <sub>4r</sub>	F6P + E4P = GAP + S7P
v <sub>5</sub>	E4P + P5P = F6P + GAP
v <sub>5r</sub>	F6P + GAP = E4P + P5P
v <sub>6</sub>	F6P + ATP = ADP + 2GAP
v <sub>7</sub>	GAP + ADP + NAD = PG + ATP + NADH
v <sub>8</sub>	PG + ADP = PYR 1 + ATP
v <sub>9</sub>	mPYR + CoA + NAD = mAcCoA + NADH + CO <sub>2</sub>
v <sub>10</sub>	mAcCoA + mOAA + H <sub>2</sub> O = mCIT + CoA
v <sub>11</sub>	mCIT + NAD = mAKG + NADH + CO <sub>2</sub>
v <sub>12</sub>	mAKG + ADP + NAD = mSUC + NADH + CO <sub>2</sub> + ATP
v <sub>13</sub>	FAD + mSUC + H <sub>2</sub> O = FADH + mMAL; mMAL + NAD = mOAA + NADH
v <sub>14</sub>	PG + ADP + NAD = SER + ATP + NADH
v <sub>15</sub>	SER + TTHF = GLY + MTTHF
v <sub>15r</sub>	GLY + MTTHF = SER + TTHF
v <sub>16</sub>	SER = PYR 2 + NH <sub>4</sub>
v <sub>17</sub>	PYR 2 (+GLU) = ALA (+AKG)
v <sub>18</sub>	mCIT = AcCoA + MAL
v <sub>19</sub>	mMAL + GLU = MAL + mAKG
v <sub>19r</sub>	MAL + mAKG = mMAL + GLU
v <sub>20</sub>	MAL + NADP = PYR + CO <sub>2</sub> + NADPH
v <sub>21</sub>	ASP (+AKG) = MAL (+GLU)

## APPENDIX

---

V <sub>22</sub>	GLU = mAKG
V <sub>23</sub>	PYR 2 + CO <sub>2</sub> + NADPH = MAL + NADP
V <sub>24</sub>	PYR 1 = PYR 2
V <sub>25</sub>	PYR 2 = mPYR
V <sub>26</sub>	PYR 1 = LAC
V <sub>27</sub>	PYR 2 = LAC
V <sub>28</sub>	PYR 1 (+GLU) = ALA (+AKG)
V <sub>29</sub>	mPYR (+GLU) = ALA (+AKG)
V <sub>30</sub>	mICIT = GLOX + mSUC
V <sub>31</sub>	GLOX (+ALA) = GLY (+PYR)
V <sub>32</sub>	THR + NAD + CoA = GLY + mAcCoA + NADH
V <sub>33</sub>	CO <sub>2</sub> + NH <sub>3</sub> = GLY
V <sub>34</sub>	AcCoA = Fatty acids

### **Reactions for external fluxes:**

<b><u>Reaction no.</u></b>	<b><u>Biochemical equation</u></b>
V <sub>ext1</sub>	GLC + ATP = ADP + G6P
V <sub>ext2</sub>	extPYR = PYR 2
V <sub>ext3</sub>	GLY = extGLY
V <sub>ext4</sub>	SER = extSER
V <sub>ext5</sub>	CYS (+mAKG) = PYR (+GLU)
V <sub>ext6</sub>	THR = mSUC
V <sub>ext7</sub>	ASP = extASP
V <sub>ext8</sub>	ASN = ASP+NH <sub>4</sub>
V <sub>ext9</sub>	TYR + CoA (+AKG) = mSUC + 2AcCoA + CO <sub>2</sub> (+GLU) & PHE + NADPH = TYR + NADP
V <sub>ext10</sub>	ILE + ATP + CoA + 3NAD (+AKG) = mSUC + mAcCoA + ADP + 3NADH (+GLU)
V <sub>ext11</sub>	MET + 4ATP + 2NAD + 4H <sub>2</sub> O (+SER) (+THF) = mSUC + NH <sub>4</sub> + 4ADP + 2NADH (+CYS) (+MTHF)
V <sub>ext12</sub>	VAL+2ATP+COA+4NAD (+AKG)=mSUC+2ADP+4NADH+CO <sub>2</sub> (+GLU)
V <sub>ext13</sub>	PRO + 2NAD = GLU + 2NADH
V <sub>ext14</sub>	ARG + NAD (+AKG) = GLU + NADH (+GLU)

## APPENDIX

---

- V<sub>ext15</sub>**     $\text{HIS} + \text{THF} + \text{NADPH} = \text{GLU} + \text{MTHF} + \text{NADP} + 2\text{NH}_4$
- V<sub>ext16</sub>**     $\text{GLN} = \text{GLU} \ \& \ \text{GLN} = \text{GLU} + \text{NH}_4$
- V<sub>ext17</sub>**     $\text{LEU} + \text{ATP} + 2\text{NAD} + 3\text{CoA} (+\text{mAKG}) = 3\text{AcCoA} + 2\text{NADH} + \text{ADP} (+\text{GLU})$
- V<sub>ext18</sub>**     $\text{LYS} + 2\text{CoA} + 0.5\text{O}_2 + 4\text{NAD} (+\text{mAKG}) = 2\text{AcCoA} + 2\text{CO}_2 + \text{NH}_4 + 4\text{NADH} (+\text{GLU})$
- V<sub>ext19</sub>**     $\text{LAC} = \text{exLAC}$
- V<sub>ext20</sub>**     $\text{ALA} = \text{exALA}$
- V<sub>ext21</sub>**     $\text{GLU} = \text{extGLU}$

## 9.5 Biomass composition of CHO cells

The **Cellular Composition** of the cell used was taken from Altamirano et al. (2001) and is given below:

Macromolecules	% Dry Weight
DNA	1.9
RNA	5.8
Lipids	7.7
Carbohydrates	7
Proteins	70.6

The **cell dry weight** was calculated to 0.32 mg/10<sup>6</sup> cells.

The **Amino acid** composition of cellular protein is taken from Altamirano et al. (2001) and is shown below:

Amino Acid	Molar Fraction	Amino Acid	Molar Fraction
ALA	0.095	LEU	0.088
ARG	0.063	LYS	0.089
ASP	0.048	MET	0.020
ASN	0.039	PHE	0.021
CYS	0.028	PRO	0.028
GLN	0.052	SER	0.057
GLU	0.064	THR	0.061
GLY	0.078	TRP	0.006
HIS	0.022	TYR	0.020
ILE	0.052	VAL	0.059

The Average Molecular Weight was thus calculated to be **108**. The Molar requirement for each amino acid per gram biomass was calculated from this.

The **Carbohydrates** are taken as polyglucose with a molecular weight of **162**.

The GC content of the **DNA** is taken as 41% (Lander et al., 2001):

DNA	Content (mol/mol)	MW(g/mol)	Content % (w/w)	mmol/g biomass
dAMP	0.295	331.2	0.318	0.018
dTMP	0.295	304.2	0.291	0.018
dGMP	0.205	304.2	0.197	0.012
dCMP	0.205	289.2	0.192	0.012

The average molecular weight is **307.52**

## APPENDIX

The GC content of **RNA** is taken as an average of 52% (Lander et al., 2001):

<b>RNA</b>	<b>Content (mol/mol)</b>	<b>MW(g/mol)</b>	<b>Content % (w/w)</b>	<b>mmol/g biomass</b>
AMP	0.24	329.2	0.246	0.043
UMP	0.24	306.2	0.228	0.043
GMP	0.26	345.2	0.279	0.047
CMP	0.26	305.2	0.246	0.047

The average molecular weight is **321.6**

The average molecular weight of **lipids**, calculated from the composition described below and assuming only the major classes, is found to be **717**.

The Lipid Composition is taken from Mackenzie et al. (1967) for mammalian cell :

<b>Lipid Fraction</b>	<b>% total lipid</b>	<b>Average Mol. Wt</b>
Sterol Esters + Hydrocarbons	2.7	636
Triglycerides	7.2	895.4
Cholesterol+ Diglycerides	8.8	386
Polar lipids	81	742.7

The major components of the polar lipids are given below (Tombaccini et al., 1981):

<b>Lipid Class</b>	<b>% Polar Lipid</b>	<b>Mol Wt.</b>
Phosphatidylcholine	46.3	747
Phosphatidylethanolamine	25.2	705
Phosphatidylinositol+ Phosphatidylserine (1:2)	13.6	811
Sphingomyelin	14.7	741

The average molecular weight of the polar lipids is 742.7

The Fatty acid Composition was determined using GC-MS. The major fatty acids detected are given below and the others being neglected, taken as 100%:

<b>Fatty acid</b>	<b>% Fatty Acid</b>	<b>Molecular Wt:</b>
18:1	44%	281
18:0	27%	283
16:0	22%	255
16:1	5%	253

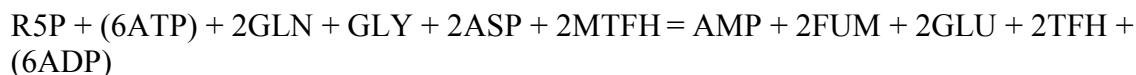
The Average Molecular Weight was calculated as: 268.8

**EQUATIONS FOR BIOMASS COMPONENTS FOR CHO CELLS:**

The biomass equations were determined from known biochemistry of biosynthesis and the cellular composition.

**Purine Biosynthesis:****AMP (Adenosine monophosphate)**

Biosynthesis:



*For CHO cells DNA:*



*For CHO cells RNA:*

**GMP (Guanosine monophosphate)**

Biosynthesis:



*For CHO cells DNA:*



*For CHO cells RNA:*



**Pyrimidine Biosynthesis:****UMP (Uridine monophosphate)**

Biosynthesis:

*For CHO RNA:***dTMP (Thymidine monophosphate)**

Biosynthesis:

*For CHO DNA:***CMP (Cytidine monophosphate)**

Biosynthesis:

*For CHO DNA:**For CHO RNA:*

**Combined CHO DNA**

$$0.295R5P + (1.47ATP) + (0.59GLN) + 0.295GLY + 0.59ASP + 0.59MTHF = 0.295dAMP + 0.59FUM + (0.59GLU) + 0.59THF + (1.47ATP)$$

$$0.205R5P + (1.025ATP) + (0.605GLN) + 0.205GLY + 0.205ASP + 0.41MTHF = 0.205GMP + 0.205FUM + (1.025ADP) + (0.605GLU) + 0.41THF$$

$$0.295R5P + (1.18ATP) + 0.295ASP + 0.295MTHF = 0.295dTMP + 1.18ADP + 0.295THF$$

$$0.205R5P + (1.025ATP) + 0.205ASP + (0.41GLN) = 0.205CMP + (0.41GLU) + 1.025ADP$$

**DNA biosynthesis equation CHO cells:**

$$R5P + (4.7ATP) + 1.295ASP + 0.5GLY + 1.29MTHF + (1.6GLN) = \mathbf{DNA} + (4.7ADP) + 1.29THF + (1.6GLU) + 0.205FUM$$

**Combined CHO RNA**

$$0.24R5P + (1.2ATP) + (0.48GLN) + 0.24GLY + 0.48ASP + 0.48MTHF = 0.24AMP + 0.48FUM + (0.48GLU) + 0.48THF + (1.2ATP)$$

$$0.26R5P + (1.3ATP) + (0.78GLN) + 0.26GLY + 0.26ASP + 0.52MTHF = 0.26GMP + 0.26FUM + (1.3ADP) + (0.78GLU) + 0.52THF$$

$$0.24R5P + (0.96ATP) + 0.24ASP + (0.24GLN) = 0.24UMP + (0.24GLU) + (0.96ADP)$$

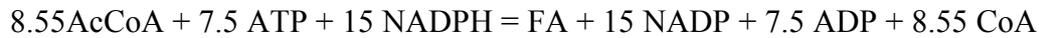
$$0.26R5P + 1.3ATP + 0.26ASP + (0.52GLN) = 0.26CMP + 0.52GLU + (1.3ADP)$$

**RNA biosynthesis equation for CHO cells:**

$$R5P + (4.67ATP) + 1.24ASP + 0.5GLY + MTHF + (2GLN) = \mathbf{RNA} + (4.67ADP) + 0.26FUM + (2GLU) + THF$$

**Lipid biosynthesis:****Fatty Acid**

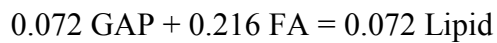
Considering an average carbon chain of 17.1 as determined from the lipid composition

**Triglycerides (TG)**

Biosynthesis:



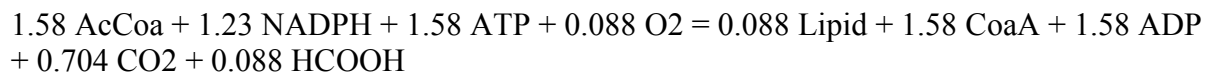
*For CHO cells:*

**Cholesterol (CHOL)**

Biosynthesis:



*For CHO cells*

**Sterol Esters (SE)**

Biosynthesis (without ATP and reductive elements):



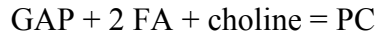
*For CHO cells*



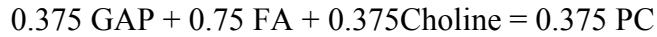
**Polar Lipids**

***Phosphatidylcholine (PC)***

Biosynthesis (Reductive factors not considered and DHAP is replaced with GAP):



*In CHO Cells:*

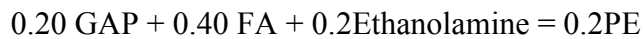


***Phosphatidylethanolamine (PE)***

Biosynthesis:

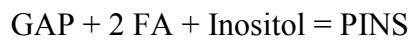


*In CHO cells:*

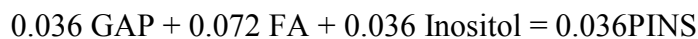


***Phosphatidylinositol (PINS)***

Biosynthesis:



*In CHO cells:*

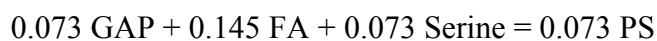


***Phosphatidylserine (PS)***

Biosynthesis:

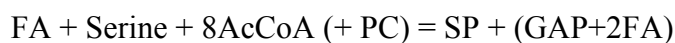


*In CHO Cells:*

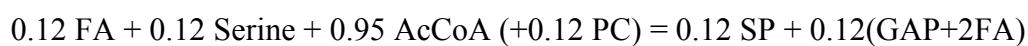


***Sphingomyelin (SP)***

Biosynthesis:



*In CHO cells:*



**Total polar lipids**

$$0.375 \text{ GAP} + 0.75 \text{ FA} + 0.375 \text{ Choline} = 0.375 \text{ PC}$$

$$0.20 \text{ GAP} + 0.40 \text{ FA} + 0.2 \text{ Ethanolamine} = 0.2\text{PE}$$

$$0.036 \text{ GAP} + 0.072 \text{ FA} + 0.036 \text{ Inositol} = 0.036\text{PINS}$$

$$0.073 \text{ GAP} + 0.145 \text{ FA} + 0.073 \text{ Serine} = 0.073 \text{ PS}$$

$$0.12 \text{ FA} + 0.12 \text{ Serine} + 0.95 \text{ AcCoA} (+0.12 \text{ PC}) = 0.12 \text{ SP} + 0.12(\text{GAP}+2\text{FA})$$

**Combined equation polar lipids**

$$0.68 \text{ GAP} + 1.49 \text{ FA} + 0.193 \text{ Serine} + 0.95 \text{ AcCoA} + 0.375 \text{ choline} + 0.2 \text{ Ethanolamine} + 0.036 \text{ Inositol} = 0.81 \text{ lipid}$$

**Total Lipids:**

TG

$$0.072 \text{ GAP} + 0.216 \text{ FA} = 0.072 \text{ Lipid}$$

CHOL

$$1.58 \text{ AcCoA} + 1.23 \text{ NADPH} + 1.58 \text{ ATP} + 0.088 \text{ O}_2 = 0.088 \text{ Lipid} + 1.58 \text{ CoA} + 1.58 \text{ ADP} + 0.704 \text{ CO}_2 + 0.088 \text{ HCOOH} + 1.23 \text{ NADP}$$

SE

$$0.027 \text{ FA} + 0.486 \text{ AcCoA} = 0.027 \text{ Lipid}$$

Polar Lipids

$$0.68 \text{ GAP} + 1.49 \text{ FA} + 0.193 \text{ Serine} + 0.95 \text{ AcCoA} + 0.375 \text{ choline} + 0.2 \text{ Ethanolamine} + 0.036 \text{ Inositol} = 0.81 \text{ lipid}$$

Combining the individual lipid equations for CHO cells (not including NADPH, NADP, ATP, ADP, CO<sub>2</sub>, O<sub>2</sub>, CoA and HCOOH):

$$0.75 \text{ GAP} + 1.73 \text{ FA} + 3.02 \text{ AcCoA} + 0.193 \text{ Serine} + 0.375 \text{ choline} + 0.2 \text{ Ethanolamine} + 0.036 \text{ Inositol} = \text{Lipids}$$

**Total lipid biosynthesis equation for CHO cells:**

Final Equation only based on precursors:

$$0.75 \text{ GAP} + 17.8 \text{ AcCoA} + 0.193 \text{ SER} + 0.375 \text{ choline} + 0.2 \text{ Ethanolamine} + 0.036 \text{ Inositol} = \text{Lipids}$$

**EQUATIONS FOR BIOMASS BIOSYNTHESIS IN CHO CELLS:**

**Protein:**

0.095ALA+0.048ASP+0.039ASN+0.063ARG+0.028CYS+0.052GLN+0.064GLU  
 +0.078GLY+0.022HIS+ 0.089LYS+0.02MET+0.021PHE+0.028PRO+0.057SER  
 +0.061THR+0.006TRP+0.02TYR+0.059VAL+(4ATP)=**PROTEIN**+(4ADP)

**Carbohydrates**

G6P+3.5ATP=**CARBO**+3.5ADP

**Lipid**

0.75 GAP+17.8 AcCoA+0.193 SER+0.375 choline+0.2 Ethanolamine  
 + 0.036 Inositol = **LIPIDS**

**DNA**

R5P+(4.7ATP)+1.295ASP+0.5GLY+1.29MTHF+(1.41GLN)=**DNA**+(4.7ADP)+1.29THF+(1.41GLU) +0.205FUM

**RNA**

R5P+(4.67ATP)+1.24ASP+0.5GLY+MTHF+(1.76GLN)=**RNA**+(4.67ADP)+0.26FUM  
 +(1.76GLU)+THF

---

**References**

- Altamirano, C., Illanes, A., Casablancas, A., Gamez, X., Cairo, J.J. and Godia, C. (2001) Analysis of CHO cells metabolic redistribution in a glutamate-based defined medium in continuous culture. *Biotechnol Prog* 17, 1032-41.
- Lander, E.S., Linton, L.M., Birren, B., Nusbaum, C., Zody, M.C., Baldwin, J., Devon, K., Dewar, K., Doyle, M., FitzHugh, W., Funke, R., Gage, D., Harris, K., Heaford, A., Howland, J., Kann, L., Lehoczky, J., LeVine, R., McEwan, P., McKernan, K., Meldrim, J., Mesirov, J.P., Miranda, C., Morris, W., Naylor, J., Raymond, C., Rosetti, M., Santos, R., Sheridan, A., Sougnez, C., Stange-Thomann, N., Stojanovic, N., Subramanian, A., Wyman, D., Rogers, J., Sulston, J., Ainscough, R., Beck, S., Bentley, D., Burton, J., Clee, C., Carter, N., Coulson, A., Deadman, R., Deloukas, P., Dunham, A., Dunham, I., Durbin, R., French, L., Grafham, D., Gregory, S., Hubbard, T., Humphray, S., Hunt, A., Jones, M., Lloyd, C., McMurray, A., Matthews, L., Mercer, S., Milne, S., Mullikin, J.C., Mungall, A., Plumb, R., Ross, M., Shownkeen, R., Sims, S., Waterston, R.H., Wilson, R.K., Hillier, L.W., McPherson, J.D., Marra, M.A., Mardis, E.R., Fulton, L.A., Chinwalla, A.T., Pepin, K.H., Gish, W.R., Chissoe, S.L., Wendl, M.C., Delehaunty, K.D., Miner, T.L., Delehaunty, A., Kramer, J.B., Cook, L.L., Fulton, R.S., Johnson, D.L., Minx, P.J., Clifton, S.W., Hawkins, T., Branscomb, E., Predki, P., Richardson, P., Wenning, S., Slezak, T., Doggett, N., Cheng, J.F., Olsen, A., Lucas, S., Elkin, C., Uberbacher, E., Frazier, M., et al. (2001) Initial sequencing and analysis of the human genome. *Nature* 409, 860-921.
- Mackenzie, C.G., Mackenzie, J.B. and Reiss, O.K. (1967) Increase in cell lipid and cytoplasmic particles in mammalian cells cultured at reduced pH. *J Lipid Res* 8, 642-5.
- Tombaccini, D., Fallani, A., Mugnai, G. and Ruggieri, S. (1981) Lipid composition of Balb/c3T3, SV3T3, and Concanavalin A-selected revertant cells grown in media containing lipid-depleted serum. *J Lipid Res* 22, 590-7.